PolyPublie
Polytechnique Montréal

POLYTECHNIQUE MONTRÉAL
UNIVERSITÉ D'INGÉNIERIE

Titre: Title:	Machining strategies of an inconel 718 shaft
Auteur: Author:	Charles Romain Galo
Date:	2006
Type:	Mémoire ou thèse / Dissertation or Thesis
Référence: Citation:	Galo, C. R. (2006). Machining strategies of an inconel 718 shaft [Master's thesis, École Polytechnique de Montréal]. PolyPublie. https://publications.polymtl.ca/7619/

Document en libre accès dans PolyPublie
Open Access document in PolyPublie

URL de PolyPublie: PolyPublie URL:	https://publications.polymtl.ca/7619/
Directeurs de recherche: Advisors:	Marek Balazinski, Ioan Sasu, & Victor Songmené
Programme: Program:	Unspecified

Ce fichier a été téléchargé à partir de PolyPublie, le dépôt institutionnel de Polytechnique Montréal
This file has been downloaded from PolyPublie, the institutional repository of Polytechnique Montréal

https://publications.polymtl.ca

UNIVERSITÉ DE MONTRÉAL

MACHINING STRATEGIES OF AN INCONEL 718 SHAFT

CHARLES ROMAIN GALO
DÉPARTEMENT DE GÉNIE MÉCANIQUE
ÉCOLE POLYTECHNIQUE DE MONTRÉAL

MÉMOIRE PRÉSENTÉ EN VUE DE L'OBTENTION
DU DIPLÔME DE MAÎTRISE ÈS SCIENCES APPLIQUÉES
(GÉNIE MÉCANIQUE)
FÉVRIER 2006

©Charles Romain Galo, 2006.

Library and Archives Canada

Published Heritage Branch

395 Wellington Street
Ottawa ON K1A 0N4
Canada

Bibliothèque et Archives Canada

Direction du Patrimoine de l'édition

395, rue Wellington
Ottawa ON K1A 0N4
Canada

Your file Votre référence
ISBN: 978-0-494-16786-1
Our file Notre référence
ISBN: 978-0-494-16786-1

NOTICE:
The author has granted a non-exclusive license allowing Library and Archives Canada to reproduce, publish, archive, preserve, conserve, communicate to the public by telecommunication or on the Internet, loan, distribute and sell theses worldwide, for commercial or non-commercial purposes, in microform, paper, electronic and/or any other formats.

The author retains copyright ownership and moral rights in this thesis. Neither the thesis nor substantial extracts from it may be printed or otherwise reproduced without the author's permission.

AVIS:
L'auteur a accordé une licence non exclusive permettant à la Bibliothèque et Archives Canada de reproduire, publier, archiver, sauvegarder, conserver, transmettre au public par télécommunication ou par l'Internet, prêter, distribuer et vendre des thèses partout dans le monde, à des fins commerciales ou autres, sur support microforme, papier, électronique et/ou autres formats.

L'auteur conserve la propriété du droit d'auteur et des droits moraux qui protège cette thèse. Ni la thèse ni des extraits substantiels de celle-ci ne doivent être imprimés ou autrement reproduits sans son autorisation.

In compliance with the Canadian Privacy Act some supporting forms may have been removed from this thesis.

While these forms may be included in the document page count, their removal does not represent any loss of content from the thesis.

Conformément à la loi canadienne sur la protection de la vie privée, quelques formulaires secondaires ont été enlevés de cette thèse.

Bien que ces formulaires aient inclus dans la pagination, il n'y aura aucun contenu manquant.

Canada

UNIVERSITÉ DE MONTRÉAL

ÉCOLE POLYTECHNIQUE DE MONTRÉAL

Ce mémoire intitulé:

MACHINING STRATEGIES OF AN INCONEL 718 SHAFT

présenté par: GALO CHARLES ROMAIN
en vue de l'obtention du diplôme de: Maîtrise ès sciences appliquées
a été dûment accepté par le jury d'examen constitué de:

M. MAYER René, Ph.D., président
M. BALAZINSKI Marek, Ph.D., membre et directeur de recherche
M. SASU Ioan, Ph.D., membre et codirecteur de recherche
M. SONGMENÉ Victor, Ph.D., membre et codirecteur de recherche
M. ENGIN Serafetin, PhD., membre

ACKNOWLEDGEMENT

I would like to thank my co director M. Ioan Sasu for his support during this study. His expertise and advices have been useful to conduct this project and avoid technical traps.
I would also like to thank M. Serafetin Engine for his interest to this project and his advices.
I would like to express my gratitude to my thesis director M. Marek Balazinski. He has been more than a director for me during the difficult periods of my study. I would like to thank him for his patience.
I would like to thank my co director Victor Songmene, whose advices have been appreciable to understand some aspects of this study.

ABSTRACT

This study is about the machining strategies of an Inconel 718 shaft, a super alloy used in the aerospace industry. The emphasis is put especially on the roughing and semi finishing aspects. The objectives are to increase the quality of the machined parts, the tool life and thus to reduce the machining time and the machining costs.

An overview of the roughing steps is presented, followed by the major problems encountered when machining an Inconel 718 material in turning.
Different techniques to reduce the notch wear are portrayed according to the literature review. Based on this literature review, a tool material and its geometries are selected, to start the preliminary tests.

Two different machining strategies are presented, i.e. the feed variation method and the depth of cut variation method, called ramping. The work piece material physical and metallurgical properties are also taken into account during the tests.

The advantages and drawbacks of these methods are highlighted, and several advices are given to optimize the machining of an Inconel 718 shaft.

It is shown that a good application of the ramping method is necessary, in order to eliminate the notch wear, which is the major cause of short tool life. It is also shown that an adequate choice of the tool geometry and cutting parameters make it possible to reduce or eliminate the lateral burr formation when machining Inconel 718.

For future research, a new method is presented, that is the feed variation during ramping.

RÉSUMÉ

Cette étude porte sur les stratégies d'usinage d'un arbre en Inconel 718, un super alliage utilisé en aéronautique. Elle s'intéresse en particulier à l'aspect de l'ébauche et de la demi-finition. Elle vise à améliorer la qualité des pièces, la durée de vie des outils de coupe et donc à réduire les temps de cycles et les coûts de fabrication.

Plusieurs méthodes décrites dans la littérature sont présentées, et selon cette analyse bibliographique, le matériau de l'outil de coupe et sa géométrie sont sélectionnés pour les essais préliminaires.

Deux principales stratégies d'usinage sont étudiées, à savoir la méthode de l'avance variable et celle de la profondeur de coupe variable, communément appelée ramping. Les propriétés physiques et métallurgiques du matériau usiné sont prises en compte dans l'analyse des résultats. Les avantages et les inconvénients de ces deux méthodes sont présentés, et des astuces sont fournies pour optimiser l'usinage d'un arbre en Inconel 718.

Il est montré qu'une bonne application de la méthode du ramping est nécessaire, afin d'éliminer l'apparition de l'usure en entaille, principale cause de la faible durée de vie des outils de coupe. Il est aussi montré qu'un choix adéquat de la géométrie de l'outil et des paramètres de coupe permet de réduire, voir d'éliminer l'apparition de bavures latérale pendant l'usinage de l'inconel 718.

Pour les recherches futures, une nouvelle stratégie d'usinages est présentée, à savoir la variation de l'avance pendant le ramping.

CONDENSÉ EN FRANÇAIS

La compagnie Pratt & Whitney Canada est un leader mondial dans la fabrication de turbomoteurs, turbosoufflantes et des turbopropulseurs. Le maintien de cette position de leader nécessite un investissement constant dans la recherche et développement de nouveaux procédés de fabrication. C'est dans ce cadre que s'insère la présente étude. Il s'agit de déterminer des stratégies d'usinage du superalliage Inconel 718, un alliage de nickel qui entre dans la fabrication de l'arbre de la turbosoufflante PW307.

INTRODUCTION

Les alliages de nickels sont très répandus dans l'industrie aéronautique pour des applications civiles et militaires. Cette présence est due à leur très bonne résistance mécanique et leur résistance à la corrosion à haute température. Mais ces qualités mécaniques rendent ces alliages difficiles à usiner.

L'introduction d'un nouveau matériau dans le procédé de fabrication nécessite la plupart du temps une réadaptation des méthodes d'usinage. Il devient alors nécessaire de changer les outils de coupe, les paramètres de coupe et la planification du procédé de fabrication. Le but ultime de ces recherches étant une réduction du coup de fabrication.

L'usinage de l'Inconel 718 est réputée être difficile à cause de la faible durée de vie des outils de coupe. Ce document traite des stratégies d'usinage à appliquer pour accroître la durée de vie des outils, la productivité, afin de réduire les coûts de fabrication.

Le premier chapitre traite de la problématique de l'usinage d'un arbre en Inconel 718. Il résume les différentes questions soulevées pendants les essais préliminaires effectués chez Pratt &Whitney Canada.

Le second chapitre est consacré à la revue de littérature pertinente au sujet. Il est question de résumer les informations sur les outils de coupe, les méthodes d'usinage et toutes autres informations pertinentes dans la littérature scientifique.

Le troisième chapitre traite de la méthodologie et des procédures expérimentales utilisées pour résoudre le problème posé.

Enfin le quatrième chapitre est consacré aux résultats des essais effectués. Une nouvelle technique d'usinage est proposée pour les recherches futures.

CHAPITRE I: PROBLÉMATIQUE

Pendant les essais préliminaires d'usinage effectués à Pratt & whitney, le coût de fabrication de l'arbre en Inconel 718 est resté élevé, car le procédé de fabrication n'était pas maîtrisé. L'une des raisons principales est le manque de contrôle sur le comportement des outils de coupe et leurs faibles durées de vie, pendant la phase d'ébauche et de demi-finition.
La question à résoudre est donc de définir une stratégie d'usinage de l'inconel 718 afin de réduire les coûts de l'ébauche et de la demi-finition. Cette question peut être formulée de différente manière:

- Quel est le meilleur outil à utiliser pour usiner un arbre en Inconel 718?
- Quelle est la meilleure méthode d'usinage?
- Quels sont les paramètres de coupe à utiliser pour réduire le coût de fabrication ?

A cette étape de l'étude, une analyse bibliographique s'avère nécessaire. Le chapitre suivant sera consacré à la revue bibliographique.

CHAPITRE II: REVUE DE LITTÉRATURE

2.1 Les différents procédés d'usinage de l'inconel 718

Pour résoudre le problème de l'usure en entaille de l'outil de coupe qui est l'une des causes majeures de la faible durée de vie des outils, plusieurs méthodes ont été proposées dans la littérature. Il s'agit entre autre, de la variation de la profondeur de coupe, communément appelé le ramping, de l'usinage assisté au laser, de l'usinage assisté au plasma, de l'usinage cryogénique, de l'usinage hybride et de la méthode de l'avance variable, pour ne citer que celles là.

2.1.1 Le ramping

Le ramping est une méthode qui a été abondamment traité dans les catalogues de la compagnie Greenleaf [18]. Il a pour but de faire varier la profondeur de coupe pendant l'usinage afin de repartir l'énergie qui crée l'usure en entaille sur toute l'arête de coupe.

2.1.2 L'usinage assisté au laser

L'usinage assisté au laser (LEM) a été utilisé par certains auteurs pour ramollir la couche superficielle du matériau afin de diminuer sa résistance à la traction et son écrouissage. L'auteur [36] note que l'usure de l'outil a été réduite de 40%, les efforts de coupe de 18% et le taux d'enlèvement en métal a été augmenté de 33%. Cependant le coût élevé des lasers de forte puissance, et la forte consommation d'énergie fait que ce procédé de coupe est très peu utilisé pour usiner l'Inconel 718.

2.1.3 L'usinage assisté au plasma PEM

Le PEM ou l'usinage assisté au plasma est l'utilisation d'une torche de plasma à la place d'un laser. Il vise le même objectif que la méthode au laser, c'est à dire ramollir la matière pour faciliter l'enlèvement de copeau. Cependant, cette méthode entraîne d'autres problèmes notamment l'échauffement inadmissible des outils [34,36].

3.1.4 L'usinage cryogénique CEM

Le but de l'usinage cryogénique est de refroidir l'outil à travers un système de refroidissement à l'azote liquide. Ce processus permet d'augmenter la durée de vie des outils. Néanmoins cette technique implique des coûts supplémentaires qui pourraient ainsi ne pas être justifiés.

2.1.5 L'usinage hybride

L'usinage hybride est une combinaison de l'usinage au plasma et l'usinage cryogénique. L'objectif étant de faciliter le refroidissement de l'outil dû au plasma. Les coûts d'investissement seront plus importants que les méthodes précédentes et il faudra justifier un tel investissement supplémentaire.

2.1.6 La méthode de l'avance variable

Cette méthode consiste a faire varier l'avance pendant l'usinage. Il a été montre que cette méthode permettait de réduire l'usure en cratère des outils. Il serait intéressant d'évaluer son influence sur l'usure en entaille.

2.2 Les outils de coupes

L'usinage de l'inconel 718 s'effectue avec plusieurs types d'outils dont les plus utilisés sont :

- Les carbures revêtus au TiAlN ou les carbures multi revêtus par les combinaisons (TiN, TiCN, TiAlN, Al_2O_3). La majeure partie des manufacturiers d'outils disposent de ces gammes de carbures.
- Les céramiques mixtes à base de nitrure de silicium Si_3N_4 et d'oxyde d'aluminium (Al_2O_3).
- Les céramiques renforcés de fibres de carbure de silicium SiC-whisker. On distingue les whisker à base de nitrure de silicium (Si_3N_4), utilisés la plupart du temps pour l'ébauche et les whisker à base d'oxyde d'aluminium (Al_2O_3) pour la finition. Les outils whisker utilisés dans cette étude sont commercialisés par la compagnie Greenleaf sous le nom WG 300 à base de Si_3N_4 et le WG600, qui est un WG300 revêtu.

L'analyse de la bibliographie a permis de sélectionner les meilleures catégories d'outils pour les essais préliminaires. Au moins un outil de coupe a été sélectionné dans les 3 catégories présentées. Le tableau (I) page (XIV) regroupe tous les outils employés pendant les essais. La méthodologie utilisée pour résoudre le problème posé est décrite dans le chapitre 3, sur la base des informations de la revue de littérature.

CHAPITRE III: MÉTHODOLOGIE ET PROCÉDURES EXPÉRIMENTALES

L'objectif de cette étude est d'établir la meilleure stratégie d'usinage d'un arbre en Inconel 718, afin de réduire le coût de fabrication d'un arbre en Inconel 718. Pour atteindre cet objectif, il est indispensable d'augmenter la durée de vie des outils de coupe. C'est donc autour de ce point que se focalise cette méthodologie.

3.1 Les méthodes

En se basant sur la revue bibliographique, trois méthodes sont analysées pour atteindre les objectifs d'augmentation de la durée de vie des outils de coupe:

- La méthode d'essai à profondeur de coupe constante
- La méthode du ramping
- La méthode de l'avance variable

Les essais à profondeur de coupe constante permettent de choisir les meilleures géométries d'outils et les paramètres de coupe adéquats entre plusieurs outils provenant de différents manufacturiers.

Avec les outils ainsi sélectionnés, les essais de ramping sont effectués. Deux variables sont testés avec deux plans d'expérience distincts. Ces variables sont, la pente du ramping, et la variation de la profondeur de coupe par rapport au temps. Le but étant de déterminer laquelle des deux variables peut être considérée comme la variable pertinente pour le ramping. Il sera ainsi aisé de lier mathématiquement l'usure de l'outil à cette variable, pour réaliser plus tard la minimisation de cette usure, et donc la maximisation de la durée de vie de l'outil.

3.2 Les outils de coupe

Le tableau suivant regroupe les outils de coupe et leurs caractéristiques, utilisés pour les essais d'usinage. Ces outils ont été sélectionnés selon les informations de la revue de littérature.

Tableau I : Outils de coupe pour les essais d'usinage

Outils	Manufacturer	Désignation	Plaquette	Type de plaquette	Angle de dépouille	Angle de coupe	Angle d'inclinaison
(1) Porte outil pour plaquette ronde en céramique	Greenleaf	C-CRGPL-164	RPGN-43	Céramique Whisker R-WG-300	//	5	5
(2) Porte outil pour plaquette carrée en céramique	Greenleaf	C-CSSPL-164	SPGN-432	Céramique Whisker S-WG 300	45	5	0
(3) Porte outil pour plaquette ronde en céramique	Kennametal KY1540	CRGNL-164	RNG-43T 0420	Sialon KY 1540	//	-10	-5
(4) Porte outil pour plaquette V en céramique	Greenleaf	CDJOL-164V	DPGN-443V	Céramique Whisker WG-600	-3	0	0
(5) Porte outil pour plaquette en carbure	Greenleaf	G-MSSNL-16-4D	SNGN -432	Carbure GA-5026	45	-10	-5
(6) Porte outil pour plaquette en carbure	Iscar	SDJCL-16-3	DCGT 3-1-SM	Carbure	-1	0	0
(7) Porte outil pour plaquette en carbure	Kennametal	MVJNL-163D	VNMG-332	Carbure KC5010 (TiAlN)	-3	-4	-13
(8) Porte outil pour plaquette en carbure	Kennametal	MDJNL-163D	DNGG-432LF	Carbure KC5010 (TiAlN)	-3	-5	-5
(9) Porte outil pour plaquette en carbure	Kennametal	MDJNL-163D	DNGG-432LF	Carbure GA-5026	-3	-5	-5

3.3 Les procédures expérimentales

3.3.1 La matière usinée

Deux échantillons d'Inconel 718 ont été utilisés pour ces essais. L'échantillon 1 et l'échantillon 2.

- Le premier échantillon d'Inconel 718 (échantillon 1) est une barre de 9 pouces de long et 5 pouces de diamètre.
- Le second échantillon d'Inconel 718 (échantillon 2) est une barre de 12 pouces de long et 6 pouces de diamètre.

Des essais de duretés et des observations de microstructures ont été effectués sur ces échantillons pour déterminer le lien entre leurs propriétés mécaniques et métallurgiques, et leurs comportements en usinage.

3.3.2 Les équipements de tests

- L'usinage est réalisé sur un tour CNC Mazak Nexus 200.
- La mesure de dureté est effectuée sur un testeur de dureté numérique.
- La microstructure des échantillons est analysée par un microscope électronique è balayage.
- Les efforts de coupes sont mesurés à l'aide d'un dynamomètre Kistler.
- L'usure des outils est mesuré à l'aide de photo prises par une camera numérique.

CHAPITRE IV: RÉSULTATS DES ESSAIS

4.1 Résultats du ramping

L'utilisation de la pente comme variable de ramping n'a pas donné des résultats satisfaisants, c'est pourquoi la variable utilisé pour le ramping est finalement la variation de la profondeur de coupe par rapport au temps.

La figure (I) montre la courbe de l'usure de l'outil en fonction de la variation de la profondeur de coupe par rapport au temps. La première approximation polynomiale entre les points de l'usure décrit une oscillation tout en décroissant. L'oscillation provient du fait que si la première rampe est positive, un nombre impair de rampe donne une usure inférieure à un nombre pair de rampe sur la même longueur usinée.

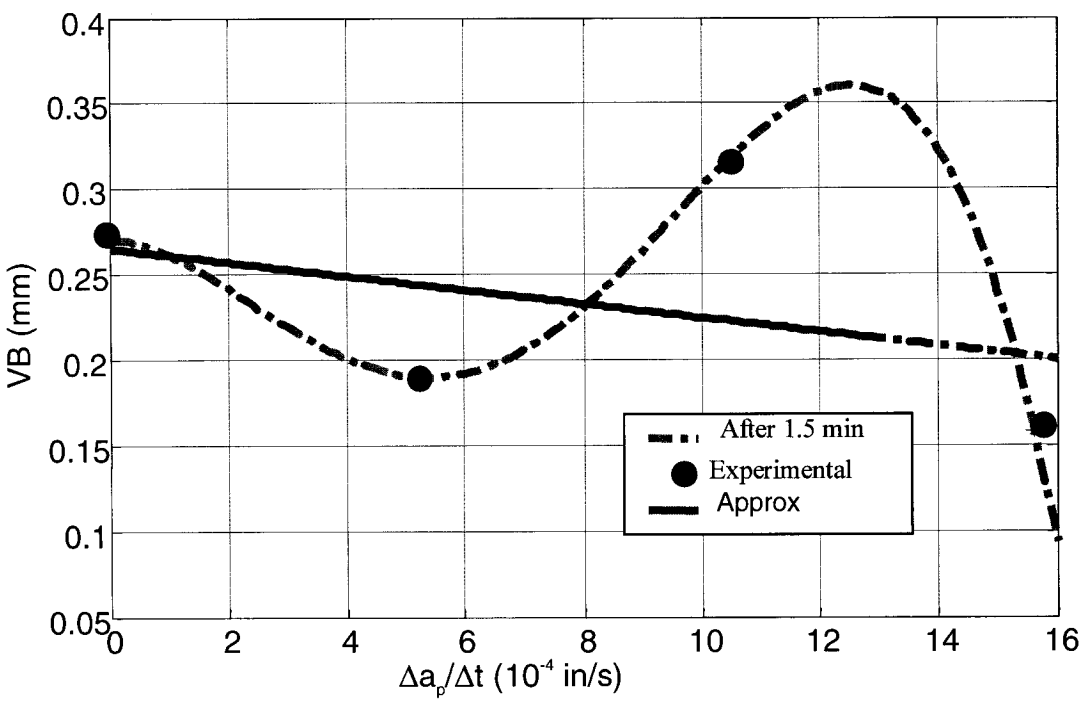

Figure I. Usure de l'outil en fonction de la variation de la profondeur de coupe par rapport au temps.

L'utilisation de ces résultats est illustrée à la page 116 de ce rapport, dans le cas général d'un arbre de diamètre et de longueur donnés.

La phase de pénétration de l'outil (rampe négative) produit une usure plus grande que la phase de rampe positive, parce que la section de copeau pendant la rampe négative est plus grande que pendant la phase positive, ce qui induit des efforts plus élevés sur l'outil. En plus durant la phase de rampe négative, la composante de la vitesse de pénétration de l'outil dans la matière contribue à réduire l'angle de dépouille de l'outil, ce qui augmentation l'usure en dépouille.

Pour palier ces phénomènes, une nouvelle stratégie de ramping a été mise sur pied. Il s'agit de réduire l'avance pendant les phases de rampes négatives et de l'augmenter pendant les phases de rampes positives, afin de conserver le même temps d'usinage tout en réduisant les effets négatifs de la rampe négative.

4.2 Les bavures latérales pendant l'usinage

Les essais pour la réduction des bavures latérales ont montré que l'angle de direction d'arête (κ_r) est la variable principale qui permet de réduire les bavures, comme illustré à la figure II. La raison est qu'un petit angle de direction donne une rigidité de la pièce en avant de la direction d'avance plus grande, ce qui limite la déformation latérale du bord de la pièce.
Cette observation est partagée par Andrey Toropov et al. [1].

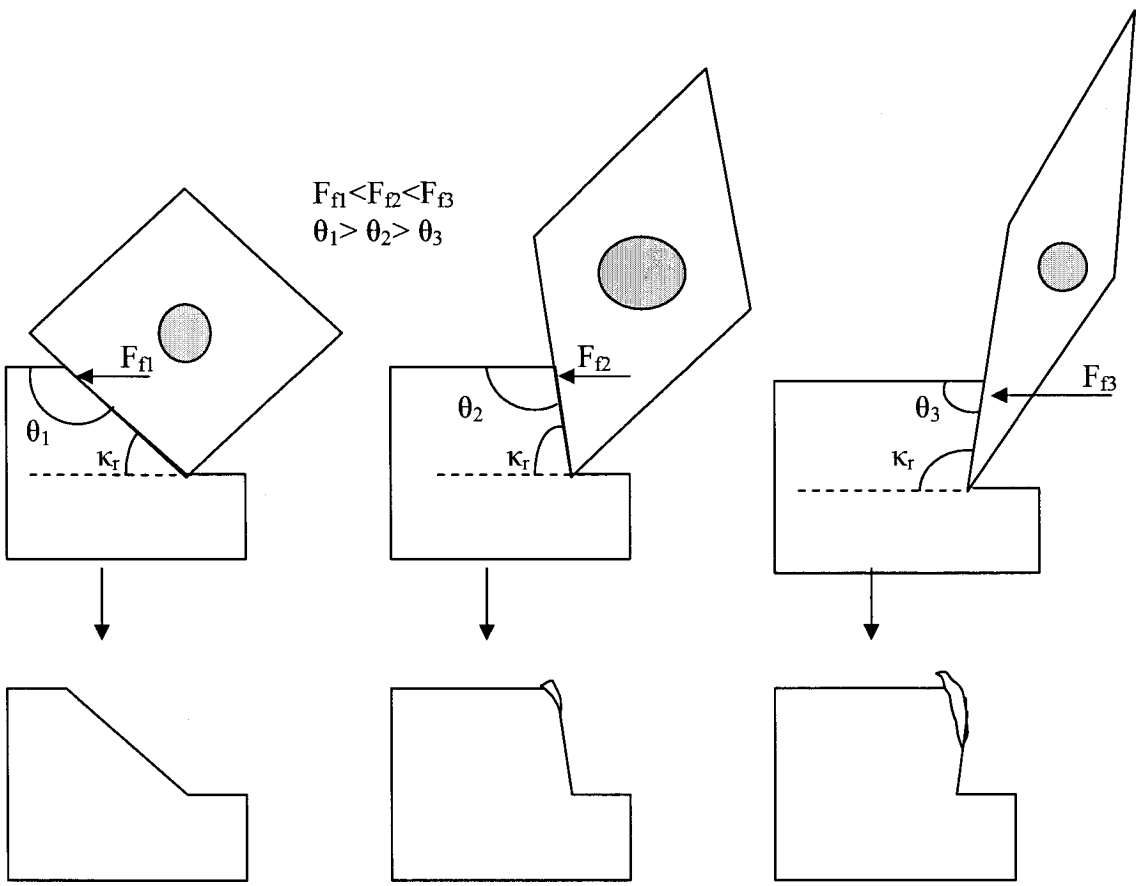

Figure II. Réduction des bavures selon l'angle de direction (κ_r)

Pour les angles de direction qui favorisent l'apparition de bavures, il est montré que la réduction de la vitesse de coupe, de l'avance ou de la profondeur de coupe permet de réduire, voir éliminer les bavures latérales.

CONCLUSION

Plusieurs stratégies d'usinage sont décrites afin d'accroître la durée de vie de l'outil pendant l'usinage de l'Inconel 718.
La méthode de l'avance variable n'a pas donné les résultats escomptés. Cependant le ramping a prouvé son efficacité dans la suppression de l'usure en entaille. La variation de la profondeur de coupe par rapport au temps est la variable indiquée pour estimer l'usure de l'outil, contrairement à la pente du ramping qui ne permet pas une bonne appréciation des usures.

Une valeur du ratio $\rho = 0.3$ permet de conserver un copeau minimum à enlever par l'outil, tout en maintenant une bonne longueur sur l'arête pour la répartition de l'énergie de l'usure en entaille.

La stratégie de ramping en zigzag est efficace sur des longueurs à usiner plus grandes. Néanmoins pour une longueur donnée, il est préférable d'effectuer si possible plus de rampes positifs (en montée) que de rampes négatifs (pénétration dans la matière).

Un trop grand nombre de rampes sur une petite longueur accroît la vitesse de pénétration de l'outils pendant les rampes négatives, ce qui a pour corollaire une usure rapide. Pour un usinage efficace, il est donc préférable de garder une valeur raisonnable de variation de la profondeur de coupe par rapport au temps (dans les limites des résultats de cette étude).

Les bavures sur les pièces usinées sont plus influencées par l'angle de direction que par les paramètres de coupe. Il suffit dès lors d'avoir un angle de direction inférieur à 90 degré, pour que cette bavure disparaisse progressivement. L'angle de 45 degré utilisé dans cette étude donne des résultats satisfaisants. Néanmoins pour les situations où l'utilisation d'un angle de 45 degré est impossible, la réduction de la vitesse de coupe, l'avance ou de la profondeur de coupe permettent de réduire voir éliminer les bavures.

Table of contents

LIST OF TABLES

LIST OF FIGURES

LIST OF EQUATIONS

LIST OF APPENDIX

NOMENCLATURE

α : Clearance angle

α_{eff}: Effective clearance angle

a_p: Depth of cut

A: Maximum depth of cut removed when ramping

b: Active tool edge length

B: Minimum depth of cut removed when ramping

C: machining time for Greenleaf ramping method

C_{tc} : Chip thickness for constant depth of cut machining

C_{tN}: Chip thickness for negative ramp

C_{tp}: Chip thickness for positive ramp

Δt: Time to machine the first pass when ramping

D: Diameter

D_f: final diameter

D_i, $D_{init.}$ Initial diameter

D_m: mean diameter

DOCVT: Depth of cut variation in time

E, ε: Slope angle

f: feed

f_{eq}: Equivalent feed

F_f: Feed force

F_r: Radial force

F_t: Tangential force

γ: Rake angle

γ_{eff}: Effective rake angle

κ_r: Lead angle

λ_s: Inclination angle

L_{ind}: indicative length

n: Spindle speed or RPM

N: number

r_ε: Tool radius

RPM: Revolution per minute

VB, VB_B: Average flank wear

VB_c: Nose wear

VB_{max}: Maximum flank wear

VB_N, V_N: Notch wear

V_c: Cutting speed

$\vec{V}_c$: Cutting speed vector

V_f: Feed rate

$\vec{V}_f$: Feed rate vector

V_p:Depth of cut point speed

V_{pe}: Tool radial penetration speed

$\vec{V}_{pe}$: Tool radial penetration speed vector

DEFINITIONS

Ramping: depth of cut variation during the machining

Positive ramp: ramping process where the tool tip describes a positive slope (moves away from the shaft axis for the external turning)

Negative ramp: ramping process where the tool tip describes a negative slope (plunge in, where the tool tip approaches the shaft axis for the external turning)

Zigzag ramping or waves: ramping process where the tool tip describes a sinusoidal path, which is a combination of positive and negatives ramps.

Introduction

The nickel alloys are widespread in the aircraft industry for civil and military applications. This presence is due to their good mechanical properties and their corrosion resistance at high temperature. But these good mechanical properties make these alloys difficult to machine.

The introduction of a new material in the production process requires most of the time a certain adaptation. It is often necessary to change the tooling, i.e. the tool geometries and the tool material. The cutting parameters must also be adapted to the new material. The choice of theses parameters requires some tests that are usually time consuming. The new tool data and the cutting parameters have to be taken into account during the process planning, in order to set an optimum process.

The final objectives of these investigations are always the reduction of the overall machining cost. This cost has four components. At first, the tooling cost which is the cost of all the inserts used during the machining process. Secondly the total operating cost, which includes the costs connected to the machine (electricity, maintenance, the dumping, the operator hourly cost...). The third cost is the tool changing cost. It comes from the additional time an operator or a system will take to change a tool if it is worn. If the tool has to be changed very often, this cost will be high. The fourth cost is the unproductive cost, which include the waste of time related to tool breakage, tiredness of the operator and the unforeseeable vibrations of the system.

The machining of a super alloy such as Inconel 718 is known to be difficult because the tool life is very short. It is therefore important to set an optimization process to ensure a minimum machining cost.

This document gives some answers to the question of how an Inconel 718 shaft machining process can be optimized. Different machining techniques are studied in order to find the best way to machine an Inconel 718 shaft.

The first chapter is devoted to the problem statement. It shows the different questions risen during the machining of an Inconel shaft at Pratt & Whitney Canada.

The second chapter summarizes some basic notions in turning used in this document.
The third chapter is devoted to the review of the literature relevant to the turning of Inconel 718 material. This chapter deals with the problems of tooling, machining methods and all relevant information in published articles.

The chapter 4 is about the theories of machining strategies developed to solve the problems. The feed variation methods and the ramping methods are explained.

The fifth chapter deals with the tests plans proposed according to the different machining strategies and the experimental procedures used to solve the problems raised in the first chapter.

The chapter 6 is about the machining results and the analysis. This chapter gives some answers for the different issues raised when machining Inconel 718. The advantages and drawbacks of the different machining strategies are highlighted. Some proposals are made about a thesis subject and a new machining method. Some practical solutions are given to machine the PW 307 shaft in roughing and semi finishing.

CHAPTER 1. PROBLEM STATEMENT

1.1. Overview of the machining process

The PW307 is an engine of the PW300 family series of advanced high by-pass ratio turbofan engines developed by Pratt & Whitney Canada. The machining of the main shaft of this engine is what concerns this study.

1.1.1. The shape of the shaft

The shaft to be machined is a thin-walled hollow shaft of Inconel 718, Figure 1.1. It has a length of more than approximately 53.01 in, a diameter varying from 1.75 to 2.7 in. At certain places, the wall thickness is only 0.16 in, which makes its machining difficult. Therefore the knowledge of the cutting forces may be an important issue.

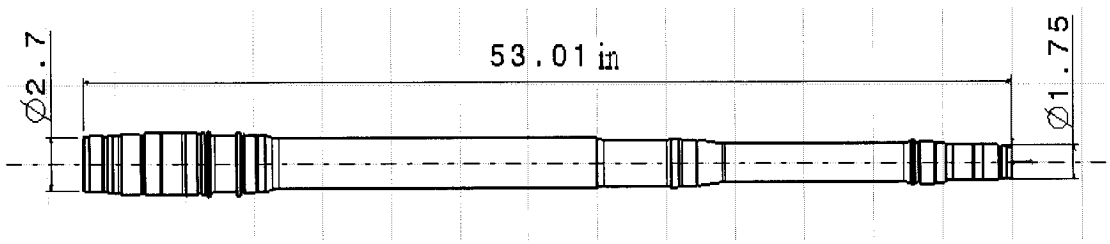

Figure 1.1. PW307 shaft

1.1.2. Overview of the roughing process

The machining process of the shaft from rough material to finished part is quite complex. But for the roughing and semi finishing aspect, a simplified process is represented in Figure 1.2. Phase 1 is a roughing process, for which goal is to define the first starting surfaces. It includes a straight turning and a facing. Phase 2 consists in machining a certain number of surfaces on the part for the steady rest positioning. Phase 3 consist in removing the maximum amount of material in order to approach the final

roughing shape. Phase 4 is a semi finishing operation. It aims to have the exact roughing shape, by removing a certain amount of material in order to have a constant thickness all around the finished shape. This operation in generally made with a constant depth of cut (DOC) machining. Many other operations are performed to obtain the final shaft. We can mention the gun-drilling (drilling over the entire length of the shaft), the grinding, and many related operations.

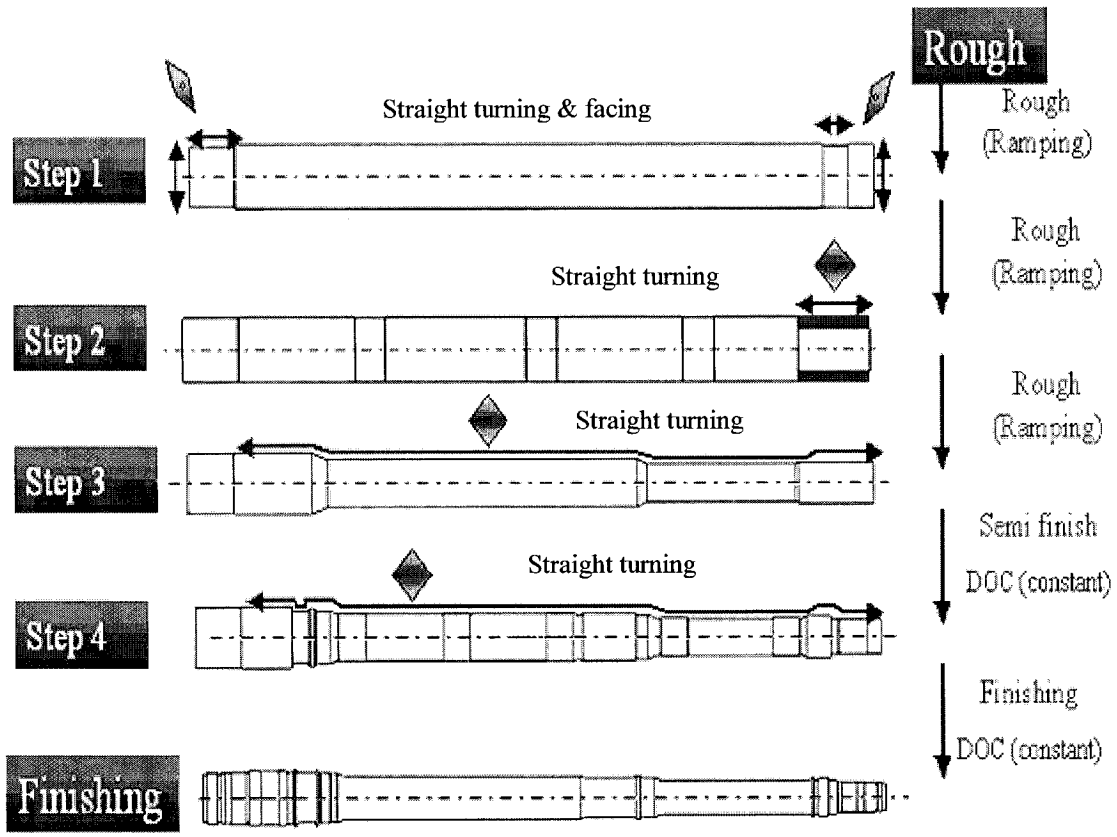

Figure 1.2. Simplified roughing process

1.1.3. The quality requirements

The surface roughness is a quality requirement during machining, but this aspect is less important in this case, since this study focuses only on the roughing and semi-finishing aspects.

The emphasis will be put on the material behavior in certain cases like the build up edges and burrs on the machined part which can cause degradation of the machined surfaces properties

1.1.4. The Inconel 718 machining issue

Inconel 718 is a difficult to machine super alloy. Its low thermal conductivity generates during machining a localization of heat at the tool tip. This heat induces high temperatures which causes premature tool wear.

Notch wear is the most frequent wear and Inconel 718 has a strong work hardening tendency. During the machining in certain conditions, lateral burrs formations are observed.

All these problems were addressed during the preliminary tests performed at Pratt & Whitney Canada. These facts explain why the tools lives are short and the machining cost are high.

1.2. The questions

The question to be solved is to define a strategy to machine an Inconel 718 shaft in order to reduce the roughing and semi finishing cost. This question can be stated in different ways:

- What is the best tool to use for the machining of an Inconel 718 shaft?
- What is the best machining method?

- What are the cutting parameters to use in order to reduce the total machining cost?

To solve these questions, it is necessary to find a good tool material, tool geometry, a machining method and a good process planning.

In the next chapter, some basic notions in turning are presented related to this study.

CHAPTER 2. Basic notions in turning

This chapter deals with some basic notions in turning which are going to be used during this study. The notions of tool geometries, cutting parameters, cutting forces and tool wear criteria are explained.

2.1. The cutting parameters and the cutting forces

The constant depth of cut machining is a classical machining process where the depth of cut is set constant during the process. Three major machining parameters can be noticed:

a_p: The depth of cut (in)

V_c: The cutting speed (ft/min)

f : The feed (in/rev)

Figure 2.1 shows the basic geometry of a turning process

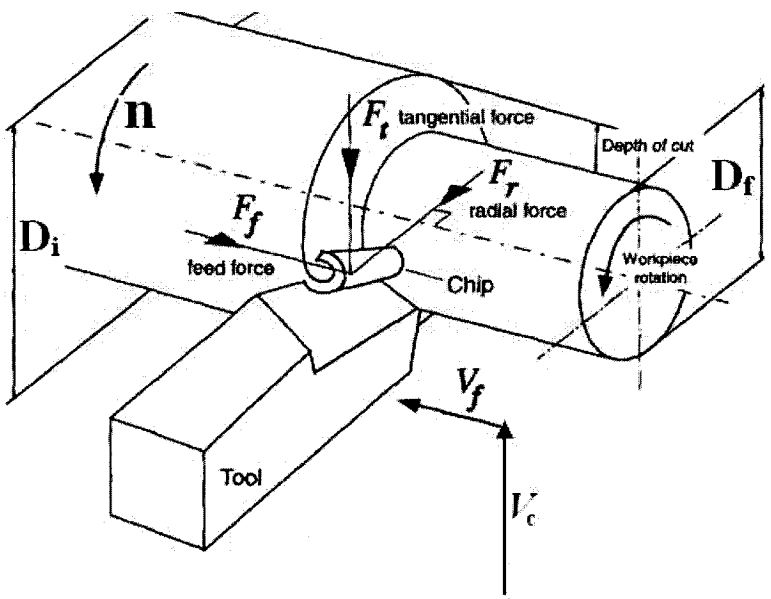

Figure 2.1. Geometry of turning process. Source [36]

D_i: The initial diameter

D_f: The final diameter

n: The spindle speed or RPM (rev/min)

V_f: The feed rate = nf (in/min)

The cutting force during the turning process has 3 components as indicated in Figure 2.1:

F_r: The radial force (N)

F_f: The feed force (N)

F_t: The tangential force (N)

In this document, we define the tool relative velocity vector V to the workpiece as a combination of the 3 component vector of tool velocity

$$V = V_f + V_c + V_{pe} \qquad \text{Equation (1)}$$

The norm of V can be expressed with the norm of V_f, V_c and V_{pe} as:

$$V=\sqrt{V_f^2+V_c^2+V_{pe}^2} \qquad \text{Equation (2)}$$

Where V_{pe} is the tool radial penetration speed vector when the process requires the tool to move toward the radial direction. In the case described in Figure 2.2, the tool plunges in the radial direction on a slope of value E:

$V_{pe}=V_f\tan(E)=nf\tan(E)$

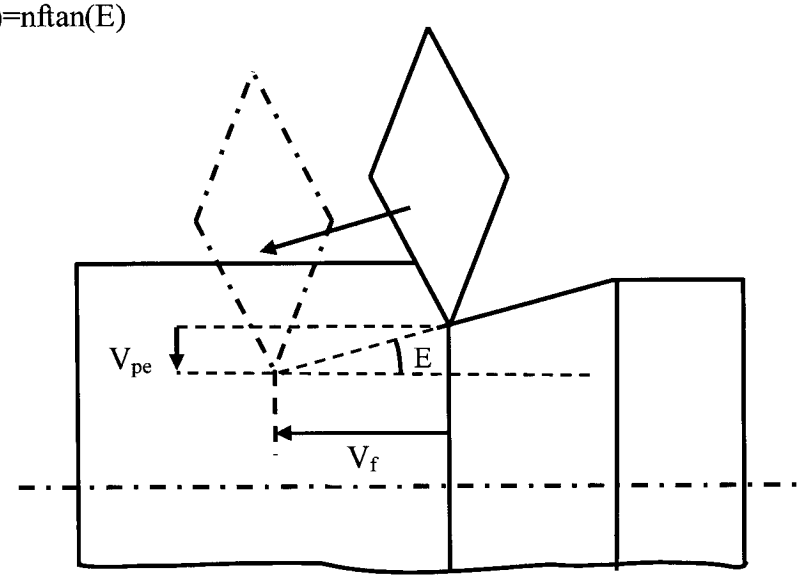

Figure 2.2. Tool penetration speed V_{pe} during negative ramping

During the plunging of the cutting tool, the tool clearance angle α can be reduced to α_{eff} because of the penetration speed. Figure 2.3 shows this phenomenon.

V_{ceff}: The effective cutting speed in the radial plan

α: The clearance angle

α_{eff}: The effective clearance angle

γ : The rake angle

γ_{eff} : The effective rake angle

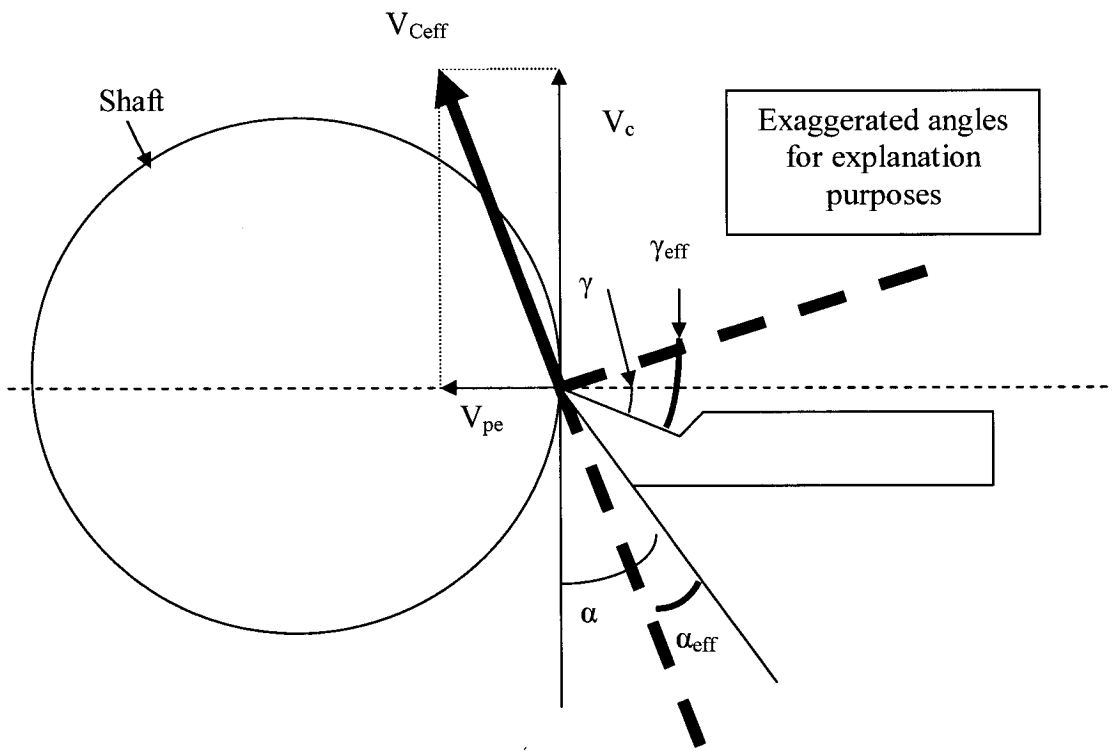

Figure 2.3. The effect of penetration speed on the reduction of clearance angle α

2.2. The cutting tool faces and wear pattern

The generic terms that are going to be used in this document are shown on Figure 2.4. The rake face and the flank face are indicated according to the feed and the cutting speed direction of the insert.

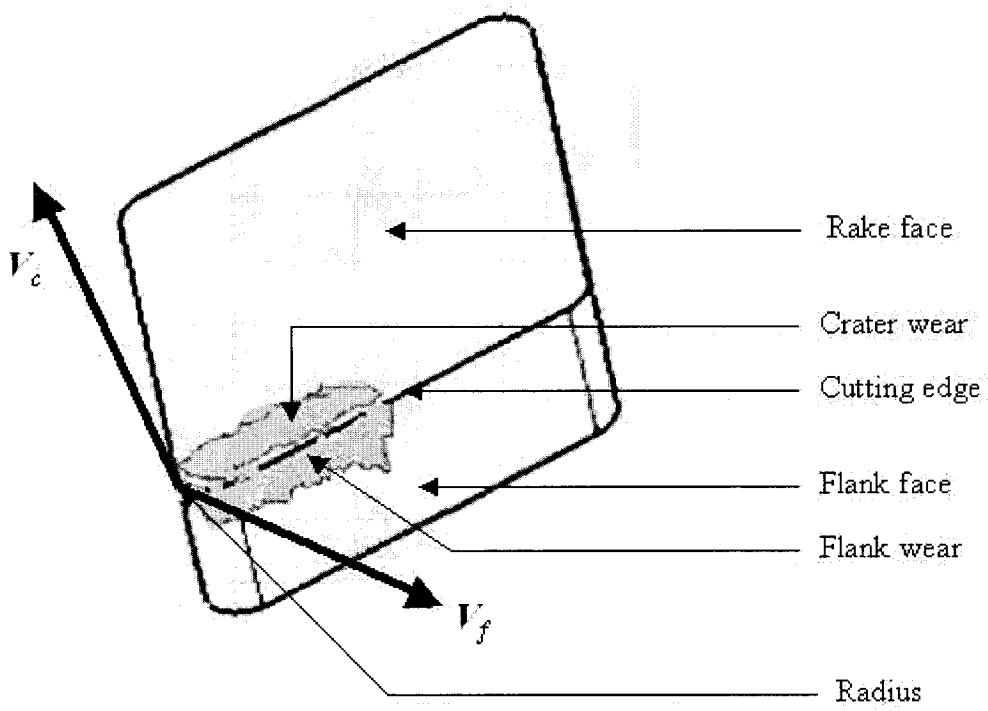

Figure 2.4. Cutting tool insert basic faces

Generally the tool wear pattern can be seen on the flank face, called flank wear and on the rake face called crater wear. Figure 2.4 shows what these types of wear can look like. The tool wear criteria are standardized by ISO 3685:1993F. Figure 2.5 shows the different flank wear and crater wear criteria established by ISO.

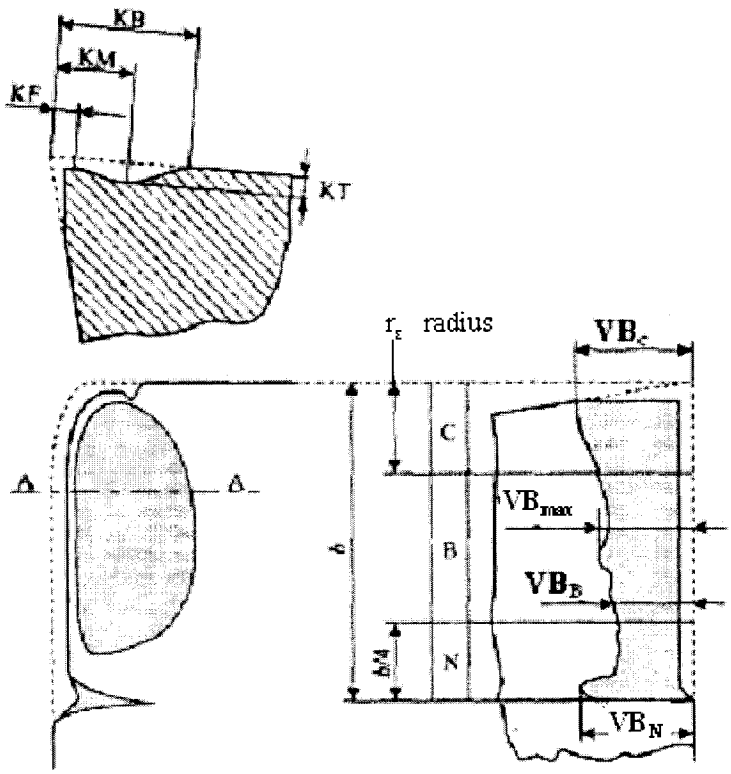

Figure 2.5. Cutting tool faces, Source (ISO 3685 :1993F)

Figure 2.5 establishes the tool wear criteria as:

- The notch wear VB_N, also called V_N in this document
- The average flank wear VB_B, also called VB in this document
- The nose wear VB_C
- The maximum flank wear VB_{max}
- The crater depth KT
- The crater position KF
- The crater width KB
- The crater center position KM

The tool wear limit on the flank face is determine by VB=0.3 mm, VB_c=0.3 mm and VB_N=0.6 mm. The nose wear VB_c is measured on the zone C of length r_ε (insert radius).

The notch wear is measured on the zone N of length b/4, wear b is the active length of the insert. The wear VB is measured on the remaining zone B.

2.3. The chip thickness

The chip thickness plays an important role in machining. It helps to estimate the cutting forces. Higher chip thicknesses give higher cutting forces. The real chip thickness when the chip is cut is different from the theoretical one call undeformed chip thickness C_{tc}. The undeformed chip thickness is linked to the feed f and the tool lead angle κ_r as shown on Figure 2.6.

$C_{tc}=f\sin(\kappa_r)$ Equation (3)

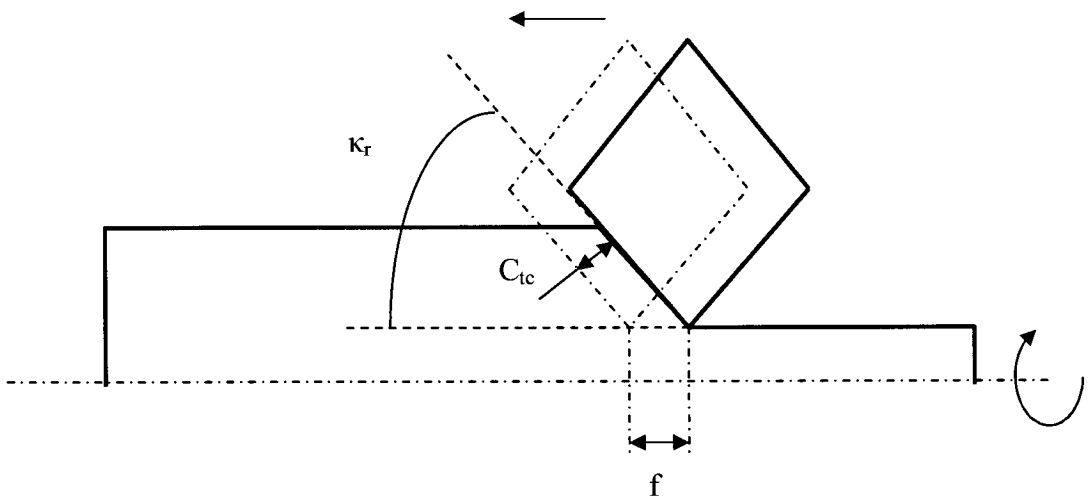

Figure 2.6. The undeformed chip thickness C_{tc}

After an overview of the basic notions in turning which are going to be used in this document, the next chapter deals with the literature review about Inconel 718 machining.

CHAPTER 3. LITERATURE REVIEW

3.1. Inconel 718

Inconel 718 is a nickel based super alloy. It is used in the situations where a high temperature is required, generally in the hot sections of engines.

3.1.1. Chemical Composition

In the Inconel 718, the nickel (Ni) has 53% of the total mass, chromium (Cr) has about 18% and iron (Fe) has approximately 17%. Table 1 shows a basic elements mass composition. Many other addictive elements are in the material (Nb, Al, Mo...) which may influence its properties.

Table 1: Company Inconel 718 chemical composition

%Ni	%Cr	%Fe	%Nb	%Mo	%Ti	%Al	%Mn	%Si	%C	%S
53.92	18.31	17.29	5.31	3.04	0.00	0.65	0.07	0.09	0.04	0.001

3.1.2. The microstructure

The microstructure of Inconel is composed of matrix, precipitates and possible inclusions in certain cases. It undergoes some heat treatment which affects the microstructure.

3.1.2.1 Matrix and precipitates

Inconel 718 is a super alloy whose microstructure is largely influenced by the ternary diagram Ni-Cr-Fe (nickel-chromium-iron), with additions of Nb, Mo, Ti and Al elements. According to G. Pottlacher et al. [17] the cold structure of the Inconel 718 is a

γ (austenite) face-centered cubic. Inconel 718 is a precipitated hardened material. That means its strength comes from the effect of the precipitate in the matrix. The main precipitate are γ' (Ni_3(Al, Ti)) and/or γ'' (Ni_3Nb) phases from which Inconel 718 draws its mechanical performances. These phases are observed in Figure 3.1.

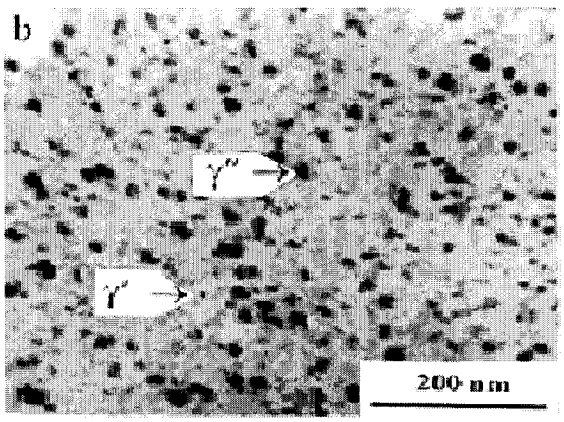

Figure 3.1. Transmission electron microscope image of Inconel 718. Source [35]

3.1.2.2 Inclusions

Inclusions are particles obtained during the solidification process of a material. In the matrix of Inconel 718 the common inclusions are MC type carbide, where 'M' is Nb or Ti and the inclusions can then be NbC and TiC. These inclusions play an abrasive role on tools during machining because of their high hardness (H.G. Prengel et al. [20]).

Primary niobium carbide (NbC) phase is more stable and is also responsible for hot cracking in Inconel 718 because of its presence at the grain boundaries (M.B. Henderson et al. [26]).

The secondary NbC type are formed during the ageing process of Inconel 718, and can give $M_{23}C_6$ (refractory carbide) beyond 973 K according to Ming Gao et al. [27].

3.1.2.3 Heat treatments

According to Allvac [35], the Inconel 718 generally undergoes two types of heat treatments. The solution heat treatment, which consist in maintaining the material at a suitable temperature (1010 to 1037 °C) for a sufficient time (1 hour for example), to ensure the setting of the various elements, generally followed by a fast water quench to preserve this solid solution and to obtain the desired microstructure.

They also undergo an ageing treatment, which consist in maintaining the material at a temperature within 774 to 802° C during a few hours, followed by an air cooling. This treatment aims to homogenize the distribution of the γ' and γ" precipitates between the grains.

G.Pottlacher et al. [17] also note that the thermo physical properties of Inconel 718 largely depend on the type of heat treatment of which it is subjected to. The γ' and γ" phases appears during the aging process, and their microstructure depend on this aging time.

3.1.3. The physical and mechanical properties

Table 2 shows that Inconel 718 is heavier than carbon steel (Pw 245 or AMS 6304) which is used in the company. The elasticity modulus of Inconel 718 is slightly higher, but the ultimate strength is higher, so more strength is needed to cut an Inconel 718 material than a steel material. The thermal conductivity is lower for Inconel 718, that is why the heat is not easily evacuated when machining, compared to steel. Inconel 718 is

Table 2: Physical and mechanical properties

	True Ultimate Stress (Gpa)	Thermal Conductivity (W/mK)	Thermal Expansion Coefficient 10^{-6}/K	Modulus of Elasticity (Gpa)	Density kg/m3
Pw245 (Steel)	1,02	42,8	14,7	204	7832
Inconel 718	1,73	15	11	206	8470

less sensitive to high temperatures because the thermal expansion coefficient is low. All these physical properties make the machining of Inconel 718 more difficult compared to carbon steel Pw 245.

3.2. The machining of Inconel 718

3.2.1. The machining methods

There are several machining methods used to machine Inconel 718. We can mention the constant depth of cut machining, the ramping technique, the laser enhanced machining, the plasma enhanced machining, the cryogenic machining and the hybrid machining.

3.2.1.1 Ramping technique

To deal with the notch wear problem during the machining of Inconel 718, the most widespread tendency is to proceed by ramping. It consists in varying the depth of cutting so that the energy that creates the notch wear is distributed all over the tool edge. The tool life is thus increased. Many aspects of this technique have been developed by Greenleaf [18], to reduce the notch wear when machining nickel alloys such as Inconel 718. Figure 3.2 shows the basic ramping technique used by Greenleaf [18].

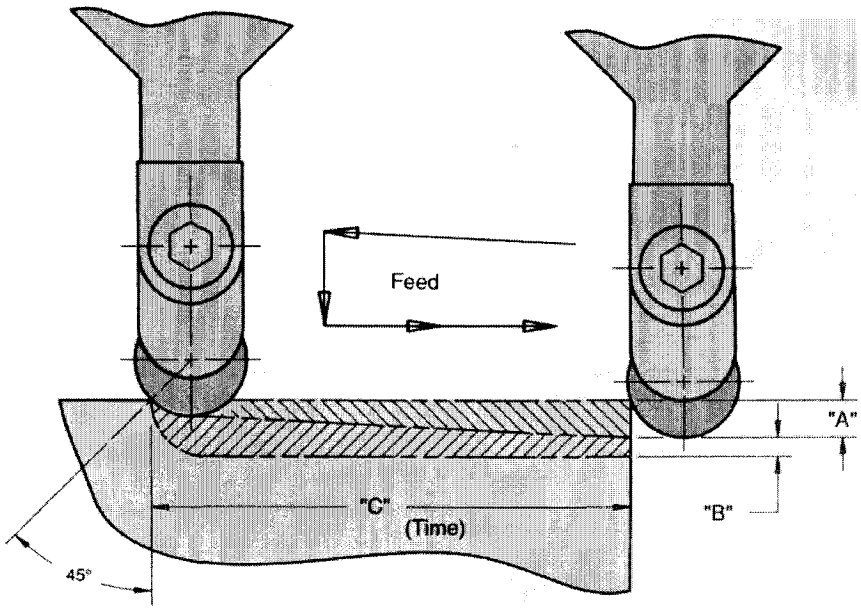

Figure 3.2. Ramping technique with a round whisker ceramic insert WG-300. (Source Greenleaf [18])

The calculations of the cutting conditions are made according to variables A, B and C, Table 3.

Table 3: Ramping conditions as a function of the insert diameter

Diameter		"A"		"B"		"C"
Inches	mm	Inches	mm	Inches	mm	Minutes
.250	6,3	.080	2,0	.040	1,0	3
.375	9,5	.120	3,0	.060	1,5	4
.500	12,7	.160	4,0	.080	2,0	5

(Source Greenleaf [18])

The technique is as followed:

- The cutting feed and speed are set up according to the insert diameter, in the conditions of constant depth of cut machining proposed in the manufacturer's catalog. These conditions are supposed to be the 100% condition at the mid-point of the ramp.

- The ramping starts at the depth of cut value A. The cutting feed and speed percentage for the start point are determined by a chart, for the depth of cut value A. Their values are then deduced from the mid-point values which are supposed to be 100%.
- Both feed and speed are supposed to vary during the machining until the time C and the final depth of cut value B are reached.

Multiple ramping waves techniques are also proposed by Greenleaf [18], Figure 3.3. But no detailed information is presented to explain the methods to perform these techniques and their advantages.

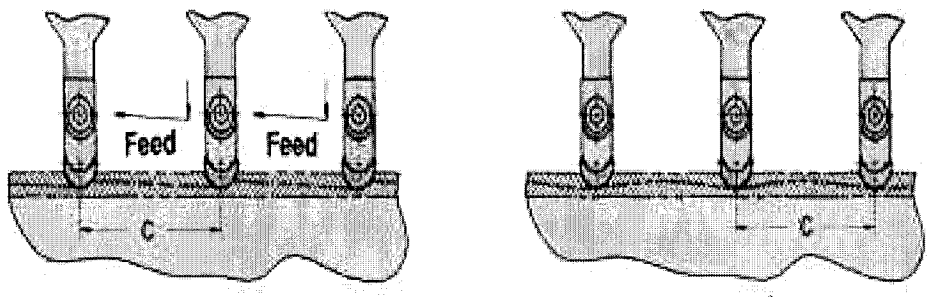

Figure 3.3. Plunging in and multiple ramp (waves) techniques. (Source [18])

3.2.1.2 Laser enhanced machining (LEM)

The laser enhanced machining method was used by some authors to soften the surface layer of material in order to reduce its tensile strength (Z.Y. Wang et al. [36]). These authors note that the tool wear was reduced by 40%, the cutting forces by 18% and the metal removed rate increased by 33%. However the high cost of high power lasers (15 kilowatts of $C0_2$), and the high consumption of energy makes that process difficult to use in production. Figure 3.4 shows a global ideal of the LEM process.

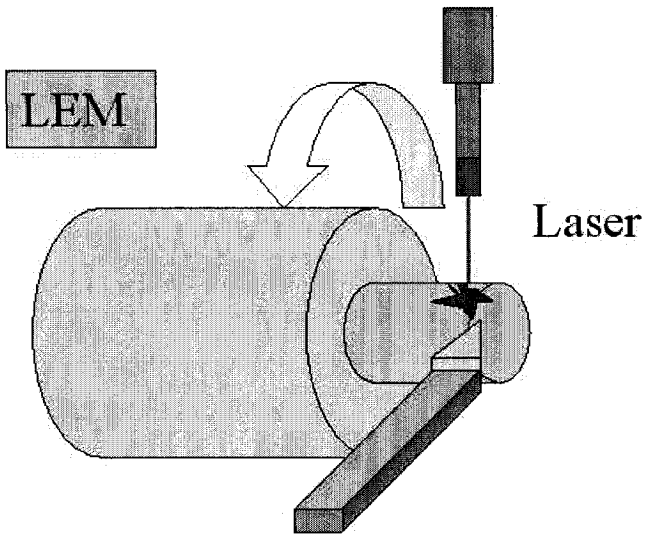

Figure 3.4. Laser enhanced machining

3.2.1.3 Plasma enhanced machining (PEM)

The plasma enhanced machining has the same objectives as the laser machining, but instead of a laser, a plasma torch is used to soften the material. The cost is lower than high power laser. However this method involves another problem in particular the inadmissible heating of the tools [34, 36]. To cool the cutting tool, another method is used, that is the cryogenic enhanced machining. Figure 3.5 shows a global ideal of the LEM process

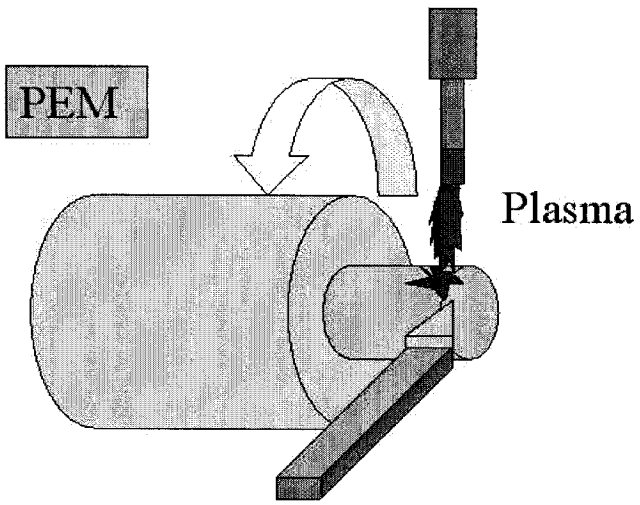

Figure 3.5. Plasma machining

3.2.1.4 Cryogenic enhanced machining (CEM)

The goal of cryogenic machining is to cool the tool through a system of cooling by liquid nitrogen as schematized in Figure 8. This process makes it possible to increase the tool life (Z.Y. Wang et al. [34]). This technique requires a special tool holder and a cooling system. Nevertheless, to be profitable, all these additional cost must be justified by a significant increase in tool life. Figure 3.6 shows the toolholder system used for cryogenic machining, and Figure 3.7 shows a simplified drawing of the CEM technique.

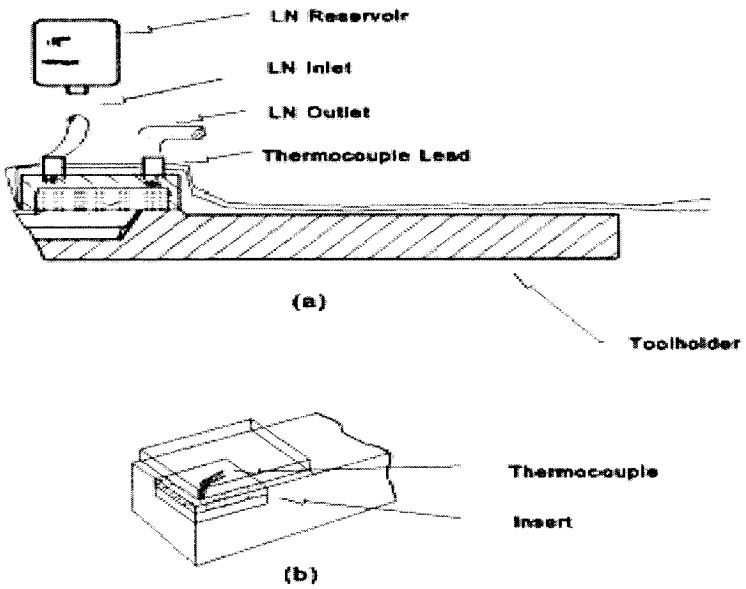

Figure 3.6. Cryogenic machining (Source [34])

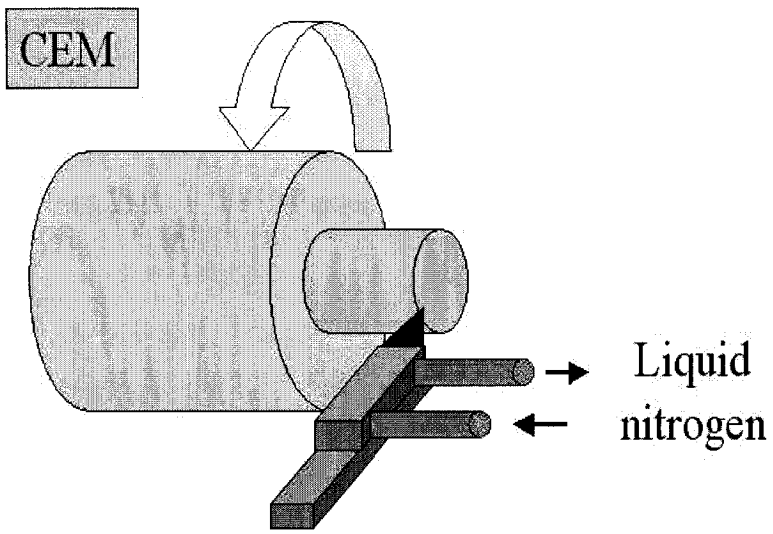

Figure 3.7. Cryogenic machining

3.2.1.5 Hybrid machining

Hybrid machining is the combination of cryogenic and plasma machining. The objective is to use the benefit of both methods, that is the softening of the work piece material and at the same time the cooling of the tool. This method, according to Z.Y. Wang [36], can reduce the flank wear. As mentioned previously, the obstacle of these methods is that additional cost will have to be economically justified in a cost effective machining process. Figure 3.8 shows a simplified drawing of this technique.

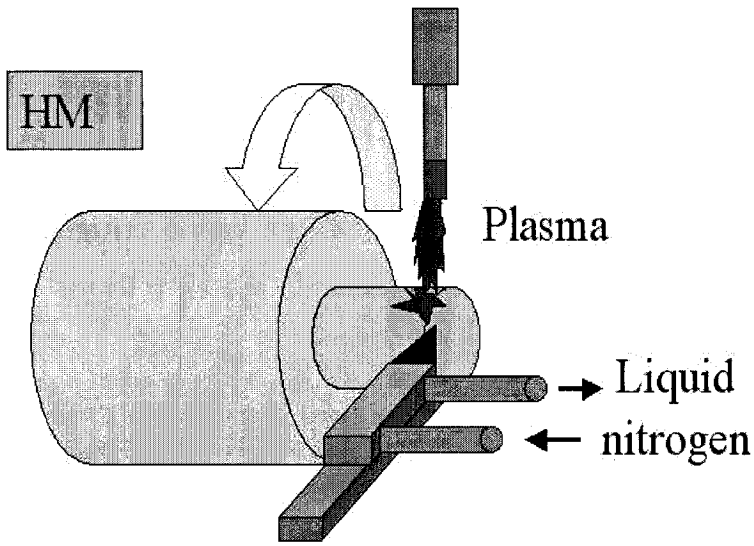

Figure 3.8. Hybrid machining

3.2.2. Effect of cutting conditions

3.2.2.1 Environment

a) Atmosphere

According to E. O. Ezugwu [9], Nitrogen and Argon rich machining environment can accelerate the appearance of notch wear, whereas oxygen tends to reduce it. The author explains that by the fact that oxygen will form oxides at the surface of tools having a

strong tendency for oxidation at high temperature. This effect will reduce the local forces because of the reduction of friction coefficient and consequently the tool wear.

b) The coolant

The machining of Inconel 718 is characterized by very high temperatures in the cutting zone consecutive to the low conductivity of the material. The use of coolant consequently is recommended. According to El-Wardany et al. [10], the temperature at the tool tip can reach about 1000 °C, which is beyond the softening temperature of the majority of carbides [7]. This temperature is for example the softening temperature of the β' phase of sialon tools (mixed ceramics of Si_3N_4). In the literature, the lubricants used are often water based.

According to Ezugwu et al. [9], the use of high pressure coolant nevertheless gives bad results. That can be explained by the fact that high pressure coolant makes it possible to reduce the tool chip contact length. Since the cutting forces remain unchanged, the pressure will be higher on small portion of the edge, which will be worn more quickly.

3.2.2.2 The chip

a) Chip types

Choudhury et al. [6] and R.Komanduri et al. [31] affirm that the continuous chips are formed when the workpiece material has a face centered cubic (CFC) or centered cubic (CC) crystalline structure, and has a low hardness and a good thermal conductivity. The fragmented chips are obtained in the case when work piece material has a high hardness, low thermal conductivity and has a hexagonal close packed (Hcp) crystalline structure.

As mentioned in the section 3.1.2.1, Inconel 718 matrix has a CFC crystalline structure, with a high hardness and low thermal conductivity. A continuous chip is therefore more likely to appear. But the low thermal conductivity can lead to discontinuous chips, because of the high stress generated by the high temperatures during the cutting process, at certain cutting conditions.

El-Wardany et al. [10] show the effect of cutting parameters on the tool tip temperature when machining Inconel 718. Figure 3.9 shows these effects.

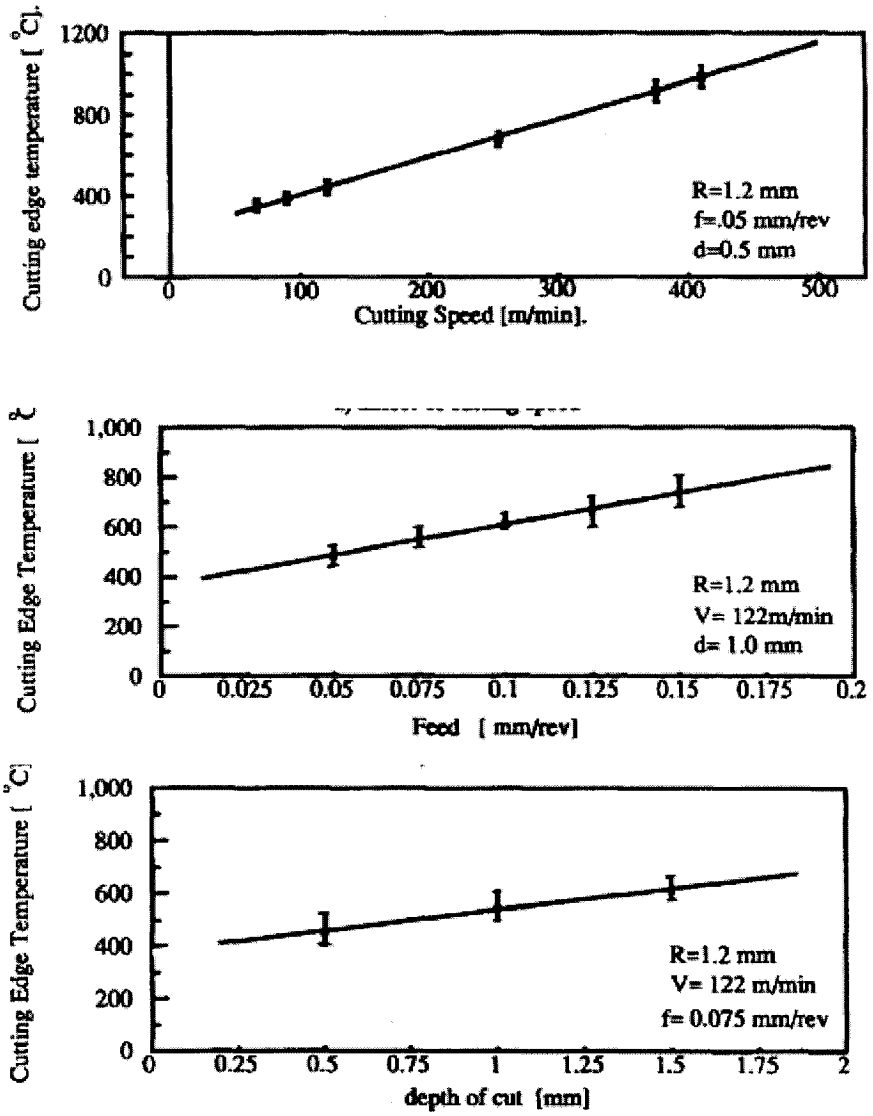

Figure 3.9. Tool temperature according to cutting parameters (speed, feed and depth of cut) (Source [10])

b) Factors affecting the chip shape

In addition of the work piece material properties, the chip shape is influenced by the tool geometry. For example chip width is influenced by the lead angle, while the chip upsetting depends on the rake angle.

The friction at the tool chip interface also influences the chip shape, Guoqin et al.[19]. If the friction coefficient is high, the chip undergoes an upsetting.

During the machining of Inconel 718, authors Kitagawa et al. [22] noted the apparition of burr on the machined part. He noted that the burr height was correlated with the notch wear and the surface roughness, Figure 3.10 and 3.11.

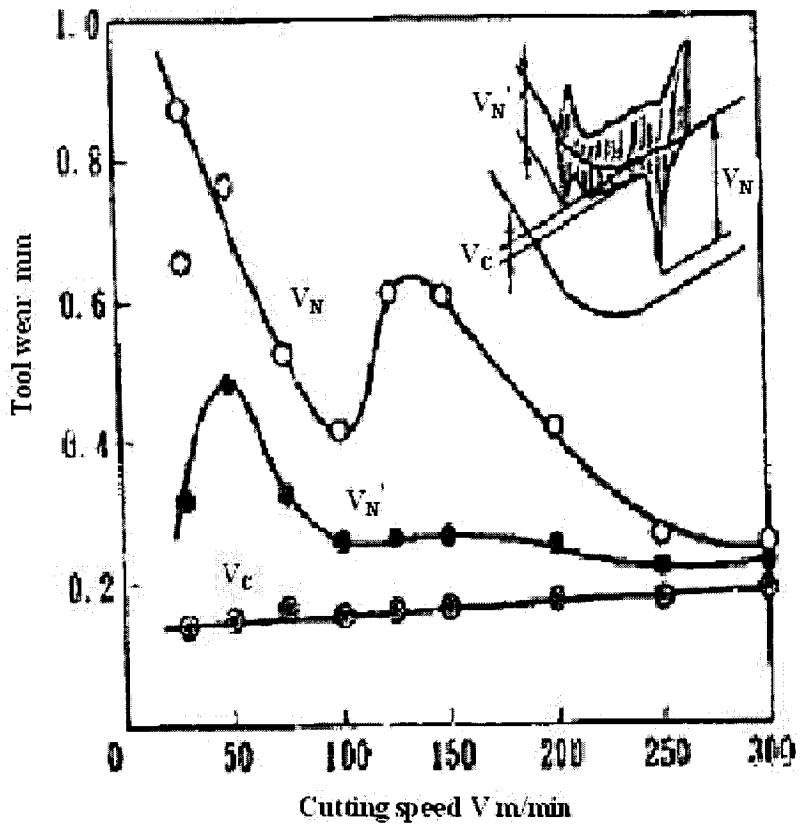

Figure 3.10. Tool notch wear V_N, secondary notch V_N' and corner wear V_C as a function of the cutting speed. (Source [22])

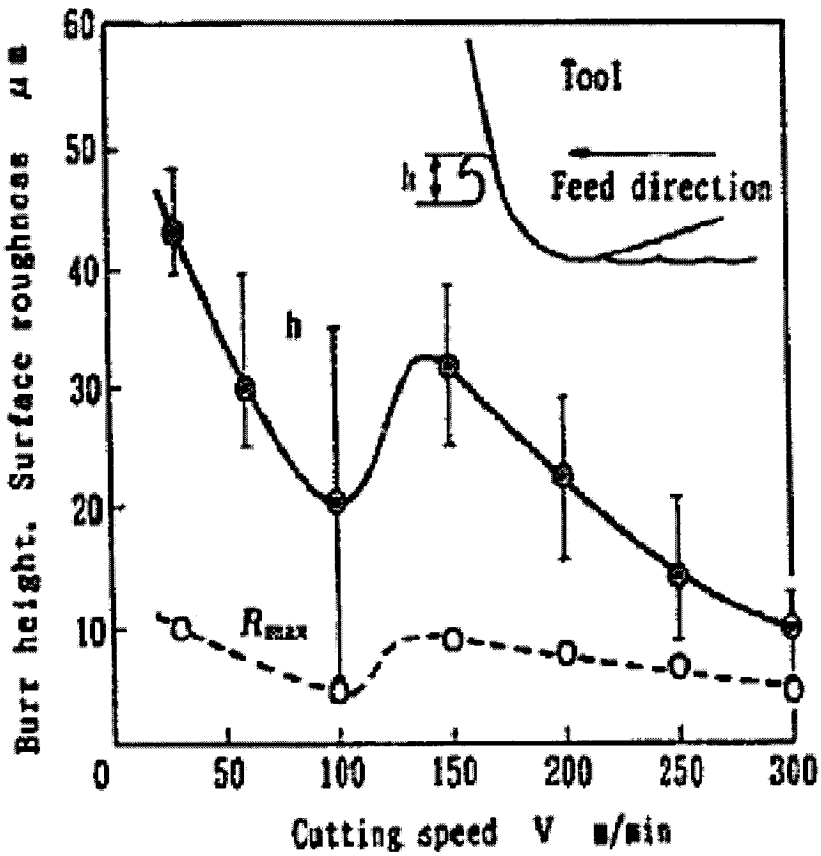

Figure 3.11. Burr height (h) and surface roughness R_{max} as a function of cutting speed (Source [22])

Figure 3.12 shows a result of a test carried out at Pratt & Whitney Canada, (a) is lateral burr formation on the machined part and (b) is a saw type chip.

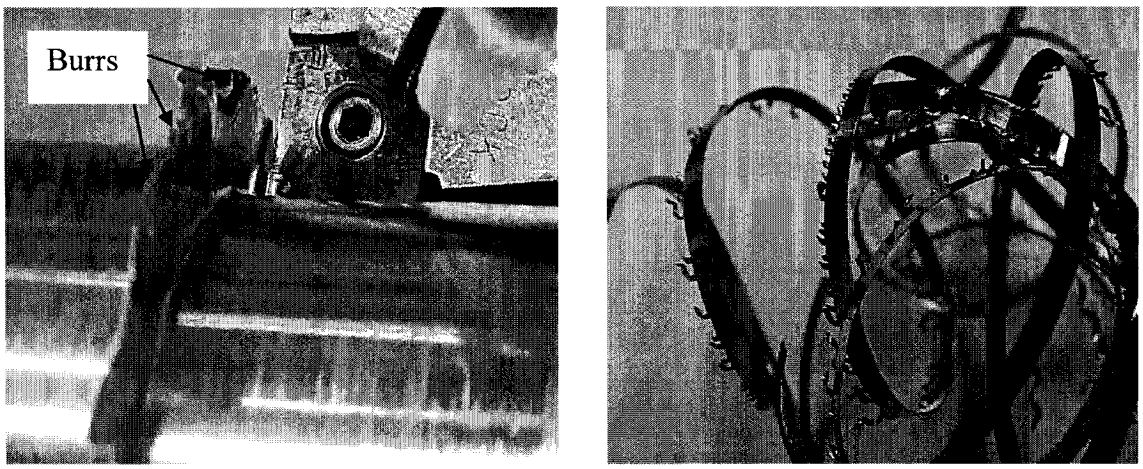

(a) *burr formation on the part* (b) *Saw type chip*

Figure 3.12. Burr formation on the machined part

The correlation obtained by Kitagawa et al. [22] is the index which enables us to deduce that the phenomenon of pronounced notch wear during the machining of Inconel 718 is in certain cases closely related to burrs formation.

3.2.3. The cutting tool

Appendix I gives a detailed literature review of the cutting tool and the tool geometries used by different authors to machine Inconel 718. Three types of cutting tool material can be mentioned to machine Inconel 718. The carbide tools, the mixed ceramics and the whisker reinforced ceramics. The summary of this review is given in the following section.

3.3. Summary of the cutting tool data

This summary is made according to the literature review information gathered in appendix I, page 140 to page 171. The machining parameters and results of each article of the literature review have been used to compare different cutting tool performances. The comparison is made upon the total machining time required by a tool to remove an amount of 300 in^3 of material. 300 in^3 is approximately the volume of material to remove for the roughing process of the studied shaft. Table 4 gives the results of the calculations.

Table 4: Best tool material (from number 1 to number 5)

	Number 1	Number 2	Number 3	Number 4	Number 5
	Ceramic				Carbide
	SiC whisker reinforced			Mixed	coated
	Al_2O_3 CrN coated	nano Al_2O_3	Al_2O_3	Al_2O_3	TiCN/TiN/TiCN
Estimated total machining time (min)	158	162	208	210	265
Volume of material removed per insert (in^3)		17	16	10	61
Tool life (min)			10	13	48
Material removal rate (in^3/min)				5,6	1,2
Effective cutting time (min)					240

According to Table 4, the best tool material is the CrN coated alumina oxide SiC whisker reinforced ceramic (Al_2O_3 SiC-Whisker).

The tool classification table Appendix I page 166 shows an alternative to the Al_2O_3 SiC-Whisker, which is the Si_3N_4 SiC-Whisker reinforced ceramic tool. A good coating is a multiple coating PVD TiN/TiCN/TiN. But the single TiAlN is a good alternative. The ideal would be a combination of TiAlN, TiN and TiCN.

3.3.1.1 The tool geometry

According to the literature the better tool geometry is a 45 degree lead angle, with a positive rake angle.

3.4. Conclusion of the literature review

The best tool material and geometry, and the best machining conditions have been proposed. Greenleaf company is the only whisker reinforced ceramic tool manufacturer in Canada, that is why for the whisker ceramics this company tools are chosen. Different machining techniques are portrayed, but the laser, plasma, cryogenic and Hybrid machining techniques are not going to be studied because of extra equipment cost generated. Only machining strategies based on the cutting parameters variations will be considered.

The next chapter is devoted to the theories of the different machining strategies developed in this study.

CHAPTER 4. THEORIES OF MACHINING STRATEGIES

In this chapter, the theories which underlie the proposed machining strategies are explained. Based on the literature review, three different machining strategies are studied. The constant depth of cut machining, the ramping method and the feed variation method.

4.1. The constant depth of cut machining

The constant depth of cut machining is the classical method in turning. It consists in machining with a constant depth of cut, constant feed and constant cutting speed or RPM as explained in chapter 2.

4.2. The ramping method

4.2.1. Overview

The goal of the ramping is to vary the depth of cut so that the notch wear is distributed all over the length of the edge. To study this method it is necessary to define the physical variables of the process.

4.2.2. The description of the ramping methods

Figure 4.1 shows a simplified ramping process based on the Greenleaf model in Figure 3.2, page 17.

D_{ext}: The external diameter (in)

D: The average diameter (in)

Δt: The time of single ramping pass (s)

Δap : The depth of cut variation (in/s)

E: The slope (°)

vol: volume of material removed during both ramping passes (in^3)

ρ : The ratio, ρ =B/A

P1: The material removed during the first pass

P2: The material removed during the second pass

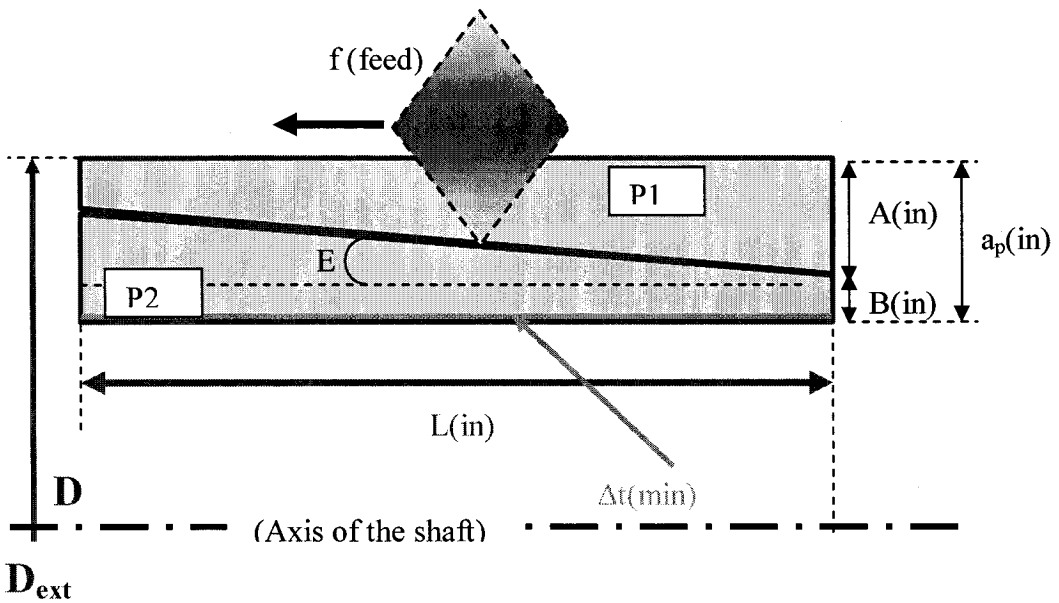

Figure 4.1. Simplified ramping process

Two methods are used to study the ramping technique. These methods are based on the fact that the ramping slope E or the depth of cut variation in time $\frac{\Delta a_p}{\Delta t}$ (calculated while keeping the ratio B/A as constant) (Figure 4.1), can be taken as the main ramping variable separately. The use of the slope E as the main variable can lead to a variation of the ramping wear length by varying the ratio B/A, while the use of the ratio B/A as the main variable leads to the variation of the slope during ramping while keeping the ramping wear length constant. More detail can be seen on page 34-36.

4.2.2.1 Comparison of ramping slope and depth of cut variation in time

To reduce the notch wear, it is important to vary the position of the point where this notch wear appears, that is on the depth of cut line. The rate of change in position of the contact point P (Figure 4.2) between the tool edge and the depth of cut line can be expressed by a speed V_p.

The expression of this speed V_p according to Figure 4.3 is:

$$V_p = V_f \frac{\sin(E)}{\sin(\chi_r - E)}$$ Equation (4)

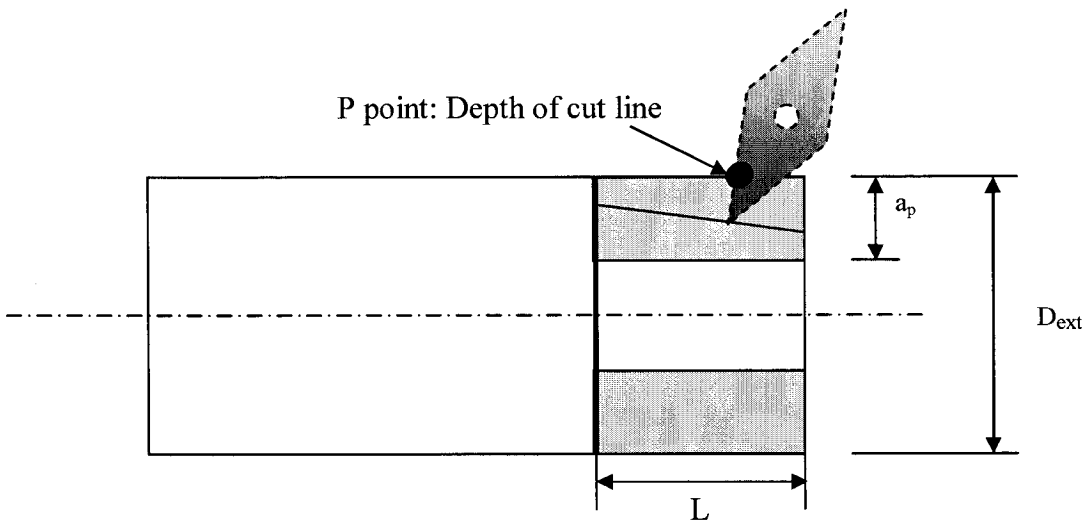

Figure 4.2. Localization of depth of cut line

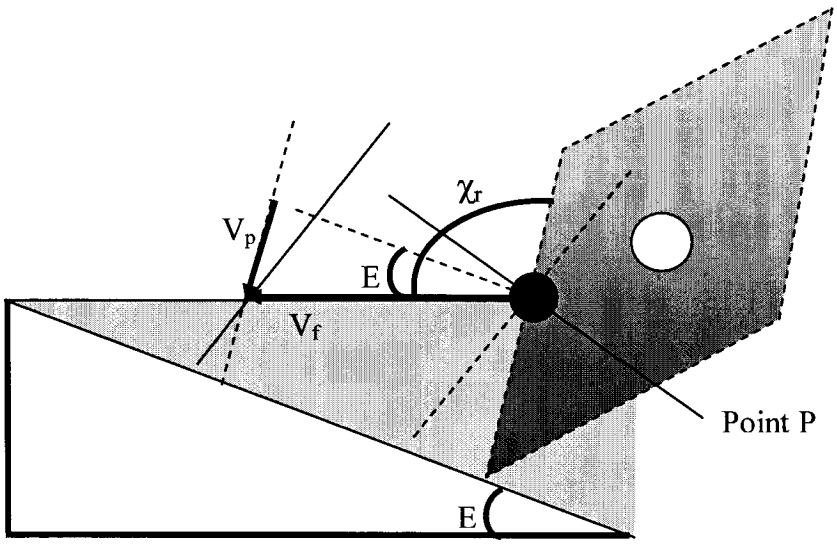

Figure 4.3. Depth of cut point speed

The main variable for a ramping process is then the slope, because the variation of slope produces the variation of the speed V_p. However the choice of the value of E requires some analysis.

Let's define the material removed model as in Figure 4.1.

The slope can be expressed as:

$$E=\frac{\Delta a_p}{\Delta L} \qquad \text{Equation (5)}$$

The length of cut L is:

L = fnt,

that is $\Delta L=fn\Delta t$.

For a constant feed and a constant RPM, the slope becomes:

$$E=\frac{1}{fn}\left(\frac{\Delta ap}{\Delta t}\right) \qquad \text{Equation (6)}$$

To keep a linear relation between the slope and the depth of cut variation in time (DOCVT), the spindle speed n and the feed f should be constant. But the surface speed V_c will vary during machining because of the diameter variation.

$$n=\frac{V_c}{\pi D}$$ Equation (7)

Moreover the variation of depth of cut Δa_p in the slope Equation (6) must be kept constant; if not the ramping wear length can be anarchic. Here are 2 examples to explain this phenomenon.

The same operation (with the same variables) carried out with different diameters should give the same results. The variation of the depth of cut can be done while keeping a constant slope or by keeping a constant ratio $\rho=B/A$ for all diameters of the workpiece.

Case 1: Ratio $\rho=B/A$ = constant for all diameters. The slope E is not constant ($E_1 \neq E_2$)

For this case, ramping wear length obtained on the edge of the tool is identical from one diameter to another, because the ratio $\rho=B/A$ remains constant, Figure 4.4. On the other hand the progression speeds V_p of the tool point on the two slopes are different, because the slopes are different.

This progression speed can have an effect on the results.

For the smaller diameters, the progression speed on the ramping slope will be smaller than for the higher diameters. That is due to the fact that the length of cut for the smaller diameter is higher since $D_2<D_1$, Figure 4.4.

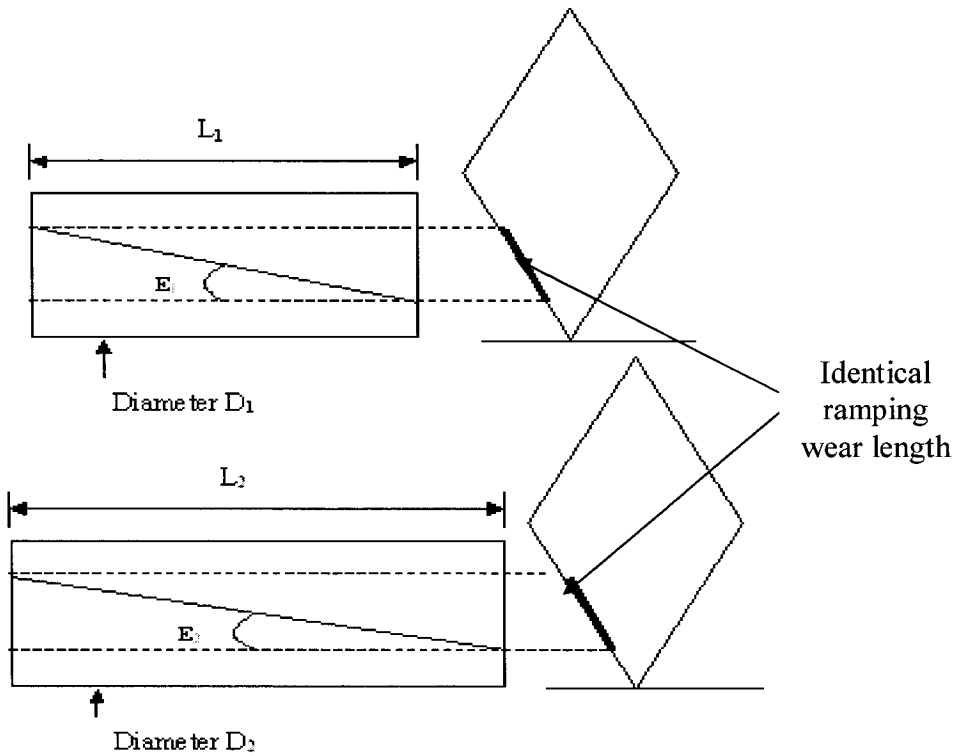

Figure 4.4. Variable slope and constant depth of cut variation

Case 2: The slopes $E_1 = E_2$. The Ratio ρ=B/A is not constant for all diameters

For this case Figure 4.5, the wear length is different, even if the progression speed on the slope is identical from one diameter to the other because of the constant slope. The disadvantage is that the superposition of wears will be done in an anarchistic way; the results of measurements will not be easily comparable. For example the average wear VB which is measured on the machined total edge will not be identical to the accumulation of the tests on the same edge. The repeatability will not be respected.

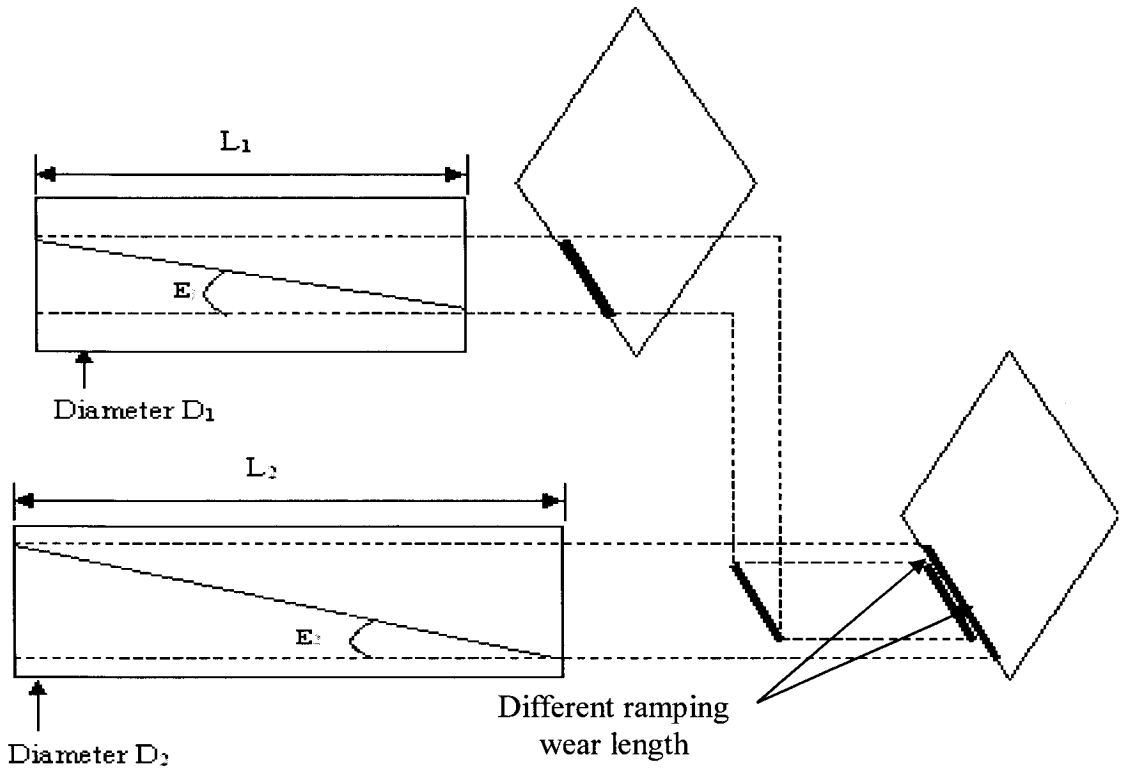

Figure 4.5. Constant slope and variable depth of cut variation

According to Equation (6), if the ratio $\frac{\Delta ap}{\Delta t}$ is constant, the variation of the slope can be expressed by:

$$\frac{\Delta E}{E} = \frac{\Delta D}{D} \qquad \text{Equation (8)}$$

To be sure that during the tests the difference of diameter will not influence the results of the slope, the change in diameter will be kept as small as possible for the same cutting conditions.

Moreover, in a real case the slope is less than 3°. The variation of slope ΔE for 2 different diameters can be neglected.

The ratio $\frac{\Delta ap}{\Delta t}$ will be taken as a ramping variable to be controlled. It is another way of controlling the slope. The results of the tests with this variable will be used to deduce the effects of the change in slope for different diameters, because of Equation (6).

Hence two variables have been identified for the ramping process. The slope E and the depth of cut variation in time (DOCVT).

The effect of depth of cut variation in time on the tool wear will have to be measured. That is the relation between the tool wear and the variable $\frac{\Delta ap}{\Delta t}$.To do so, a length L of the part is going to be divided into 2 and 3 parts.

Let Δt be the time to remove the half volume of the part (P1), Figure 4.1. The variation of the depth of cut Δa_p is indicated Figure 4.6.

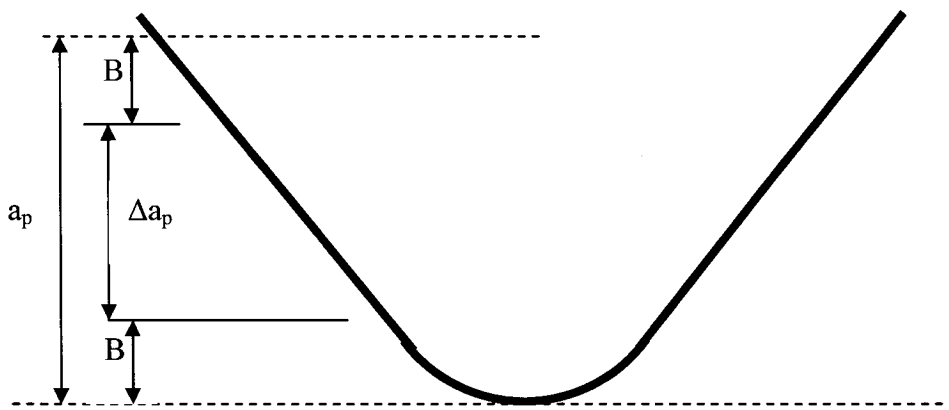

Figure 4.6. Depth of cut variation Δa_p

$$a_p = B\left(1+\frac{1}{\rho}\right) \qquad \text{Equation (9)}$$

$$\Delta a_p = a_p \frac{1-\rho}{1+\rho}$$

$$\text{So } \frac{\Delta a_p}{\Delta t} = \frac{1-\rho}{1+\rho} \times \frac{a_p}{\Delta t} \qquad \text{Equation (10)}$$

The interval of time Δt to remove the half volume of length L (Figure 4.1) is,

$$\Delta t=\frac{L}{fN}=\frac{\pi DL}{fV_c} \qquad \text{Equation (11)}$$

The variable $\frac{\Delta a_p}{\Delta t}$ should be kept constant for the same tests. So keeping Δt, ρ and a_p, constant solves this problem.

- For strategy I Figure 4.7, for an indicative time Δt, and a diameter D, the length to machine is:

$$L=\frac{fV_c\Delta t}{\pi D} \qquad \text{Equation (12)}$$

$$\left.\frac{\Delta a_p}{\Delta t}\right|_{(I)}=\frac{1-\rho}{1+\rho}\times\frac{a_p}{\Delta t} \qquad \text{Equation (13)}$$

- For strategy II Figure 4.7 , the time is $\frac{\Delta t}{2}$

$$\left.\frac{\Delta a_p}{\Delta t}\right|_{(II)}=2\frac{1-\rho}{1+\rho}\times\frac{a_p}{\Delta t}=2\left.\frac{\Delta a_p}{\Delta t}\right|_{(I)} \qquad \text{Equation (14)}$$

- For strategy III Figure 4.7, the time is $\frac{\Delta t}{3}$

- $\left.\frac{\Delta a_p}{\Delta t}\right|_{(III)}=3\frac{1-\rho}{1+\rho}\times\frac{a_p}{\Delta t}=3\left.\frac{\Delta a_p}{\Delta t}\right|_{(I)}$ Equation(15)

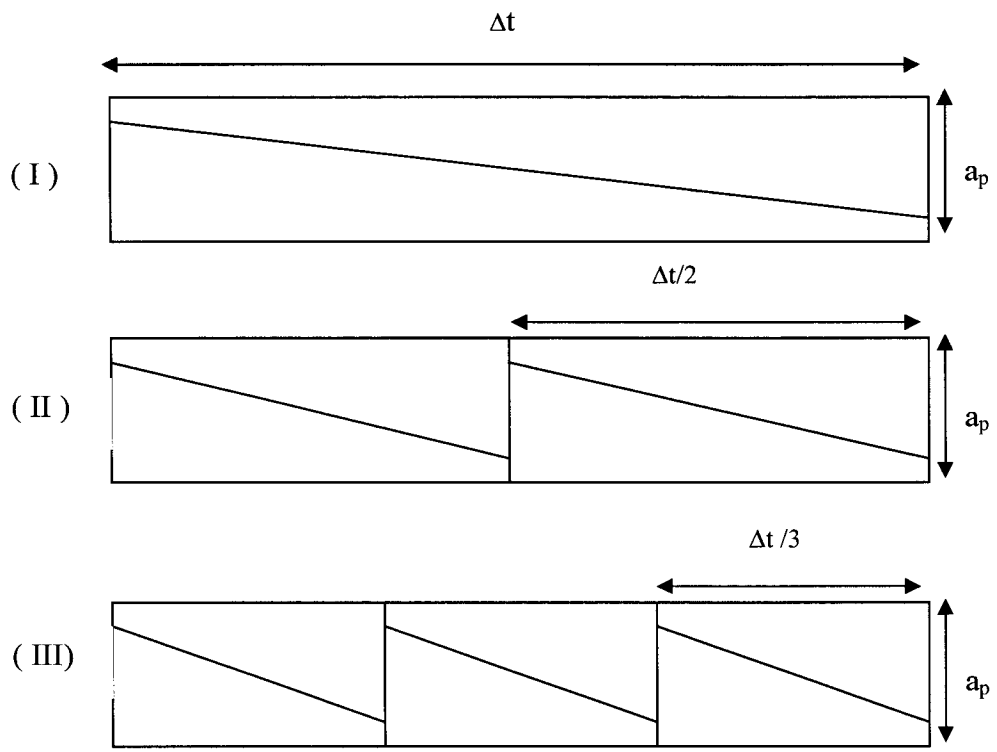

Figure 4.7. Ramping strategies

The rough estimation of the trajectory time to remove the material for the strategies I, II and III is given in Appendix VI. This estimation allowed the choice of six configurations equivalent to strategies I, II and III, Figure 4.8. Configuration (A) is composed of strategies of ramping starting with a negative ramp and configuration (B) is composed of strategies of ramping starting with a positive ramp. These configurations are going to be considered for the test plan.

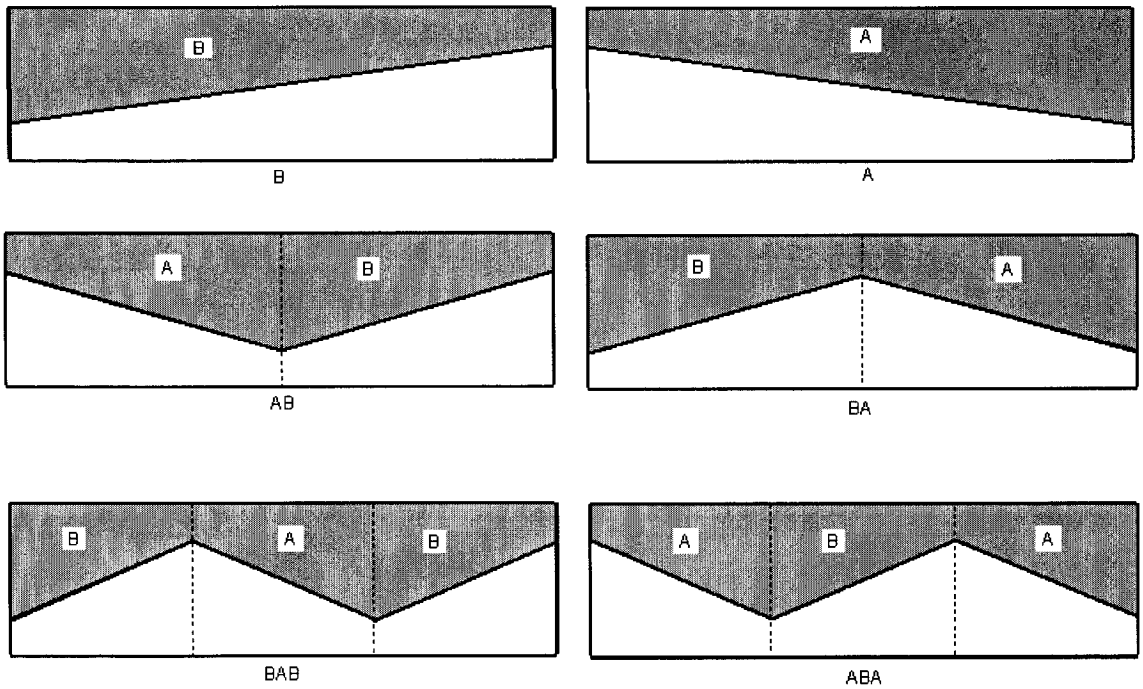

Configuration (A) Configuration (B)

Figure 4.8. The six ramping configurations to test

It is now possible to build a plan to assess the tool wear behavior as a function of different depth of cut variation in time.

4.2.2.2 The number of ramps effect

The number of ramps (or waves) effect will be estimated by a model. This model is based on the assumption that the tool average wear is related to the total energy absorbed by the tool during the machining.

For example, it is known that tool abrasive wear comes from the friction between the tool and the work piece. This friction forces remove the material from the tool at a certain speed, during a certain time. It is possible to calculate the total energy absorbed by the tool.

The objective of this part is not to demonstrate this assumption, but to establish the more likely criteria to estimate the tool wear, in order to compare different ramping strategies.

- The components of the energy generated by the components F_r and F_f (radial and feed) of the cutting force will be assumed to be negligible compared to the one generated by the tangential cutting force component F_t.
- The cutting force F_t will be assumed to be $F_t=K_c.S_c$, where K_c is a constant and S_c the undeformed chip section.

The explanation of the hypothesis is as followed:
If 2 cutting tools of the same characteristics have to follow the trajectory in the same material, the one which will generate the highest force will be more badly worn than the one which will generate the lowest force, if the speed is identical. The same conclusion can be said about the speed. The fastest will be more badly worn than the slowest.
Also the longest the machining time is, the more the tool will be worn.
The total energy absorption is an assumption that can be seen as a first approximation of the insight of the tool wear. Even if the force and speed have an effect on tool wear, the marginal effects of each variable can be different. That is, the force may affect the tool wear more than the speed and vice versa. In the total energy absorption assumption, it is supposed that both force and speed affect the tool wear the same way. That may not be true. But in the case of this study, the average cutting speed will always remain the same; only the cutting force will have a significant effect on this energy absorption.

Total energy absorption is $\int_{(AB)} F_t.V.\,dt$

The instantaneous power at a point (i) is: $Pc_i=F_{t_i}V_i$ Equation (16)

Where the speed V is the combination of the cutting speed V_c, the feed rate V_f and the penetration speed V_{pe} (see Equation (2) page 8).

Therefore the total energy absorption is:

$$E_t=\sum_{i=1}^{M}P_{c_i}dt_i=\sum_{i=1}^{M}F_{t_i}V_i dt_i=K_c\sum_{i=1}^{M}S_{c_i}V_i dt_i \qquad \text{Equation (17)}$$

where K_c is a constant that will be determined by a cutting force test, and M the number of subdivisions of the cutting length.

The objective of this chapter is to estimate the energy absorption during a ramping strategy (1, 2, 3 ...waves). If this energy increases, it will be deduced that the tool wear will also increase.

Before establishing the model, the cutting force should be measured experimentally to determine the constant K_c linking the tangential force to the chip section.

4.2.2.3 The cutting force measurement

The test plan used to measure the cutting force is a full 3^3 design, 3 factors and 3 levels design. The 3 factors are the depth of cut, the feed and the cutting speed. The data can be seen in Table 6 and 7. Table 5 shows the factors and their levels for this test.

Table 5: Factors and their levels

Level	Depth of cut a_p (in)	Feed f (in/rev)	Cutting speed V_c (ft/min)
1	0.01	0.006 (0.15 mm/tr)	500 (152 m/min)
2	0.02	0.007 (0.17 mm/tr)	700 (213 m/min)
3	0.05	0.008 (0.20 mm/tr)	800 (243 m/min)

The test is performed with a square whisker ceramic WG 300 Greenleaf [18]. A water based coolant is used during the tests.

a) Cutting force results

Figure 4.9 shows an example of the radial cutting force Fr result for a given condition a_p= 0.05 in, V_c= 500 ft/min and f = 0.008 in/rev.

The cutting force data analysis is performed with the module design of experiments of the software Statistica.

The cutting forces data Table 6 have been transformed into logarithm expressions $\ln(a_p)$, $\ln(V_c)$, $\ln(f)$, $\ln(F_r)$, $\ln(F_f)$ and $\ln(F_t)$ in Table 7, which are respectively the logarithm of, depth of cut a_p, feed f, radial force F_r, feed force F_f and tangential force F_t.

The objective is to determine a response surface profile for each cutting force component, that is to determine for each $\ln(F_r)$, $\ln(F_f)$ and $\ln(F_t)$, a polynomial function of 3 variables $\ln(a_p)$, $\ln(V_c)$ and $\ln(f)$.

For the case of the component $\ln(F_r)$ in Table 8, the effects of the function are shown in the column effect. The effects are the coefficients of a 1 degree polynomial. The column variables show to which variable belong the effects. $\mathrm{Ln}(a_p)$ is considered variable 1, $\ln(V_c)$ variable 2 and $\ln(f)$ the variable 3. The two-way interaction effect of variables $\mathrm{Ln}(a_p)$ and $\ln(V_c)$ is expressed by 1L by 2L, meaning the linear effect of variable 1 by the linear effect of variable 2 (1Q would mean quadratic effect).

In many areas of research, the alpha error probability p of 0.05 (5%) is customarily treated as a "border-line acceptable" error level. The effects estimates show that some effects can be neglected, see column 'p' of Table 8. The values of variables giving p higher than 5% (p>5%) will be neglected. The regression coefficient can then be obtained by removing the variables which gave a value of p higher than 5%. Table 9 shows these variables and the regression coefficient associated to them.

Table 6: Cutting forces data

	a_p (in)	Vc (in)	f (in)	Fr (N)	F_f (N)	F_t (N)
1	0,01	500	0,006	140,9581	33,8506	132,4285
2	0,01	500	0,007	197,0872	56,8691	160,221
3	0,01	500	0,008	169,5604	39,7762	165,9429
4	0,01	700	0,006	149,0876	51,9279	130,9522
5	0,01	700	0,007	211,6389	60,5484	161,278
6	0,01	700	0,008	206,3364	52,9373	172,4147
7	0,01	800	0,006	167,3881	44,4009	133,3393
8	0,01	800	0,007	218,656	63,2245	161,7173
9	0,01	800	0,008	186,8057	45,9685	166,1162
10	0,02	500	0,006	291,3891	125,447	261,7636
11	0,02	500	0,007	351,846	163,7934	314,8483
12	0,02	500	0,008	331,2867	128,3751	321,6765
13	0,02	700	0,006	323,2696	152,8809	271,9685
14	0,02	700	0,007	365,6288	170,9052	308,2436
15	0,02	700	0,008	351,8453	156,2072	330,3716
16	0,02	800	0,006	323,6825	137,0271	263,7624
17	0,02	800	0,007	383,5836	177,9305	308,7945
18	0,02	800	0,008	339,055	143,3647	321,4685
19	0,05	500	0,006	530,9236	305,2569	592,5725
20	0,05	500	0,007	332,6755	233,146	640,0034
21	0,05	500	0,008	590,8764	327,7443	732,5549
22	0,05	700	0,006	252,5875	172,2286	524,7883
23	0,05	700	0,007	366,0506	259,6875	638,5853
24	0,05	700	0,008	299,2658	197,1149	675,3941
25	0,05	800	0,006	604,6794	343,5371	589,7254
26	0,05	800	0,007	415,8871	297,711	650,3732
27	0,05	800	0,008	244,5644	149,0207	637,2559
28	0,02	700	0,007	382,09	181,27	313,16

Table 7: Cutting force data transformed into logarithm

$\ln(a_p)$	ln(Vc)	ln(f)	ln(Fr)	$\ln(F_f)$	$\ln(F_t)$
-4,605	6,215	-5,116	4,948	3,522	4,886
-4,605	6,215	-4,962	5,284	4,041	5,077
-4,605	6,215	-4,828	5,133	3,683	5,112
-4,605	6,551	-5,116	5,005	3,950	4,875
-4,605	6,551	-4,962	5,355	4,103	5,083
-4,605	6,551	-4,828	5,330	3,969	5,150
-4,605	6,685	-5,116	5,120	3,793	4,893
-4,605	6,685	-4,962	5,387	4,147	5,086
-4,605	6,685	-4,828	5,230	3,828	5,113
-3,912	6,215	-5,116	5,675	4,832	5,567
-3,912	6,215	-4,962	5,863	5,099	5,752
-3,912	6,215	-4,828	5,803	4,855	5,774
-3,912	6,551	-5,116	5,778	5,030	5,606
-3,912	6,551	-4,962	5,902	5,141	5,731
-3,912	6,551	-4,828	5,863	5,051	5,800
-3,912	6,685	-5,116	5,780	4,920	5,575
-3,912	6,685	-4,962	5,950	5,181	5,733
-3,912	6,685	-4,828	5,826	4,965	5,773
-2,996	6,215	-5,116	6,275	5,721	6,384
-2,996	6,215	-4,962	5,807	5,452	6,461
-2,996	6,215	-4,828	6,382	5,792	6,597
-2,996	6,551	-5,116	5,532	5,149	6,263
-2,996	6,551	-4,962	5,903	5,559	6,459
-2,996	6,551	-4,828	5,701	5,284	6,515
-2,996	6,685	-5,116	6,405	5,839	6,380
-2,996	6,685	-4,962	6,030	5,696	6,478
-2,996	6,685	-4,828	5,499	5,004	6,457
-3,912	6,551	-4,962	5,946	5,200	5,747

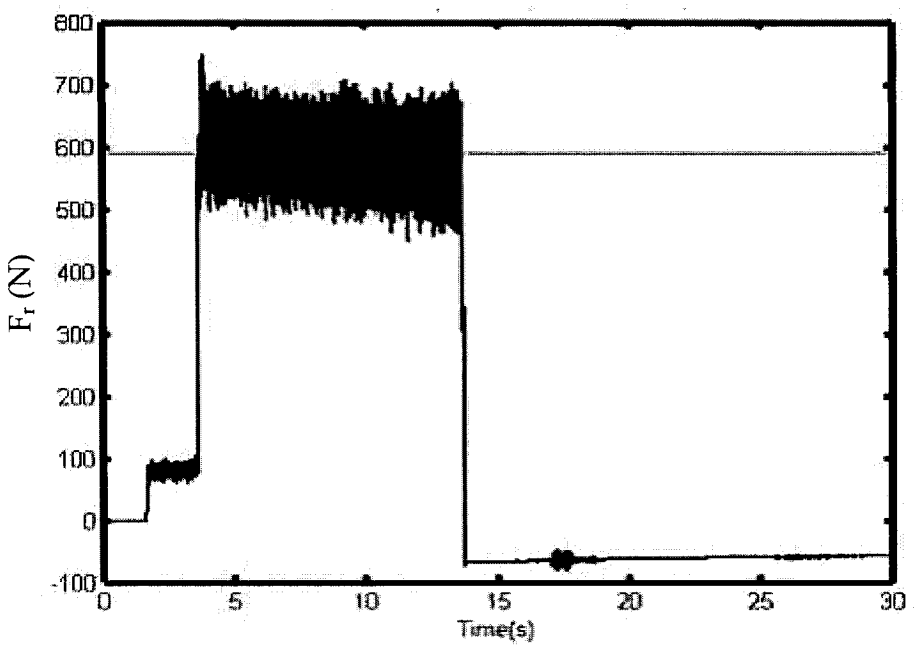

Figure 4.9. The component Fr of the cutting force a_p= 0.05 in, V_c= 500 ft/min and f = 0.008 in/rev.

Table 8: Effect estimates for radial component

Variables	Effect	Std.Err.	t(21)	p	-95,% Cnf.Limt	+95,% Cnf.Limt	Coeff.	Std.Err. Coeff.
Mean/Interc.	5,69	0,05	109,58	0,00%	5,58	5,79	5,69	0,05
(1)Ln(a_p) (L)	0,75	0,13	5,86	0,00%	0,49	1,02	0,38	0,06
1L by 3L	-0,22	0,15	-1,40	17,58%	-0,54	0,11	-0,11	0,08
1L by 2L	-0,20	0,15	-1,34	19,31%	-0,51	0,11	-0,10	0,08
2L by 3L	-0,14	0,15	-0,95	35,16%	-0,46	0,17	-0,07	0,08
(3)Ln(f) (L)	0,04	0,13	0,35	73,35%	-0,22	0,31	0,02	0,06
(2)Ln(V_C) (L)	-0,02	0,12	-0,13	90,08%	-0,27	0,24	-0,01	0,06

:

Table 9: The regression coefficients for F_r component of the cutting force after ignoring some effects

Regr. Coefficients; Var.:LnFr; R-sqr=,55553; Adj:,53844 3 3-level factors, 1 Blocks, 28 Runs; MS Residual=,0718612 DV: LnFr						
	Regressn Coeff.	Std.Err.	t(26)	p	-95,% Cnf.Limt	+95,% Cnf.Limt
Mean/Interc.	5,94	0,0694	85,609	0,00%	5,7958	6,08096
(1)Ln(a_p) (L)	0,45	0,0782	5,7006	0,00%	0,2852	0,60691

Using the regression coefficient in Table 9 to express the polynomial Ln(F_r):

$$\ln(F_r)=5.94+0.45\ln(a_p)$$

$$F_r=379a_p^{0.45} \qquad \text{Equation (18)}$$

F_r expressed in N and a_p in mm.

The same procedure is used to express the coefficients of the feed component F_f and the tangential component F_t of the cutting force. See Appendix IV.

$F_f= 222a_p^{0.97}$ (F_f expressed in N and a_p in mm) Equation (19)

$F_t=1840a_p^{0.87} f^{0.73}$ (F_t expressed in N, a_p and f in mm) Equation (20)

b) Summary of the cutting force tests

After the cutting forces test, the conclusion from equations 18, 19 and 20 is that the effect of the cutting speed on the cutting force is negligible in the range of the tests. That is between 152 m/min (500 ft/min) and 243 m/min (800 ft/min), the cutting speed does not effect the cutting force. During the machining of Inconel 718 with whisker ceramics, this range of cutting forces is commonly used.

The second conclusion is that the radial and feed components of the cutting force depend only on the depth of cut for the tool geometry used. The effect of feed can be neglected in the parameter range.

The third conclusion is that the tangential component of the cutting force depends on both feed and depth of cut.

4.2.3. The energy absorption model

In section 4.2.2.2, the tangential component of the cutting force was assumed to be $F_t=K_c.S_c$, where K_c is a constant and S_c the undeformed chip section. Using the tangential component of the cutting force, the constant K_c value is determined; K_c=3003 N/mm^2, see details in Appendix V page 192.

With the value of K_c, the energy absorption expression is determined by Equation (17).

4.2.3.1 The ramping energy estimation

In the energy estimation formula, the chip section S_c is a parameter to estimate. To facilitate these calculations, the workpiece section is divided in many parts, Figure 4.10 and 4.11.

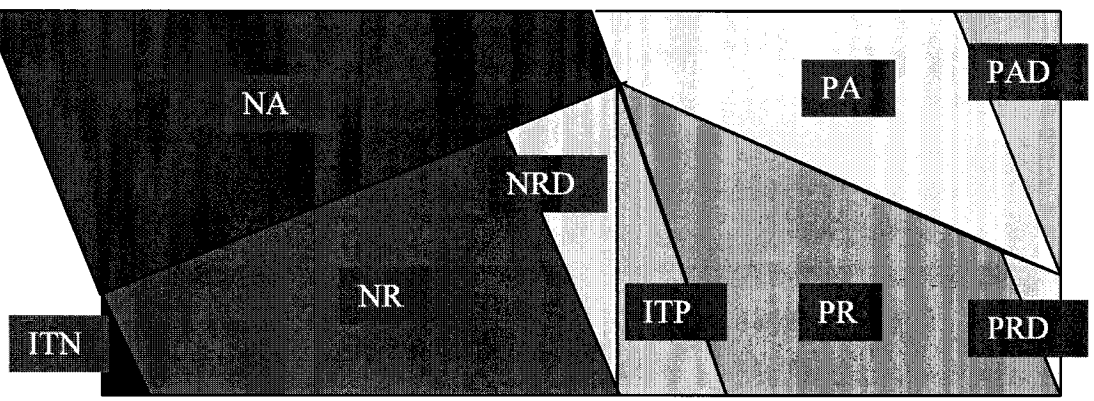

Figure 4.10. Two waves ramping starting with a positive ramp

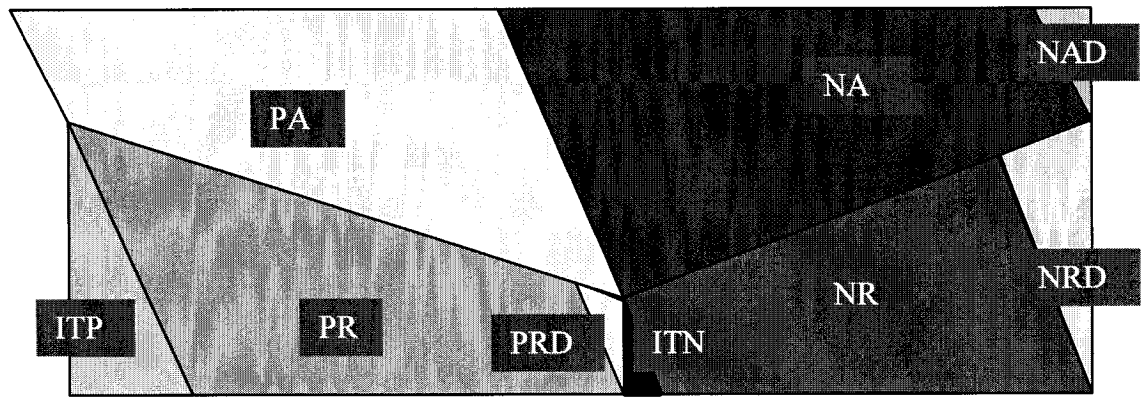

Figure 4.11. Two waves ramping starting with a negative ramp

Each part of the sections is named differently:

PAD: The section removed at the beginning when the tool enters into the material when the ramp is positive during the first pass.

PA: The section removed when the ramp is positive during the first pass.

NA: The section removed when the ramp is negative during the first pass.

NAD: The section removed at the beginning when the tool enters into the material when the ramp is negative during the first pass.

PRD: The section removed at the beginning when the tool enters into the material when the ramp is positive, during the second pass.

NRD: The section removed at the beginning when the tool enters into the material when the ramp is negative, during the second pass.

NR: The section removed when the ramp is negative, during the second pass.

PR: The section removed when the ramp is positive, during the second pass.

ITN: The remaining material when the ramp is negative during the second pass.

ITP: The remaining material when the ramp is positive during the second pass.

The calculation of section is made in detail in the Appendix II page 172-181.

4.2.3.2 The cutting force and the cutting power curves

With a Matlab program it's now possible to draw the cutting force component F_t and the cutting power. The cutting power expression is given by Equation (16). The energy can then be easily determined later.

Let's go back to the 3 configurations (B) Figure 4.8. Let's suppose the cutting conditions:

V_c=900 ft/min, a_p=0.14 in, f=0.007 in/rev, ρ=0.3, L=4 in, initial diameter Dinit=5 in, κ_r=45°.

a) For one positive ramp configuration (B)

The cutting force curves modeled when performing this single positive ramp is shown in Figure 4.12.

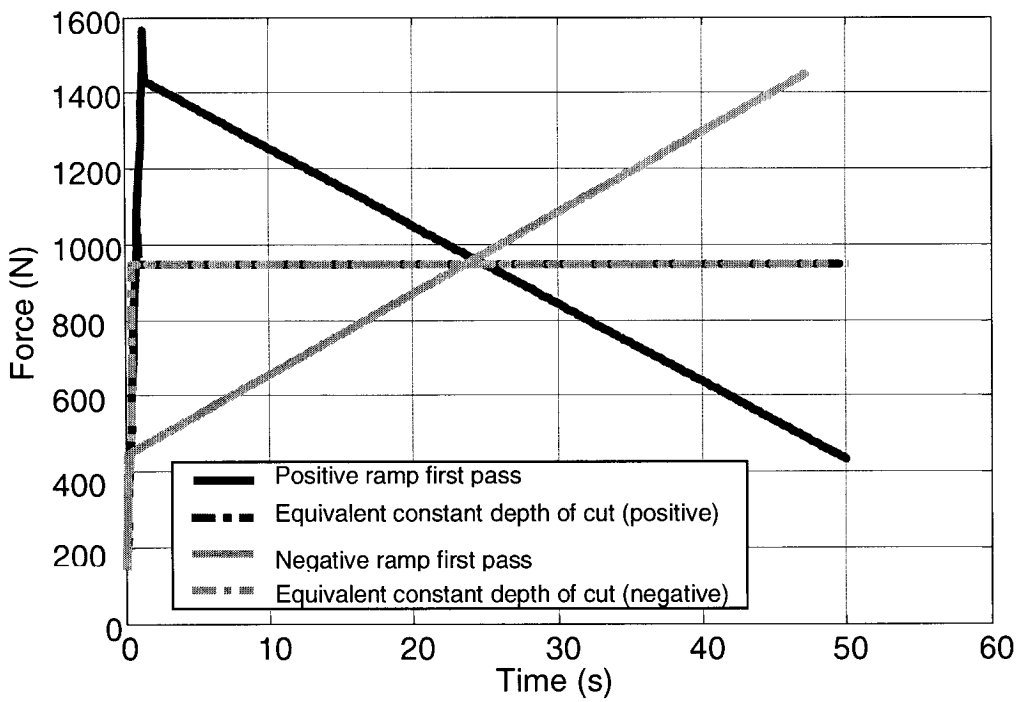

Figure 4.12. Cutting force as a function of time for one ramp, V_c=900 ft/min, a_p=0.14 in, f=0.007 in/rev, ρ =0.3, L=4 in, Dinit= 5 in, κ_r=45°.

The instantaneous power expression can also be drawn (Figure 4.13).

Figures 4.12 and 4.13 show that the cutting force and the power have the same shape as a function of time. Therefore only the instantaneous power will be used to represent the next ramping methods, and its variations will be considered the same as the cutting force variations.

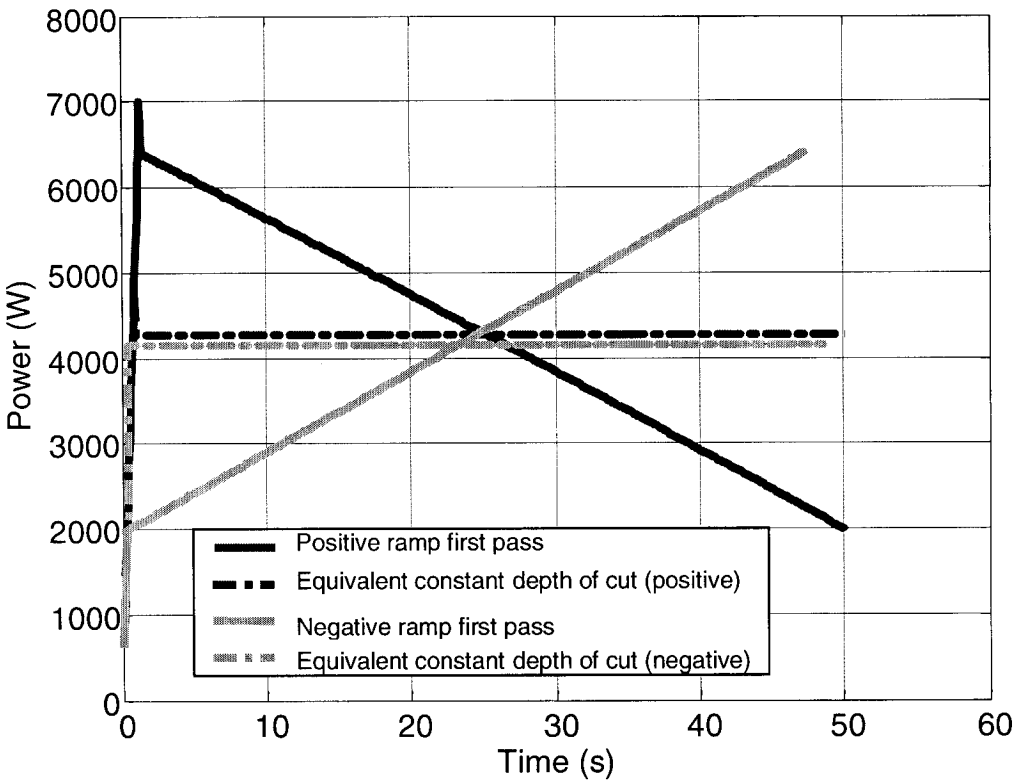

Figure 4.13. Cutting power as a function of time for one ramp, V_c=900 ft/min, a_p=0.14 in, f=0.007 in/rev, ρ =0.3, L=4 in, Dinit= 5 in, κ_r=45°.

b) For 2 and 3 ramps configuration (B)

Figure 4.14 and 4.15 show the instantaneous power shape of the 2 ramps and 3 ramps configuration (B).

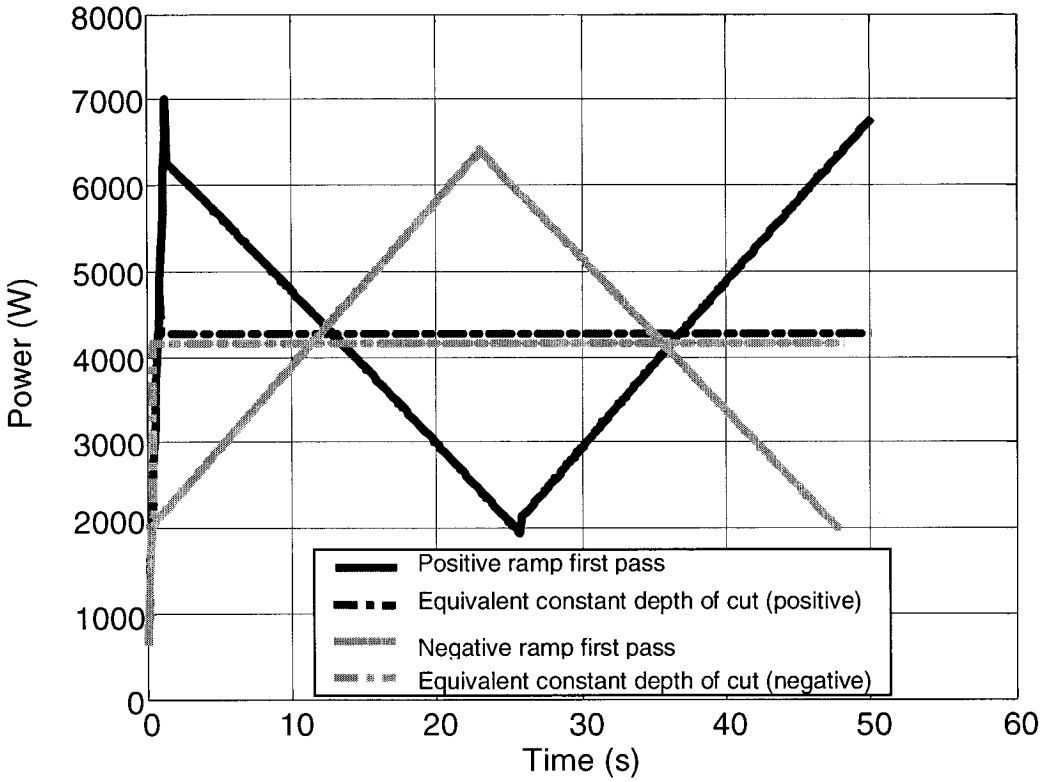

Figure 4.14. Cutting power as a function of time for 2 ramps, V_c=900 ft/min, a_p = 0.14 in, f=0.007 in/rev, ρ =0.3, L=4 in, Dinit= 5 in, κ_r=45°.

At the beginning of the first pass ramping Figures 4.14 and 4.15, the power reaches a peak before decreasing. This is due to the fact that the cutting force increases until the point (1) Figures 4.15, where the positive ramping starts. Seconds before this point, the tool movement was supposed horizontal (constant depth of cut), Figure 4.16. Seconds after this point, the positive ramping starts. Since the chip thickness for a constant depth of cut is bigger for a positive ramp (see Figure 4.17), there is an abrupt drop of power function at this point.

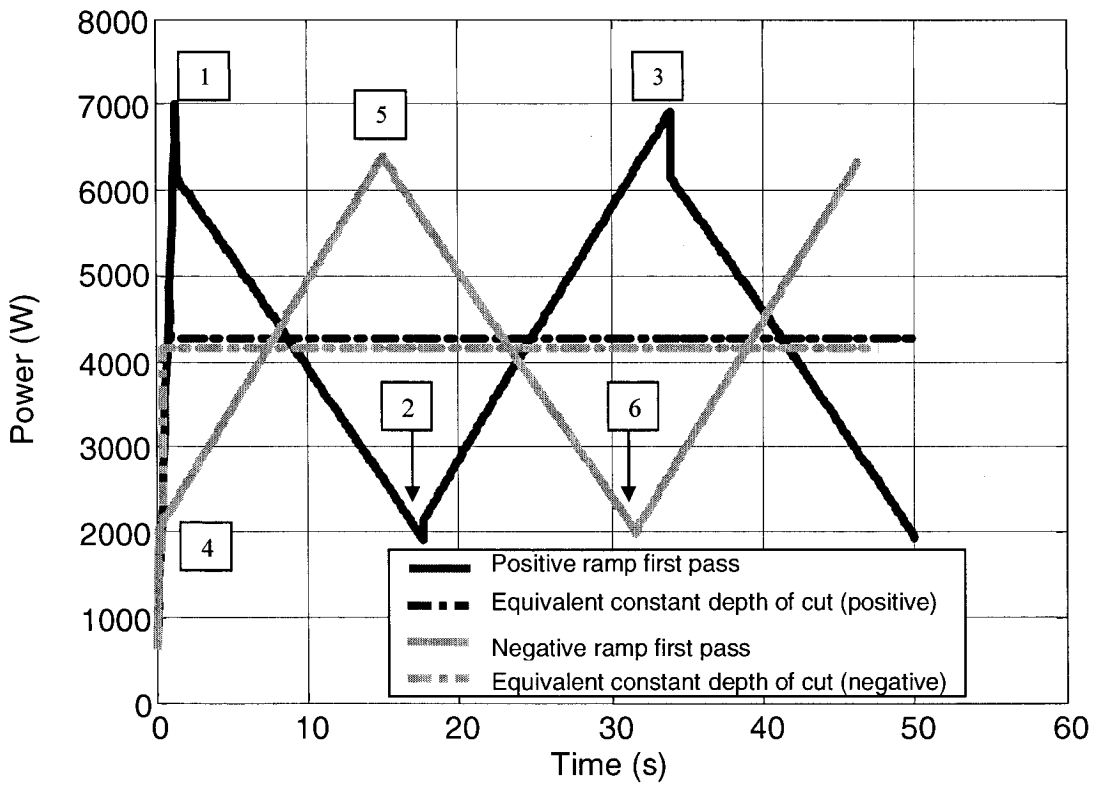

Figure 4.15. Cutting power consumption as a function of time for 3 ramps, V_c=900 ft/min, a_p =0.14 in, f=0.007 in/rev, ρ =0.3, L=4 in, Dinit= 5 in, κ_r=45°.

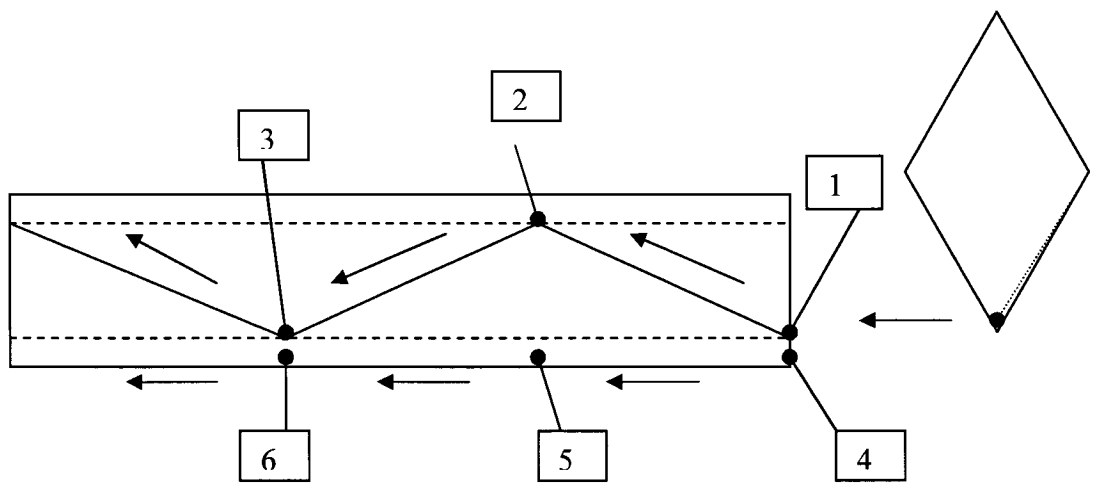

Figure 4.16. Tool trajectory and positions during a 3 waves ramping (first and second pass)

The same phenomenon is observed at point (2) where there is an abrupt power jump, because the chip thickness for the positive ramp is less than the one for the negative ramp. At the point (3), it is the contrary. There is an abrupt decrease of power due to the fact that there is a passage from a negative to positive ramp.

The second pass power curve is more continuous, because the chip thickness remains the same during this constant depth of cut machining. But because of the variation of depth of cut, the power function decreases and increases, point (4), (5) and (6).

When the tool is at the points (3) and (5), the depths of cut are the same, but Figure 4.16 indicates that the power reached at the point (3) is higher than at the point (5). Also at the points (2) and (6), the depths of cut are the same, and the power reached at the point (6) is higher than at the point (2).

This phenomenon can be explained by the fact that the chip thickness is bigger for the negative ramps than for constant depth of cut, which is bigger than the positive ramp; giving the highest cutting section, the highest force and the highest power.

Figure 4.17 shows the chip thickness variation for the same feed, when at one point of the cutting, the tool moves on a positive ramp, negative ramp or constant depth of cut (zero ramp).

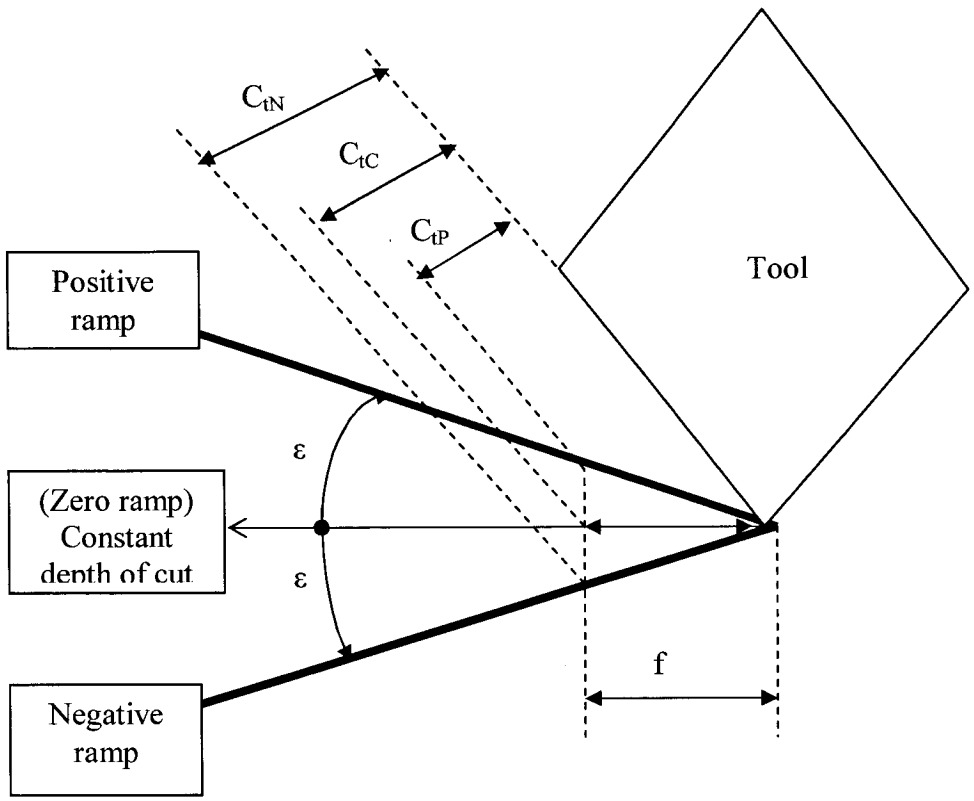

Figure 4.17. The chip thickness comparison for positive, negative and zero ramp

The positive ramping chip thickness C_{tP}, the negative ramping chip thickness C_{tN} and the constant depth of cut machining chip thickness C_{tC} expressions are respectively :

$$C_{tP}=f\frac{\sin(\kappa_r-\varepsilon)}{\cos(\varepsilon)} \qquad \text{Equation (21)}$$

$$C_{tN}=f\frac{\sin(\kappa_r+\varepsilon)}{\cos(\varepsilon)} \qquad \text{Equation (22)}$$

$$C_{tc}=f\sin(\kappa_r) \qquad \text{Equation (23)}$$

4.2.3.3 Energy absorption as a function of DOCVT

As it was stated earlier, the energy absorption during a ramping technique will be associated to the tool average wear.

A number of 1, 2,.., 5 ramps are simulated with a Matlab program, and the depth of cut variation in time is calculated for each 1,2,…5 ramps.

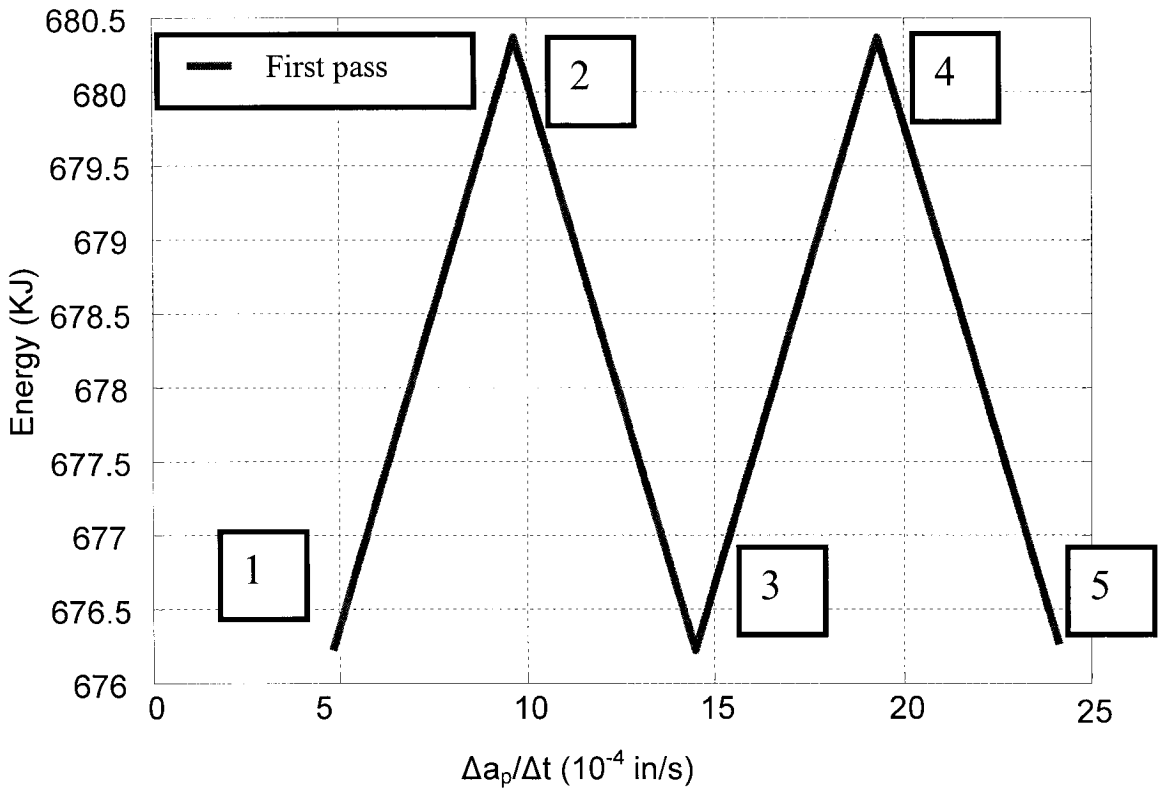

Figure 4.18. First pass for 5 waves ramping for a_p=0.14 in, ρ=0.3, κ_r=45 , Δt=156 s, V_c=900 ft/min, f=0.007 in/rev

Figures 4.18, 4.19 and 4.20 show the energy absorbed by the tool as a function of the depth of cut variation in time. The points (1), (2), (3), (4) and (5) are respectively the number 1, 2, 3, 4 and 5 ramps (waves), simulated on the same length during the time Δt =156 s. The energy absorbed by the tool as function of depth of cut variation in time as

the shape of an oscillation. If the 5 considered points are linked by a polynomial the shape will be closed to a sinusoid.

- The first thing to notice is that the amount of energy absorbed during the first pass of ramping reaches the value of 676.5 KJ, while for the secondary pass it is of 657.7, less than for the first pass. That is because the amount of material removed during the first pass of ramping is always more than the one removed at the second pass, since the diameter of the shaft is reduced after the first pass.

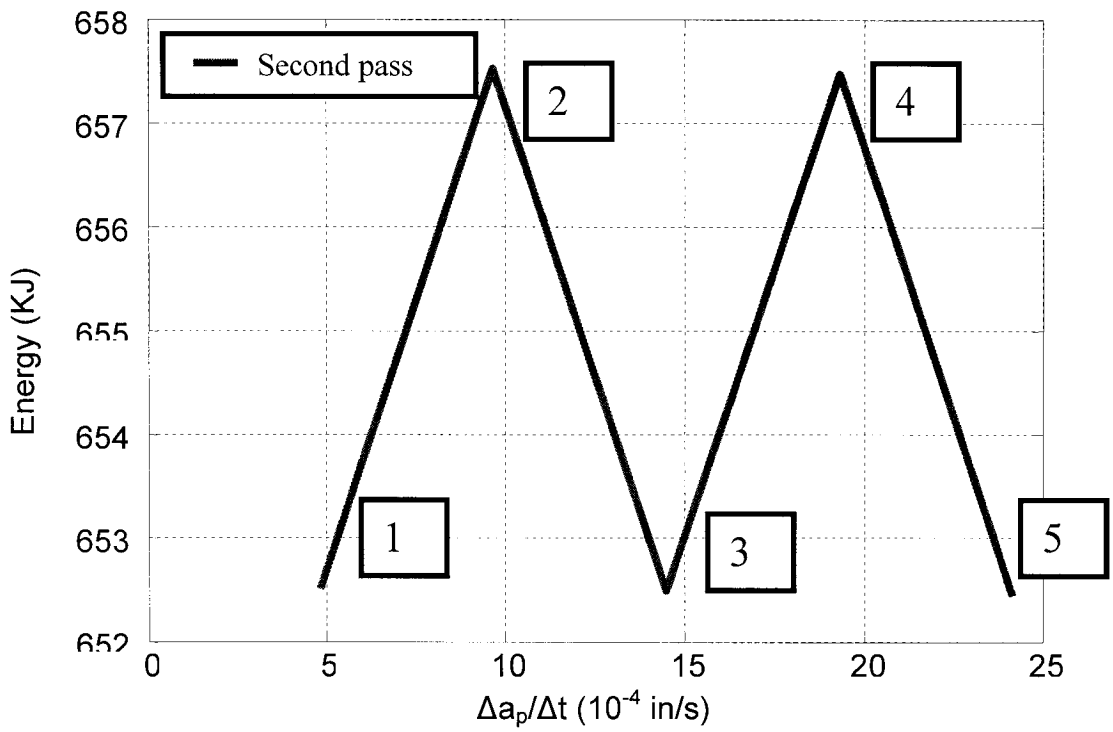

Figure 4.19. Second pass for 5 waves ramping, for a_p=0.14 in, ρ=0.3, κ_r=45, Δt=156s, Vc=900 ft/min, f=0.007 in/rev

- Another interesting result is that when the number of waves is odd, the energy absorbed is less then when the number of waves is even.

- In spite of the number of waves, the energy absorbed is the same for all odd numbers of waves (1, 3, and 5), and the same for all the even numbers (2, 4).

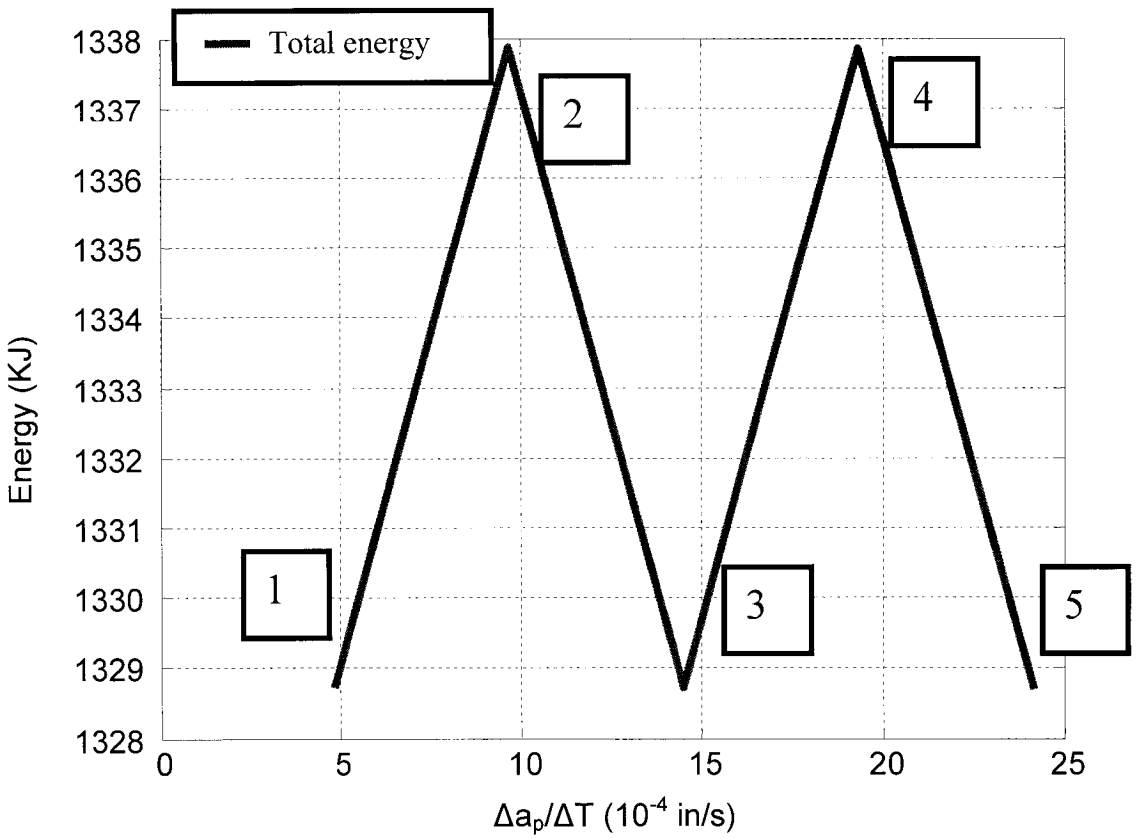

Figure 4.20. Total ramping energy (first +second pass) for 5 waves ramping, for a_p=0.14 in, ρ=0.3, κ_r=45, ΔT=156s, Vc=900 ft/min, f=0.007 in/rev

This result can be generalized for N waves. The implications of these results for the initial hypothesis are as follow:

1. The average tool wear should theoretically be higher for the first pass than for the second pass
2. It would be better to make odd numbers of ramps or waves for a certain length to minimize the average wear.

3. The average wear should theoretically be the same in spite of the number of waves, for the same categories, even and odd waves.

Even if the hypothesis of the direct link between energy absorption and tool wear is not proven, it's interesting to have a criteria to compare the different ramping techniques, since it's not possible to make unlimited test runs because of the material cost.
The experimental results are going to be compared to these model observations.

4.3. The feed variation method

4.3.1. An overview of the variable feed method

The variation of feed during a cutting operation makes it possible to vary the tool chip contact length in order to reduce crater wear. The reduction of crater wear has been demonstrated by many researchers, Zdzilaw et al [39], Balazinski & Songmene, [3].
The objectives of these investigations are not to demonstrate this fact, but to know if this method can allow reducing the notch wear. Balazinski & Songmene [3] stated that feed variation method could probably reduce notch wear when machining Inconel 900. It was shown that the principal factors influencing this wear are the amplitude of the feed variation and the number of discretization step of the feed function. To verify this hypothesis a simple feed variation test was performed. This model accounts for:

- The monotonous variation of feed (because the functions which give abrupt jumps in feed while remaining constant for long periods are less useful)
- The effect of the amplitude
- The number of discretization intervals
- The periodicity
- The oscillation of the function

The feed model retained is:

$$\begin{aligned} t\in[0;\tfrac{T}{4}] \quad & F(t)=\tfrac{4A}{T}t+f \\ t\in[\tfrac{T}{4};\tfrac{3T}{4}] \quad & F(t)=-\tfrac{4A}{T}t+f+2A \\ t\in[\tfrac{3T}{4};T] \quad & F(t)=\tfrac{4A}{T}t+f-4A \end{aligned} \qquad \text{Equation (24)}$$

T is the period, f the average feed and A the amplitude of the function.

Since it is not possible to program this function using CNC controllers, a discretization is necessary.

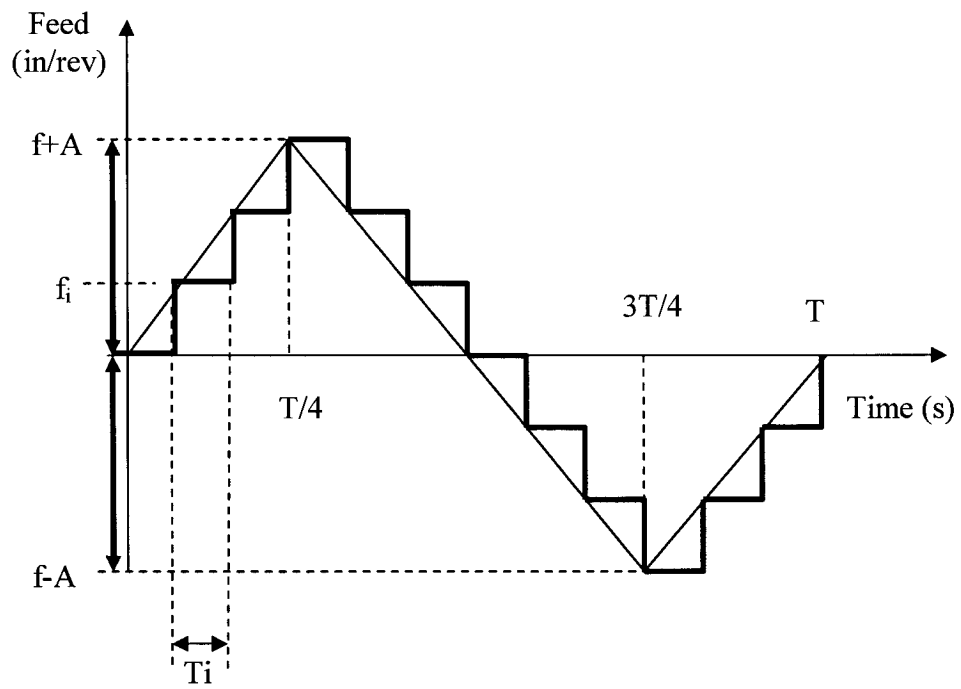

Figure 4.21. Feed variation function

The objective of this method is to divide the feed function into N intervals. Each interval represents a time T_i where the value of feed remain constant and equal to f_i. The function can then be represented by a multiple steps function which can be programmed in a CNC controller.

To compare this feed variation method with a constant feed method, it is important to estimate the value of the equivalent feed to be used for this constant feed machining. The estimation of this equivalent feed is as followed (Zdzilaw et al [39]):

N: The number of discretization intervals of the feed function.

T: The period of feed function

A: The maximum amplitude

Ti: The duration of each step

Q: The volume of material removed for one period

V_c: The cutting speed

f: The average feed

f_{eq}: The equivalent feed when the volume of material removed is Q for the period T

a_p: The depth of cut

For an operation without variation of feed, the volume of material removed is:

$$Q_1 = a_p f_{eq} V_c T \qquad \text{Equation (25)}$$

With a variation of feed according to the function represented Figure 4.21, the volume of material removed is:

$$Q_2 = \sum_{i=1}^{N} a_p f_i V_c T_i = a_p V_c = \sum_{i=1}^{N} f_i T_i = \frac{a_p V_c T}{N} = \sum_{i=1}^{N} f_i \qquad \text{Equation (26)}$$

So, both operations are comparable if there is equality between the amount Q_1 and Q_2.

That is $Q_1 = Q_2$ $\quad f_{eq} = \sum_{i=1}^{N} f_i$ Equation (27)

In this case, the feed function is odd, so Equation (14) always gives $f_{eq} = f$

Let say L_i, the incremental displacement of the tool for the period T_i:

$$Li = \frac{f_i V_c T_i}{\pi D} = \frac{f_i V_c T}{\pi N D} \qquad \text{Equation (28)}$$

A graphical representation of the feed variation function represented by Equation (24) is shown in Figure 4.22. The same function is represented in Figure 4.23 using the discretization in the conditions the N=24, T=30 s, A=0.001 in/rev and f=0.007 in/rev

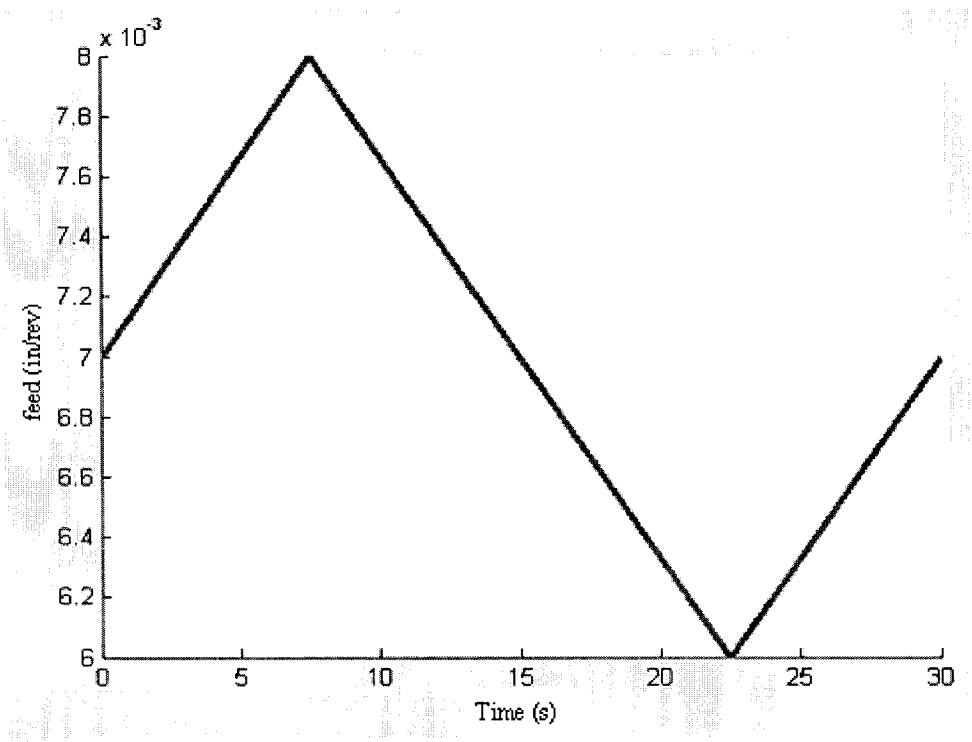

Figure 4.22. Representation of the feed variation function for N=24, T=30 s, A=0.001 in/rev, f=0.007 in/rev

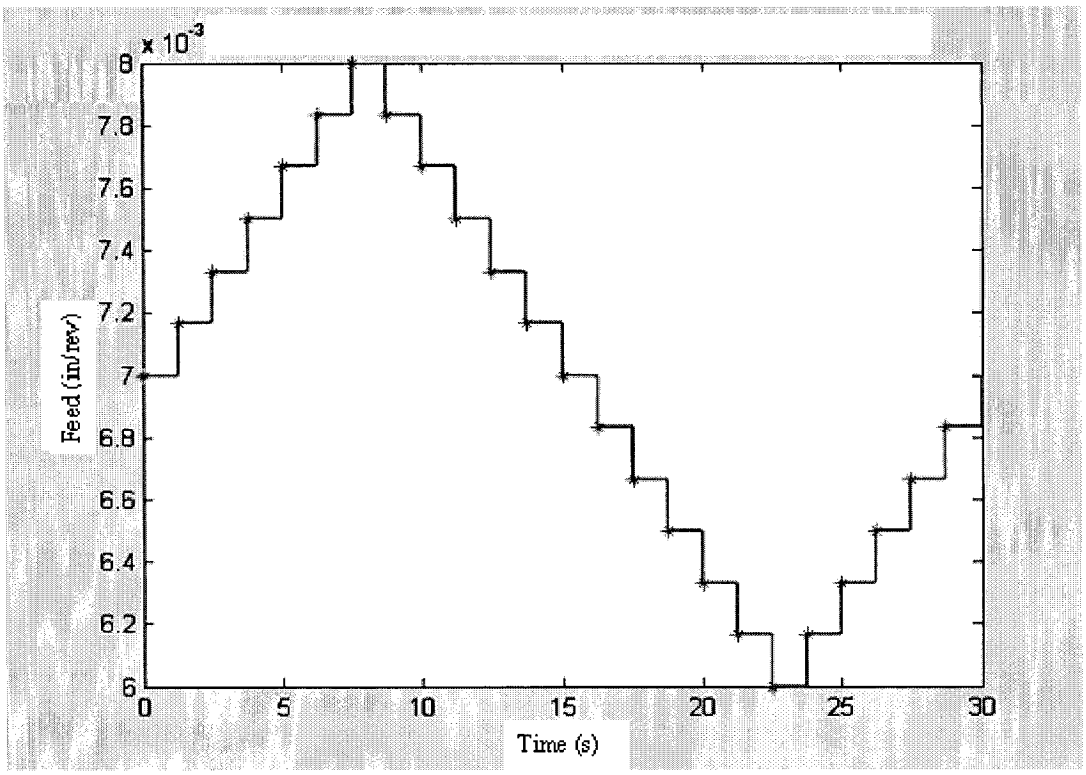

Figure 4.23. Feed discretization as a function of time by 24 steps

After a the explanations of the theories behind the machining strategies developed in this document, the next chapter deals with the tests plans used to carry out these models.

CHAPTER 5. THE TESTS PLANS

This chapter deals with the different test plans used to solve the issues raised in the problem statement chapter. These test plans are established to validate the machining theories explained in chapter 4.

5.1. The Inconel 718 samples

Two Inconel 718 samples are used during these tests. These samples are going to be called sample 1 and sample 2.

- The first Inconel 718 sample called sample1 is a bar of 9 in long of diameter 5 in.
- The second Inconel 718 sample called Sample 2 is a bar of 12 in long of diameter 6 in.

A hardness tests and a microstructure tests are performed on these two samples to further determine the link between their mechanical and metallurgical properties, and their machining properties.

5.2. The test equipments

- The machining tests are performed on a CNC lath Mazak Nexus 200
- The hardness test is performed on a numerical hardness tester
- The microstructure is observed and analyze by a scanning electron microscope
- The cutting force is measured by kistler dynamometer for turning
- The wear is measured using a picture from a high definition digital camera

Figures 5.1 and 5.2 show respectively the machine tool and the wear capturing system.

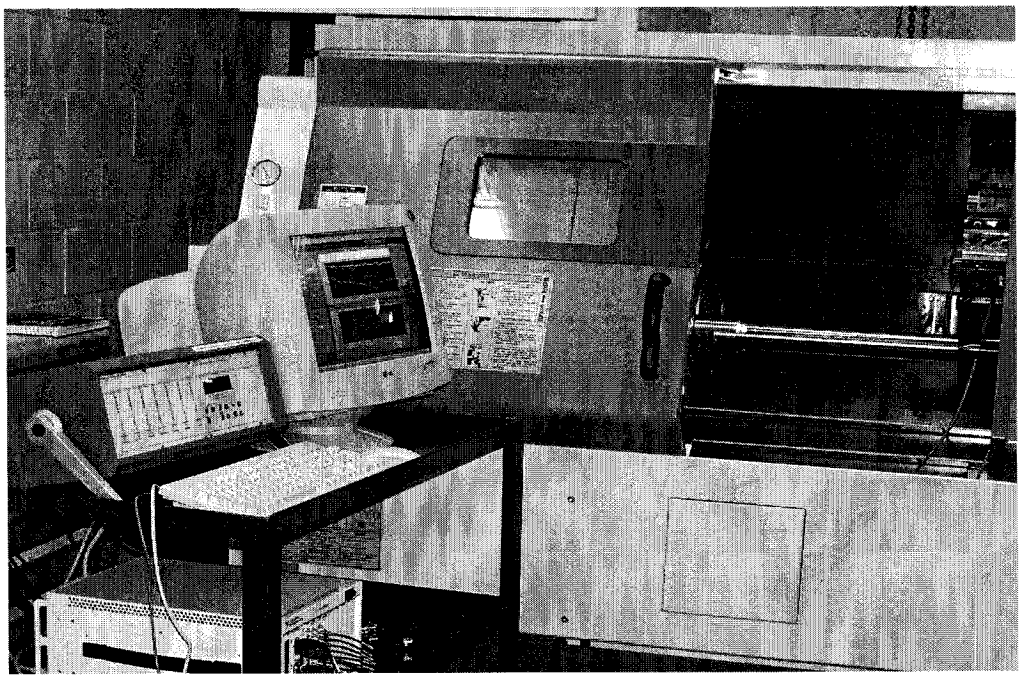

Figure 5.1. Mazak nexus 200 lathe and the cutting force measuring system

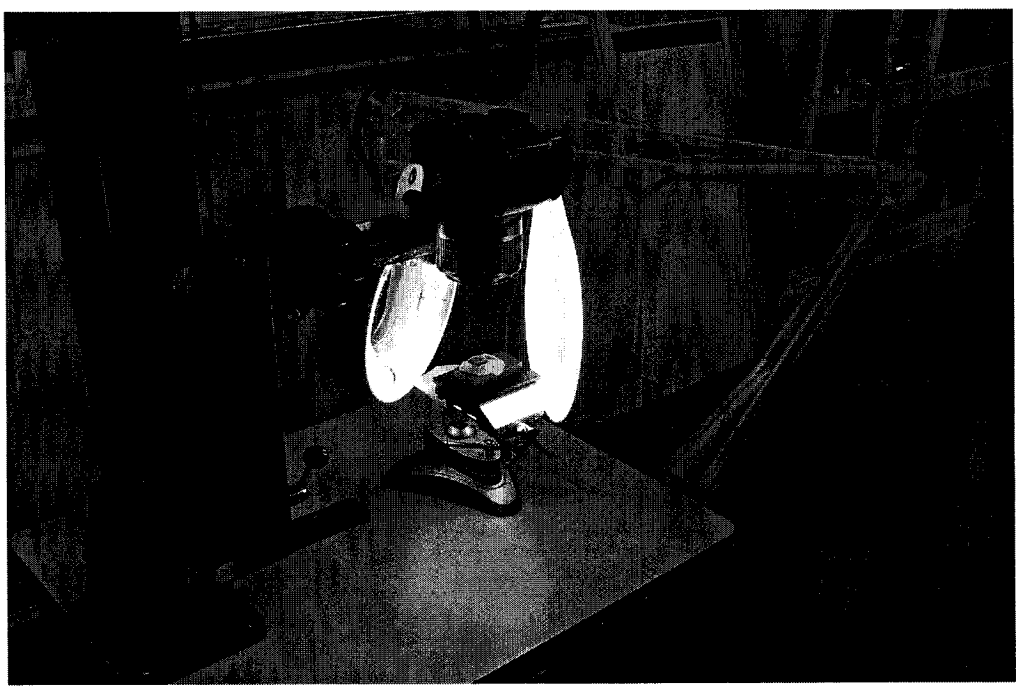

Figure 5.2. The tool wear capturing camera

5.3. The constant depth of cut method

The constant depth of cut is used with different cutting tool geometries and material to choose the best tool and to find the best cutting conditions. These tools are selected according to the literature review.

- A round and square whisker ceramic from Greenleaf corporation
- A mixed ceramic from Kennametal
- A TiAlN coated carbide from Kennametal
- A TiN coated carbide from Iscar

This method helps to confirm the appearance of notch wear, its effects on tool life, and to compare the performances of the cutting tools selected. Table 11 shows the cutting tool used during this phase.

5.3.1. The constant depth of cut tests with sample 1

This test is performed with only one cutting tool, the square whisker WG-300 of Greenleaf.

Because of the material cost, and the machining time expected to reach a significant level of tool wear, it was decided to start with a certain design point and complete the plan according to the results. Table 10 gives the cutting parameters used for this test.

The semi finished aspect is also tested, that is with the small depth of cut a_p=0.0175 in. The effects of feed during the semi finishing is tested, see Table 10 test numbers 3, 4 and 5.

Table 10: Test parameters

Number	f (in/rev)	a_p (in)	V_c (ft/min)
1	0,007	0,07	400
2	0,007	0,07	800
3	0,007	0,0175	800
4	0,005	0,0175	800
5	0,009	0,0175	800
6	0,007	0,0175	900
7	0,007	0,07	900
8	0,009	0,07	900

5.3.2. The constant depth of cut tests with sample 2

5.3.2.1 The cutting tools

The sample 2 was used to test different cutting tool to compare their performances. Three categories of cutting tool are used:

- **2 types of carbides**
  - KC5010, (TiAlN coated)
  - GA-5026 (TiN coated)
- **1 mixed ceramic**
  - KY1540, (Sialon Si_3N_4 ceramic)
- **2 whiskers ceramic**
  - WG-300, (SiC whisker)
  - WG-600, (TiN coated SiC whisker).

Table 11 regroups detailed information about these cutting tools.

Table 11: Tools materials and their geometries

Item	Manufacturer	Designation	Insert	Insert type	clearance angle	Rake angle	Inclination angle
(1)Toolholder for round ceramic	Greenleaf	C-CRGPL-164	RPGN-43	Whisker ceramic R-WG-300	//	5	5
(2)Toolholder for square ceramic	Greenleaf	C-CSSPL-164	SPGN-432	Whisker ceramic S-WG 300	45	5	0
(3)Toolholder for round ceramic	Kennametal KY1540	CRGNL-164	RNG-43T 0420	Sialon KY 1540	//	-10	-5
(4)Toolholder for V ceramic	Greenleaf	CDJOL-164V	DPGN-443V	Whisker ceramic WG-600	-3	0	0
(5)Toolholder for carbide	Greenleaf	G-MSSNL-16-4D	SNGN -432	Carbide GA-5026	45	-10	-5
(6)Toolholder for carbide	Iscar	SDJCL-16-3	DCGT 3-1-SM	Carbide	-1	0	0
(7)Toolholder for carbide	Kennametal	MVJNL-163D	VNMG-332	Carbide KC5010 (TiAlN)	-3	-4	-13
(8)Toolholder for carbide	Kennametal	MDJNL-163D	DNGG-432LF	Carbide KC5010 (TiAlN)	-3	-5	-5
(9)Toolholder for carbide	Kennametal	MDJNL-163D	DNGG-432LF	Carbide GA-5026	-3	-5	-5

5.3.2.2 The test plan

The test plan used for sample 2 (Table 12) is simply the cutting conditions proposed by each tool manufacturer for the carbides. For the mixed ceramic KY1540 in Table 12, two conditions are used. The insert 1-KY1540 is the KY1540 used in the same condition as the whisker WG 300 for comparison purposes. The insert 2-KY1540 is KY1540 in the manufacturer cutting conditions.

Table 12: Cutting conditions

Item	Insert	Cost ($/edge)	Type	a_p (in)	f (in/rev)	V_c (ft/min)
(3)	1-KY1540	10	Round	0,07	0,007	900
(3)	2-KY1540	10	Round	0,07	0,005	500
(9)	GA 5026	7,5	80 degree	0,07	0,007	230
(8)	KC5010	7,5	80 degree	0,07	0,007	230
(1)	R-WG 300	10	Round	0,07	0,007	900
(2)	S-WG 300	10	square	0,07	0,007	900

5.4. The ramping test

As indicated in chapter 4, two ramping techniques are tested. The technique using the constant slope and the technique using the depth of cut variation in time. Two cutting tools are used for the ramping test.

- The TiAlN coated carbide of Kennametal (item 8, Table 11)
- The square whisker ceramic S-WG 300 of Greenleaf (item 2, table 11).

For the method using the constant slope, only the square whisker ceramic S-WG 300 of Greenleaf is used.

For the technique using the depth of cut variation in time, the TiAlN coated carbide is used to determine the link between the tool wear and the depth of cut variation in time, and the whisker S-WG 300 is used to confirm the results. The reason is because of the material cost, using carbide to evaluate the ramping is more profitable than using a whisker tool, since the amount of material to remove by a whisker tool to reach a significant wear pattern is high.

5.4.1. The constant slope test

This test plan aims to determine the link between the tool wear and the ramping slope. If this link is established, a tool life model can then be deduced for further optimizations. The set of input variables are:

- The feed f
- The cutting speed V_c
- The depth of cut a_p
- slope E
- The volume removed vol

This test is a 2^{4-1} levels fractional factorial design with 4 variables. The fifth variable, volume (vol), is kept constant, vol= 4.5 in^3. A fractional factorial design is chosen because the number of test is reduced, and it is possible to add new test conditions for more precisions.

Table 13: 2^{4-1} levels fractional factorial design with 4 variables

Test number	E (degree)	f (in/rev)	V_c (ft/min)	a_p (in)
1	-0,4	0,006	600	0,13
2	-0,4	0,006	800	0,19
3	-0,4	0,008	800	0,19
4	-0,4	0,008	600	0,13
5	0,4	0,006	800	0,19
6	0,4	0,006	600	0,13
7	0,4	0,008	600	0,13
8	0,4	0,008	800	0,19

Factor	Low value	High value
E (degree)	-0,4	0,4
f (in/rev)	0,006	0,008
V_c (ft/min)	600	800
a_p (in)	0,13	0,19

5.4.2. The constant depth of cut variation in time test

The set of variables for the second ramping test is as follows:

- The cutting speed Vc
- The feed f
- The depth of cut a_p
- The machining time Δt
- The depth of cut variation in time $\frac{\Delta ap}{\Delta t}=\frac{1-\rho}{1+\rho}\times\frac{ap}{\Delta t}$ where $\rho=\frac{B}{A}$

The plan is divided into 3 parts. The purpose of the first part of the tests is to identify the cutting speed which will make it possible to reach a tool life higher than 5 minutes with the TiAlN coated carbide. This is because a lower tool life will be difficult to deal with in practice by the operators. The second part of the tests consist in specifying the influence of the depth of cut variation in time on the tool life and in which circumstances it is profitable to use it. Table 14 shows the test plan for this second part. The third test is a confirmation of the second test using this time a square whisker ceramic WG 300.

Table 14: Effect of depth of cut variation in time

Tests	slope (E)	ρ	a_p	Δt (s)	Δa_p (in)	$\Delta a_p/\Delta t$ (in/s)
A(I)	Positive	0,1	0,14	156	0,1145	0,0007
A(II)	Positive	0,1	0,14	78	0,1145	0,0015
A(III)	Positive	0,1	0,14	52	0,1145	0,0022
B(I)	Positive	0,3	0,14	156	0,0754	0,0005
B(II)	Positive	0,3	0,14	78	0,0754	0,0010
B(III)	Positive	0,3	0,14	52	0,0754	0,0014

5.5. The feed variation test plan

The feed variation test plan is established according to the theoretical part in chapter 4 page 59. The feed variation function is described in page 60 by Equation (24). A comparison is made between this feed variation function and a constant feed machining.

5.5.1. The cutting tool

The cutting tool was chosen according to the indication of the literature review.
The tool is a whisker ceramic tool manufactured by Greenleaf Corporation (item 2, Table 11, page 68). It has a 45 degree lead angle, with a 5 degree rake angle and 0 degree inclination angle.

5.5.2. The variable feed test plan

Based on the theoretical aspect, the conditions used for this investigation are:

a) For the feed variation:

- The feed f=0.007 in/rev
- The amplitude of feed variation A= 0.002 in/rev
- The number of step N=28
- The cutting speed V_c = 700 ft/min
- The depth of cut a_p=0.080 in
- The feed function period T=30 s

b) For the constant feed:

- The feed f=0.007 in/rev
- The cutting speed V_c = 700 ft/min
- The depth of cut a_p=0.080 in

CHAPTER 6. THE MACHINING RESULTS

In this chapter the different machining results are presented according to the tests plans presented in the chapter 5. The constant depth of cut machining results is presented first, followed by the ramping method results, the feed variation results and the burr formation observation during the tests. A section devoted to proposals will follow after the presentation of the machining results.

6.1. The constant depth of cut tests results

Both Inconel 718 samples are tested. Both samples are supposed to have the same properties. A more detailed metallurgical result of theses two samples is presented in pages 101-105.

6.1.1. The constant depth of cut tests with sample 1

Based on the test plan establish in chapter 5 page 66, different machining tests are performed.

According to Figure 6.1, the notch wear increases with cutting speed. This result is due to the effect of heat as confirmed by the literature. Figure 3.9 page 24 in the literature review shows that the cutting temperature during machining increases with the cutting speed. It is also stated in Appendix I page 141 that diffusion can be a cause of notch wear at high temperature. Diffusion is a mass transfer between the tool and the workpiece, activated by temperature.

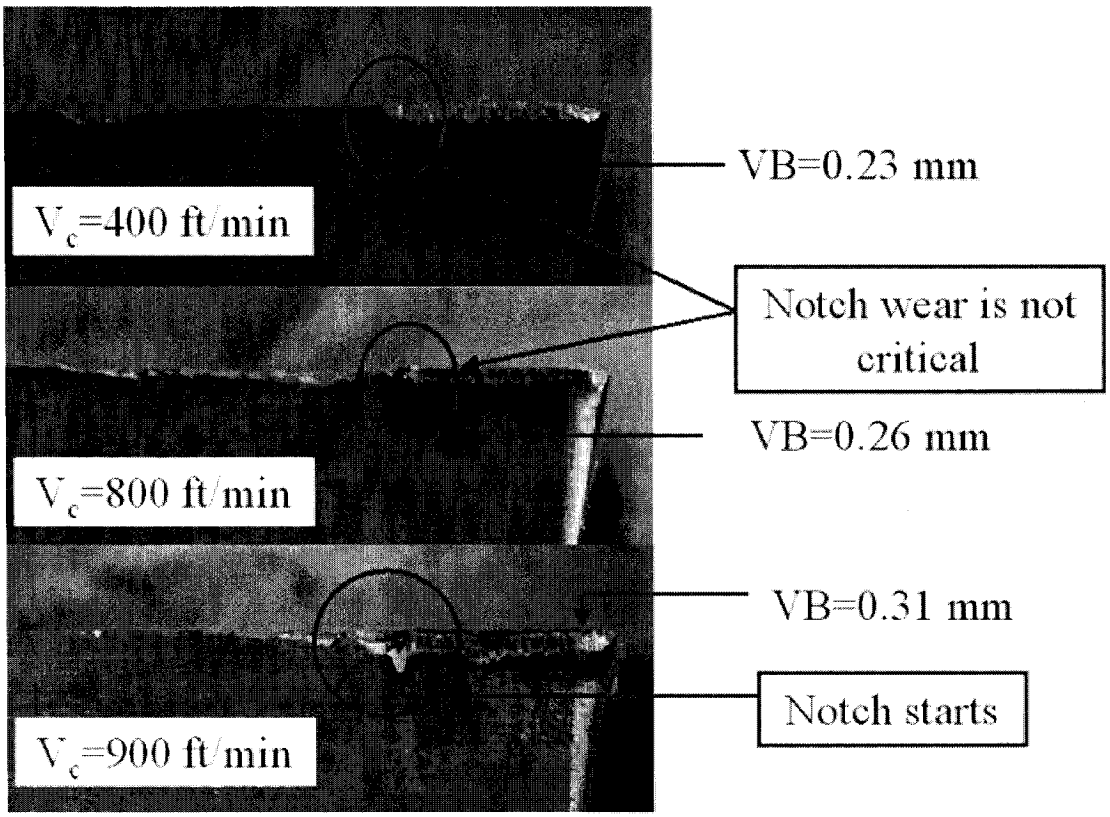

Figure 6.1. Notch wear variation in function of the cutting speed after 7 min

According to the tool wear standards ISO 3685:1993F, the acceptable notch wear for a ceramic tool is 0.6 mm, it is the same as for a carbide tool. Figure 6.2 indicates that this value of 0.6 mm is not reached after 7 min of machining even at 900 ft/min.

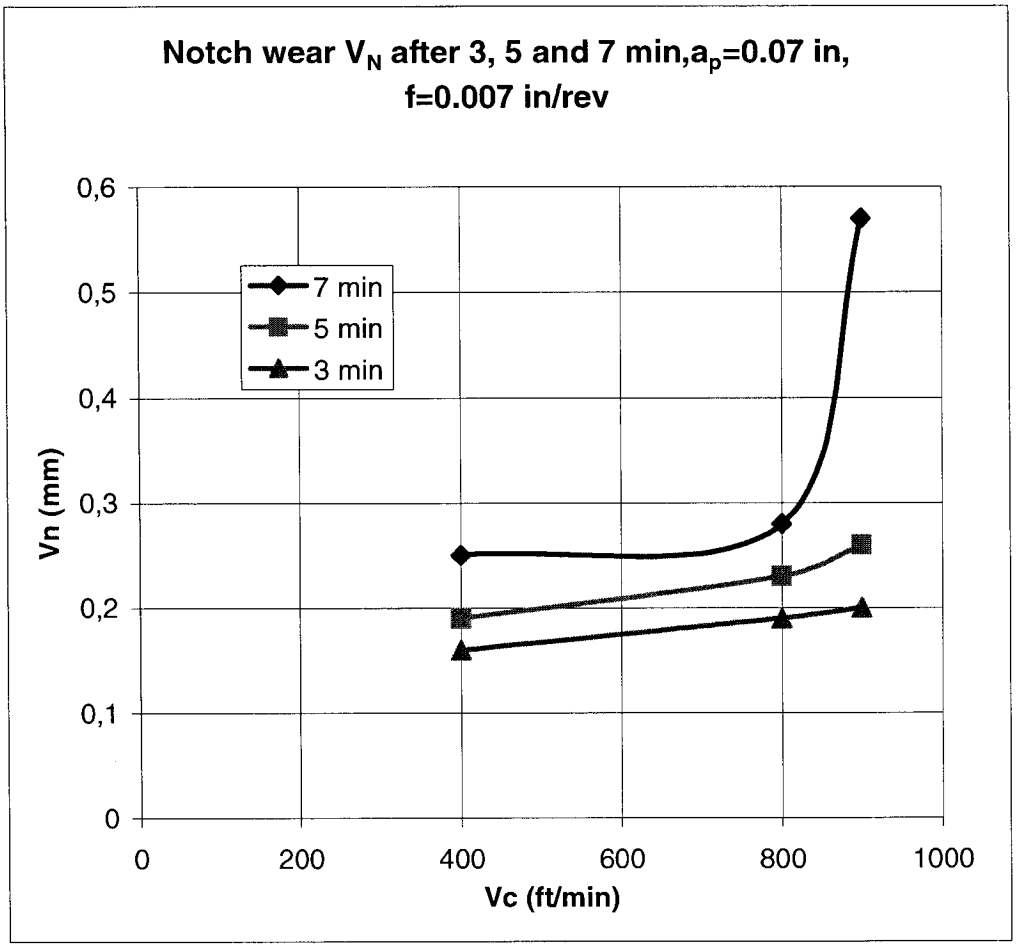

Figure 6.2. Notch wear V_N for different machining time in function of cutting speed

Let now consider the average flank wear VB. The tool life curve (Figure 6.3) shows that around 900 ft/min, the tool life is about 7 min for a_p=0.07 in, f=0.007 in/rev.

The tool is then supposed to be worn after 7 min in this case according to the VB criterion, but according to the notch wear criterion the tool is still good.

It can be deduced that for the Inconel 718 (sample 1), for a depth of cut of a_p=0.07 in, feed f=0.007 in/rev, and for a cutting speed in the range of 400 ft/min to 900 ft/min, the notch wear is not critical.

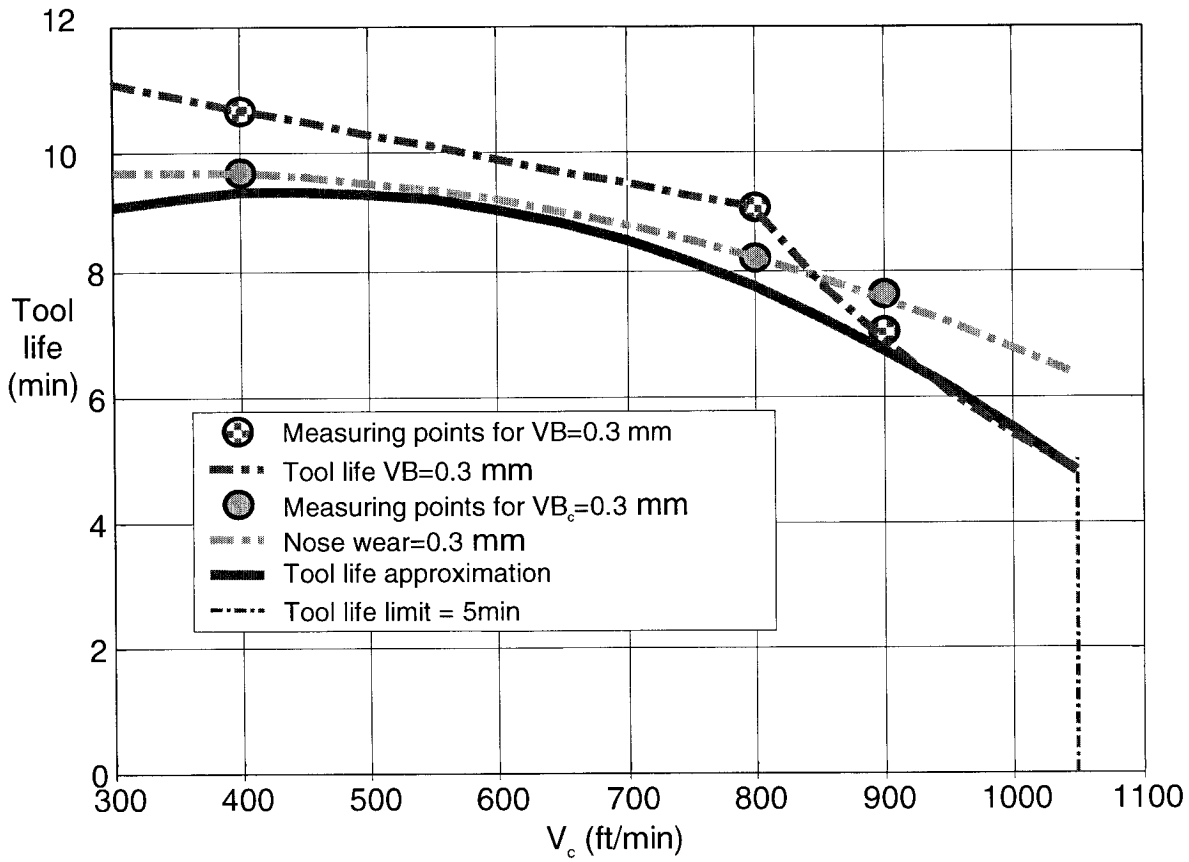

Figure 6.3. Tool life as a function of cutting speed a_p=0.07 in, f=0.007 in/rev

During the tests, the importance of the nose wear on the tool life was also noticed. Nose wear VB_c seems to be higher than flank wear VB above 850 ft/min (Figure 6.3).

The feed was increased from f=0.007 in/rev to f=0.009 in/rev, for the cutting speed V_c=900 ft/min to estimate the tool life. Figure 6.4 shows the reduction of tool life when the feed is increased.

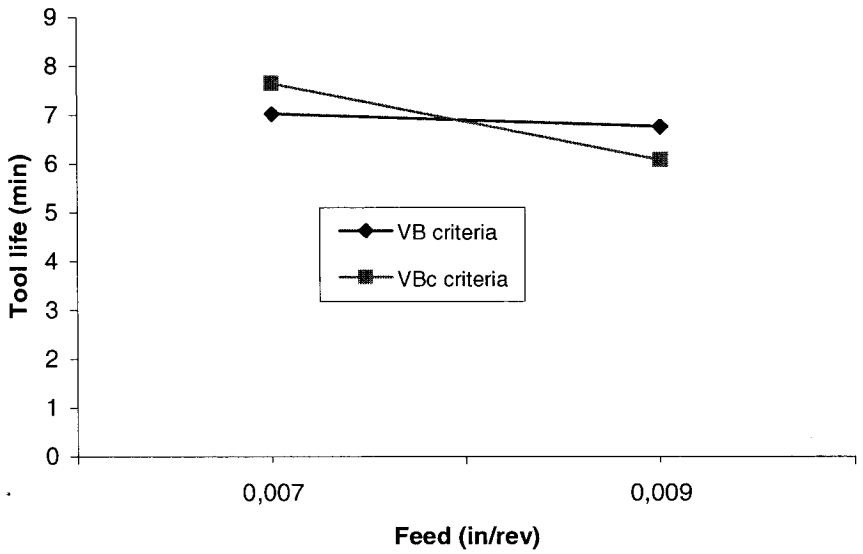

Figure 6.4. Tool life as a function of feed with a_p=0.07 in, Vc=900 ft/min

In order to find the variables that could affect this nose wear, the effect of feed was tested with a smaller depth of cut.

6.1.1.1 The effects of feed on the nose wear for a small depth of cut

The small depth of cut machining with a_p=0.0175 in is a test in the semi finished conditions. To estimate the effects of feed on the nose wear, the same cutting tool in the following conditions is used:

a_p=0.0185 in , Vc=800 ft/min, and 3 different values of feed, f=0.005 in/rev, f=0.007 in/rev, and f=0.009 in/rev, Figure 6.5. The data can be found in appendix III Table 29 page 186.

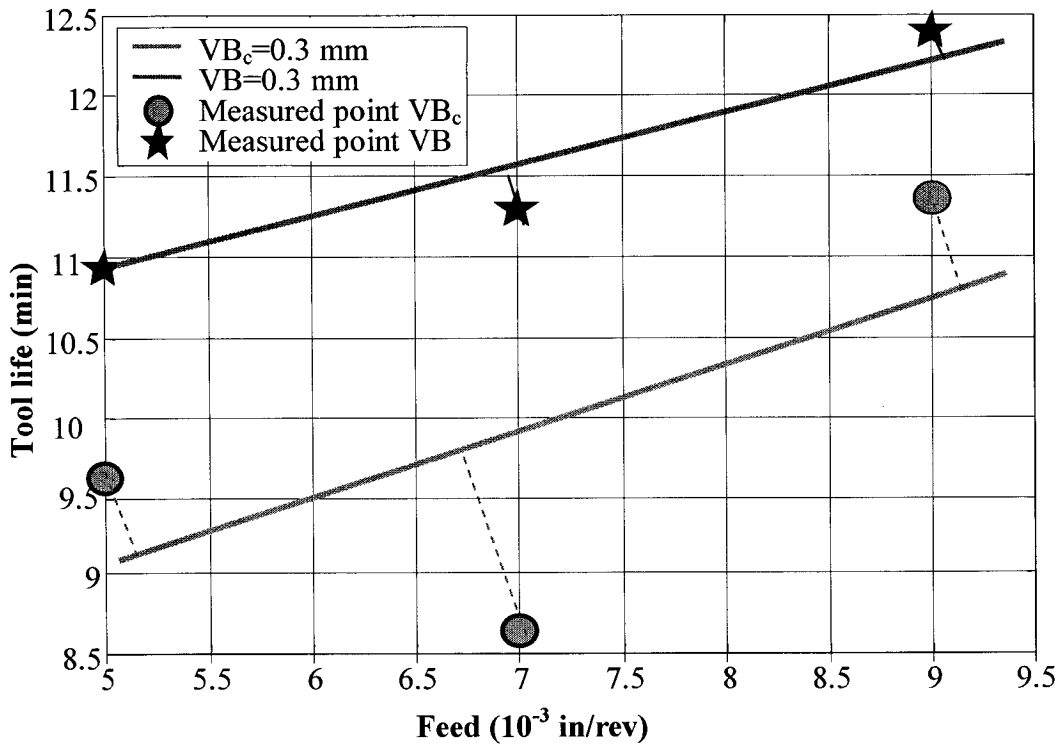

Figure 6.5. Tool life as a function of feed, for V_c=800 ft/min, a_p=0.0175 in

The tool life increases when the feed increases for both nose wear and flank wear criteria.

The feed was limited to 9 in/rev because of the surface quality and the chip which were bad above this value.

Figure 6.6 shows the wear VB variation as a function of feed for 3 machining times, 1, 4.5 and 7 min. the column 7 min shows a decrease of wear variation, from VB=0.21 mm for f=0.005 in/rev, to VB=0.20 mm for f=0.007 in/rev and VB=0.19 mm for f=0.009 in/rev.

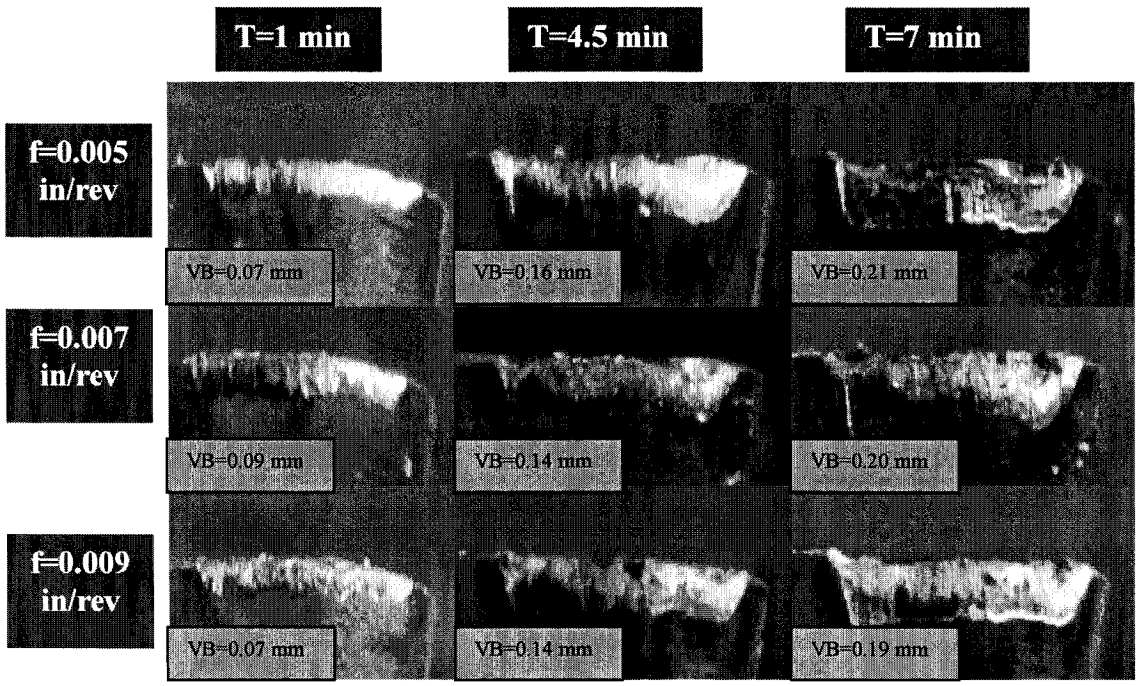

Figure 6.6. Effects of feed on the tool flank wear, with a_p=0.0175 in, Vc=800 ft/min

For the smaller depth of cut, the tool life with the VB criterion seems to increase with feed, but this phenomenon is not the same for the higher depth of cut. For higher depth of cut (more than the tool radius 0.031 in) the tool life decreases with feed, Figure 6.4.

But when looking at the crater (Figure 6.7), the crater width increases with feed while the flank wear decreases. It's a kind of compensation.

Figure 6.7 shows 9 pictures of crater wear for 3 different values of feed at 3 different machining times (1min, 4.5 min and 7 min).

The result shows an increase in crater width when the cutting feed increases despite the cutting time.

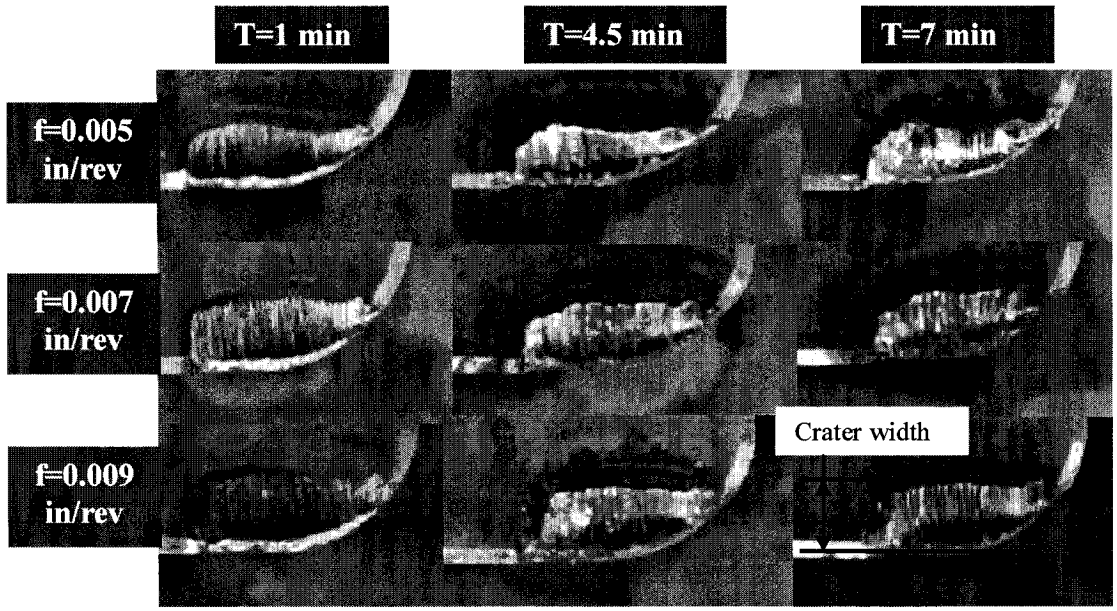

Figure 6.7. Effects of feed on the tool crater wear, with a_p=0.0185 in, Vc=800 ft/min

6.1.1.2 The effect of non stop long length machining

It was noticed in Figure 6.1 that notch wear increases with the cutting speed. That can be due to the effect of heat. If the heat has an effect on notch wear, it is necessary to determine if the time the cutting edge passes in the material could affect its wear.

For example if a test has to be done for 1 min, it is possible to machine a non stop 1 min, or to do the same machining time of 1 min in many steps (2, 3 4,...times).

In this last case, the tool has to be removed from the material as many times as the total machining time is divided.

The Figure 38 is a result of an experiment of long length and different short length machining.

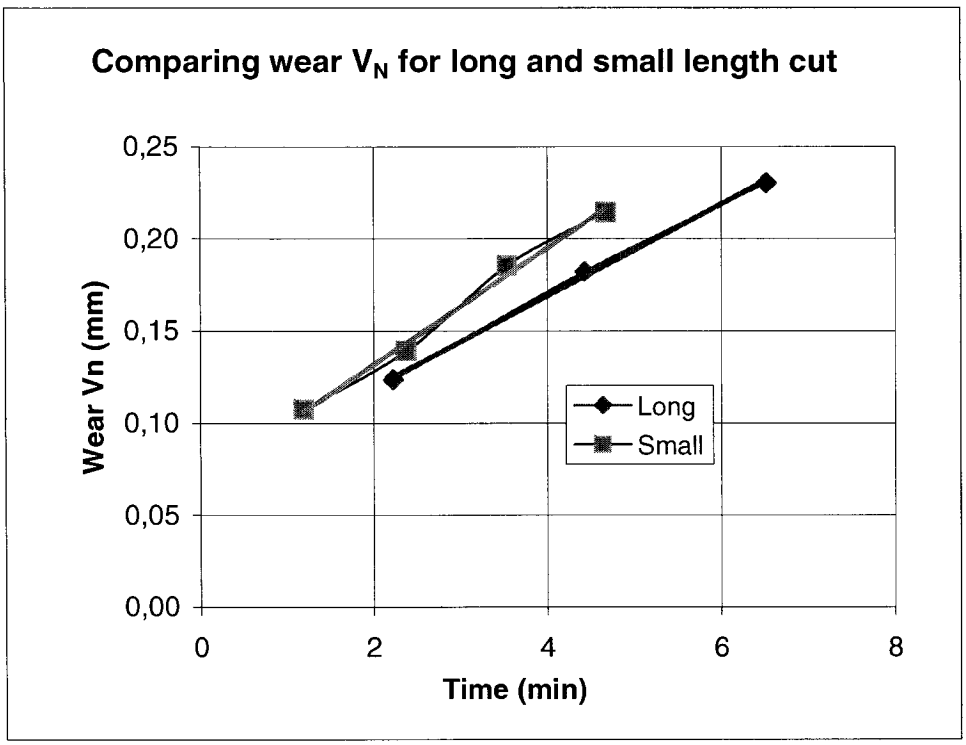

Figure 6.8. The effect of non stop machining on notch wear (V_N), comparison of long length and different small lengths machining a_p=0.07 in, V_c=800 ft/min, f=0.007in/rev.

A tool wear was measured each 2.2 min for long length machining, and each 1.1 min for small lengths (Figure 6.8). When comparing the results after 2.2 min and 4.4 min machining of both situations, the deduction was clear that machining the same length in many steps increases the notch wear. It is therefore better to make a non stop machining instead of making small steps.

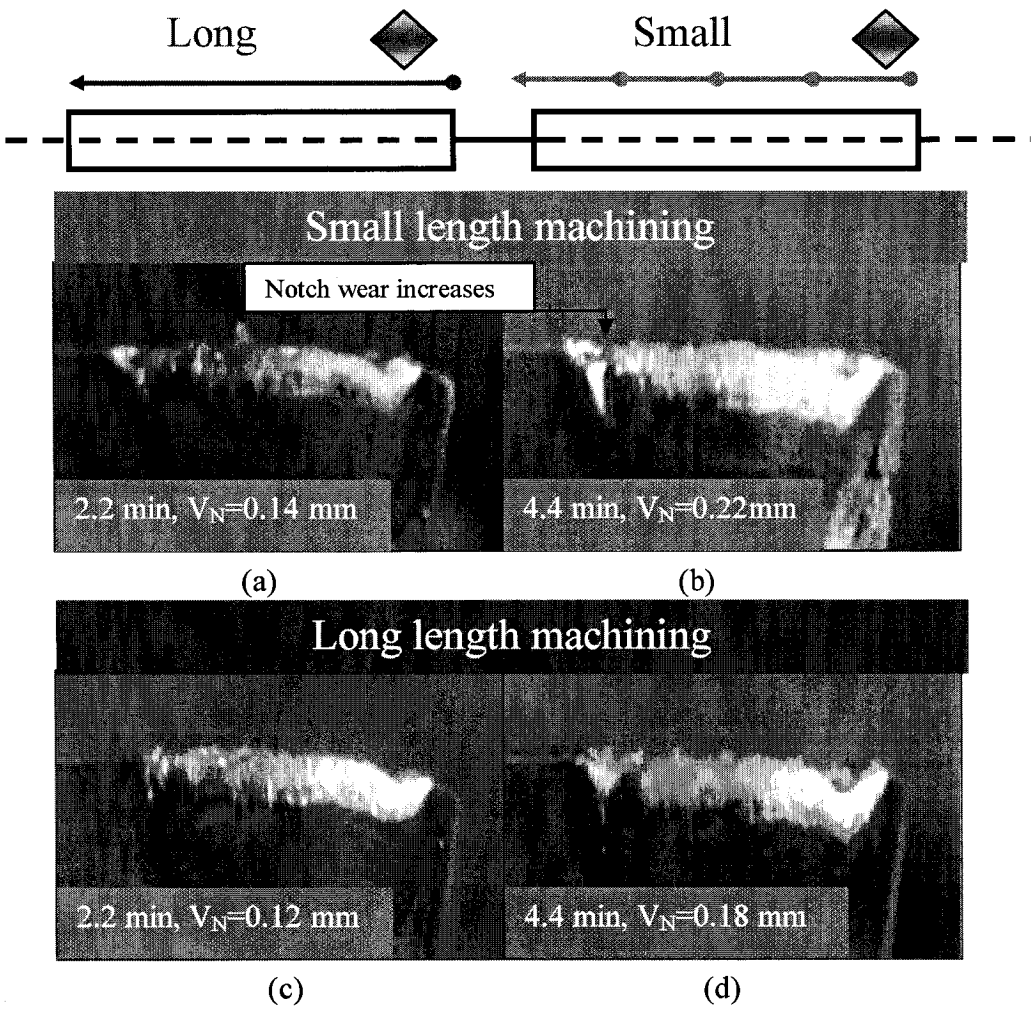

Figure 6.9. Notch wear (V_N) comparison of long length and different small lengths machining a_p=0.07 in, V_c=800 ft/min, f=0.07 in/rev.

It was expected to be the contrary, because a non stop machining means a longer tool-workpiece contact, thus increase of heat effect on the tool. But the experimental results show that the number of times a tool enters the material has also an effect on the notch wear. Figure 6.9 shows photos of the worn tools.

6.1.1.3 The chip shapes

The chip plays an important role during the machining of Inconel 718. As it was shown in the literature review, machining of Inconel 718 gives abrasive chips. It is important to establish a good chip shape domain. A more fragmented is preferable.

a) Continuous chips

The continuous chip is observed in the range of cutting speed from 500 to 900 ft/min and a feed from 0.005 to 0.009 in/rev. The chip abrasiveness may damage insert free corners even if they are not cutting, Figure 6.17.

When the feed and the cutting speed are high, the temperature increases and the chip becomes breakable.

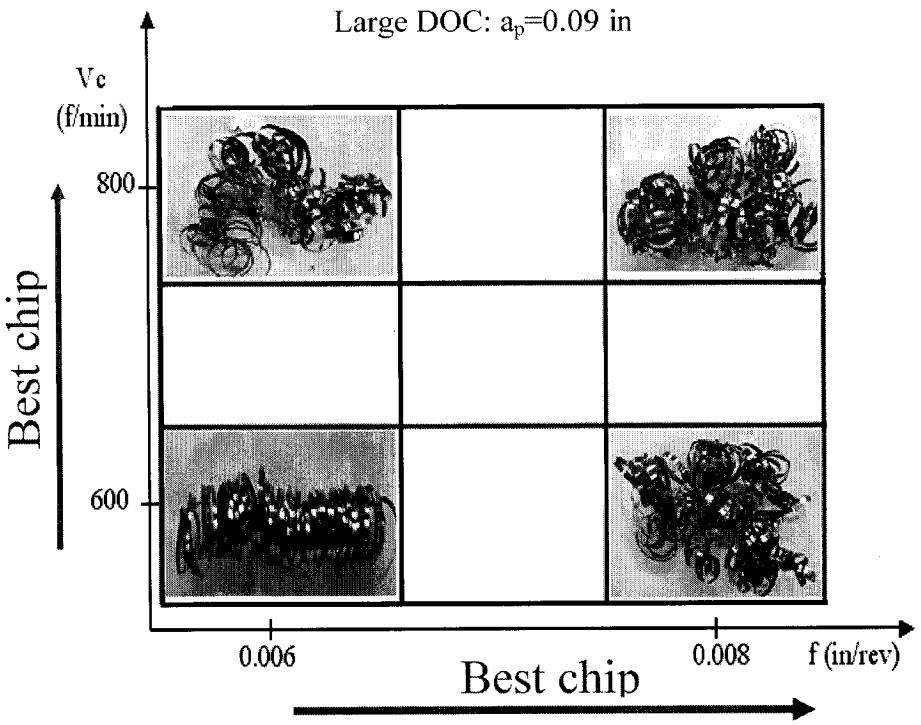

Figure 6.10. Continuous chip with depth of cut a_p=0.09 in

Figure 6.10 indicates that the worst chip occurs when both the feed and the cutting speed are low, and the better chip appears when both variables are at their highest values. The same result is shown on the Figure 6.11 with a depth of cut of a_p=0.05 in.

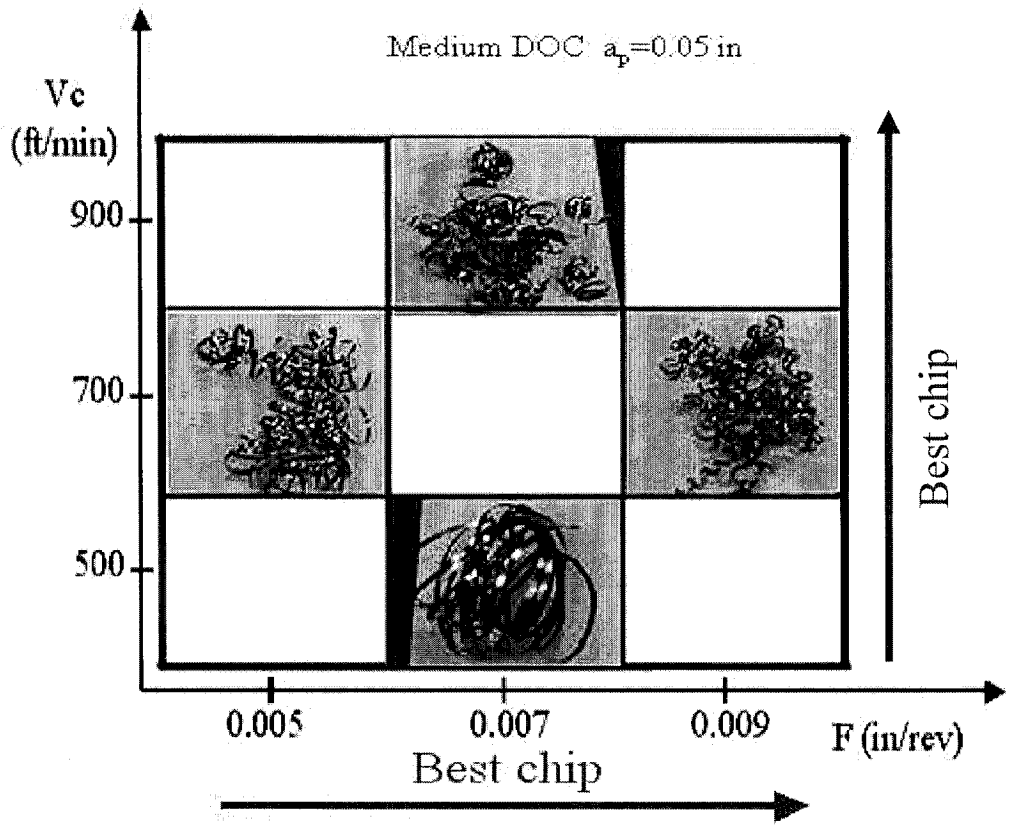

Figure 6.11. Continuous chip with depth of cut a_p=0.09 in

b) Superimposed chip

Around the cutting speed of 900 ft/min, with a feed of 0.009 in/rev, a different type of chip appears. That chip is a superimposed chip, Figure 6.12 and 6.13.

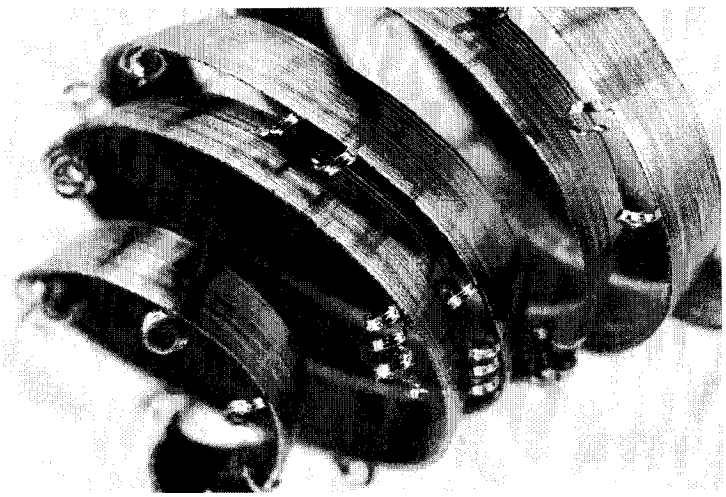

Figure 6.12. Superimposed chip Vc=900 ft/min, ap=0.07 in, f=0.007 in/rev

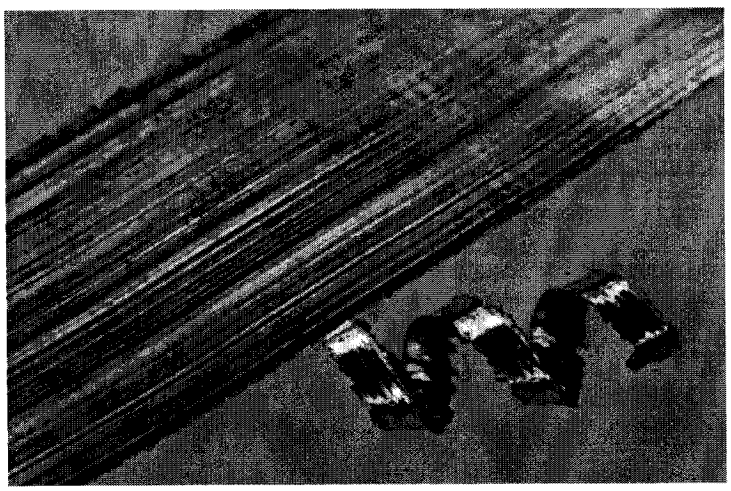

Figure 6.13. Superimposed chip V_c=900 ft/min, a_p=0.07 in, f=0.007 in/rev

The phenomena causing this new chip appearance are not known. However the appearance of this type of chip coincides with a poor surface quality, Figure 6.14.

It appears that, the superimposed chip comes from the removal of material on the workpiece surface, creating thus a bad surface quality.

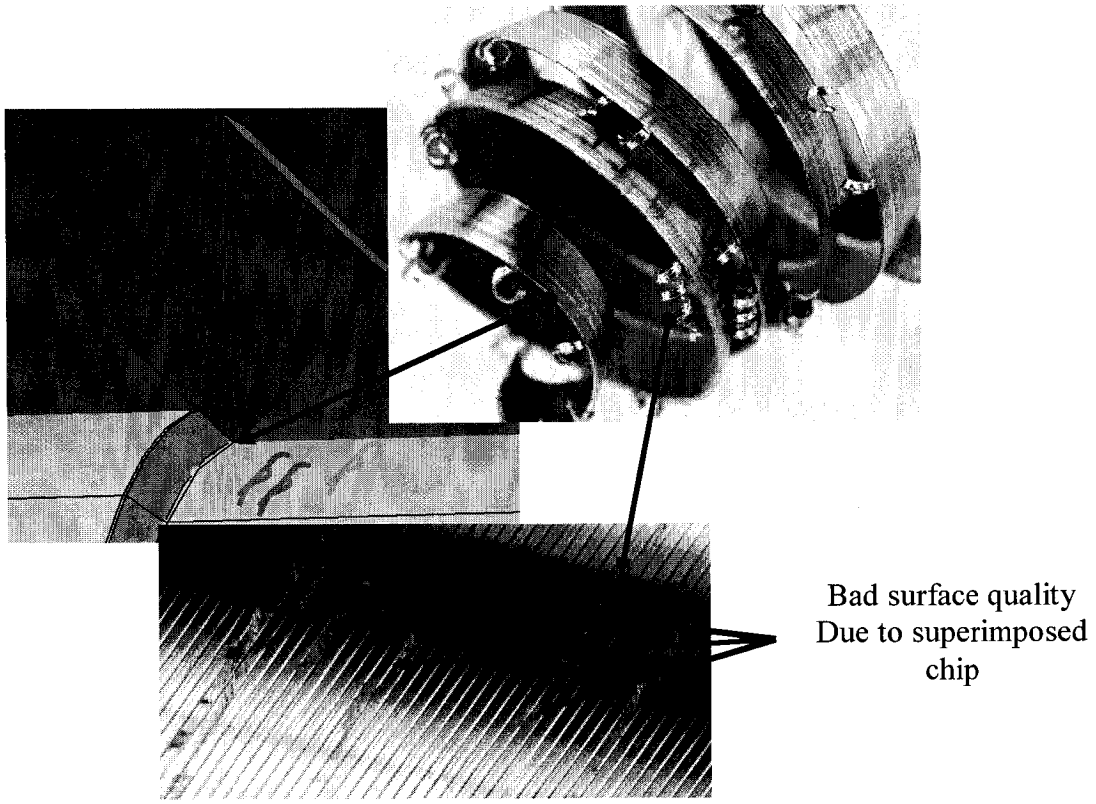

Figure 6.14. The superimposed chip and the surface quality

c) The saw type chip

A saw type chip in Figure 6.15 was observed at higher cutting speed (V_c > 900 ft/min) and higher feed (around 0.009 in/rev). This type of chip seems to come from the sideward deformation of the chip because of high constrains (temperature and stress) Figure 6.16.

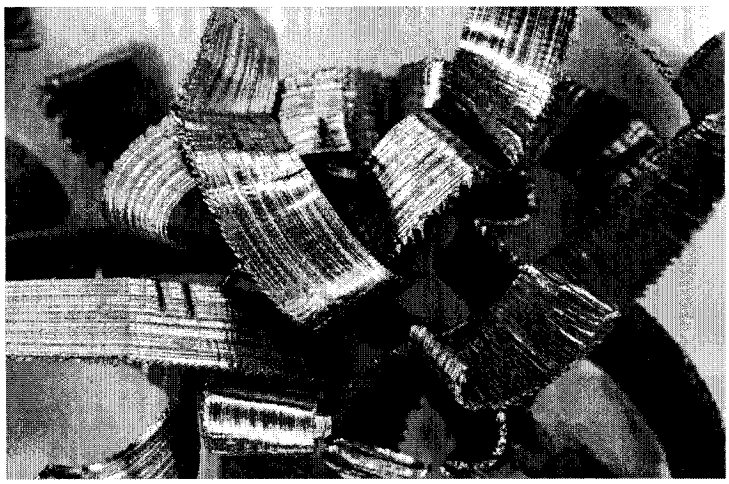

Figure 6.15. Fragmented saw type chip (V_c=900 ft/min, a_p=0.07 in, f=0.009 n/rev)

The appearance of this type of chip is good for the machining because the insert free corners are less worn. If not, when the chip is continuous, the other free corners of the square insert may be worn out by the abrasive action of continuous chips even if they are not directly involve in cutting, as shown in Figure 4.17. The saw type chip does not produce this phenomenon. However, the surface quality and the tool life decrease rapidly in this domain.

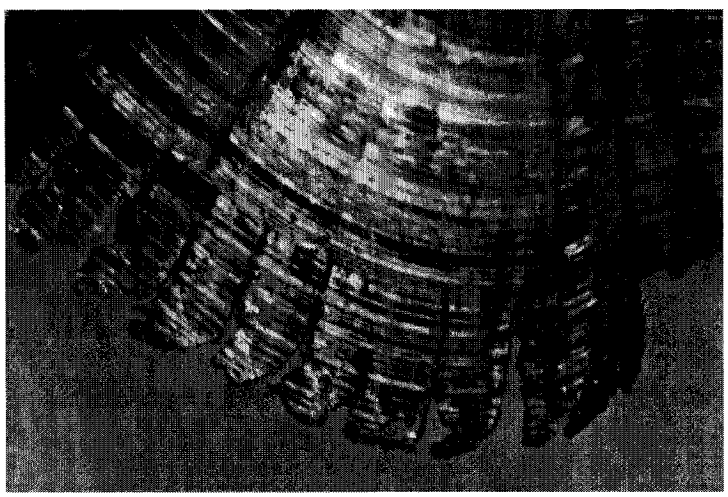

Figure 6.16. Saw type chip (Vc=900 ft/min, a_p=0.07 in, f=0.009 n/rev)

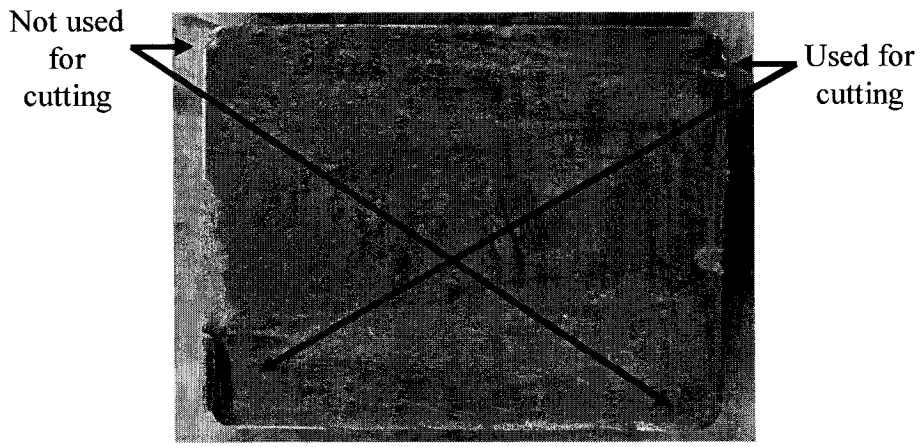

Figure 6.17. The other free corners of the square insert may be worn by chip even if not directly involve in cutting.

d) The roller type chip (spiral tubular chips)

The spiral tubular type of chip appears during machining of Inconel 718 at about the same conditions where the fragmented saw type chip appears, Figure 6.18.

Around the cutting speed of V_c= 900 ft/min and the feed of f=0.009 in/rev, the chip formation is not stable. A slight change in cutting conditions (cutting diameter, coolant direction) may affect the chip shape.

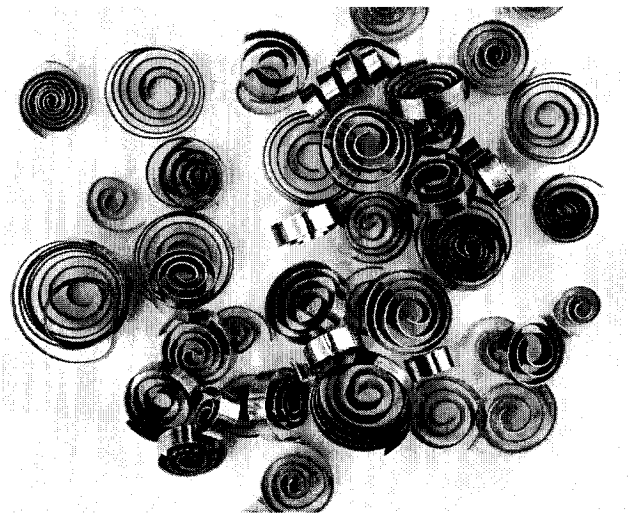

Figure 6.18. The type chip Vc=900 ft/min, a_p=0.07 in, f=0.009 in/rev

During the test, a significant change in chip shape during the same cutting operation happened frequently. Figure 6.19 shows this phenomenon.

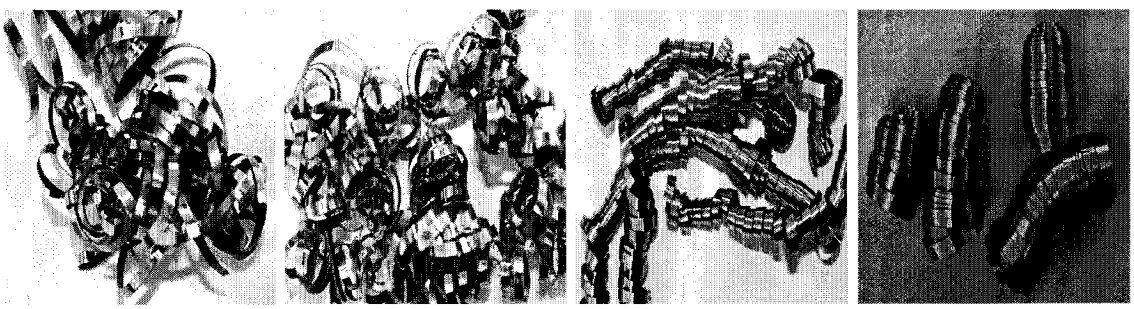

Figure 6.19. Significant change in chip shape with cutting time Vc=900 ft/min, f=0.007 in/rev, a_p=0.07 in

e) The chip shapes diagram

Figure 6.20 shows that from 400 ft/min to 800 ft/min the chip remain continuous from a feed of 0.007 to 0.009 in/rev. At about 900 ft/min, the chip is still continuous when the

feed is low 0.007 in/rev. At this point there is the phenomenon of superimposed chips. When the feed increases to 0.009 in/rev the chip is fragmented.

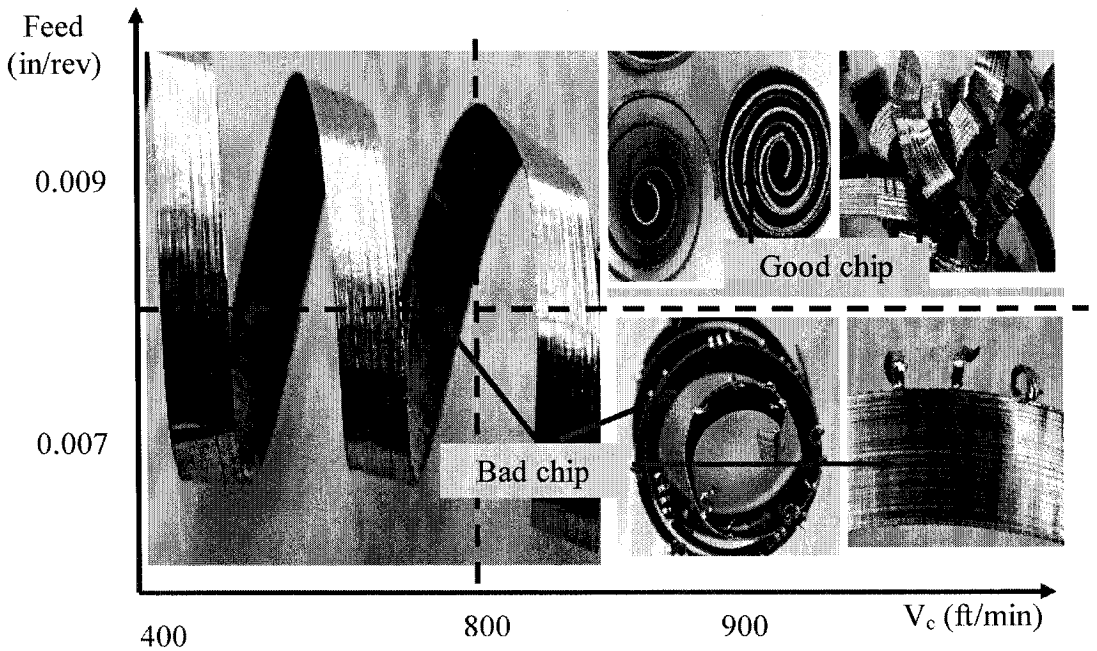

Figure 6.20. The chip diagram for a_p=0.07 in

f) The small depth of cut chip shape

When the depth of cut is small (less than the tool radius 0.031 in) the chip evacuation is not a major problem, Figure 6.21.

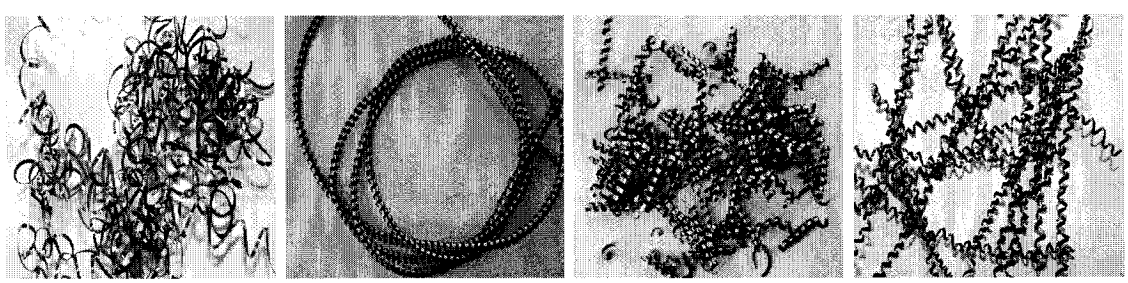

Figure 6.21. Chip shape variation with time for a small depth of cut Vc= 900 ft/min, f= 0.007 in/rev, a_p=0.0175 in

Figures 6.21 and 6.22 show the phenomena of chip shape change during machining. The continuous uncut chip is mostly observed during the early stages of cutting. After about 2 minutes of machining the chip starts to break. When the tool is near to the end of its life, the long continuous chip appears again.

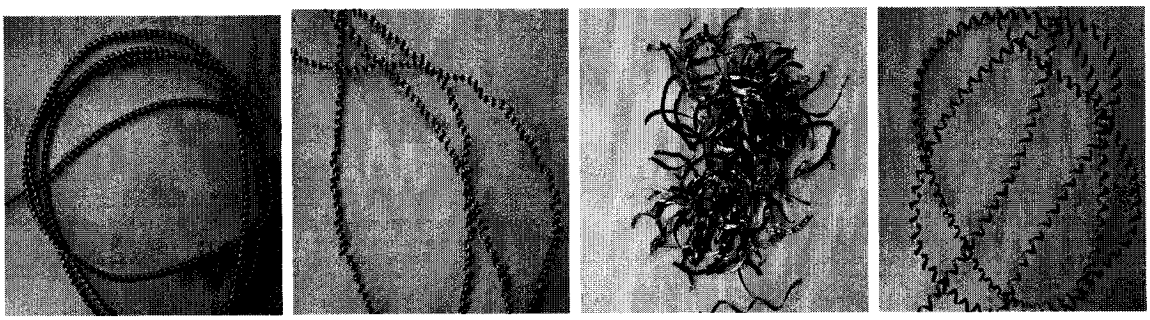

Figure 6.22. Chip shape variation with time for a small depth of cut Vc= 800 ft/min, f= 0.005 in/rev, a_p=0.0175 in

The heat effect and the tool wear are some variables to consider when investigating these changes.

But all these different chip shapes does not significantly affect the tool behavior and its life, since the depth of cut is small and the chip movement around the insert is negligible.

6.1.1.4 The layer effect on notch wear

The results of the machining for Sample 1 indicate that notch wear is not a major problem. The cutting conditions can then be easily established according to the chip diagram (Figure 6.20) and the tool life (Figure 6.3).

But the initial layer showed a different notch behavior, Figures 6.23 and 6.24.

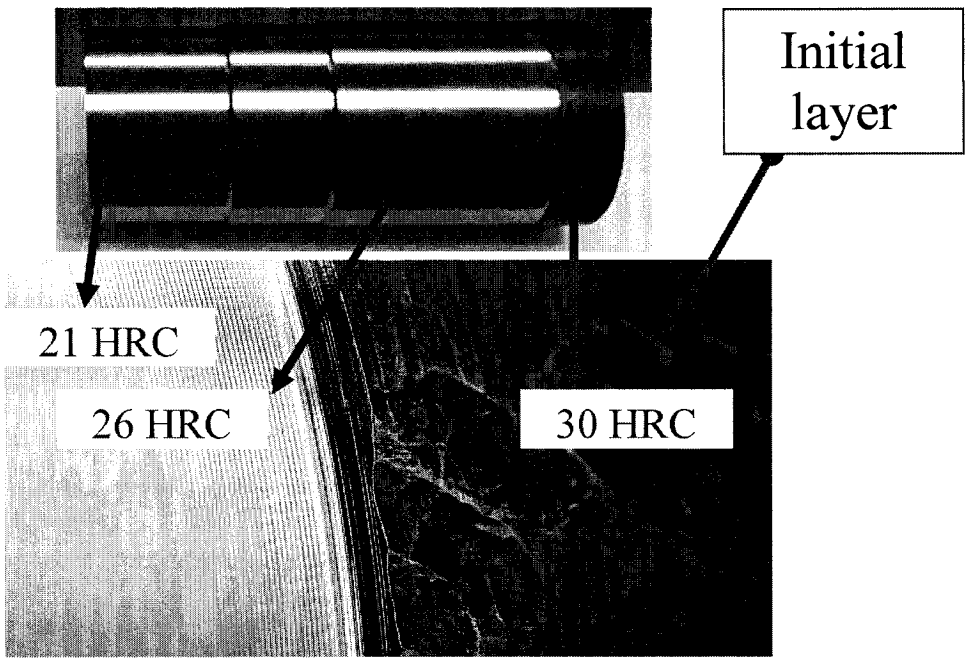

Figure 6.23. Hardness variation on the rough material

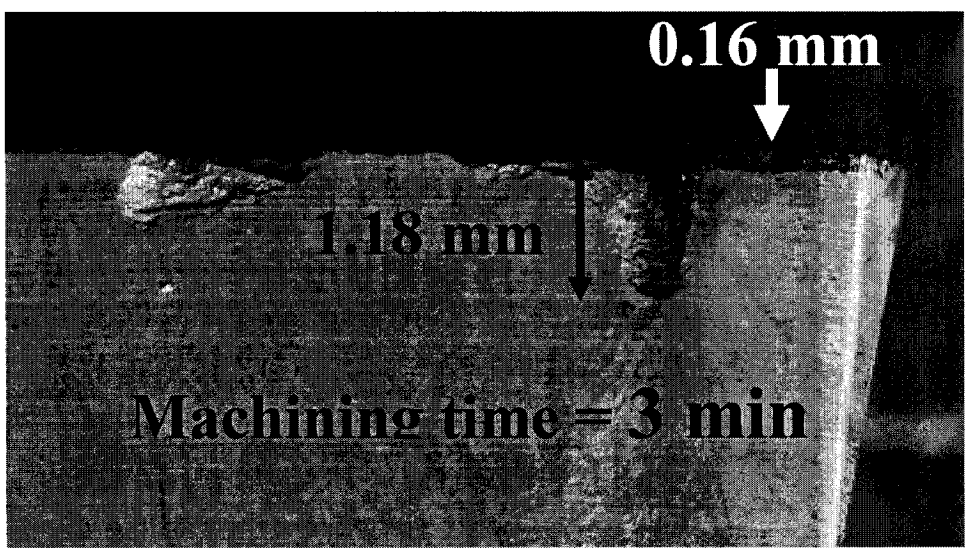

Figure 6.24. Large notch wear when machining the initial layer (V_c=600 ft/min, f=0.006 in/rev, a_p=0.05 in)

The results in Figure 6.1 page 74 indicate that notch wear increases with cutting speed, and at a cutting speed of V_c= 800 ft/min and feed f=0.007 in/rev, the notch wear is not critical. But the results of Figure 6.24 (V_c=600 ft/min, f=0.006 in/rev), is in contradiction with the previous ones.

Therefore many hypotheses may be stated like for example the effect of material hardness.

6.1.1.5 Conclusion of the Inconel 718 sample 1 tests

The conclusion is that the initial layer in this case doesn't have the same behavior than the other parts of the material. The tool life is then reduced to 3 min, instead of 6 to 7 min for the other part of the material in the same conditions.

It's important to notice on Figure 6.24 that, the average flank wear is 0.16 mm, less than 0.3 mm (the standardize VB limit) while the notch wear is about 1.18 mm, more than 0.6 mm, the standardize notch wear limit.

Therefore it should be possible to find a way to reduce the notch wear V_N beyond its limit, while keeping an acceptable average flank wear VB. The tool life will than be evaluated according to this flank wear VB. The tool life can then be increased. The ramping technique results will be discussed in the section 6.2 of this chapter.

6.1.2. The constant depth of cut tests with sample 2

Table 11 page 68 summarizes the tools and their different materials and geometries used for the test. The first set of test is carried out with the tool model (1), (2), (3), (8) and (9). Table 15 shows the results of the tests. For more details see Appendix III page 182-185.

Table 15: Cutting results

Item	Insert	Tool life (min)	MRR (in^3/min)	Volume (in^3)	Cost ($/$in^3$)
(3)	1-KY1540	1,0	5,29	5,29	1,94
(3)	2-KY1540	4,4	2,10	9,2	1,09
(9)	GA 5026	6,6	1,35	9,0	0,83
(8)	KC5010	7,9	1,35	10,7	0,70
(1)	R-WG 300	5,1	5,29	26,8	0,37
(2)	S-WG 300	6,8	5,29	35,9	0,28

Figure 6.25 indicates that square ceramic whisker S-WG 300 is by far the best cutting tool from the economic point of view (minimum $ per cubic inches), and also for the productivity (maximum volume of material per edge).

It is also clear that the cost per cubic inches removed is lower for a carbide tool than for a mixed ceramic tool. The reason is a lower cost for the carbides, and the fact that the mixed ceramic tools performances are not much higher than that of carbides.

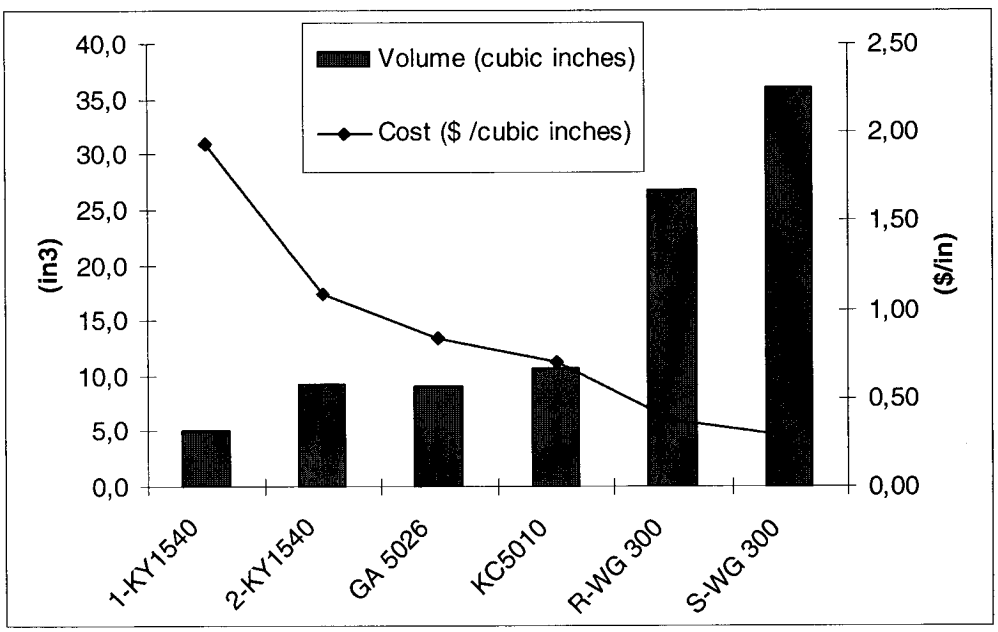

Figure 6.25. Volume of material removed per edge and the cost per cubic inches

Figures 6.26, 6.27, 6.28 and 6.29 show respectively some test results for the R-WG 300, 2-KY1540, GA 5026 and KC5010.

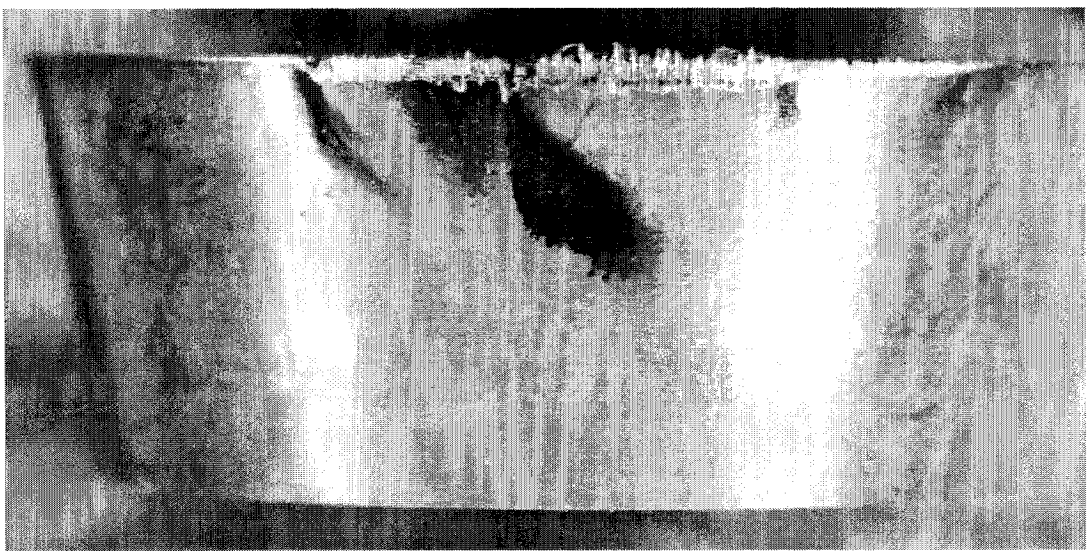

Figure 6.26. Round ceramic whisker R-WG-300 Vc=900, f=0.007, ap=0.07, after 5.2 min, VB=0.31 mm

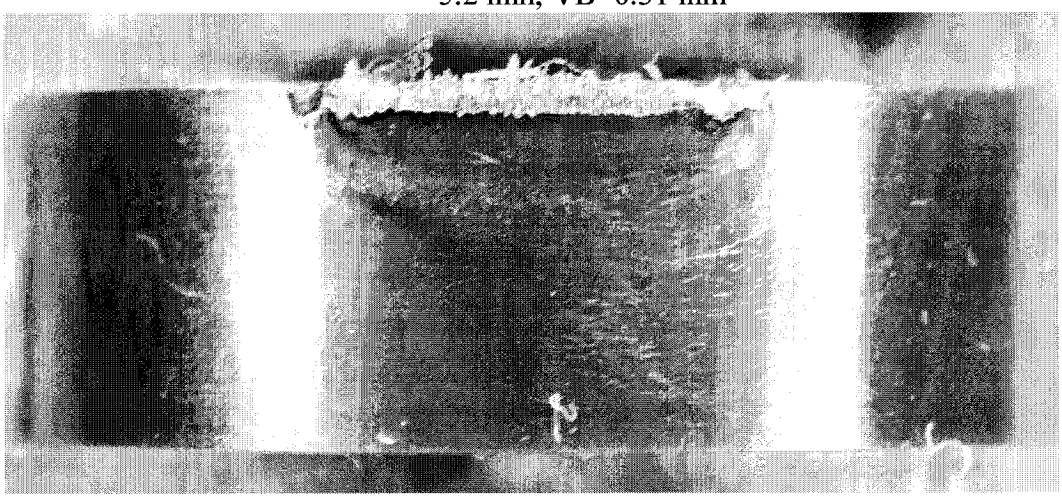

Figure 6.27. Round ceramic 2-KY 1540 Vc=500, f=0.005, ap=0.07, after7min, VB=0.38 mm

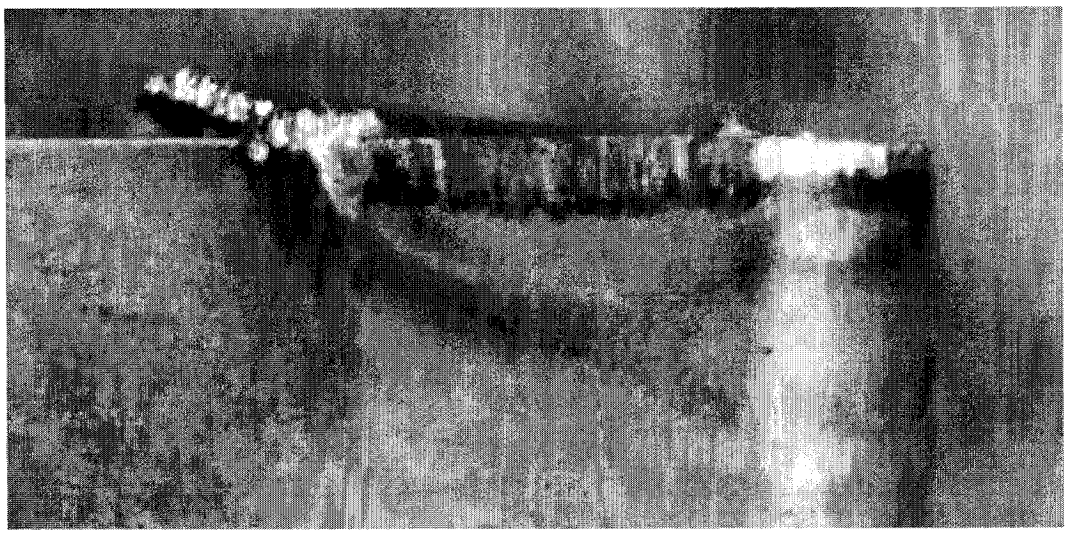

Figure 6.28. 80 degree carbide GA 5026, Vc =230 ft/min, f=0.007in/rev, ap=0.07in, after 5.2 min, VB=0.25 mm

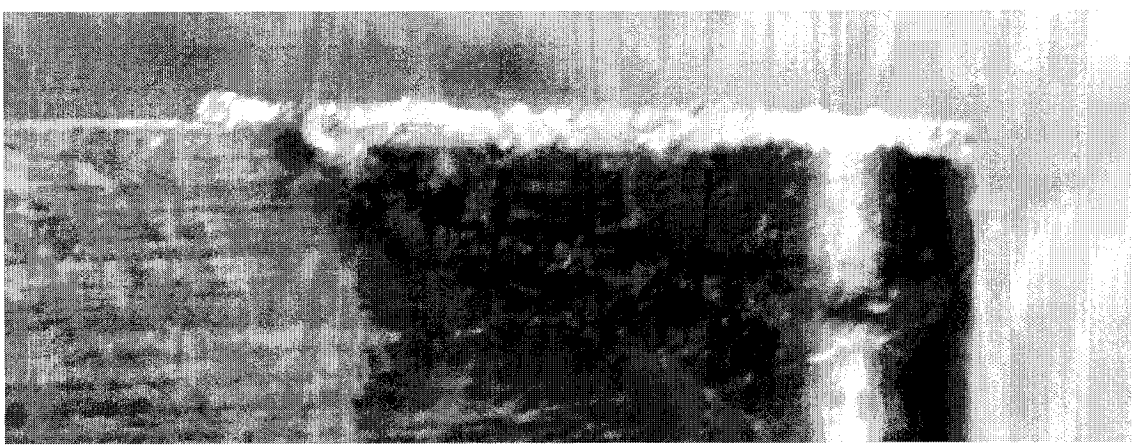

Figure 6.29. 80 degree carbide KC 5010, Vc =230 ft/min, f=0.007in/rev, a_p=0.07in, after 2.6 min, VB=0.16 mm

6.1.2.1 The S-WG 300 whisker ceramic (best tool performance)

The tests at the cutting speed of V_c =900 ft/min, and V_c=1000 ft/min confirm the fact that notch wear increases with cutting speed, Figures 6.30, 6.31 and 6.32.

Notch wear was not supposed to be critical for the first sample, while for the second sample it is.

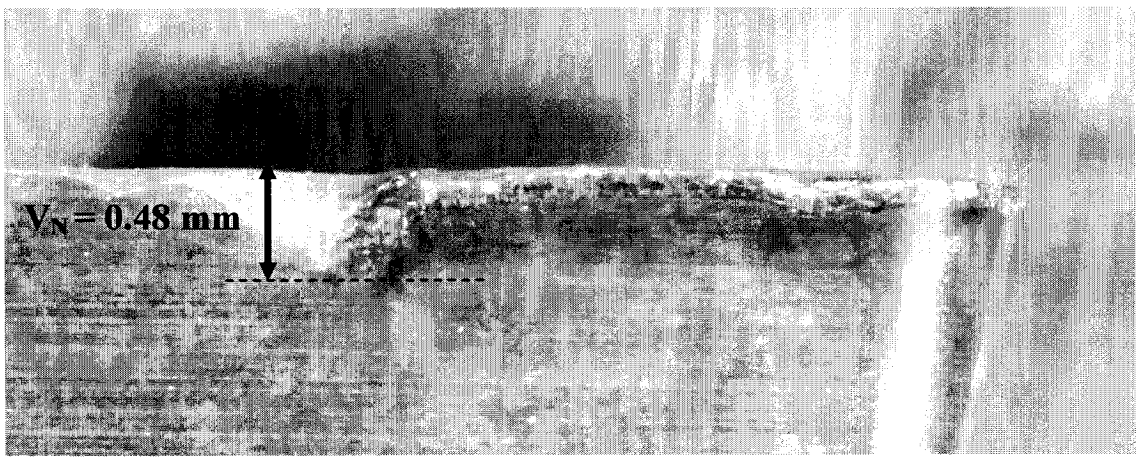

Figure 6.30. Sample 2, S-WG 300 ceramic, V_c=900 ft/min, a_p=0.07 in, f=0.007 in/rev, after 3.8 min V_N=0.48 mm

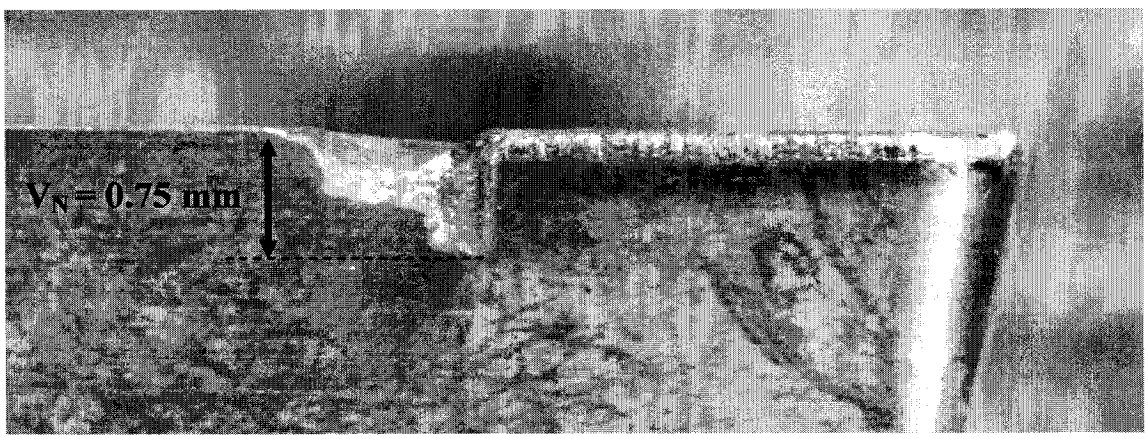

Figure 6.31. Sample 2,V_c=1000 ft/min, a_p=0.07 in, f=0.007 in/rev, after 3.5 min, V_N=0.75 mm

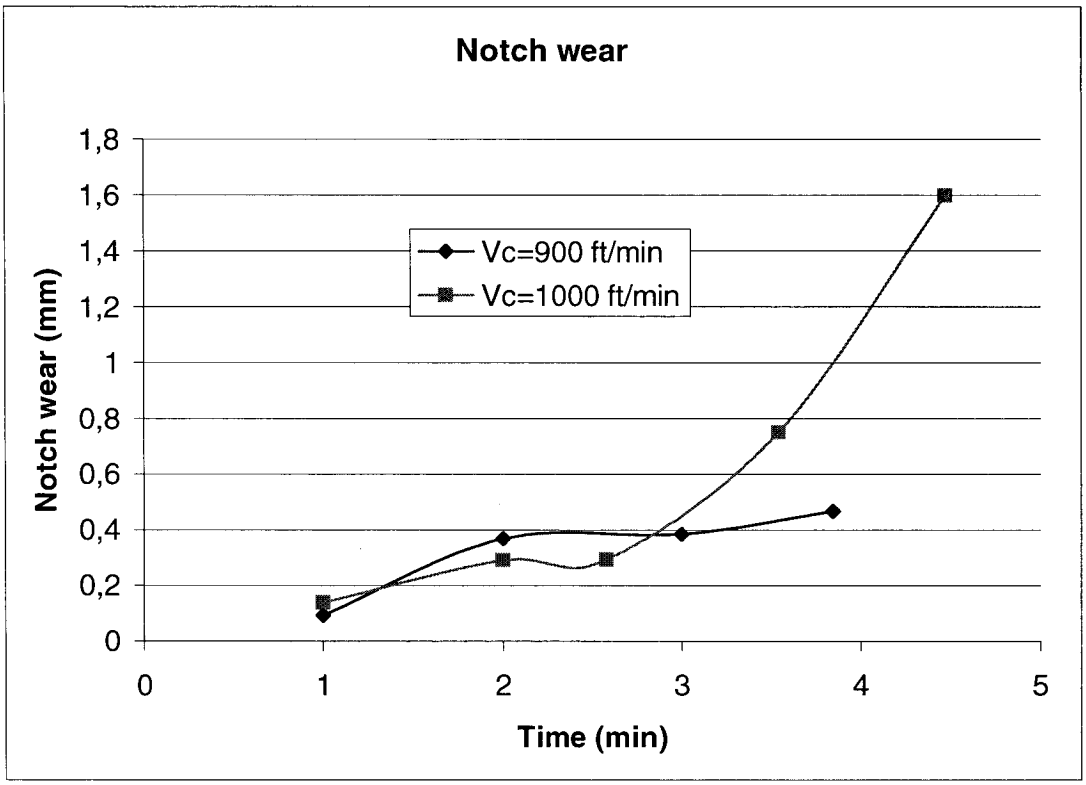

Figure 6.32. Sample 2, notch wear evolution for V_c=900 ft/min and V_c=1000 ft/min, a_p=0.07 in, f=0.007 in/rev

Since the S-WG 300 square whisker ceramic has proven to be the best tool to machine Inconel 718 with the first sample and the second one a test was performed with this tool to compare the first and the second Inconel 718 sample. Figure 6.33 shows this comparison.

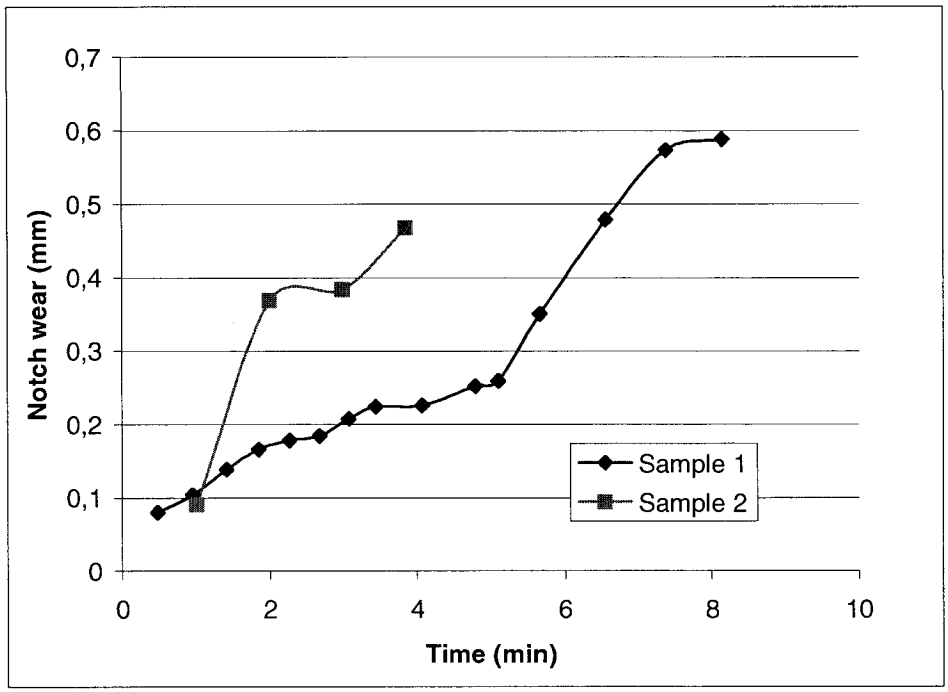

Figure 6.33. Notch wear comparison for Sample 1 and Sample 2 (V_c=900 ft/min, a_p=0.07 in, f=0.007 in/rev)

Figure 6.33 indicates that after 4 min the notch wear is about 0.48 mm for the Sample 2, while for the Sample 1, this value of notch wear is reached after about 6,3 min. However, the average flank wear VB is about the same for both Sample 1 and Sample 2, as shown on Figure 6.34.

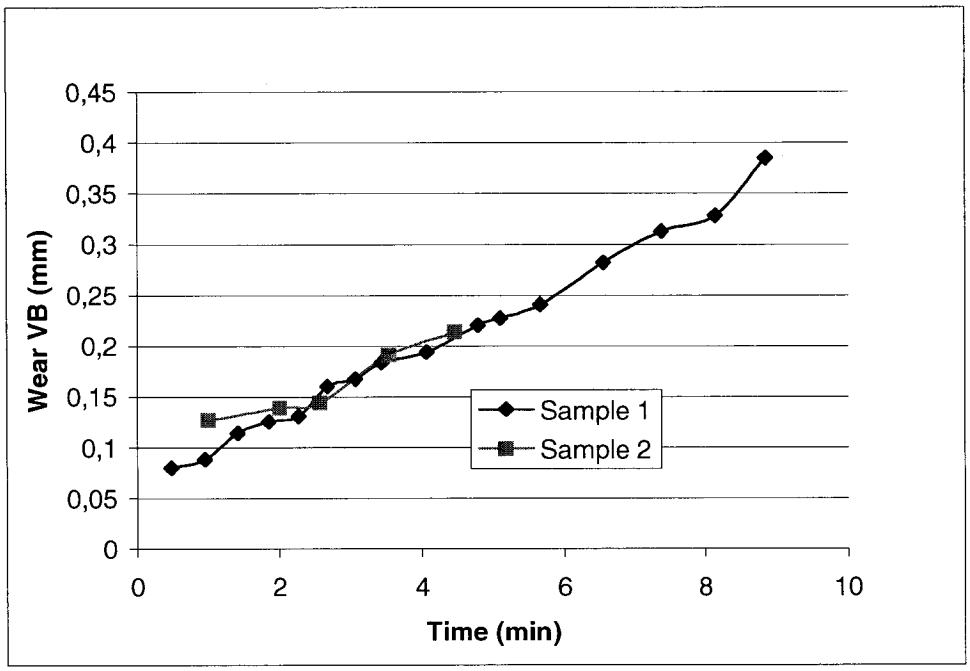

Figure 6.34. Average flank wear VB comparison for Sample 1 and Sample 2 (V_c=900 ft/min, a_p=0.07 in, f=0.007 in/rev)

To establish why both samples give different results regarding the notch wear, a hardness and a microstructure tests were performed.

6.1.3. Microstructure and hardness comparison of Inconel 718 Sample 1 and Sample 2

The previous tests were performed with 2 different Inconel 718 samples, called Sample 1 and Sample 2. Since both samples are supposed to be Inconel 718, the results should be the same. Unfortunately the notch wear evolution as function of time is not the same for both samples, while the average flank wear remain about the same.

A microstructure and a hardness test are performed for both samples for comparison.

6.1.3.1 The hardness test

The hardness test for Sample 1 gave a hardness variation from 21 HRC in the centre of the shaft to 30 HRC to the external diameter of 5 inches, Figure 6.35.

For the first sample the hardness was about 30 HRC on a layer of 0.05 inches width.

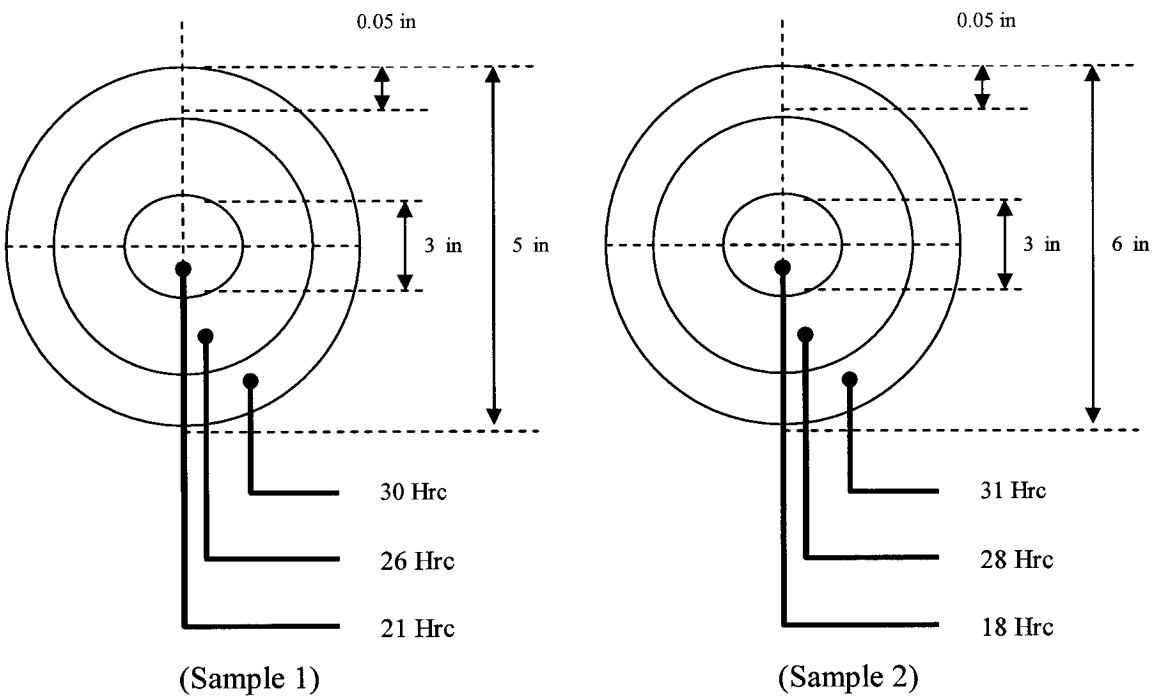

Figure 6.35. Sample 1 and 2 hardness test results

The hardness test for Sample 2 gave approximately the same hardness of 20 HRC in the centre of the shaft, and 31 HRC in the external diameter of 6 inches.

These two samples are then supposed to have the same hardness pattern.

This result is helpful to explain the difference of notch wear between both samples shown on Figure 6.33.

For the first sample the large notch observed in Figure 6.24 page 92 was obtained at the beginning of the tests when the diameter was about 5 inches, which is the zone where the hardness is about 30 HRC. But the following tests in Figure 6.1 page 74, where the notch wear was proven not critical, were carried out when the work piece diameter was about 2.5 to 3 in, that is where the hardness is about 21 to 22 HRC.

On the other hand, for Sample 2 Figure 6.32 where the notch wear reached a high value very quickly, is a result of a test performed at a diameter of 6 to 5 in. At this point, the hardness is about 31 HRC.

The conclusion about the hardness measurement and the results can than be drawn.

When the hardness is more than 30 HRC, the notch wear curve behaves like the Sample 2. Above this value, that is around 20 HRC the notch wear behaves like Sample 1. The average wear VB is about the same for both samples as shown in Figure 6.34. But it is difficult to find the critical value of hardness between 20 and 30 HRC where the notch effect start to be important.

That is why for an Inconel 718 sample, the notch wear behavior will be considered like Sample 2 (the worst) and the flank wear will be supposed to be like the Sample 1 or Sample 2.

6.1.3.2 The microstructure tests

A sample called (Petit) is taken on a portion of the Sample 1 of hardness 20 HRC (on the centre of the shaft) and another called (Grand) is taken on the second sample of hardness 30 HRC (on the layer at the diameter 6 in).

The analysis is made on a scanning electron microscope, Figure 6.36

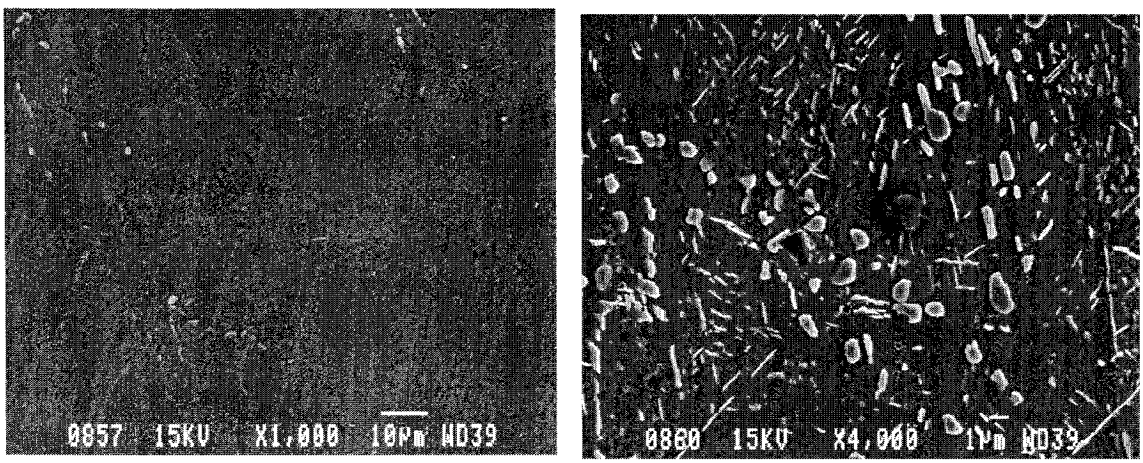

Presence of precipitates (white spots) Zoom on the precipitates

Figure 6.36. Sample Petit of hardness 20 HRC, on a Scanning Electron Microscope

The sample Petit shows a presence of precipitates. This result is not different from what is said in the literature review.

The composition of this sample shows a niobium rich particle, Figure 6.37.

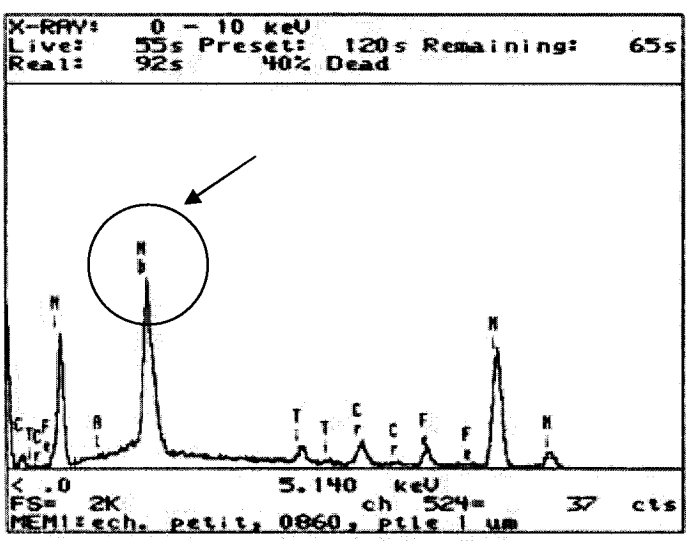

Figure 6.37. Niobium rich precipitate for the sample Petit.

Sample Grand microstructure is shown in Figure 6.38 with less precipitates in the matrix.

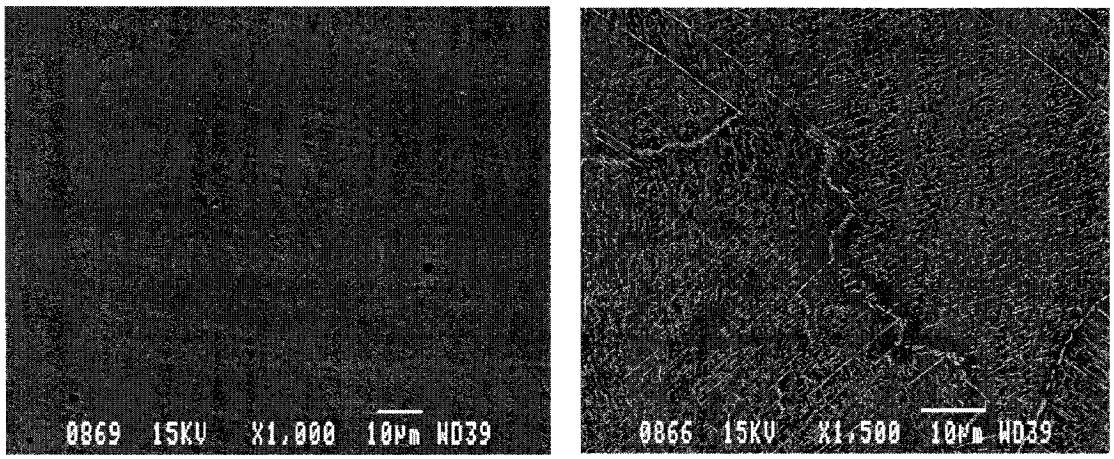

Less number of precipitates

Presence of small size precipitates at the grain joint

Figure 6.38. Sample Grand hardness 30 HRC, on a Scanning Electron Microscope

The particles at the grain boundary of the sample Grand are rich niobium particles like for the sample Petit, Figure 6.39.

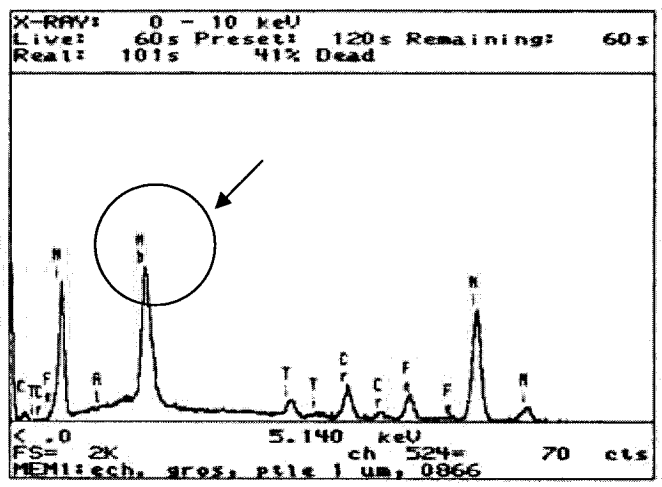

Figure 6.39. Niobium rich precipitate for the sample Grand.

The composition of both sample Petit and Grand shows the same type of elements as indicated in Figure 6.40.

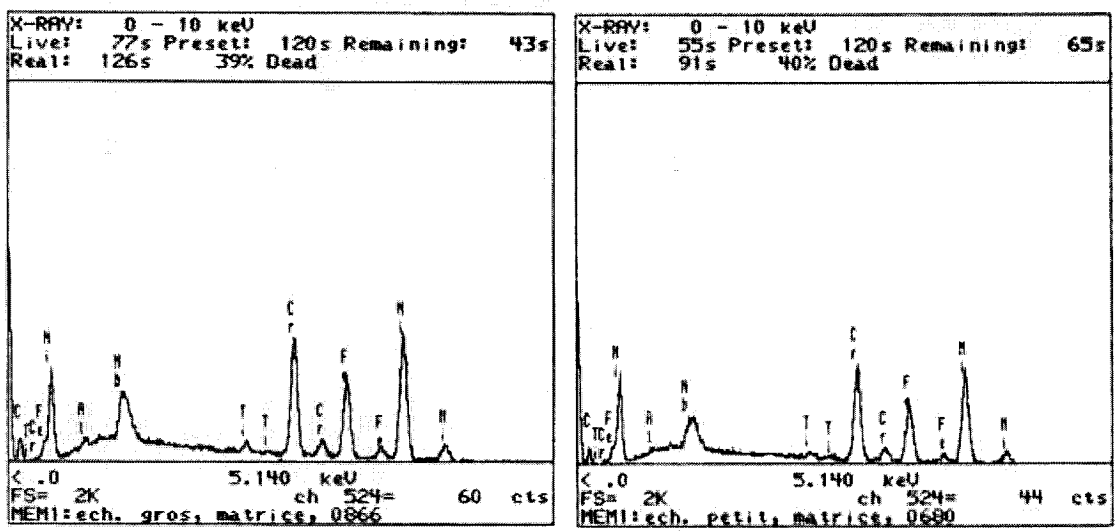

Figure 6.40. The same type of material and about the same composition for both samples Grand and Petit for the matrix.

The microstructure analysis was not pursued further because it is not the objectives of this work. But, it is clear that both Inconel 718 samples have approximately the same composition. The heat treatment seems to differ since the precipitates in the sample Petit seem to be more widespread than for the sample Grand.

The precipitates appear during the aging of a material like Inconel 718. When the aging time increases at a certain temperature, the material is hardened. But when the aging time is to long, the precipitates size increase, and the material hardness starts to decrease.

The different hardness of these two Inconel 718 samples may come from the type of heat treatment underdone by them. The difference of hardness observed at the external diameter and the internal part of the shaft may come from the cooling of the rough material. So the way the shaft material is processed explains these differences.

6.2. The ramping tests results

6.2.1. The constant slope ramping test results

As established in section 5.4.1, the constant slope ramping test is a 2^{4-1} levels fractional factorial design with 4 variables, where the volume is constant vol = 4.5 in^3.

Table 16 shows the results of this test.

For the test number 3, during the first pass, a notch wear was observed near the radius Figure 6.41. This type of wear was observed when the feed and speed were at their maximum and when the slope was negative. Because of these unexplained results, the factorial design was not analyzed in detail.

Table 16: Results of the 2^{4-1} levels fractional factorial design with 4 variables

	VB (mm)		VBmax (mm)		Vn (mm)	
Test number	Fisrt pass	Second pass	Fisrt pass	Second pass	Fisrt pass	Second pass
1	0,125	0,14	0,145	0,16	0,12	0,15
2	0,13	0,135	0,13	0,18	0,13	0,17
3	0,13	0,14	0,24	0,25	0,13	0,16
4	0,11	0,135	0,11	0,145	0,11	0,15
5	0,11	0,15	0,09	0,14	0,11	0,14
6	0,11	0,135	0,11	0,14	0,11	0,14
7	0,125	0,14	0,16	0,18	0,13	0,16
8	0,135	0,15	0,18	0,2	0,13	0,15

Figure 6.41. V_c=800 ft/min, a_p=0.19 in, f=0.008 in/rev, vol=4.5 in^3, ε =-0.4 °

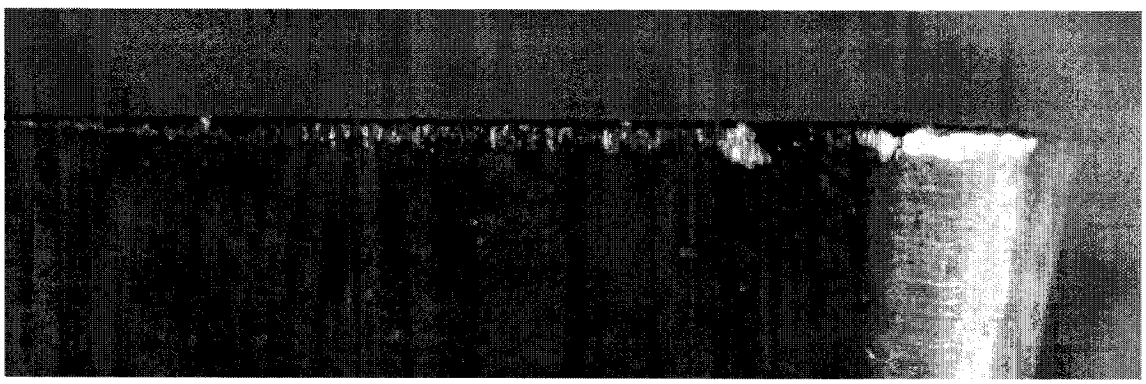

Figure 6.42. V_c=800 ft/min, a_p=0.19 in, f=0.008 in/rev, vol=4.5 in^3, ε =0.4 °

This design gave some contradictory results and some unexplained phenomena. Figures 6.41 and 6.42 show some unexplained wear patterns.

But, some interesting conclusions can be drawn with these preliminary results.

- The ramping effect on notch wear is undeniable. For almost all the tests, the notch wear V_N was reduced on the depth of cut line, compared with Figure 6.24 page 92 where a large notch wear is observed for a constant depth machining.
- The large maximum wear Figure 6.41 for the highest value of feed and speed when the ramp is negative shows a phenomenon to be explained.

- Taking the slope as a ramping variable poses some problems to evaluate the wear since the wear length variation changes with the diameter, Figure 4.5 page 36.

6.2.2. The constant depth of cut variation in time tests

The preliminary ramping test with the slope E as the main ramping variable did not give the results expected. So the constant depth of cut variation in time method is tested in this second ramping test.

6.2.2.1 Effects of positive and negative slope

To minimize the material removed during the test, a less resistant tool is used for this ramping tests, the carbide KC5010 (TiAlN coated) as explained in section 5.4.2.
In order to reduce the number of tests to the configuration (B) represented by the test plan Table 14 page 71, a comparison between the positive and negative ramping slope is carried out.

Table 17: Test plan to compare positive and negative ramping slope

Tests	slope (E)	ρ	a_p (in)	Δt (s)	Δa_p (in)	$\Delta a_p/\Delta t$ (in/s)
1	Negative	0,1	0,14	156	0,1145455	0,0007343
2	Positive	0,1	0,14	156	0,1145455	0,0007343

Cutting conditions: V_c=150 ft/min, f=0.007 in/rev

Figure 6.43 shows the comparison of a negative ramping slope (a) (small depth of cut to large depth of cut, plunging) and a positive slope (b) (large depth of cut to small depth of cut, getting off).

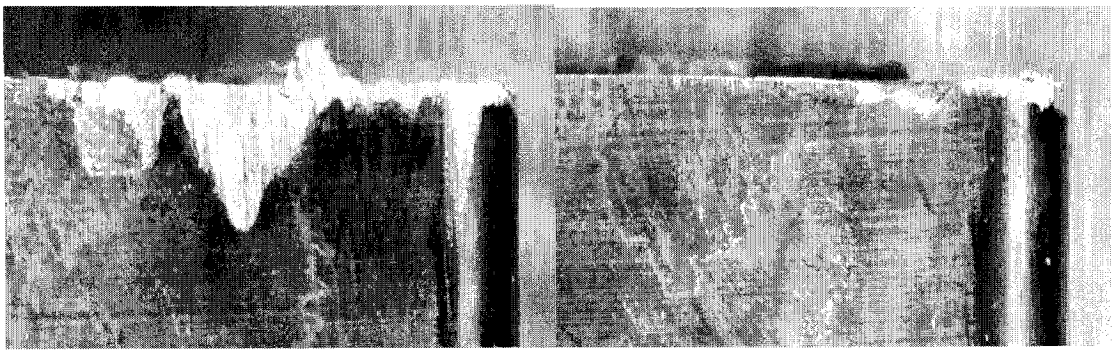

(a) (b)

Figure 6.43. Positive and negative slope ramping V_c=150 ft/min, f=0.007 in/rev, a_p=0.14 in, after 2.6 min

Figure 6.43 indicates that the negative slope (a) gives a larger tool wear than positive slope (b). Therefore the choice at this step was to privilege the set of ramping configuration (B) Figure 4.8 page 40, where the positive slope is at the beginning of the ramping.

6.2.2.2 Effects of the ratio ρ

To reduce the number of tests to perform (Table 14), two values of ratio ρ are tested to choose the best. After the test (Figure (6.44)), the test plan was reduced only for ρ = 0.3, because ρ = 0.1 gave the worst tool wear.

As previously stated, ρ = B/A, and a small value of ρ means that the ramping start with a depth of cut which is high to a depth a cut small. Hence the cutting force during the ramping will reach a higher value for a low value of ρ than for a high value. This may explain why the highest ρ seems to be better. But, a value of ρ too high will give the situation of B≈A, which is constant depth of cut machining.

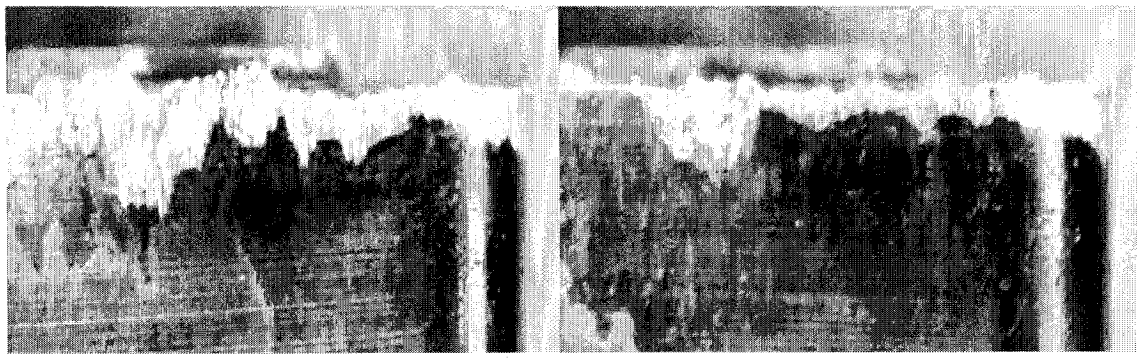

ρ = 0.1 ρ = 0.3

Figure 6.44. Effects of ratio ρ on the tool wear for V_c=225 ft/min, f=0.007, a_p=0.14 in, after 5.2 min

Figure 6.43 comparing negative and positive slope has been tested for a value ρ = 0.1. Hence the tool wear Figure 6.43 (a) is a combination of 2 bad cutting conditions, small ρ and negative slope.

When ρ is smaller, the ramping slope is higher and the penetration speed V_{pe} of the tool during ramping is higher. A high tool penetration speed during ramping causes the reduction of the tool effective clearance angle.

The reduction of the cutting tool effective clearance angle during tool penetration when the slope is negative is shown in Figure 2.3 page 9. This phenomenon can be armful for the tool flank wear. The results of the preliminary ramping test which was unexplained Figure 6.41 page 107 finds here an explanation. The effect of feed during these preliminary tests was highlighted. To reduce the penetration speed during this phase of ramping, it may be possible to reduce the feed, since V_{pe} depends on feed. This feed variation during ramping will be proposed in section 6.5.

6.2.2.3 Effect of depth of cut variation in time (DOCVT)

A constant depth of cut test was performed with a TiALN coated carbide tool as indicated in the test plan section 5.4.2. Figure 6.45 shows a result of this test. Then, a ramping test can be carried out with the final test plan after reducing the number of tests to test number B(I), B(II) and B(III) representing the configuration (B) Figure 4.8 page 40.

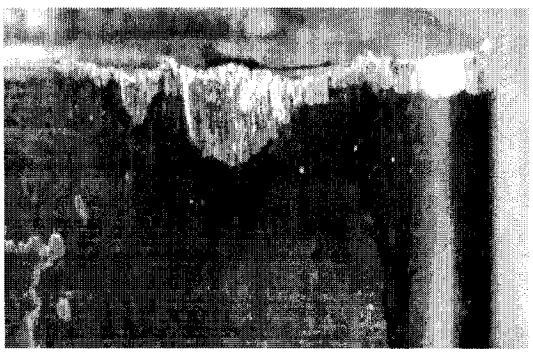

Figure 6.45. Notch wear effect on a TiALN coated carbide, constant depth of cut machining, V_c=225 ft/min, a_p=0.07 in, f=0.007 in/rev, after 5.2 min.

Figure 6.46 shows the effects of depth of cut variation in time on the flank wear VB. VB_a and VB_r are respectively the curves of the wear VB for the first and second pass of ramping. The data used for the calculations are in the Appendix III page 182.

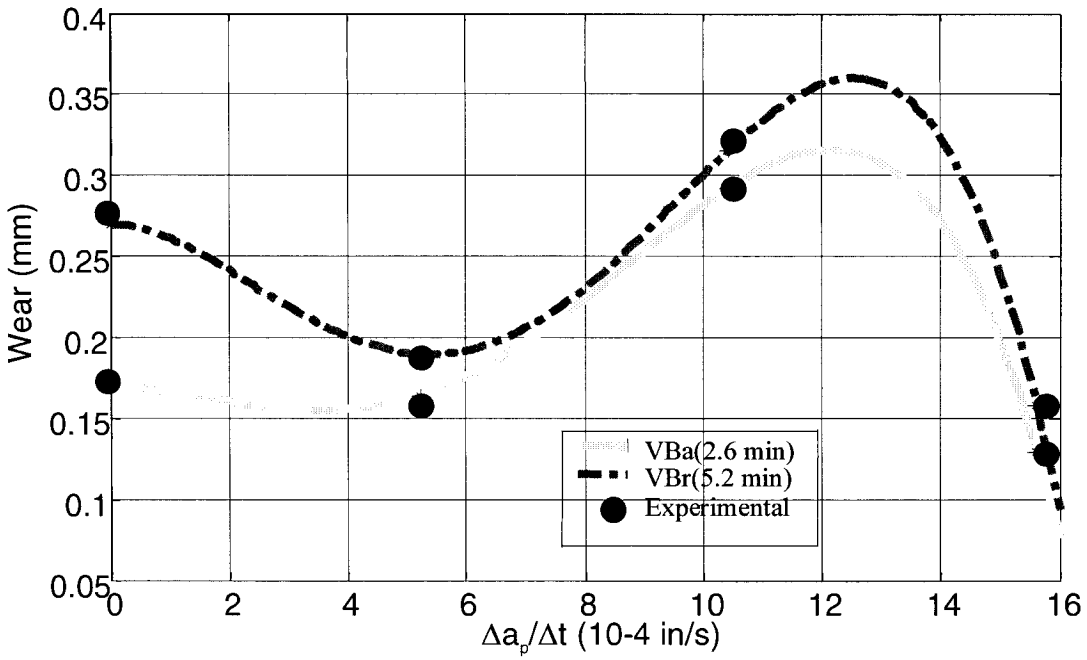

Figure 6.46. Wear in function of depth of cut variation in time, for V_c=225 ft/min, a_p=0.14 in, f=0.007 in/rev, ρ =0.3.

A polynomial approximation is chosen to link the different experimental points. Figure 6.47 is the curves of VB_r where the experimental results are approximated with a line (approx).

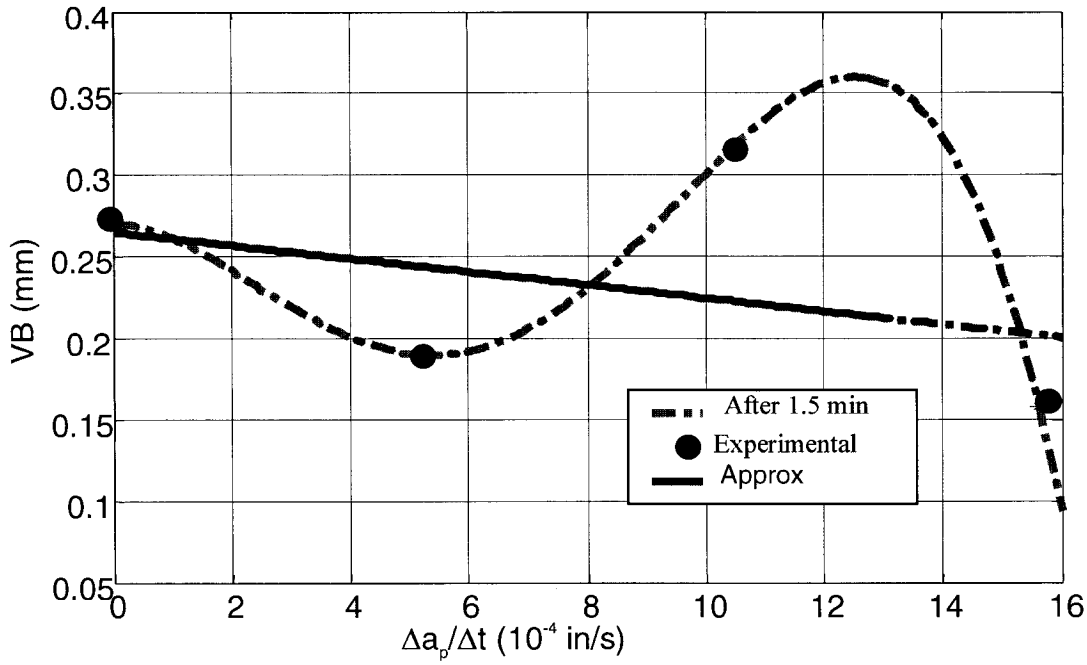

Figure 6.47. Tool wear in function of depth of cut variation in time linear approximation

The tool wear pattern used to calculate the experimental tool wear can be seen in Figure 6.48. This figure shows the first and second pass ramping results for the 3 strategies 1, 2 and 3 ramps beginning with a positive ramp.

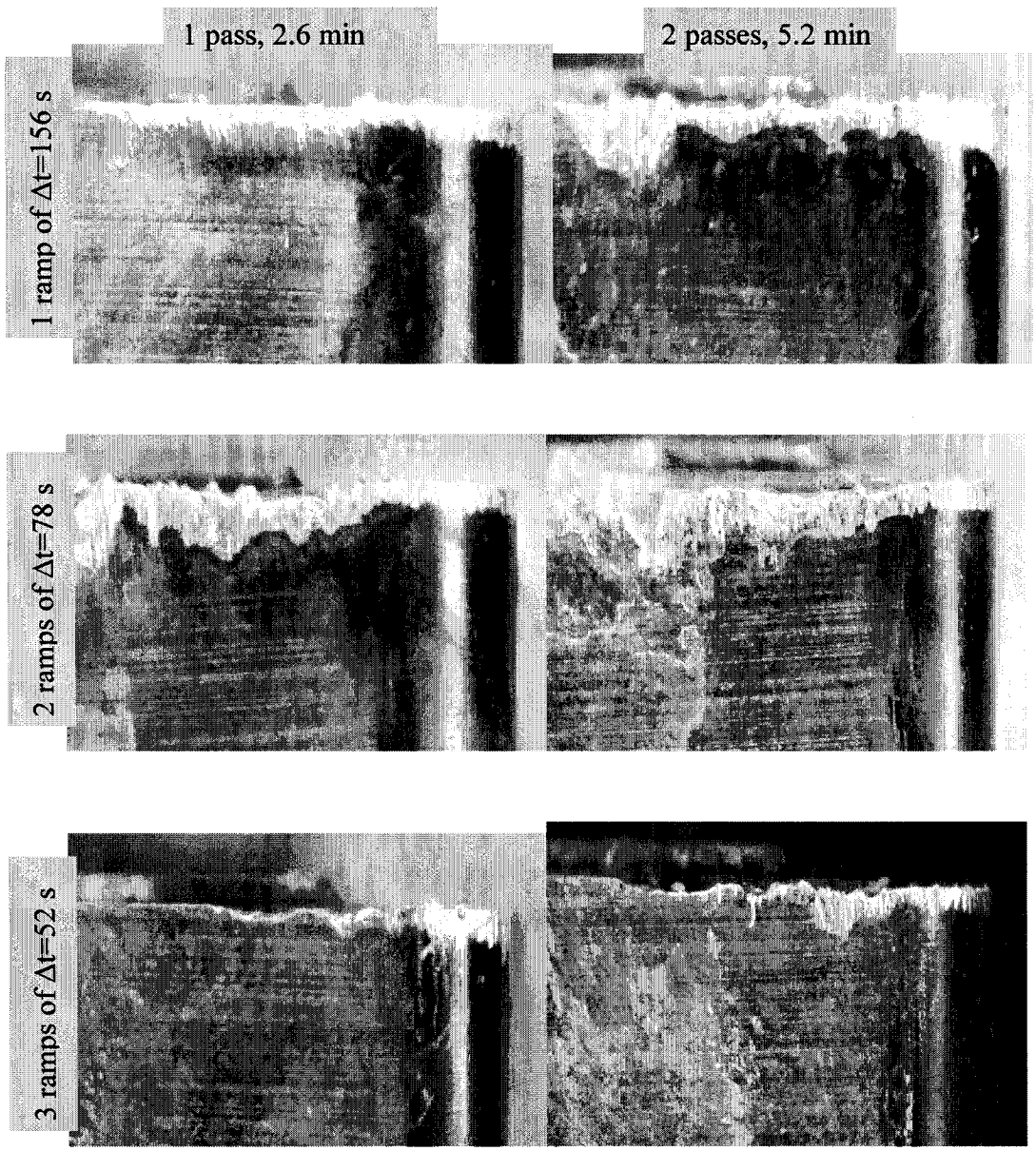

Figure 6.48. Ramping depth of cut variation in time simulations (1,2 and 3 ramps)
V_c=225 ft/min, f=0.007, a_p=0.14 in, ρ = 0.3

The value of tool wear when $\Delta a_p/\Delta t = 0$ in Figures 6.46 and 6.47 gives the average wear VB when there is no ramping, that is the constant depth of cut machining.
These figures indicate a oscillation variation of tool wear as a function of DOCVT. The tool wear seems to decrease when only one ramping is done, it increases when 2 ramping (2 waves) are performed, and finally decreases when 3 waves are performed.

This phenomenon can be explained by the fact that during an odd number of ramp (waves) (1, 3, 5 ...) there are more positive ramps, than negatives ones. Since positive ramps are better for tool wear, and negative ones are worst, the overall tool wear seems to be better. But when an even number of waves (2, 4, 6...) are performed, there is a same number of negative ramps than positive ones. The benefit effects of positive ramps are compensated by negative ones. The tool wear tends to increase.
But the results of these 3 waves examples show that the tool wear is reduced with the number of waves.

6.2.2.4 How to deal with a different length in a real machining case?

The ramping variables used are:

- The cutting speed Vc
- The feed f
- The depth of cut a_p
- The ratio ρ
- The time Δt

The depth of cut variation in time $\Delta ap/\Delta t$ is deduced from the previous 5 variables.
For example if the problem is to deal with an Inconel 718 bar of length L, what will be the ramping technique?

a) The ramping solution for a given bar length.

The solution is to use the same a_p=0.14 in, ρ=0.3, and Δt=156 s for 3 ramps. The variable $\Delta a_p/\Delta t$ will than be the same as for the test.

With the new cutting conditions for a ceramic insert WG-300, the values of V_c and f will change.

Therefore the indicative length will be:

$$Lind = \frac{f.Vc.\Delta t}{3\pi Dm} \qquad \text{Equation (29)}$$

Where Dm is the mean diameter machined during ramping

So that, on $3L_{ind}$ the machining time is Δt.

$$Dm = \frac{(Dinit - D_f)}{2} \qquad \text{Equation (30)}$$

D_{init}: initial diameter

D_f: final diameter

On each L_{ind} length, only 3 waves will be performed, so that the tool wear is minimized, (according to the previous results).

But, for a work piece length L, there will be a remaining length L_r,

$$L = L_{ind}.Q + L_r \qquad \text{Equation (31)}$$

where Q is a positive integer.

2 cases will be faced:

- If Q is odd, the best ramping choice will be to make Q ramps (or waves) on the total work piece length L, instead of making Q+1 ramps , which is a even number.
- If Q is even, the best ramping choice will be to make Q+1 ramps (or waves on the total work piece length.

b) Confirmation of the results with a test on the ceramic WG-300

The test is carried out with a square whisker ceramic S-WG-300. After 3 minutes the notch wear for the constant depth of cut machining reached 0.63 mm, which is more than the maximum acceptable notch (0.6 mm) according to the standards. But, after the 3 waves ramping in the conditions V_c =900ft/min, a_p=0.14 in, and f=0.007 in/rev, ρ=0.3, the notch wear disappeared and the average flank wear VB remained slightly the same has for the constant depth of cut machining, Figure 6.49.

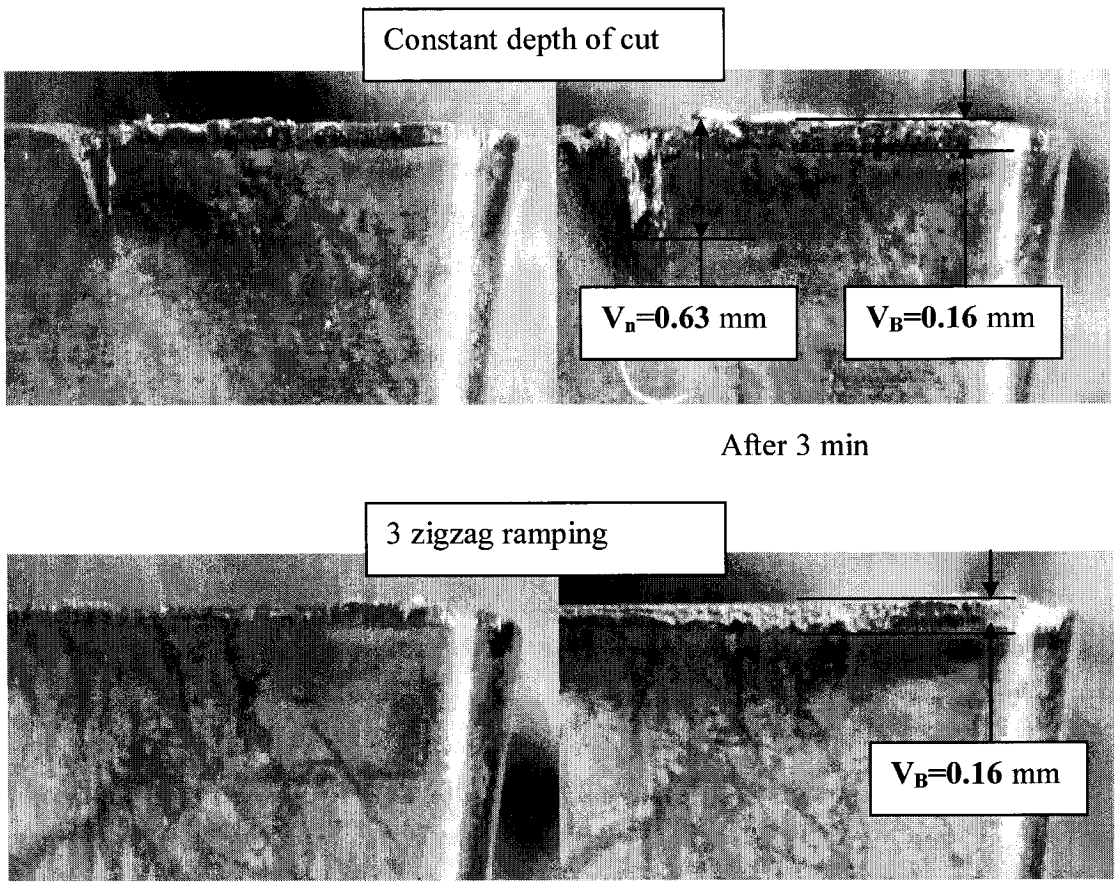

Figure 6.49. Ramping benefit effects confirmation with a WG-300, V_c=900 ft/min, a_p=0.14 in, f=0.007 in/rev

6.2.2.5 Analysis of the DOCVT results

Many conclusions can be drawn based on these results and according to the hypothesis and the theories developed in chapter 4.

a) The positive effects of depth of cut variation in time

Compare to the constant ramping slope, the constant depth of cut variation in time has proven to be the best strategy to use for a good control on the tool behavior. The notch wear is eliminated without any unexplained tool wear pattern on the flank face of the tool. This may be due to the fact that the ramping wear length on the tool edge is uniform when the constant depth of cut variation in time is used, as explained in Figure 4.4 page 35.

b) The problem of odd number of waves

The ramping test results (Figure 6.46) are obtained using 3 waves for an indicative length. But, since the curve (Figure 6.47) shows a oscillation variation of wear and its tendency to decrease, it can be assumed that it is better to use a great number of ramps, provided that this number is odd.

The model developed in section 4.2.3.3 shows an oscillation variation like what the tests results indicate. This is a confirmation of the fact that the tool wear shape as a function of depth of cut variation in time is similar to the curve of the energy absorbed during ramping. But the tendency to decrease the tool wear shown by these results is not explained by the energy model.

c) Energy hypothesis limits

The hypothesis of energy absorption by the cutting tool used to estimate the average tool wear has some limits. The major limit is the distribution of this energy on the tool. If it is

possible to assume that the energy absorbed by the tool is responsible for its wear, it is not sufficient to estimate the wear distribution on the tool by this method.

The ramping tests performed previously Figure 6.47 showed a global decrease in tool wear even if the flank wear VB curve in function of DOCVT is an oscillation.

The average energy can be seen as the total wear, on the flank, the edge, the rake etc...

If this energy is globally constant that is normal, but the distribution could be different. For example the decrease of flank wear could lead to an increase of crater width, depth etc...The energy model could be improved to focus on the amount of energy on each faces of the tool. That may be useful to confirm of infirm the decrease of tool wear with DOCVT.

6.3. The variable feed results

The average flank wear VB, the maximum flank wear VB_{max} and the notch wear were measured during theses tests. Figure 6.51 shows the average flank wear VB for both constant feed and variable feed machining.

The wear VB is smaller for the variable feed than for the constant feed machining. But both wear seem to meet at about 4 min, which is the tool life with the criteria VB=0.3 mm. The difference between both methods can not be differentiated.

The maximum flank wear shows a different pattern, 6.50. The tendency noted for the wear VB is the same for the wear VB_{max}.

Table 18: Feed variable results

Constant feed machining				Variable feed machining			
Time (min)	VB (mm)	VB_{max} (mm)	VN (mm)	Time (min)	VB (mm)	VB_{max} (mm)	VN (mm)
0.5	0.11	0.14	0.12	0.5	0.08	0.09	0.1
0.97	0.13	0.16	0.14	0.97	0.12	0.13	0.14
1.5	0.17	0.18	0.17	2	0.18	0.22	0.22
4	0.31	0.31	0.33	4	0.31	0.37	037

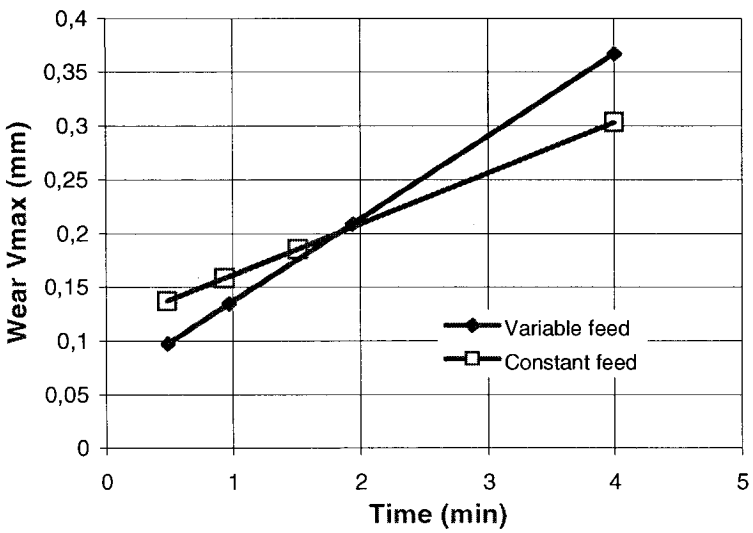

Figure 6.50. Maximum flank wear VBmax in function of time; comparison of constant and variable feed machining

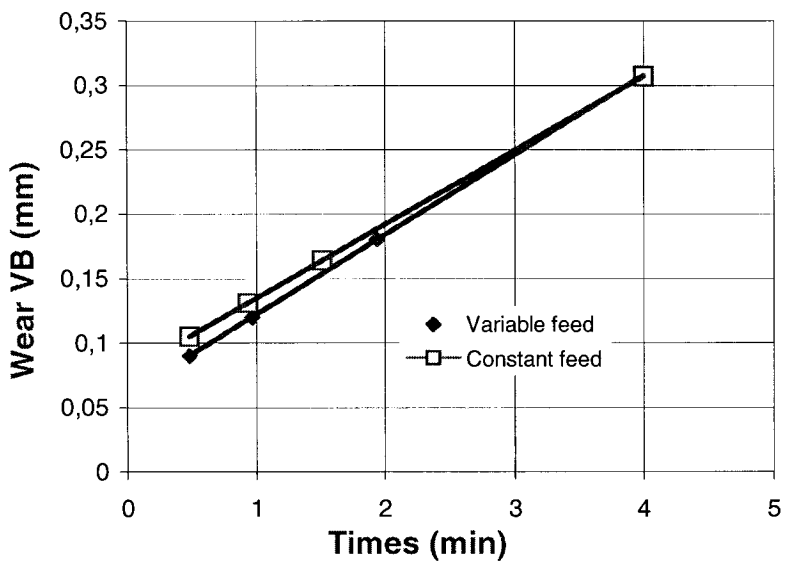

Figure 6.51. Average flank wear VB in function of time; comparison of constant and variable feed machining

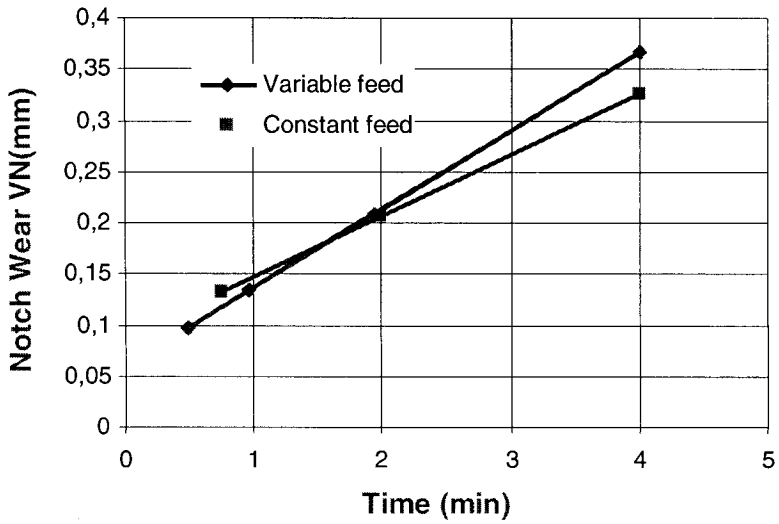

Figure 6.52. Notch wear V_N in function of time; comparison of constant and variable feed machining

The notch wear curve shows about the same results for both method, Figure 6.52, but with a slightly higher wear for variable feed when the machining time increases.

The variable feed test has not been pursued because this first test did not give the results hoped. But this method can be tested for a different feed function and could maybe show different results.

The conclusion of this first investigation did not allow to show a significant improvement on the tool life when using variable feed. This can be due to the fact that, as mentioned in the theory section, the method of feed variation affects only the rake face instead of flank face.

6.4. Burr formation and its effect on machining

Burr formation is an important issue during machining of Inconel 718. In turning operations, the sideward burr formation (appearing in the feed direction) is the one that poses problem. The preliminary test carried out at Pratt &Whitney Canada Figure 3.12 page 27 shows and important burr formation on the workpiece material. This type of burr must be eliminated.

6.4.1. The effect of feed, depth of cut and cutting speed on burr formation

6.4.1.1 The effect of feed

Figure 6.53 shows the influence of feed on the burr formation. The burr height for the feed of f = 0.009 in/rev (B) is higher than for the feed of f = 0.007 in/rev (A). It is clear that burr height increases with feed, for these two tests.

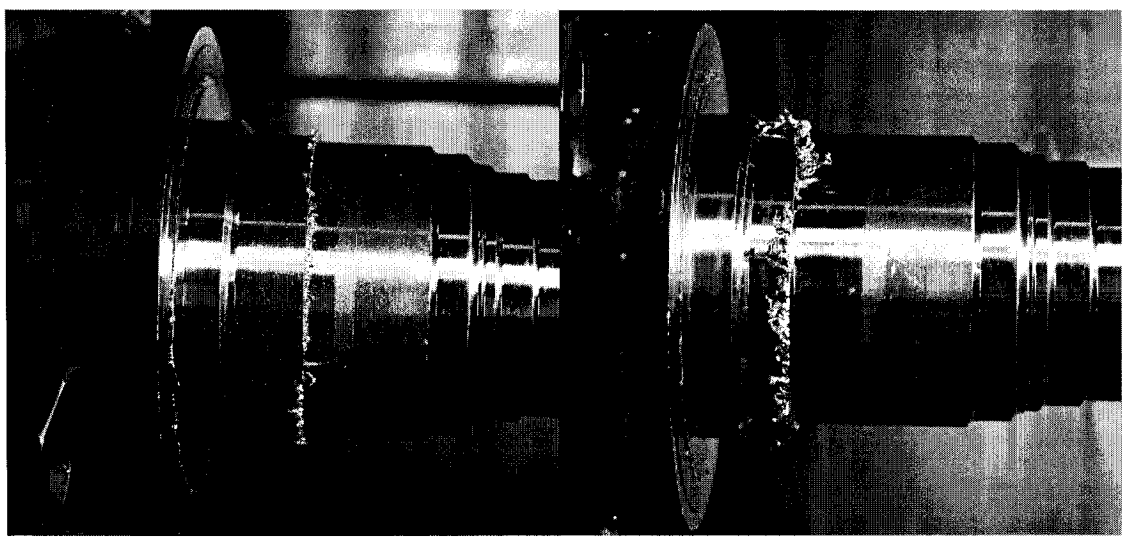

(A) f=0.007 in/rev (B) f=0.009 in/rev

Figure 6.53. The effects of feed for V_c=150 ft/min, a_p=0.07 in

The tool used for the test is a coated whisker WG-600, number (4) Table 11 page 68. Figure 6.54 shows the result of an experiment made by Andrey Toropov et al [1] which confirms that lateral burr or sideward burr generally increases with feed despite the workpiece material.

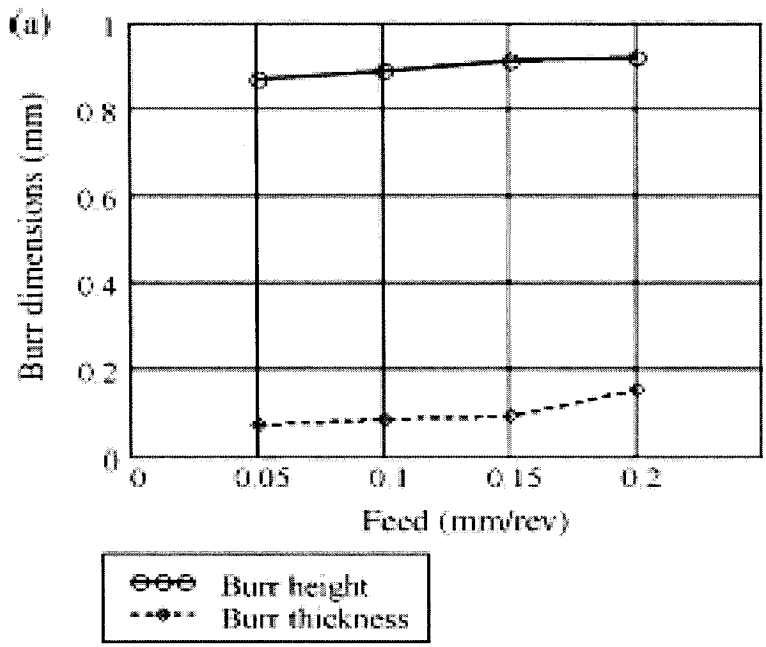

Figure 6.54. The effects of feed on the burr height and thickness, (source [1])

6.4.1.2 The effect of cutting speed

The effects of cutting speed on burr formation are shown in Figure 6.55. The burr height Figure 6.55 (A) with a cutting speed of V_c=150 ft/min is smaller than that of (B) V_c=210 ft/min.

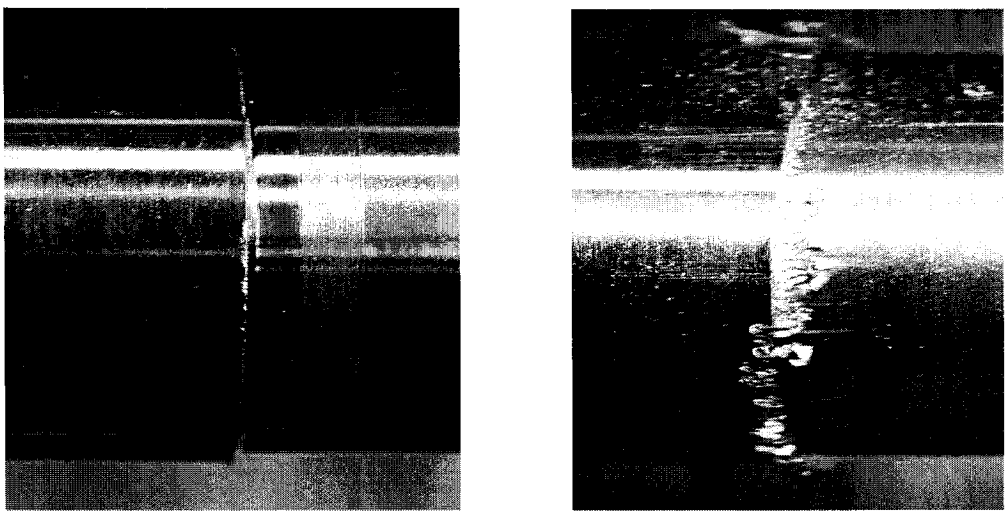

(A) V_c=150 ft/min (B) V_c=210 ft/min

Figure 6.55. The effects of the cutting speed on burr formation, for f = 0.005 in/min, a_p=0.7 in

6.4.1.3 The effect of depth of cut

The effects of depth of cut have not been tested during the experiments, but a result of Andrey Toropov et al [1] indicates that the burr height increases with the depth of cut Figure 6.56.

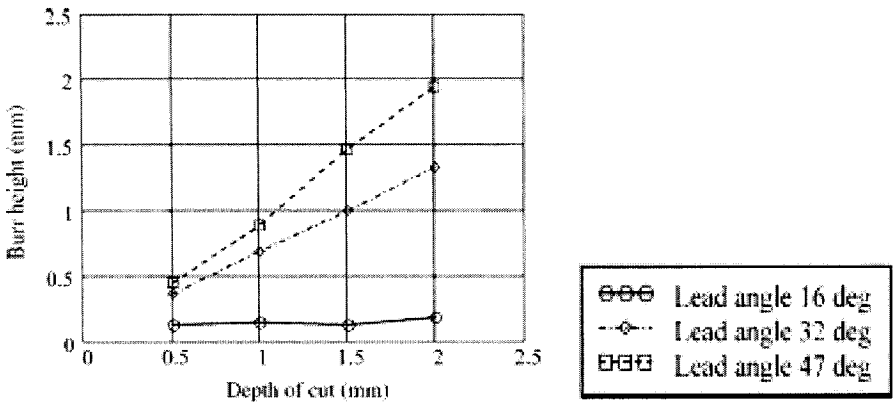

Figure 6.56. Effects of depth of cut on the burr height , Source [1]

6.4.1.4 The effect of lead angle

Before analyzing the effects of the lead angle on burr formation, a small recall should be made.

According to the results of Gillespie [23], burr is formed by the deformation of the material at its side when it is compressed (Poisson burr), and the material tearing (tear burr). The rollover burr is the chip that bended rather than shearing, and the cut-off burr results from the cut of a work material.

The lateral burr formation in turning process can than be seen as a combination of Poisson burr, tear burr (coming from the tearing of the material in the shear zone) and rollover burr.

An important explanation of why burr is not present when the lead angle is small can be seen in the works of Andrey Toropov et al. [1].

These authors show that the plastic bending of the material in the feed direction depends on the rigidity of the remaining part, see Figure 6.57.

This rigidity is characterized by the angle θ. When θ is high, the remaining part is more rigid, so the bending deformation is weak, hence burr is reduced.

$\theta = \pi - \kappa_r$.

So, if the lead angle κ_r is small, the remaining part of the work piece is more rigid, and when the lead angle is high the remaining part is less rigid.

Moreover, according to the cutting theory the smaller lead angles give a smaller feed forces F_f and the higher lead angles give higher F_f. These two observations can explain why burr formation is more pronounced when the lead angle is higher.

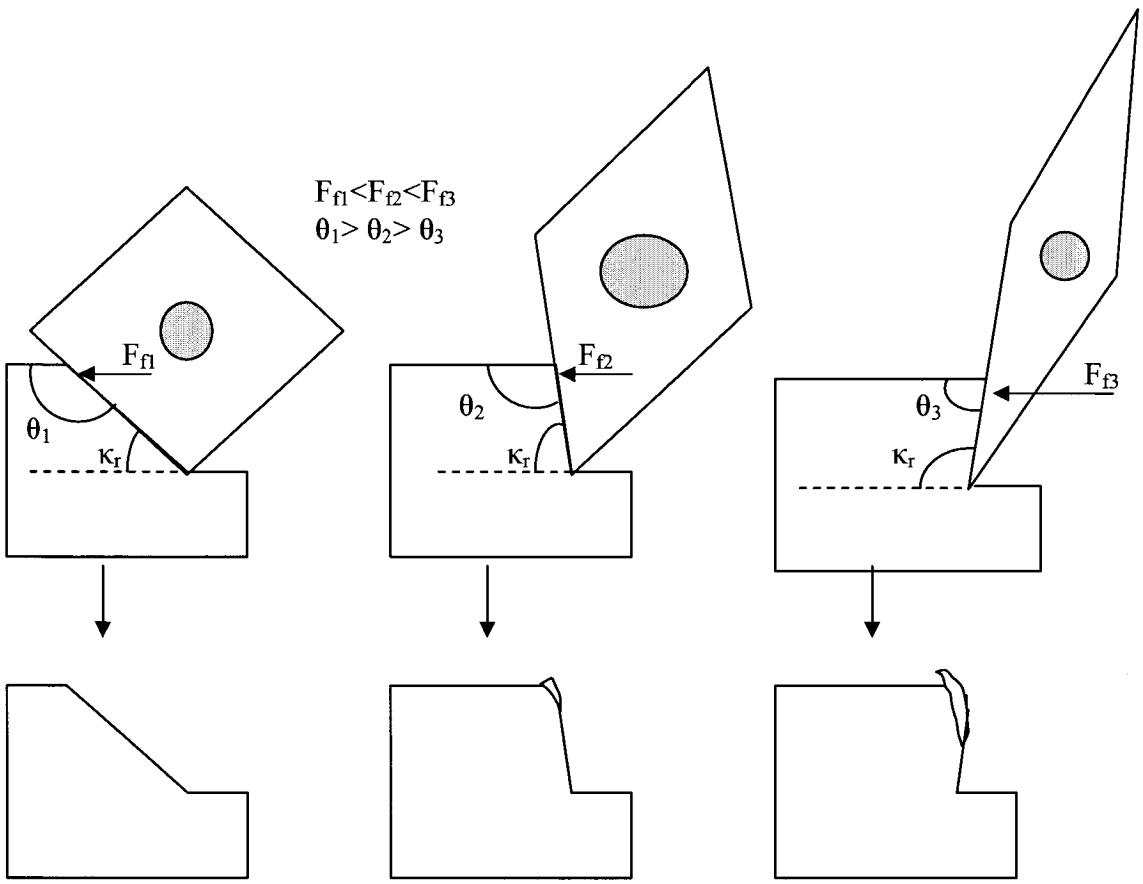

Figure 6.57. Remaining part of the work piece according to the rigidity factor θ

6.4.1.5 Burr formation summary

To reduce the burr formation during machining of Inconel 718, the main parameter to take into account is the lead angle. A small lead angle (about 30, 45 °) eliminates burr, as for the whisker ceramic S-WG 300 of 45 ° lead angle. The reduction of the cutting speed, the depth of cut and the feed also reduce considerably the burr height.

6.5. PROPOSALS

6.5.1. Thesis proposal

An interesting thesis subject could be to link the energy absorbed by the tool and the tool wear. The estimation of the energy distribution ratio on each face of the tool as a function of the geometry and the cutting conditions could help to demonstrate mathematically the decrease or increase of tool wear as a function of the machining strategy.

6.5.2. New ramping technique proposal

This proposal is based on the fact that the tool wear is more pronounced during the negative ramp than when the ramp is positive. The reason is that the chip thickness is bigger when the ramp is negative. Hence the cutting forces reach high levels during this phase. To reduce this phenomenon and compensate the negative effects of ramping, a feed variation can be introduced. The chip thickness depends on the feed. Reducing the feed is a way of reducing the cutting forces during the negative ramp, reducing the feed lead to the reduction of the penetration speed. So the feed reduction during this phase could be positive for the machining.

But if the feed is reduced during the negative phase f_N of ramping it is necessary to increase it during the positive phase f_P, so that the machining time remains the same, and the chip thickness becomes equal for both negative and positive ramping. The positive chip thickness C_{tp} and the negative one C_{tN} are:

$$C_{tp}=f_p\frac{\sin(\kappa_r-\varepsilon)}{\cos(\varepsilon)} \qquad C_{tN}=f_N\frac{\sin(\kappa_r+\varepsilon)}{\cos(\varepsilon)}$$

$$C_{tp}=C_{tN}\text{, implies } f_N=f_p.\frac{\sin(\kappa_r-\varepsilon)}{\sin(\kappa_r+\varepsilon)}=\xi.f_p$$

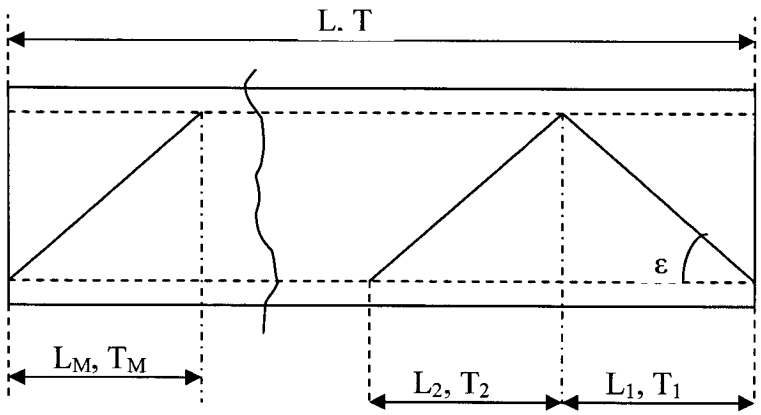

Figure 6.58. Feed variation during ramping

An integer M can be expressed by : M=2Q+R, where Q is an integer, and R= 0 if M is even and R=1 when M is odd.

Since the speed RPM is constant, the total machining time T is the sum of each time Ti of length Li for i=1,2,..M.

$$T=\sum_{i=1}^{M} T_i=\sum_{i=1}^{M}\frac{L_i}{f_i.Rpm}=\frac{L}{f.Rpm}$$

$$\text{so } \frac{1}{M}\sum_{i=1}^{M}\frac{1}{f_i}=\frac{1}{f}$$

When 'i' is odd $f_i=f_N$ and when 'i' is even $f_i=f_p$

$$\frac{M}{f}=\frac{Q+R}{f_p}+\frac{Q}{f_N}$$

$$\begin{cases} f_p=f+\dfrac{fQ}{M}(\xi-1) & \text{Equation (32)} \\ f_N=\xi.f_p & \text{Equation (33)} \end{cases}$$

where $\xi=\dfrac{\sin(\kappa_r-\varepsilon)}{\sin(\kappa_r+\varepsilon)}$ and $\varepsilon=\dfrac{ap.(1-\rho)}{L.(1+\rho)}$

Knowing the number M of ramps to make, the tool lead angle κ_r, the ramping variable ρ, the depth of cut a_p, the length to machine L, it's possible to determine the feed f_p to use

on the positive ramps and the feed f_N on the negative ones, so that the machining time is the same like if a nominal feed f was used on the same length L.

6.5.3. Shaft machining proposal

After the machining tests and the results analysis, a proposal can be made to machine the PW 307 shaft in roughing and semi finishing. The cutting tool is the square WG 300 of Greenleaf. Figure 6.59 shows two cutting tools for the turning and the boring processes.

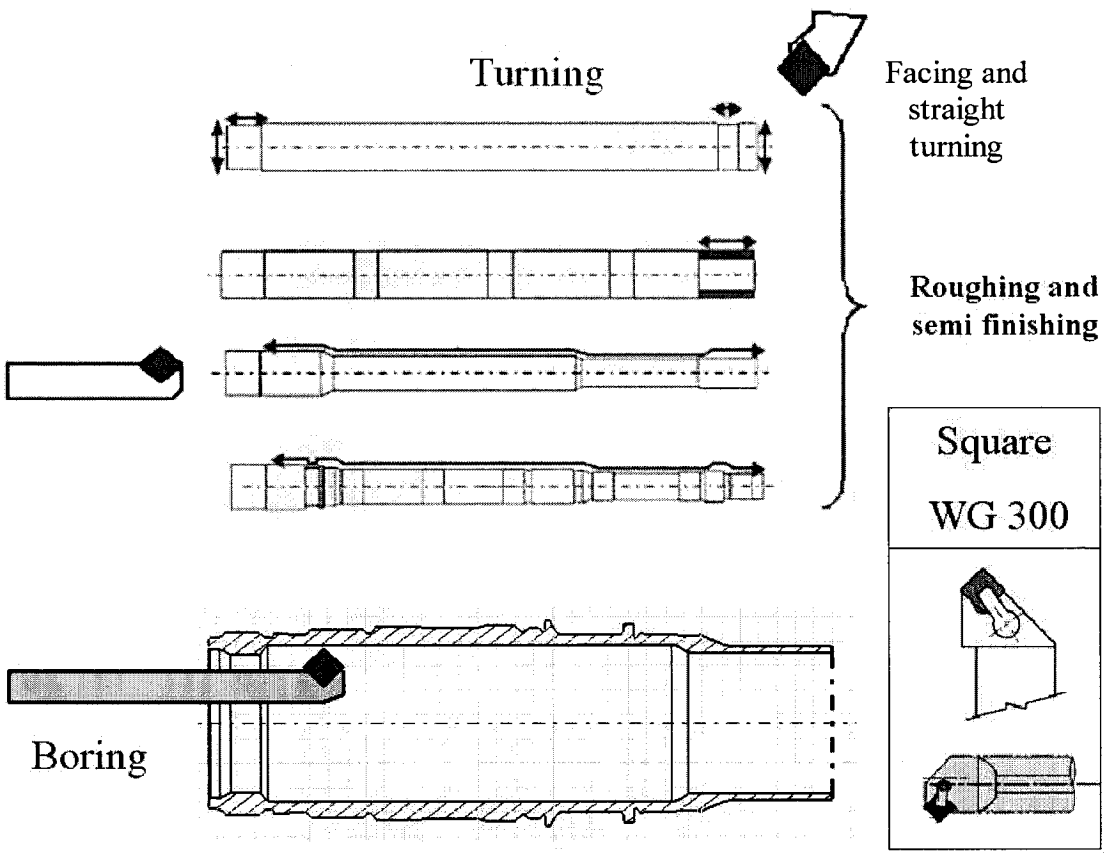

Figure 6.59. Cutting tools for the shaft machining process in roughing and semi finishing

The cutting conditions depend on the material hardness as discussed in section 6.1.3. Table 19 summarizes the machining strategies according to the Inconel 718 material

hardness. If the material to machine has a hardness between 20 and 30 HRC, the ramping technique will be chosen to avoid the reduction of tool life due to notch wear. However, the material hardness is a parameter to assess before establishing an Inconel 718 shaft machining. The ideal would be a hardness around 20 HRC for all the sample to be machined in production.

Table 19: Machining strategy according to material hardness

	Machining strategy	
Conditions	Hardness < 21 HRC	Hardness > 29 HRC
Roughing	Constant depth of cut machining Vc=900 ft/min f=0.009 in/rev ap=0.07 in Tool life expected: 6 min	Ramping ρ = 0.3 Δt = 52 s Vc=900 ft/min f=0.007 in/rev ap=0.14 in Tool life expected: 6 min
Semi finishing	Constant depth of cut machining Vc=800 ft/min f=0.007 in/rev ap < 0.02 in Tool life expected: 9 min	Constant depth of cut machining Vc=800 ft/min f=0.007 in/rev ap < 0.02 in Tool life expected: 3 min

For more details, Appendix VII gives some explanations and some operations for the PW307 machining which require the use of Table 19.

CONCLUSION

Different machining strategies have been highlighted during this study in order to improve the machining of an Inconel 718 shaft. The study focuses only on the aspects of roughing and semi finishing.

Inconel 718 should ideally be machined at higher cutting speeds and feeds for roughing aspect in order to get a better chips. This high speeds require the use of whisker ceramic tools. The whisker ceramic WG 300 has been found to be the best tool among the cutting tools used during this study.

To reduce the burr height when machining Inconel 718 the lead angle should be reduced. For a given cutting tool, another way to reduce the burr height is to reduce the cutting parameters (feed, cutting speed and depth of cut).

The feed variation method did not give satisfying results to reduce the notch wear, but the ramping technique successfully reached this objective. However this method should be used with care, because in addition to reducing the notch wear, it could increase the average wear.

To make a good ramping in order to reduce the notch wear, it is important to keep some variables at a reasonable level:

1. The variable ρ was 0.3, because it is important to keep a minimum depth of cut (variable B), and this variable value should be less than 1 which is a constant depth of cut machining.

2. An odd number of ramps (with more positive ramps than negative ones) is better than an even number of ramps, because positive ramp reduce the chip load, while negative ones increase it.

3. The major problem of increasing the number of ramps on a small length is the penetration speed during negative slopes. When the number of ramps increases on a given length, the slope increases and the penetration speed increases. Than, it is more likely to have an increases flank wear since the effective clearance angle decreases.

4. Another advantage of studying the effects of number of waves is the length to be machined. When the work piece is too long, it is not possible to make only one ramp on this length, because the slope will be too small, and the results could be closed to constant depth of cut machining. Only one ramp could be better in the cases were the length to machine is small. Otherwise, according to the value of depth of cut in time, more than one ramp should be considered. The calculations depend on the value of depth of cut in time, section 6.2.2.4.

5. Since it is difficult to test the ramping methods with many levels of variables, it is better for the practice of Inconel 718 machining to keep close to the one used in this study because they have been found to give good results.

The application of the machining strategy studied in this report to a shaft should not be a major problem if the cutting tool suggested are used, and if the geometries are chosen to minimize the burr formation and the tool wear. The work piece material mechanical properties should be closed to the one used in the study, in order to transpose the results.

REFERENCES

1. Andrey Toropov, Sung-Lim Ko, Byung-Kwon Kim, Experimental study of burrs formed in feed direction when turning aluminum alloy Al6061-T6, International Journal of Machine Tools & Manufacture 45 (2005) 1015–1022

2. A Military Handbook - MIL-HDBK-5H. Metallic Materials and Elements for Aerospace Vehicle Structures (Knovel Interactive Edition). 2003.

3. Balazinski M., Songmene V., Improvement of tool life through variable feed milling of Incone 600, Annals CIRP, 1995, vol. 44/1

4. Bhattacharyya, Amitabha. Design of cutting tools : use of metal cutting theory. 1969: Dearborn, Mich. : American Society of Tool and Manufacturing Engineers

5. C. Ducros, V. Benevent2003; 163 .164, (681.688): Mecachrome, Avenue Eugene Casella, 18700 Aubigny Sur Nere, France , CEA Grenoble, 17 av. des Martyrs, 38054 Grenoble Cedex, France

6. Choudhury, I. A. and El-Baradie, M. A. Machinability of nickel-base super alloys: A general review. Journal of Materials Processing Technology. 1998; 77(1-3. May 1):278-284; ISSN: 0924-0136.

7. Deng Jianxin, Ai Xing. Wear behavior and mechanisms of alumina-based ceramic tools in machining of ferrous and non-ferrous alloys. 1997: Department of Mechanical Engineering Jinan 250061, Shandong, China

8. E. O. Ezugwu, J. Bonney. Evaluation of the machinability of Nicke-base, Inconel 718 with nano-ceramic cutting tools. 2002: South Bank uviversity, London, SEI OAA, UK.

9. E. O. Ezugwu, Z.M Wang. The machinability of nickel-based alloys; a review. 1999: Machining Research Center, school of Engineerong Systemes and Design, London SEI OAA, UK, Federal Universidade de Uberlandia, MG-Brazil, Brazil.

10. El-Wardany, T. I.; Mohammed, E., and Elbestawi, M. A. Cutting temperature of ceramic tools in high speed machining of difficult-to-cut materials. International Journal of Machine Tools & Manufacture. 1996; 36(5. May):611-634; ISSN: 0890-6955.

11. Ezugwu, E. O. and Tang, S. H. Surface abuse when machining cast iron (G-17) and nickel-base superalloy (Inconel 718) with ceramic tools. Journal of Materials Processing Technology. 1995; 55(2. Nov 15):63-69; ISSN: 0924-0136.

12. Ezugwu, E. O.; Wang, Z. M., and Machado, A. R. Wear of coated carbide tools when machining nickel (Inconel 718) and titanium base (Ti-6A1-4V) alloys. Tribology Transactions. 2000; 43(2. Apr):263-268; ISSN: 1040-2004.

13. F. Klocke, T. Krieg. Coated Tools for Metal Cutting - Features and Applications. 1999; 48.

14. Felloni, L.; Gatto, A.; Ippolito, R., and Iuliano, L. On the performance of a CrN coated SiC whiskers reinforced ceramic tool high speed machining of

Ni-base super-alloys. Industrial Ceramics. 1997; 17(3. Sep-Dec 1997):153-157; ISSN: 1121-7588.

15. G. Appa Rao [a], Mahendra Kumar [a]. Effect of standard heat treatment on the microstructure and mechanical properties of hot isostatically pressed superalloy inconel 718. 2002: [a] Defence Metallurgical Research Laboratory, Defence Research and Development Organisation, Ministry of Defence, Government of India, POKanchanbagh, Hyderabad-500058, India[b] Department of Metallurgical Engineering, Institute of Technology, Banaras Hindu University, Varanasi 221 005, India

16. G.L. Chern, D.A. Dornfeld. Burr/breakout model development and experimental verification. 1996; 118 (4), (201206).

17. G.Pottlacher [1], H.Hosaeus[1]. Thermophysical properties of solid and liquid Inconel 718 Alloy. 2002; 31, (161-168): [1] Institut fur Experimentalphysik, Technische Universitât, Graz, Graz, Austria, [2]Otrerreicisches Gieerei-Institut, Leoben, Austria.

18. Greenleaf corporation Inc. www.greenleafcorporation.com

19. Guoqin Shi, Xiaomin Deng. A finite element study of the effect of friction in orthogonal metal cuttiing. Dep. Of. Mechanical Eng., University of south carolina, Columbia, SC 29208, USA

20. H.G. Prengel a, P.C. Jindal b. A new class of high performance PVD coatings for carbide cutting tools 2001; 139, (2534): a Kennametal Hertel AG, 90766 Fuerth, Germany, b Kennametal Inc., Latrobe, PA 15650, USA. v. 139.

21. J. A. Arsecularatne, P. Mathew. The Oxley modeling approach, its applications and future directions. 2000; 4(3), School of Mechanical and Manufacturing Engineering, The University of New South Wales, UNSW 2052, Australia.

22. Kitagawa, T.; Kubo, A., and Maekawa, K. Temperature and wear of cutting tools in high-speed machining of Inconel 718 and Ti-6Al-6V-2Sn. Wear. 1997; 202(2. Jan):142-148; ISSN: 0043-1648.

23. L.K. Gillespie, J. Eng. Ind., 98 (1976) 64 74.

24. L. Ken , Lauderbaugh Saunders. A finite element model of exit burrs for drilling of metals. 2003; 40, (139-158): Mechanical and Aerospace Engineering, University of Colorado, 1867 Austin Blues Parkway Ste. 202E, Colorado Springs, CO 80918,USA.

25. L.Li, N.He. High speed cutting of Inconel 718 with coated carbide and ceramic inserts. 2002: Institute of Mechanical and Electrical, Nanjing University of eronautics and Astronautics, Nanjing 210016

26. M.B. Henderson+, D. Arrellb. Nickel-Based Superalloy Welding Practices for Industrial Gas Turbine Applications. +ALSTOM Power Technology Centre, Whetstone, UK, *ALSTOM Power Technology Centre, Daettwil, CH.

27. Ming Gao, Robert P. Wei. Grain boundaryNiobium carbides in Inconel 718. 1996: department of mechanical engineering and mechanics. Lehigh university, bethlehem, PA 18015 USA.

28. Norme Internationale ISO 3002/2-1982 (F).

29. Norme internationale ISO 3685:1993 (F).

30. P.C Jindal, A.T. Santhanam. Performance of PVD TiN,TiCN, and TiAlN coated cemented carbide tools in turning. Kennametal Inc. Corporate Technology, PO Boc 231, Latrobe, PA 15650, USA; 1999.

31. R.Komanduri, T.A. Schroeder. On shear stability in machining nickel-based superalloy. 1986; 108, (93-100).

32. Rahman, M.; Seah, W. K. H., and Teo, T. T. Machinability of inconel 718. Journal of Materials Processing Technology: Proceedings of 1996 3rd Asia Pacific Conference on Materials Processing,Nov 12-14 1996. 1997; 63(1-3. Jan):199-204; ISSN: 0924-0136.

33. Uhlmann, E. and Ederer, G. High-speed turning of Inconel 718. Industrial Diamond Review. 2001; 61(590):169-174; ISSN: 0019-8145.

34. Wang, Z. Y. and Rajurkar, K. P. Cryogenic machining of hard-to-cut materials. Wear. 2000; 239(2. Apr):168-175; ISSN: 0043-1648.

35. www.allvac.com.

36. Yusuf Altintas, Manufacturing Automation: meta cutting mechanics, machine tool vibrations, and CNC design, Cambridge University press 2000

37. Z.Y. Wang, K.P Rajurkar. Hybrid machining of Inconel 718. 2003: Nevada Manufacturing Reasearch Center, Department of mechanical Engineering, University of nevada, Las Vegas, Nevada, Industrial and Management

Systems Engineering Department, University of Nebraska-linconln, NE 68588-0518, USA.

38. Zhao, Jun; Deng, Jianxin; Zhang, Jianhua, and Ai, Xing. Failure mechanisms of a whisker-reinforced ceramic tool when machining nickel-based alloys. Wear. 1997; 208(1-2. Jul):220-225; ISSN: 0043-1648.

39. Zdzilaw klim, Emekki Ennajimi, Marek Balazinski Clement Fortin, Study of the influence of feed variation on tool wear, ASME 1990, vol.43

APPENDIX I. Cutting tools

I.1. The wear mechanism

The machining of Inconel 718 shows about all the ranges of wears noted during the machining of super alloys, in particular abrasion wear, adhesion wear, and diffusion. Each wear mechanism is prevalent according to the operating conditions and the tool type. During the machining at low cutting speed (20 m/min), Zhao et al [38] note the presence of adhesion wear, responsible for crater formation on the rake face.

(a) T_iN (b) T_iCN (c) T_iAlN

Figure 8.1. Crater wear on a T_iN, T_iCN and T_iAlN tool at 20 m/min. Source ([38])

Crater wear is not however considered as more alarming in the literature since the hardness of the tools used (often ceramic) limit this mode of wear and machining is generally carried out at speeds higher than 50 m/min. The wear mechanism which consequently becomes prevalent is abrasion wear. The zone considered by this type of wear is the flank face and particularly the notch zone.

Notch wear is by far the major cause of the weak performances of tools when machining of Inconel 718.

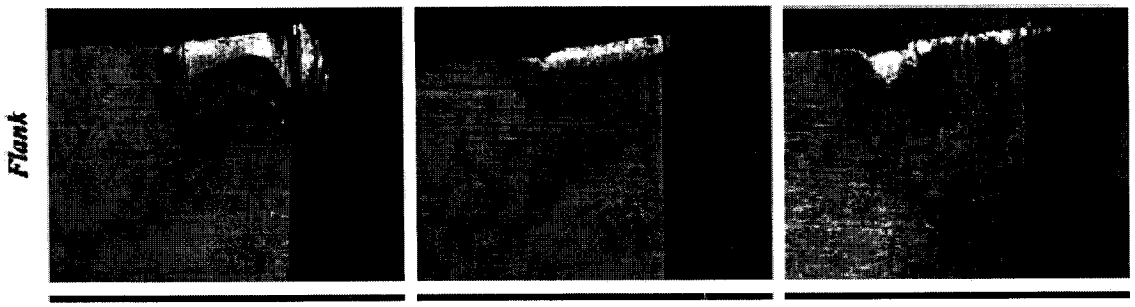

(a)T_iN (b) T_iCN (c) T_iAlN

Figure 8.2. Notch wear on a TiN, TiCN and TiAlN tool at Vc= 46 m/min. Source ([38])

I.2. Causes of notch wear

The appearance of notch wear is due to chemical causes (diffusion) and/or mechanical causes (abrasion) according to certain manufacturers. But the most frequently evoked cause in the literature is abrasion. The phenomenon of diffusion is rather frequent at high temperature, whereas notch wear appears practically at all the tested temperatures when machining Inconel 718. According to L.Li et al. [25], in the case of ceramics, the major mechanism of wear is the interaction between abrasion, adhesion and chipping. According to E. O. Ezugwu et al.[8], abrasion noted in the case of ceramics is due to the presence in Inconel 718 of hard phases of carbide, which are taken in sandwich during machining. These particles tear off portions of tool by abrasion. The same author also note that wear in the zone C of the tool tip becomes prevalent in the neighborhood of 250 m/min due to excessive temperature at this tool tip. According to Kitagawa et al.[22] and C. Ducros et al.[5], another cause of notch wear located in the depth of cut zone is, the work-hardened burrs , and lateral chip flow acting as abrasives on the tool by the formation of burrs on the machined part. E. O. Ezugwu et al.[9] note that the phenomenon of diffusion is also a prevailing mode at high cutting speeds (400 m/min). The diffusion of Ni (nickel) and Cr (chromium) of Inconel 718 in certain ceramic tools involves the formation of M_iS_i or CrS_i, weakening the tool. Uhlmann et al.[33] note that in turning with the PCBN (polycrystalline cubic Boron nitride), the notch wear tends to

decrease beyond 400 m/min, but crater wear takes the top. The phenomenon of diffusion is evoked to explain this tendency. It can arrive during the machining of Inconel 718 that the curve of notch wear has a shape of camel back as notes by Kitagawa et al.[22]. Tests carried out at a given speed can give the impression of an improvement of wear, but this tendency can be reversed by the following speeds. The author Kitagawa et al.[22] indicates that the phenomenon of material softening can explain this shape. The Testing of each type of tool to be used in production environment is necessary to identify these phenomena. But beyond 400 m/min, diffusion becomes more important and the tool wear becomes critical. Ezugwu et al.[12] also note some cases of deformation and thermal cracking of cutting the edge, chipping, some frequent ruptures of ceramic tools due to high temperatures.

I.2.1. Tool material

To compare different cutting tool performances during the machining of Inconel 718, the tools performance data was established base on tests performed by various authors. This database gathers different authors, different types of tools, coatings, geometries, cutting parameters and the tools wears.

To be able to compare the gathered information, a criterion has been established. The comparison will be made upon the total machining time required by a tool to remove an amount of 300 in^3 of material. 300 in^3 is approximately the volume of material to remove for the roughing process of the studied shaft. This time includes the tool changing time and the effective time the tool is in contact with the material. The total machining time (TmT) formula is then:

$TmT = (T + Tco)N$

T : Tool life (min)

T_{co}: Tool changing time (taken approximately 3 min)

$N = \frac{VolP}{VolA}$: Number of tool to use

$VolA = fa_p V_c T$: Volume of material removed by a tool

VolP: volume of material to remove (taken approximately $300in^3$)

f: feed (in/rev)

a_p : depth of cut (in)

V_c : Cutting speed (ft/min)

I.2.1.1 Carbide tools

a) The T_iN (Titanium nitride)

The TiN coating is less hard than TiC, but on the other hand it increases the tool chip friction coefficient. Several tests were described in the literature with TiN coated carbide tools. Three authors held our attention. The authors [12, 30, 32]. The substrate used for carbide is composed of WC (94%) and Co(6%).

Tool Number	Supplier	Insert	Tool type	Coating
14	Kennametal	CNGP 12 04 08	Carbide	TiN with PVD
8		Rhomboids ISO CNMP 120408	Carbide	TiN with PVD
10	Sumitomo Electric L.td	Rhomboids	Carbide	TiN with PVD

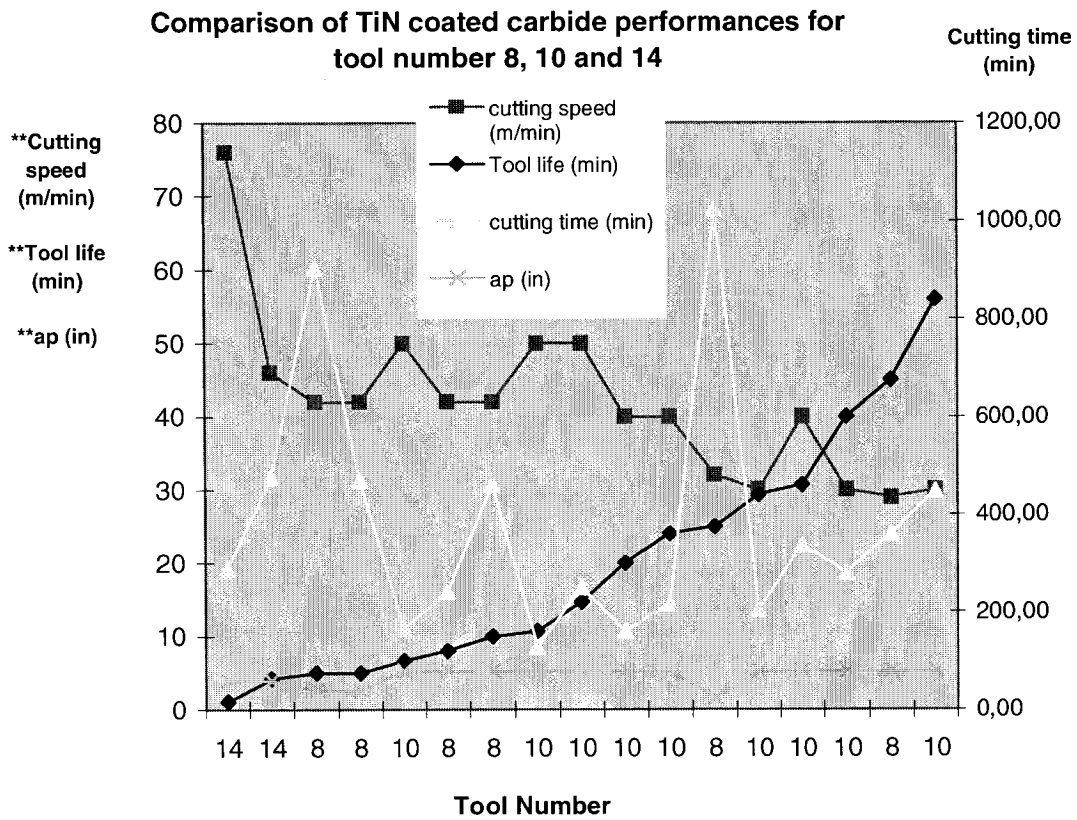

Figure 8.3. Comparison of TiN coated carbide performances for tool number 8, 10 and 14

Table 20: Cutting conditions for TiN coated tools

Tool Number	a_p (mm)	f (mm/tr)	Vc (m/min)	Tool life (min)	DOC (in 10^{-3}in)	f (10^{-3}in/ rev)	Speed (ft/min)	Cutting Time (min)
14	1,5	0,15	76	1,07	59,06	5,91	249,34	288,00
14	1,5	0,15	46	4,20	59,06	5,91	150,92	475,08
8	1	0,13	42	5,00	39,37	5,12	137,80	905,00
8	1	0,25	42	5,00	39,37	9,84	137,80	470,00
10	2	0,3	50	6,67	78,74	11,81	164,04	166,67
8	2	0,25	42	8,00	78,74	9,84	137,80	240,00
8	2	0,13	42	10,00	78,74	5,12	137,80	460,00
10	2	0,4	50	10,67	78,74	15,75	164,04	128,00
10	2	0,2	50	14,67	78,74	7,87	164,04	249,33
10	2	0,4	40	20,00	78,74	15,75	131,23	160,00
10	2	0,3	40	24,00	78,74	11,81	131,23	216,00
8	0,6	0,25	32	25,00	23,62	9,84	104,99	1025,00
10	2	0,4	30	29,33	78,74	15,75	98,43	205,33
10	2	0,2	40	30,67	78,74	7,87	131,23	337,33
10	2	0,3	30	40,00	78,74	11,81	98,43	280,00
8	2	0,25	29	45,00	78,74	9,84	95,14	360,00
10	2	0,2	30	56,00	78,74	7,87	98,43	448,00

These three curves represent the cutting speed used, the tool life and the depth of cut for 3 different tools used in different conditions by different authors. Table 20 gives the values used to draw the curves. It can be noticed that the cutting speed range is between 30 and 80 m/min. Logically the shape of the curve indicates that if the cutting speed decreases, the tool life tends to increase. For example for the tool number 10, the tool life reaches approximately 1 hour in these conditions. There is on the other hand a cutting speed zone in the neighborhoods of 40 to 50 m/min which seems to be ideal, because for this particular zone, the cutting time for the specified volume is minimum. We can also notice some peaks of cutting times which are specific to tool 8. It will be noticed that these peaks correspond to the depths of cut a_p (rather low, 1 mm and 0.6 mm, 39.37 10^{-3} in and 23.63 10^{-3} in). So the use of depth of cut of this size is non-

productive for this type of tool, because cutting times are unnecessarily longer. The ideal is around 2 mm, that is $78,74.10^{-3}$ in.

b) The TiCN (Titanium carbonitride)

The TiCN coating has the role to combine the hardness of the TiC (which resists well the abrasion and the low friction coefficient of the TiN.

Author P.C Jindal et al.[30] carried out tests with a TiCN coated carbide tool under the following conditions.

Table 21: Cutting conditions for TiCN coating tool

Tool number	Type of insert	a_p (mm)	f (mm/tr)	Vc (m/min)	DOC (10^{-3} in)	f (10^{-3}in/rev)	Speed (ft/min)	Tool life (min)
15	CNGP 12 04 08	1,5	0,15	76	59,06	5,91	249,34	1,60
15	CNGP 12 04 08	1,5	0,15	46	59,06	5,91	150,92	6,15

Comparing tool number 14 and and 15 which are tested in the same cutting conditions, the Figure 8.4 shows that the performances of TiCN are higher than the TiN for more than 40% in term tool life. This result is not surprising considering TiCN has the role to combine the properties of the TiN and the TiC.

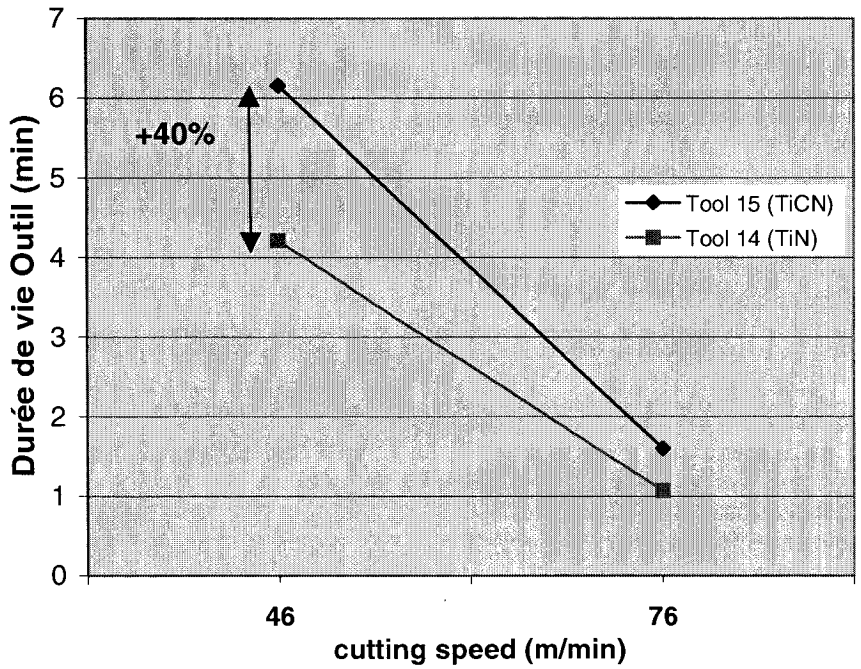

Figure 8.4. Comparison between TiN and TiCN

c) The TiALN coated tools

The TiAlN coating has a hardness which depends on the Al/Ti ratio according to F. Klocke et al.[13]. It reaches its higher hardness when this ratio is equal to 1. The author P.C Jindal et al.[30] carried out tests with the TiAlN under same the conditions as previously Table 22.

Table 22: Cutting conditions for TiAlN coating

Tool number	Type d'insert	ap (mm)	f (mm/tr)	Vc (m/min)	DOC (in)	f (in/rev)	Speed (ft/min)	Tool life (min)
16	CNGP 12 04 08	1,5	0,15	46	59,06	5,91	150,92	9,75
16	CNGP 12 04 08	1,5	0,15	76	59,06	5,91	249,34	3,20

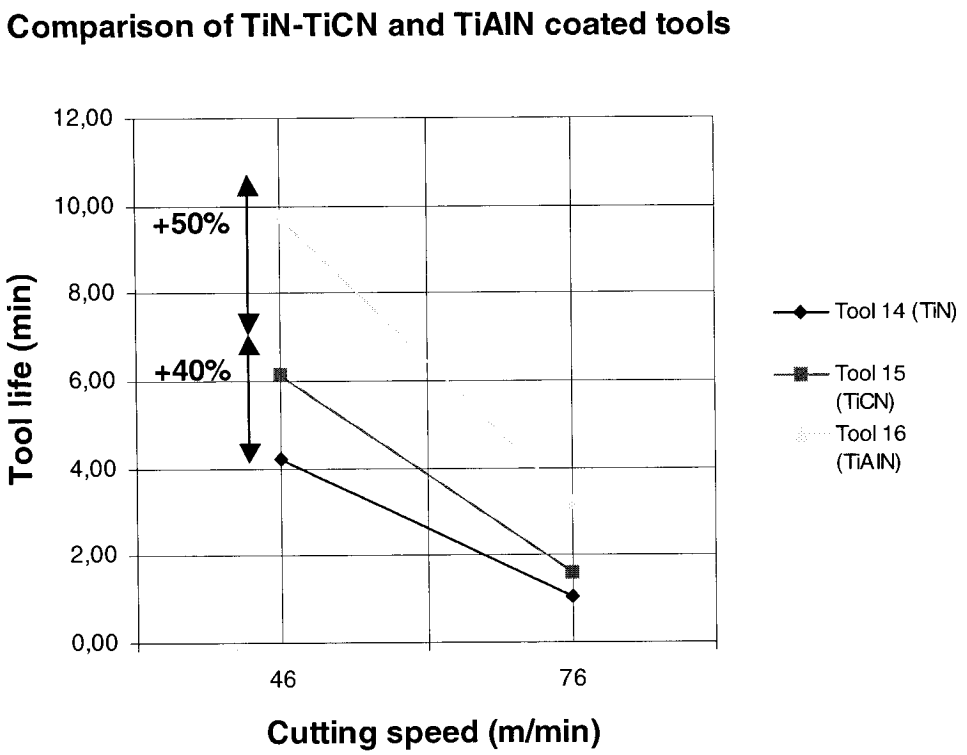

Figure 8.5. Comparison of TiN-TiCN and TiAlN coated tools

The tool life of TiAlN coating is higher than the TiCN coating for more than 50%. The Vickers hardness curve as a function of temperature of these coating (TiN, TiCN and TiAlN) Figure 8.6 gives a reason of the superiority of TiAlN over TiCN.

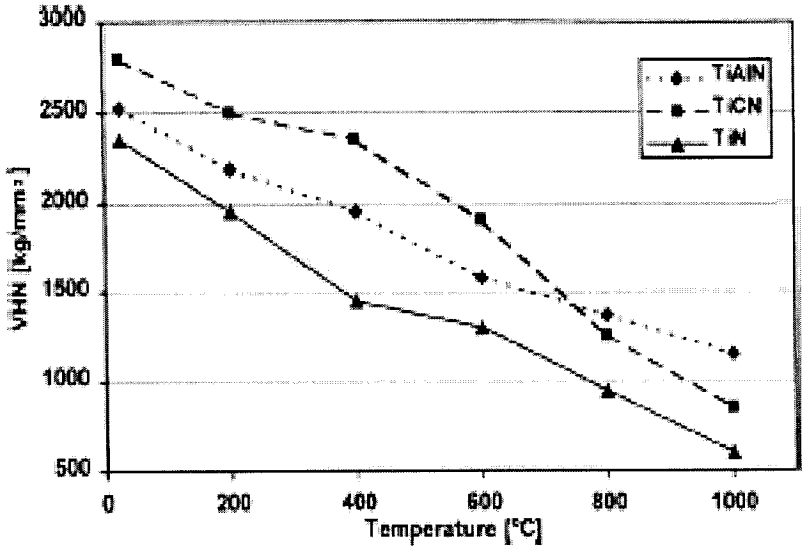

Figure 8.6. Vickers hardness according to the temperature of the TiN, TiCN and TiAlN (Source [10])

According to Figure 8.6, beyond 800 °C the hardness of TiAlN becomes higher than that of TiCN, even if the cold TiCN is the hardest. It is known that a harder tool will better resist the phenomenon of abrasion. So this curve can be an explanation.

d) The Al_2O_3 coating

The Al_2O_3 coating is a refractory coating which resists high temperatures. According to F. Klocke et al.[13] the (PVD) process is not suitable for the ceramic coatings like Al_2O_3. The process used for this case is the CVD which requires a higher temperature of the substrate to carry out the deposit. To decrease the harmful effect of temperature on the substrate transverse strength, a moderate temperature (MT-CVD) about 850 degree is used, instead of 1100 degree for the CVD. The authors Rahman et al.[32] and of P.C Jindal et al.[30] studied Al_2O_3 coatings and their performances were close to those of TiCN and TiAlN.

Table 23: Cutting conditions for a Al_2O_3 coating tools

Number	ap (mm)	f (mm/tr)	Vc (m/min)	DOC (in)	f (in/rev)	Speed (ft/min)	Tool life (min)
11	2	0,2	50	78,74	7,87	164	3,5
11	2	0,2	30	78,74	7,87	98	3,75
14	1,5	0,15	46	59,06	5,91	151	4,2
11	2	0,2	40	78,74	7,87	131	6
15	1,5	0,15	46	59,06	5,91	151	6,15
11	2	0,2	50	78,74	7,87	164	8,5
16	1,5	0,15	46	59,06	5,91	151	9,75
11	2	0,2	30	78,74	7,87	98	10
11	2	0,2	40	78,74	7,87	131	12,5

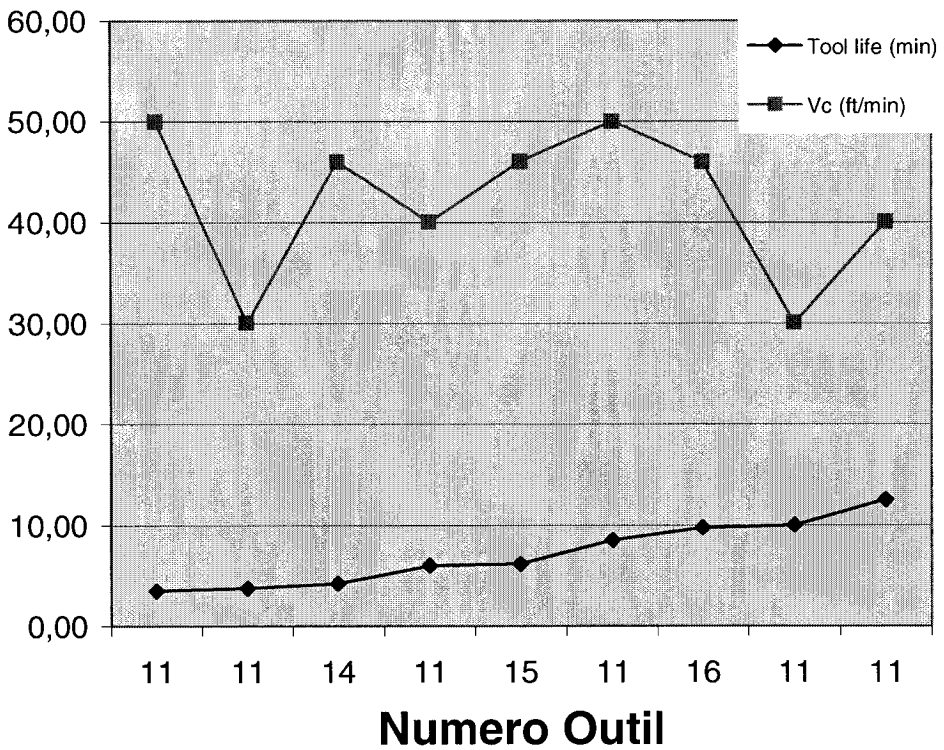

Figure 8.7. The Al_2O_3 coating compare to TiAlN and TiCN

e) The multi-layer coated carbides

Several combinations can be made with the coatings mentioned previously i.e. the TiN, TiCN, TiAlN, Al2O3 and CrN to obtain a multi-layer coating. The goal of these combinations is to create a good adhesion with the substrate tool, to improve the mechanical properties like hardness and tenacity of the tool et also to reduce the tool chip friction coefficient. Many combinations exist in the market, and according to the manufacturer the tool behavior can be different.

f) The ceramic tools

f_1) Pure ceramics

Pure ceramics does not give good results for the machining of Inconel 718 because of their low fracture strength according to Ezugwu et al.([9] ,[11]). Ezugwu et al [11] carried out test on the oxide (Al_2O_3+ZrO_2). The operating conditions are as followed:

Number	Item	Type of insert	Composition	a_p(mm)	f (mm/tr)	Vc (m/min)	Tool life (min)
12	Oxyde pure (Al_2O_3+ ZrO_2)	CNGN 12 04 12T	(Al_2O_3+ZrO_2) 99%+1%	2	0,125	152	0,01

Under these conditions of operation the tool life is lower than 30 seconds what is not enough for the industrial applications.

f_2) Mixed ceramics

There are two types of mixed ceramic commonly used to machine Inconel 718. The alumina oxide base ceramic (Al_2O_3) and the Silicon nitride base (Si_3N_4).

f_{21}) Alumina oxide base ceramic (Al_2O_3)

Tools number 13 (Al_2O_3+TiC) and 4 (Al_2O_3+TiC -Mo-Ni) have short lives for the cutting conditions used, i.e lower than 1 min. These two types of tool used by different authors Ezugwu et al [11] and Zhao et al.[38] are in fact the same type of mixed ceramics tool 13 (Al_2O_3+TiC). Even if in the neighborhoods of 50 m/min the lives of these tools are slightly higher than 1 min, that remains very short. The increase of material removal rate of ceramics compared to carbides is obvious, but this increase in the case of these tools does not make it possible to remove sufficient volumes of material per edge in a reasonable time. The tool which comes in second position is the (Al_2O_3 -(W, Ti)C) which contains tungsten. This tool although better than the precedent, does not give good results in term of tool life. In the neighborhoods of 100 m/min the tool life is about 1.5 min, which is not enough.

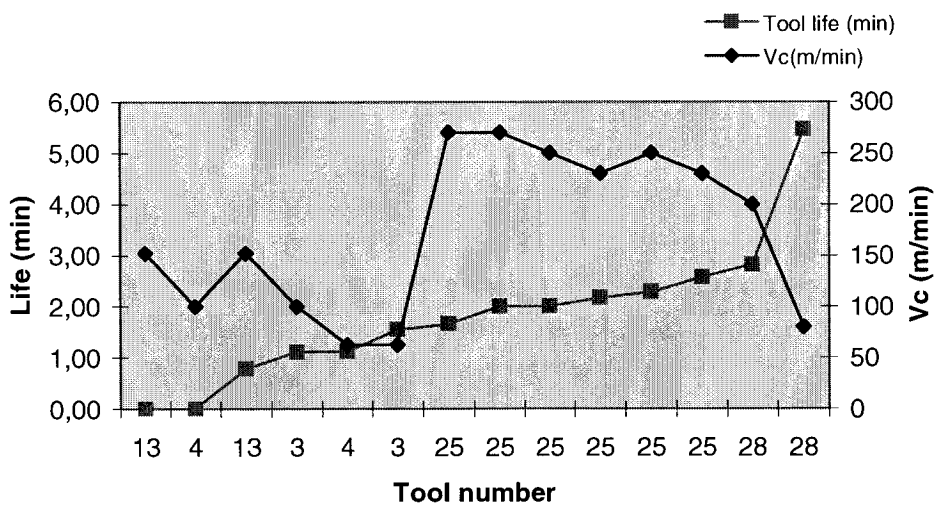

Figure 8.8. Tool life and cutting speed for a Al_2O_3 based ceramic

For tools number 25 (Al_2O_3 +TiCN+ZrO2) and 28 (Al_2O_3+TiB_2) the tool life is about 3 min, for cutting speeds from 200 to 230 m/min (656 to 755 ft/min). Good results can be obtain in term of productivity, since material removal rate is about of about 5 in^3/min.

Under these conditions of operation, cutting time is about 100 min to remove 300 in^3, whereas average time in industry for this same removed volume is of 165 min.
The addition of TiCN and TiB_2 to Al_2O_3 mixed ceramics can improve the productivity.

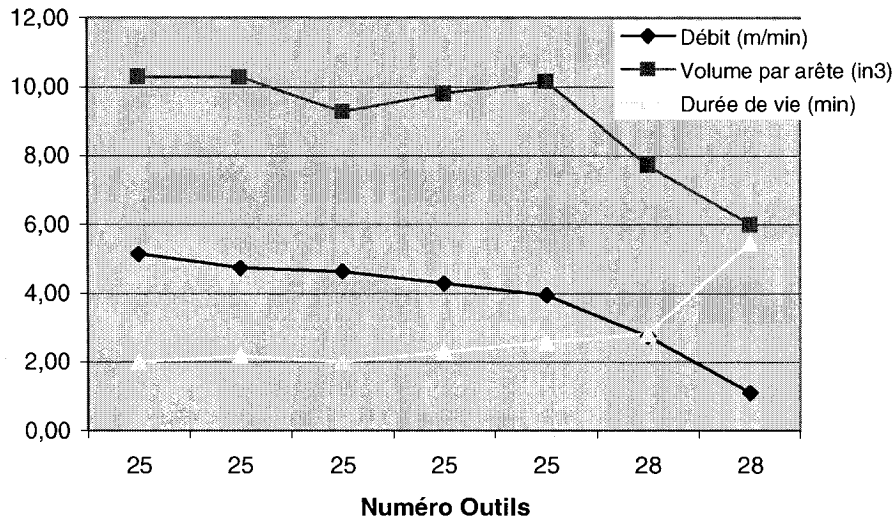

Figure 8.9. Tool life and cutting speed for a Al_2O_3 based ceramic with TiCN and Tib_2

f_{22}) Silicon nitride base ceramics

A certain number of authors used Silicon nitride ceramics to machine Inconel 718 under various cutting conditions. For example tool number 5 of Si_3N_4 was used by author Kitagawa et al. [22], Sialon tools by authors Zhao et al.[38] and L.Li et al.[27]. Under the specified conditions in the Table 24, the comparison of the various tools grades was performed.

Table 24: Data of test for ceramics Silicon nitride base ceramics

No	Item	supplier	Type of insert	a_p (mm)	f (mm/tr)	Vc (m/min)	DOC(in)	f (in/rev)	Vc (ft/min)	Tool life (min)
6	Si3N4		Carré	0,5	0,19	100	19,69	7,48	328,08	1,18
1	Sialon		SNG15083	0,3	0,15	100	11,81	5,91	328,08	1,63
23	Sialon Grade KY3000	Kennametal	SNG 433T0420	0,4	0,2	100	15,75	7,87	328,08	2,05
20	Sialon Grade KY2000	Kennametal	SNG 432	0,4	0,2	100	15,75	7,87	328,08	4,74
22	Sialon Grade KY2100	Kennametal	SNG 433T0420	0,4	0,2	100	15,75	7,87	328,08	7,57
21	Sialon Grade KY2100	Kennametal	RNG 45T0420	0,4	0,2	100	15,75	7,87	328,08	7,65

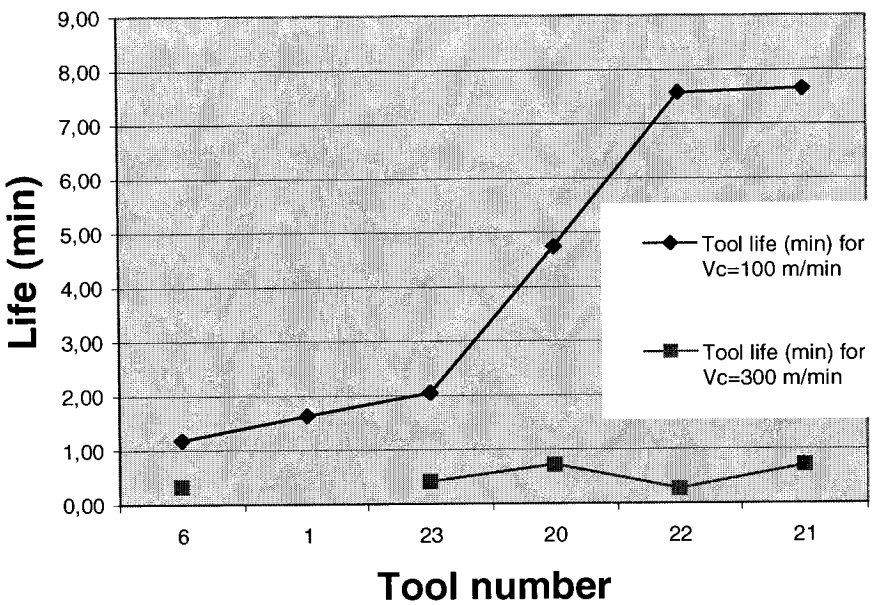

Figure 8.10. Tool life of Si_3N_4 mixed ceramics according to the cutting speed for different tool number

The tool lives are very short, about 1 min for tool number 6 (pure Si_3N_4) from the author Kitagawa et al.[22]. For the other tools in Sialon, those of Kennametal mark seem to be the best (21, Sialon Rank KY2100 of Kennametal). But in term of cutting time, the sialon are not better than mixed ceramics of alumina oxide Al_2O_3. Even if the cutting time of all these Sialon joined together seems to be about 200 min, with the cutting speeds of 300 m/min (984 ft/min), compared to 100 min for 200 m/min for mixed ceramics of Al_20_3, it is not possible to conclude about the superiority of one type of tool compared to the other. The reason is that the depth of cut used for the preceding study is about 1.5 to 2.25 mm instead of 0.3 to 0.4 mm for that case. Obviously the operating conditions are not identical and no comparison is possible. On the other hand it seems that the depths of cut used by the authors are not optimal. These tools could be used for roughing operations with depth of cut of about 2 to 2.25 mm.

f_{23}) Whisker reinforced ceramics

The most used ceramic reinforcement for the machining of nickel alloys is the silicon carbide fibbers called Sic-whisker (shortened SiCw). This reinforcement contributed to increase considerably the tool life when machining of Inconel 718. The reason is according to Ezugwu et al.[9], notch decreases with the cutting speed. It is thus possible to reach cutting speeds of 400 m/min while maintaining a good tool life. But the author notes that at very high temperatures the phenomenon of diffusion becomes prevalent. The diffusion of Ni and Cr of Inconel 718 in the tool, involves the formation of MiSi or CrSi which weakens it. The reinforcement can relate to ceramics containing Silicon nitride (Si_3N_4), Ezugwu et al [8] or those based on alumina Al_20_3, Z.Y. Wang [36], Deng Jianxin et al.[7] and Zhao et al.[37].

Num	Insert	Ap (mm)	f (mm/tr)	Vc (m/min)	DOC (in)	f (in/rev)	Speed (sfm)	MRR (in3/min)	Cutting time	tool life (min)
26	SNGN 120	2,25	0,15	270	88,58	5,91	885,83	5,56	54,29	0,57
26	SNGN 120	2,25	0,15	250	88,58	5,91	820,21	5,15	58,29	0,86
26	SNGN 120	2,25	0,15	230	88,58	5,91	754,59	4,74	63,77	1,03
26	SNGN 120	2,25	0,125	270	88,58	4,92	885,83	4,63	65,14	0,86
26	SNGN 120	2,25	0,125	250	88,58	4,92	820,21	4,29	69,94	1,03
26	SNGN 120	2,25	0,125	230	88,58	4,92	754,59	3,95	76,57	1,14
29	SNGN 120	1,5	0,15	200	59,06	5,91	656,17	2,75	113,65	5,98
27	SPGN	0,76	0,127	300	29,92	5	984,25	1,77	171,07	4,89
27	SPGN	0,76	0,127	300	29,92	5	984,25	1,77	171,66	2,72
27	SPGN	0,76	0,109	300	29,92	4,29	984,25	1,52	200,2	3,64
2	SPGN	0,3	0,15	280	11,81	5,91	918,64	0,77	390,72	0,83
2	SPGN	0,3	0,15	280	11,81	5,91	918,64	0,77	390,86	0,86
2	SPGN	0,3	0,15	230	11,81	5,91	754,59	0,63	475,28	1,04
2	SPGN	0,3	0,15	180	11,81	5,91	590,55	0,49	607,11	1,75
2	SPGN	0,3	0,15	125	11,81	5,91	410,1	0,34	874,67	2,13
2	SPGN	0,3	0,15	125	11,81	5,91	410,1	0,34	874,8	1,2
2	SPGN	0,3	0,15	100	11,81	5,91	328,08	0,27	1096,09	5,62

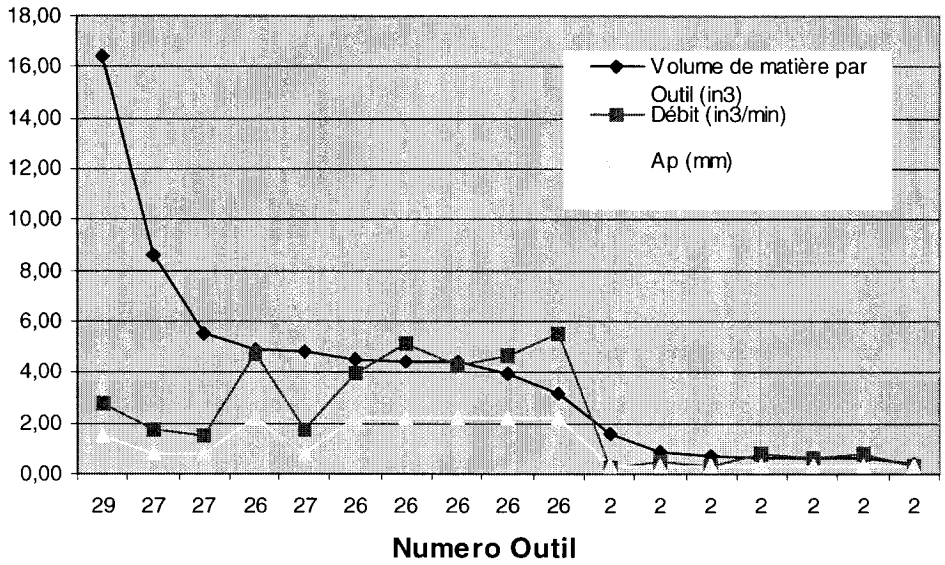

Figure 8.11. Volume of material, material remove rate of the Sic whisker reinforced tools according to the tool number under various cutting conditions

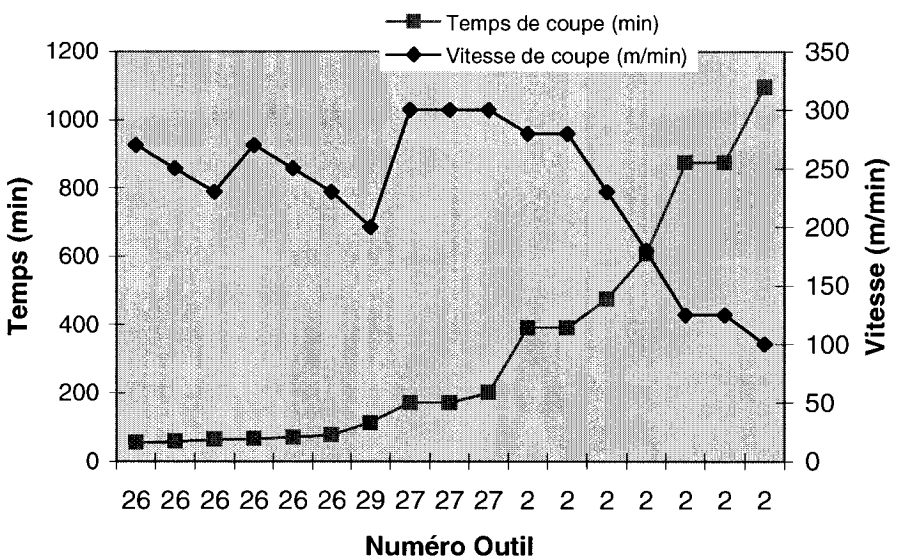

Figure 8.12. Effective cutting time of the Sic whisker reinforced tools according to the tool number used under various cutting conditions

For SiC whisker reinforced ceramics, the cutting speeds generally used are beyond 200 m/min (650 ft/min). According to data obtained from the articles, the best tool in term of volume of material removed is tool 29 ($Al_2O_3/TiB_2/SiCw$) for a volume of 3.18 in^3 per edge. We saw previously that the mixed aluminum oxide (with addition of TiB_2) was a good combination in term of productivity. The same tool material reinforced this time with Sic-Whisker thus seems to be among the best in term of volume of material removed per edge. For this tool the cutting time is about 113 min what is rather correct compared to the industrial conditions of about 165 min. The best cutting time (55 min) is obtained for the tool 26 (Si_3N_4+SiCw)(75%+35%) which is a ceramic containing silicon nitride. For this tool, the volume of material removed per edge is approximately 5 in^3. Tool 27 (SiCw+ Al_2O_3) and Tool 2 (25% by volume of SiCw + Al_2O_3) are the same tools used by different authors under different cutting conditions. It is noticed however that although having cutting times of approximately 200 min, one can not deduce compared to the present data that (SiCw+ Al_2O_3) is better or worst than (Si_3N_4+SiCw) in term of productivity, because the depth of cutting used by the author of the tests on (SiCw+ Al_2O_3) is about 0.76 mm instead of 2.25 mm for (Si_3N_4+SiCw). It is thus logical that the cutting time of the first ranks above the second. One can on the other hand assume that the contribution of TiB_2 makes tool 29 definitely better than (SiCw+ Al_2O_3) without TiB_2. That is confirmed by Ezugwu et al.[9]. The same author also affirms [8] that the mixed ceramic of Al_2O_3 is better than mixed ceramics of Si_3N_4 in term of tool life. The reinforcement in SiCw in general gives better volumes of material removed for the tools compared to the configurations without reinforcements, because these reinforcements increase the tool life under the same cutting conditions or even under higher cutting conditions [9].

f_{23}) The coated ceramics

According to Felloni et al.[14], the chromium coating (CrN) can increase a ceramic tool life. The author carried out tests with two variables, the cutting feed (f) and the cutting speed (Vc). He thus determines the influence of CrN coating on the variables zone (f and

Vc) where the tool can be used efficiently. He concluded that the increase in tool life is due to the fact that the CrN coating extends the thermal barrier of the tool.

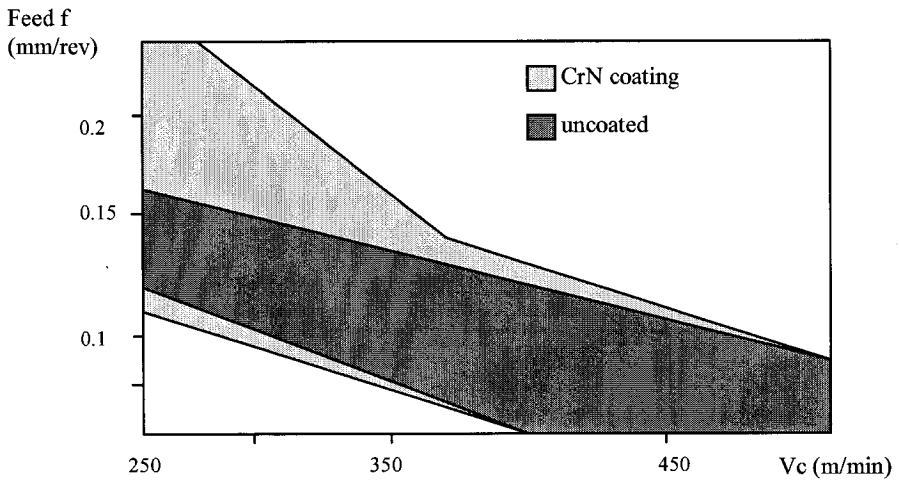

Figure 8.13. Cutting zone to avoid tool breaking after a volume of 40 cm^3 of material removed.

The presence of CrN coating on the ceramic tool gives, according to the author, a model of VB wear which does not follow the Taylor law ($Vb=A.ap^{\alpha}f^{\beta}Vc^{\gamma}$). For the same volume of material removed, the shape of VB wear as a function of cutting feed and speed is shown in the following curves.

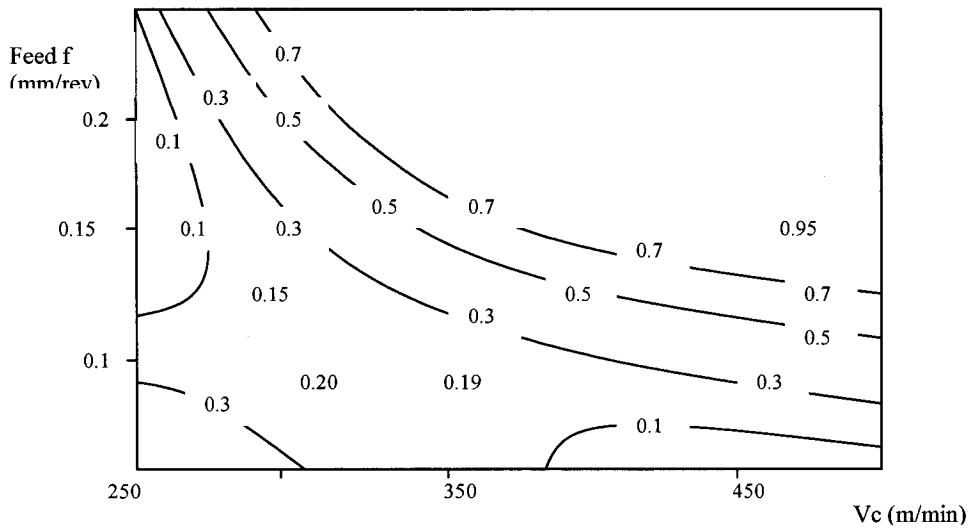

Figure 8.14. Flank wear VB (mm) of the CrN coated tools versus cutting speed and feed; experimental results refer to machined volume of $40x10^{-6}$ m3

The fact that the wear curves does not respect the Taylor law makes approximate the data obtained from the analysis for certain cutting parameters. It is thus necessary to carry out tests to be able to suitably exploit provided information.

g) The cubic boron nitride (CBN)

The tests with PCBN tools (polycrystalline CBN) were carried out by certain authors including author Uhlmann et al.[33]. In these tests the author used chamfered and non chamfered tools. The Figure 8.15 indicates that the best cutting conditions for the CBN are around the cutting speed of 400 m/min i.e 1312 ft/min. This cutting speed is rather high compared to the conditions which we indexed until there. Nevertheless the cutting time noted is about 250 min, which is very large compared to the cutting time in industry of about 165 min, or the cutting time of tool 26 of whisker (Si_3N_4+SiCw) about 55 min.

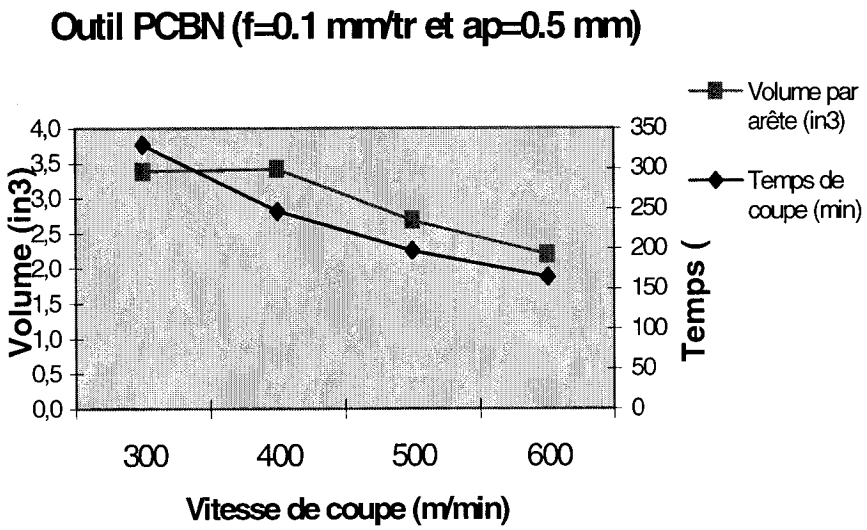

Figure 8.15. Volume of material removed and effective cutting time for a PCBN tool.

That can be explained by the operating conditions of the author, that is to say a depth of cut of 0.5 mm instead of 2 mm for tool 26 for example. Nevertheless, if the author had used these same depths of cut, it is not clear that the cutting speed of 400 m/min would give a shorter tool life. In spite of this small depth of cut of 0.5 mm, the tool life of the PCBN tool is of 2.75 min, the same range as the reinforced ceramic tools we treated previously. It is thus not sure that the PCBN is better than reinforced ceramics. Its high cost is also a considerable factor which makes its use in production not frequent.

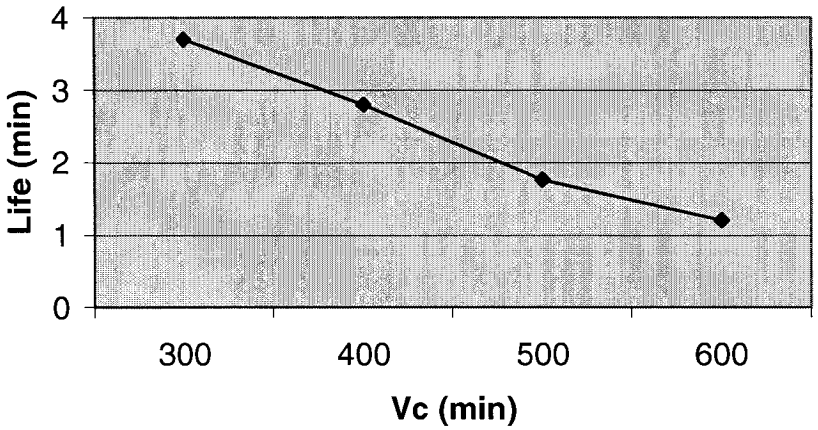

Figure 8.16. Tool life of PCBN tool as a function of cutting speed

I.2.2. Tool geometry

I.2.2.1 Chamfered edge

To avoid edges breakage, cutting edge can be chamfered. The author [33] carried out some tests on the PCBN, which enable us to say the chamfered tools are less productive than the non chamfered ones. In the following Figure 8.17, we can note that the volume of material removed per edge for the chamfered tools is lower than that of the tools whose edge is not chamfered. This volume decreases with the length of the chamfer.

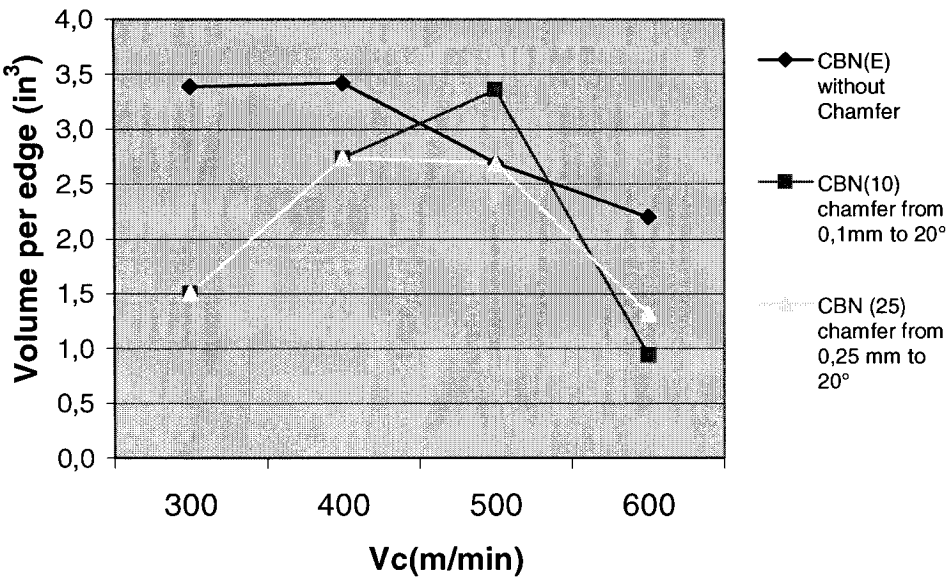

Figure 8.17. Comparison of chamfered and non chamfered edges

I.2.2.2 The effect of tool angles

a) The effect of lead angle

To analyze the effect of lead angle on the machining of Inconel 718, we retain the article of author Rahman et al. [32]. The tool number 11 is used for these tests:

Table 25: Operating conditions to assess the effects of lead angle

Number	Item	Insert	Rake	Lead	a_p(mm)	f (mm/tr)	Vc (m/min)	Tool life (min)
11	AC25 Carbure cementé	Rhomboïdes	0	-5	2	0,2	40	1,25
11	AC25 Carbure cementé	Rhomboïdes	0	15	2	0,2	40	6,00
11	AC25 Carbure cementé	Rhomboïdes	0	45	2	0,2	40	12,50

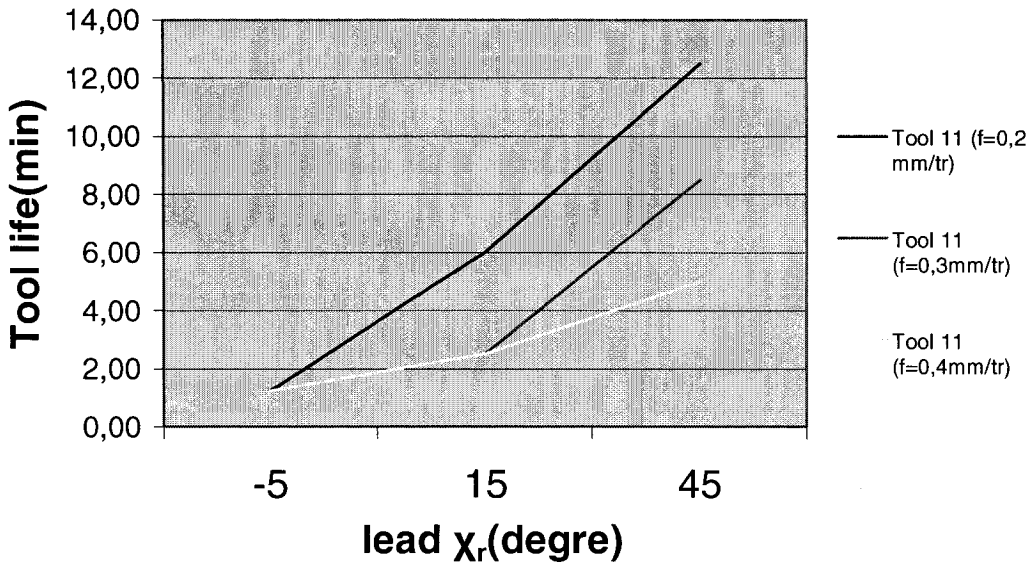

Figure 8.18. Tool life in function of lead angle

For the conditions tested by the author while varying the feed from (0.2, 0.3 and 0.4 mm/tr), the tool life increases with the complementary lead χ_r, so decreases with the lead angle κ_r, Figure 9.19.

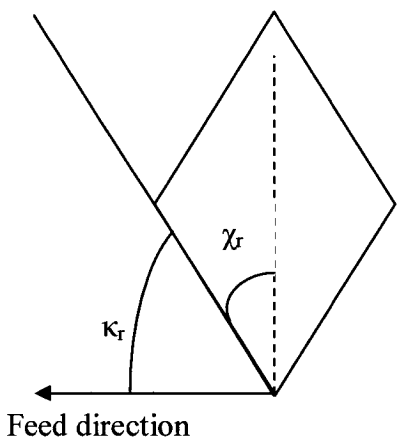

Figure 8.19. Lead angle κ_r and complementary lead angle χ_r

b) The effects of the rake angle

The author L.Li et al.[25] was chosen to analyze the effect of the rake angle on the tool life. These authors used different ceramic tools in different machining conditions.

Table 26: Operating conditions to assess the effect of the rake angle

Number	Tool type	Rake	Lead angle	a_p (mm)	f (mm/tr)	Vc (m/min)	Tool life (min)
22	Sialon Grade KY2100	-15	0	0,4	0,2	100	14,03
22	Sialon Grade KY2100	-7	0	0,4	0,2	100	7,57
22	Sialon Grade KY2100	5	0	0,4	0,2	100	32,98
23	Sialon Grade KY3000	-15	0	0,4	0,2	100	3,62
23	Sialon Grade KY3000	-7	0	0,4	0,2	100	2,05
23	Sialon Grade KY3000	5	0	0,4	0,2	100	3,85

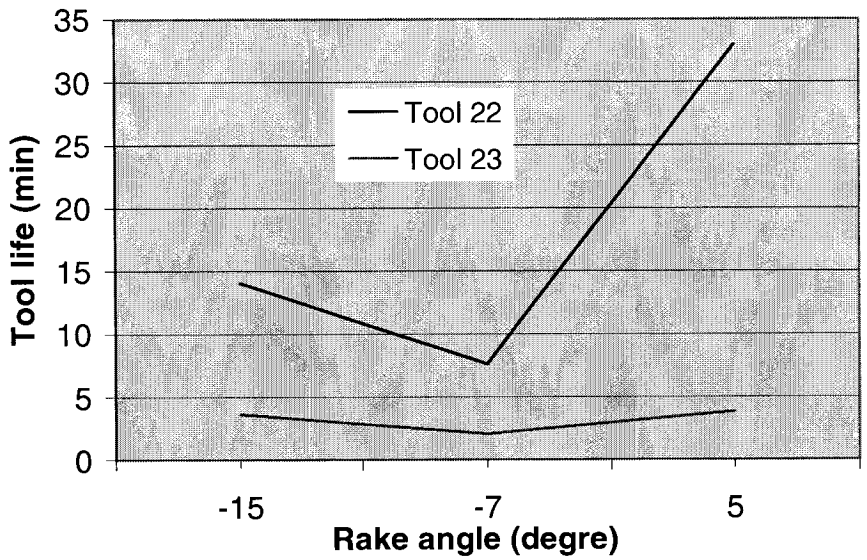

Figure 8.20. Tool life as a function of rake angle

The Figure 120 indicates that the tool life when machining Inconel 718 in longer when the rake angle is positive. The problem raised by this observation is the possibility to find a tool with a highest rake angle without weakening the insert.

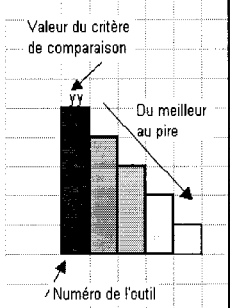

	Carbures						Céramiques						CBN
	Non revêtu	Mono revêtement				Multi revêtement		Pur	Mixtes		Renforcés			Revêtus	PCBN
		TiN	TiCN	TiAlN	Al2O3	Al2O3/TiCN/TiN	TiCN/TiN/TiCN		Si3N4	Al2O3	Si3N4	Al2O3	nano-Al2O3	CrN	
Meilleurs Temps Total de coupe (minute)	5019 (5)	390 (8)	722 (15)	870 (16)	280 (11)	1845 (19)	265 (9)	1374 (12)	721 (22)	210 (25)	373 (26)	208 (29)	162 (24)	158 (33)	686 (30)
Meilleurs Volumes de matière enlevée par arête (in3)	1 (5)	40 (8)	3 (15)	6 (16)	22 (11)	2 (19)	61 (9)	1 (12)	16 (22)	10 (25)	5 (26)	16 (29)	17 (24)	18 (33)	3 (30)
Meilleurs durées de vie d'Outil (minute)	1 (5)	45 (8)	6 (15)	9 (16)	15 (11)	10 (19)	48 (9)	2 (12)	32 (22)	13 (7)	1,1 (26)	10 (29)	4 (24)	4 (33)	3 (30)
Meilleurs débits de matière enlevée par arête (in3/minute)	1 (5)	1,2 (8)	1 (15)	1 (16)	2,4 (11)	1 (19)	1,2 (9)	2,3 (12)	1,7 (6)	5,6 (6)	5,6 (29)	2,8 (29)	5,6 (24)	6 (33)	1,5 (30)
Meilleurs temps effectifs de coupe (minute)	1092 (5)	240 (8)	288 (15)	288 (15)	123 (11)	614 (19)	240 (9)	129 (12)	172 (6)	54 (6)	54 (29)	114 (29)	54 (24)	49 (33)	78 (30)

Steel cutting time

Number	Supplier	Item	Coating	Composition	Doc (10^{-3} in)	f (10^{-3} in/rev)	Speed (ft/min)	Tool life (min)	MRR (in^3/min)	Volume(in^3)	Cutting time (min)	Total Time (min)	Tool number
33		Ceramic renforce SiCw revetu	CrN with PVD	(Al2O3+SiCw)(20% SiC)	59	9	689	4,3	4,23	18	73	158	17
24		nano-ceramic Al2O3 renforce SiCw	none	(Al2O3+SiC)(70%+30%)	89	5	820	4,0	4,29	17	72	162	18
29		Ceramic Al2O3 renforce SiCw	none	(Al2O3/TiB2/SiCw)vol 72% 18% 10%	59	6	656	6,0	2,75	16	114	209	19
25		Ceramic mixte Al2O3	none	(Al2O3+TiCN+ZrO2)(75 %+20%+5%)	89	6	820	2,0	5,15	10	60	210	30
9		Carbure multi revetu	PVD TiN/TiCN/TiN	Wc (94%) Co(6%)	79	10	138	48,0	1,28	62	240	255	5
11	Sumitomo Electric L.td	Carbure mono revetu	CVD multi Al2O3		79	16	98	15,0	1,46	22	210	260	14
26		Ceramic Si3N4 renforce SiCw	none	(Si3N4+SiC)(75%+35%)	89	6	755	1,0	4,74	5	64	374	62
8		Carbure mono revetu	TiN with PVD	Wc (94%) Co(6%)	79	10	138	8,0	1,28	10	240	330	30
30		PCBN	none	PCBN DBC50 CBn=50%, grain size 2 micron	20	4	1312	2,8	1,22	3	246	666	88
22	Kennametal	Ceramic mixte Si3N4	none	Sialon	16	8	328	33,0	0,49	16	627	722	19
16	Kennametal	Carbure mono revetu	TiAlN with PVD	WC-6%wtCo	59	6	151	9,8	0,63	6	478	723	49
15	Kennametal	Carbure mono revetu	TiCN with PVD	WC-6%wtCo	59	6	151	6,2	0,63	4	480	870	78
12		Ceramic pur	none	(Al2O3+ZrO2) 99%+1%	79	5	499	0,5	2,32	1	130	1375	249
19	Kennametal	Carbure multi revetu	CVD Al2O3/TiC/Ti CN		16	8	164	10,0	0,24	2	1230	1645	123
5		Carbure non revetu	none	(Carbure K10 (WC-Co)	12	6	205	2,7	0,17	0	1750	6020	654

Best volume of material removed per edge

Number	Supplier	Item	Coating	Composition	Doc (10^{-3} in)	f (10^{-3} in/rev)	Speed (ft/min)	Tool life (min)	MRR (in^3/min)	Volume(in^3)	Cutting time (min)	TotalTime (min)	Tool number
9		Carbure multi revetu	PVD TiN/TiCN/TiN	Wc (94%) Co(6%)	79	10	138	48,0	1,28	62	240	265	5
8		Carbure mono revetu	TiN with PVD	Wc (94%) Co(6%)	79	10	95	45,0	0,88	40	360	400	8
11	Sumitomo Electric L.td	Carbure mono revetu	CVD multi Al2O3		79	16	98	15,0	1,46	22	210	280	14
33		Ceramic renforce SiCw revetu	CrN with PVD	(Al2O3+SiCw)(20 % SiC)	59	9	689	4,3	4,23	18	73	158	17
24		nano-ceramic Al2O3 renforce SiCw	none	(Al2O3+SiC)(70% +30%)	89	5	820	4,0	4,29	17	72	162	18
29		Ceramic Al2O3 renforce SiCw	none	(Al2O3/TiB2/SiC w)vol 72% 18% 10%	59	6	656	6,0	2,75	16	114	209	19
22	Kennametal	Ceramic mixte Si3N4	none	Sialon	16	8	328	33,0	0,49	16	627	722	19
25		Ceramic mixte Al2O3	none	(Al2O3+TiCN+Zr O2)(75%+20%+5 %)	89	6	820	2,0	5,15	10	60	210	30
16	Kennametal	Carbure mono revetu	TiAlN with PVD	WC-6%wtCo	59	6	151	9,8	0,63	6	478	723	49
26		Ceramic Si3N4 renforce SiCw	none	(Si3N4+SiC)(75% +35%)	89	6	755	1,0	4,74	6	64	374	62
15	Kennametal	Carbure mono revetu	TiCN with PVD	WC-6%wtCo	59	6	151	6,2	0,63	4	480	870	78
30		PCBN	none	PCBN DBC50 CBn=50%, grain size 2 micron	20	4	1312	2,8	1,22	3	246	686	88
19	Kennametal	Carbure multi revetu	CVD Al2O3/TiC/TiCN		16	8	164	10,0	0,24	2	1230	1845	123
12		Ceramic pur	none	(Al2O3+ZrO2) 99%+1%	79	5	499	0,5	2,32	1	130	1375	249
5		Carbure non revetu	none	(Carbure K10 (WC-Co)	12	6	205	2,7	0,17	0	1750	5020	654

Best tool life

Number	Supplier	Item	Coating	Composition	Doc (10^{-3} in)	f (10^{-3} in/rev)	Speed (ft/min)	Tool life (min)	MRR (in^3/min)	Volume(in^3)	Cutting time (min)	TotalTime (min)	Tool number
9		Carbure multi revetu	PVD TiN/TiCN/TiN	Wc (94%) Co(6%)	79	10	138	48,0	1,28	62	240	265	5
8		Carbure mono revetu	TiN with PVD	Wc (94%) Co(6%)	79	10	95	45,0	0,88	40	360	400	8
22	Kennametal	Ceramic mixte Si3N4	none	Sialon	16	8	328	33,0	0,49	16	627	722	19
11	Sumitomo Electric L.td	Carbure mono revetu	CVD multi Al2O3		79	16	98	15,0	1,46	22	210	280	14
7		Ceramic mixte Al2O3	none	(Al2O3+TiC) (70% +30%)	20	7	82	13,3	0,14	2	2080	2860	156
29		Ceramic Al2O3 renforce SiCw	none	(Al2O3/TiB2/SiCw)vol 72% 18% 10%	59	6	262	10,0	1,1	12	273	398	25
19	Kennametal	Carbure multi revetu	CVD Al2O3/TiC/TiCN		16	8	164	10,0	0,24	2	1230	1845	123
16	Kennametal	Carbure mono revetu	TiAlN with PVD	WC-6%wtCo	59	6	151	9,8	0,63	6	478	723	49
15	Kennametal	Carbure mono revetu	TiCN with PVD	WC-6%wtCo	59	6	151	8,2	0,63	4	480	870	78
33		Ceramic renforce SiCw revetu	CrN with PVD	(Al2O3+SiCw)(20% SiC)	59	9	689	4,5	4,23	18	73	158	17
24		nano-ceramic Al2O3 renforce SiCw	none	(Al2O3+SiC)(70%+30%)	89	5	755	4,5	3,95	17	77	167	18
30		PCBN	none	PCBN DBC50 CBn=50%, grain size 2 micron	20	4	984	3,7	0,92	3	329	774	89
5		Carbure non revetu	none	(Carbure K10 (WC-Co)	12	6	205	2,7	0,17	0	1750	5020	654
26		Ceramic Si3N4 renforce SiCw	none	(Si3N4+SiC)(75%+35%)	89	5	755	1,1	3,9475	5	77	412	67
12		Ceramic pur	none	(Al2O3+ZrO2) 99%+1%	79	5	499	0,5	2,32	1	130	1375	249

Best material removal rate

Number	Supplier	Item	Coating	Composition	Doc (10^{-3} in)	f (10^{-3} in/rev)	Speed (ft/min)	Tool life (min)	MRR (in^3/min)	Volume(in^3)	Cutting time (min)	TotalTime (min)	Tool number
33		Ceramic renforce SiCw revetu	CrN with PVD	(Al2O3+SiCw)(20% SiC)	59	9	984	0,1	6,04	1	50	2100	410
24		nano-ceramic Al2O3 renforce SiCw	none	(Al2O3+SiC)(70%+30%)	89	6	886	2,3	5,56	13	55	175	24
26		Ceramic Si3N4 renforce SiCw	none	(Si3N4+SiC)(75%+35%)	89	6	886	0,6	5,56	3	54	529	95
25		Ceramic mixte Al2O3	none	(Al2O3+TiCN+ZrO2)(75 %+20%+5%)	89	6	886	1,7	5,56	9	55	220	33
30		PCBN	none	PCBN DBC50 CBn=50%, grain size 2 micron	20	4	4101	0,2	3,81	1	79	2704	525
29		Ceramic Al2O3 renforce SiCw	none	(Al2O3/TiB2/SiCw)vol 72% 18% 10%	59	6	656	6,0	2,75	16	114	209	19
11	Sumitomo Electric L.td	Carbure mono revetu	CVD multi Al2O3		79	16	164	0,5	2,44	1	123	1353	246
12		Ceramic pur	none	(Al2O3+ZrO2) 99%+1%	79	5	499	0,2	2,32	0	129	3519	678
6		Ceramic mixte Si3N4	none	Si3N4	20	7	984	0,3	1,74	1	173	3003	566
9		Carbure multi revetu	PVD TiN/TiCN/TiN	Wc (94%) Co(6%)	79	10	138	48,0	1,28	62	240	265	5
8		Carbure mono revetu	TiN with PVD	Wc (94%) Co(6%)	79	10	138	8,0	1,28	10	240	390	30
15	Kennametal	Carbure mono revetu	TiCN with PVD	WC-6%wtCo	59	6	249	1,6	1,04	2	288	1188	180
16	Kennametal	Carbure mono revetu	TiAlN with PVD	WC-6%wtCo	59	6	249	3,2	1,04	3	288	738	90
19	Kennametal	Carbure multi revetu	CVD Al2O3/TiC/TiCN		16	8	328	0,7	0,49	0	615	4965	870
5		Carbure non revetu	none	(Carbure K10 (WC-Co)	12	6	328	0,6	0,27	0	1092	10832	1948

Best effective cutting time

Number	Supplier	Item	Coating	Composition	Doc (10^{-3} in)	f (10^{-3} in/rev)	Speed (ft/min)	Tool life (min)	MRR (in^3/min)	Volume(in^3)	Cutting time (min)	TotalTime (min)	Tool number
33		Ceramic renforce SiCw revetu	CrN with PVD	(Al2O3+SiCw)(20% SiC)	59	9	984	0,1	6,04	1	50	2100	410
24		nano-ceramic Al2O3 renforce SiCw	none	(Al2O3+SiC)(70%+30%)	89	6	886	2,3	5,56	13	55	175	24
26		Ceramic Si3N4 renforce SiCw	none	(Si3N4+SiC)(75%+35%)	89	6	886	0,6	5,56	3	54	529	95
25		Ceramic mixte Al2O3	none	(Al2O3+TiCN+ZrO2)(75 %+20%+5%)	89	6	886	1,7	5,56	9	55	220	33
30		PCBN	none	PCBN DBC50 CBn=50%, grain size 2 micron	20	4	4101	0,2	3,81	1	79	2704	525
29		Ceramic Al2O3 renforce SiCw	none	(Al2O3/TiB2/SiCw)vol 72% 18% 10%	59	6	656	6,0	2,75	16	114	209	19
11	Sumitomo Electric L.td	Carbure mono revetu	CVD multi Al2O3		79	16	164	0,5	2,44	1	123	1353	246
12		Ceramic pur	none	(Al2O3+ZrO2) 99%+1%	79	5	499	0,2	2,32	0	129	3519	678
6		Ceramic mixte Si3N4	none	Si3N4	20	7	984	0,3	1,74	1	173	3003	566
9		Carbure multi revetu	PVD TiN/TiCN/TiN	Wc (94%) Co(6%)	79	10	138	48,0	1,28	62	240	265	5
8		Carbure mono revetu	TiN with PVD	Wc (94%) Co(6%)	79	10	138	8,0	1,26	10	240	390	30
15	Kennametal	Carbure mono revetu	TiCN with PVD	WC-6%wtCo	59	6	249	1,6	1,04	2	288	1188	180
16	Kennametal	Carbure mono revetu	TiAlN with PVD	WC-6%wtCo	59	6	249	3,2	1,04	3	288	738	90
19	Kennametal	Carbure multi revetu	CVD Al2O3/TiC/TiCN		16	8	328	0,7	0,49	0	615	4965	870
5		Carbure non revetu	none	(Carbure K10 (WC-Co)	12	6	328	0,6	0,27	0	1092	10832	1948

APPENDIX II. Chip thickness calculations

II.1. Calculation of PA: The section removed when the ramp is positive during the first pass.

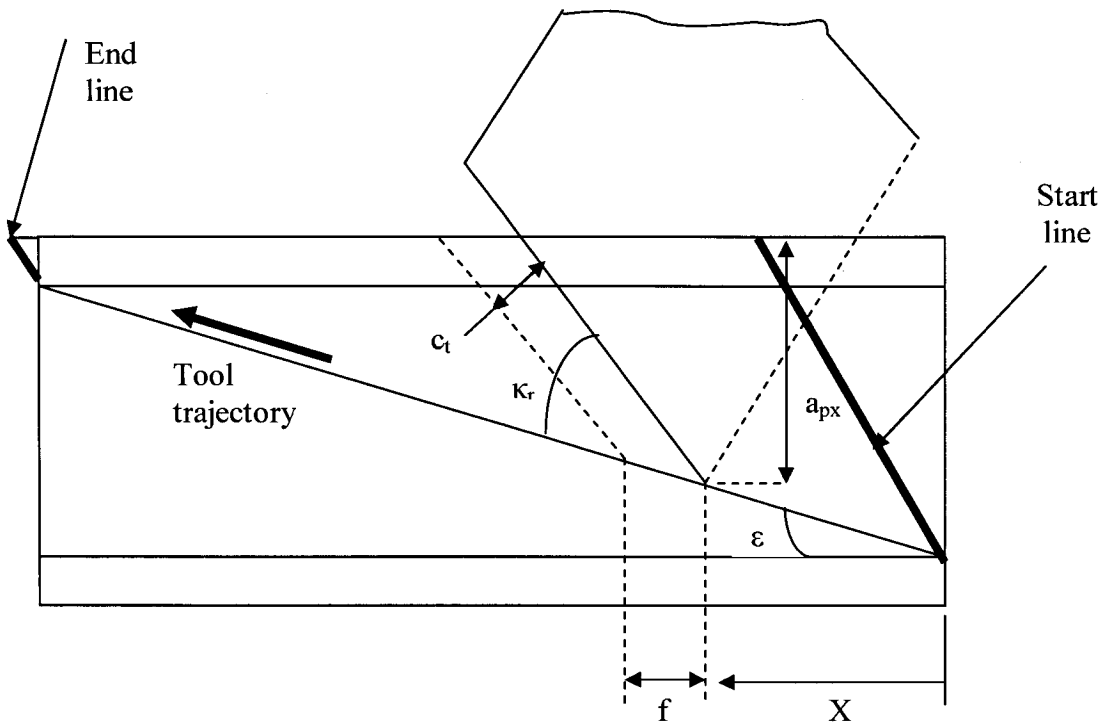

Figure 8.21. The section removed when the ramp is positive during the first pass.

$$Ct=f.\frac{\sin(\kappa r-\varepsilon)}{\cos(\varepsilon)} \qquad a_{px}=A-X.\tan(\varepsilon) \qquad Vcx=Dinit-2a_{px}$$

$$ds=C_t.\frac{a_{px}-f.\tan(\varepsilon)}{\sin(\kappa_r)}+\frac{f2}{2}\tan(\varepsilon)(1-\frac{\tan(\varepsilon)}{\tan(\kappa_r)}) \qquad X=[0;L] \qquad Fx=Ks.ds \qquad Px=Fx.Vcx$$

C_t: The chip thickness

ds: The cutting section

L: The cutting length

a_{px}: The depth of cut at the position X

ε: The slope

κ_r:The lead angle

F_x, P_x and V_{cx}, D_{init}; The cutting force, the cutting power, and the cutting speed at the position X, and the initial diameter.

II.2. Calculation of PAD: The section removed at the beginning when the tool enters into the material when the ramp is positive during the first pass.

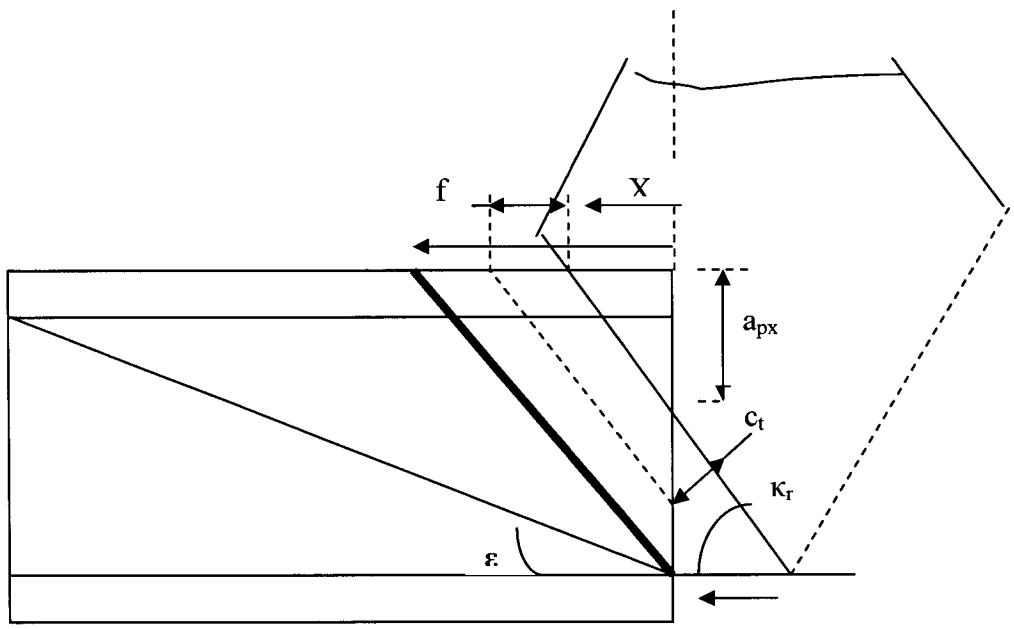

Figure 8.22. The section removed at the beginning when the tool enters into the material when the ramp is positive during the first pass.

$$Ct=f\sin(\kappa_r) \qquad a_{px}=X.\tan(\kappa_r) \qquad Fx=Ks.ds \qquad Px=Fx.Vcx$$

$$ds=\tan(\kappa_r)(f.X+\frac{f2}{2}) \qquad X=[0;\frac{A}{\tan(\kappa_r)}] \qquad Vcx=Dinit-2A$$

C_t: The chip thickness

ds: The cutting section

L: The cutting length

a_{px}: The depth of cut at the position X

ε: The slope

κ_r :The lead angle

F_x, P_x and V_{cx}, D_{init}; The cutting force, the cutting power, and the cutting speed at the position X, and the initial diameter.

II.3. Calculation of PR: The section removed when the ramp is positive, during the second pass.

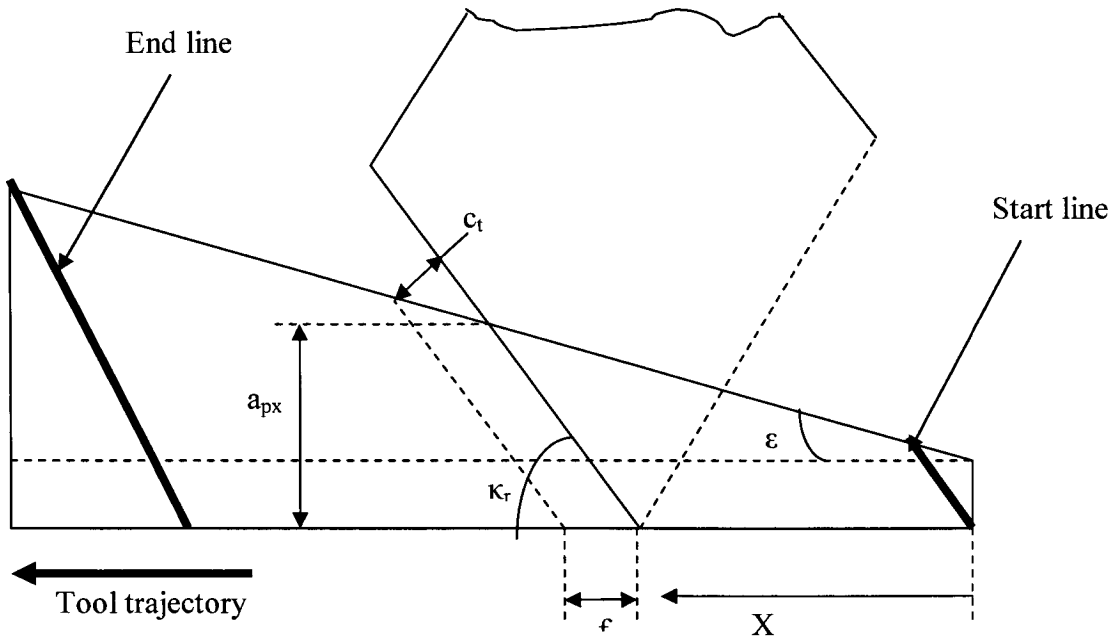

Figure 8.23. The section removed when the ramp is positive, during the second pass.

$$Ct=f\sin(\kappa_r) \qquad X=[0;L-\frac{A}{\tan(\kappa_r)}] \qquad Fx=Ks.ds \qquad Px=Fx.Vcx$$

$$ds=f.a_{px}+\frac{f^2}{2}\frac{\sin(\kappa_r)\sin(\varepsilon)}{sn(\kappa_r-\varepsilon)}) \qquad a_{px}=\tan(\kappa_r)\frac{B+X.\tan(\varepsilon)}{\tan(\kappa_r)-\tan(\varepsilon)} \qquad Vcx=Dinit-2(A+B)$$

C_t: The chip thickness

ds: The cutting section

L: The cutting length

a_{px}: The depth of cut at the position X

ε: The slope

κ_r :The lead angle

F_x, P_x and V_{cx}, D_{init}; The cutting force, the cutting power, and the cutting speed at the position X, and the initial diameter.

II.4. PRD: the section removed at the beginning when the tool enter into the material when the ramp is positive, during the second pass.

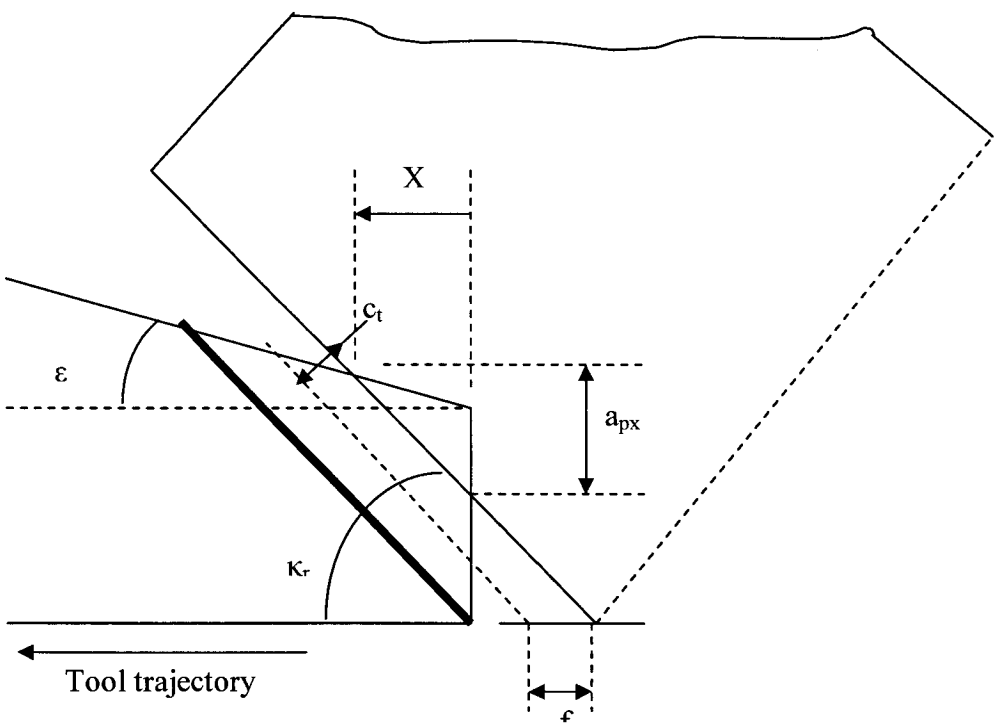

Figure 8.24. PRD: The section removed at the beginning when the tool enters into the material when the ramp is positive, during the second pass.

$$Ct=f\sin(\kappa_r) \quad X=[0;\frac{B}{\tan(\kappa_r)}] \quad Fx=Ks.ds \quad Px=Fx.Vcx \quad a_{px}=\frac{X\tan(\kappa_r)^2}{\tan(\kappa_r)-\tan(\varepsilon)}$$

$$ds=(f.X+\frac{f2}{2})\frac{tan(\kappa_r)^2}{\tan(\kappa_r)-\tan(\varepsilon)} \quad Vcx=Dinit-2(A+B)$$

C_t: The chip thickness

ds: The cutting section

L: The cutting length

a_{px}: The depth of cut at the position X

ε: The slope

κ_r :The lead angle

F_x, P_x and V_{cx}, D_{init}; The cutting force, the cutting power, and the cutting speed at the position X, and the initial diameter.

II.5. NR: The section removed when the ramp is negative, during the second pass.

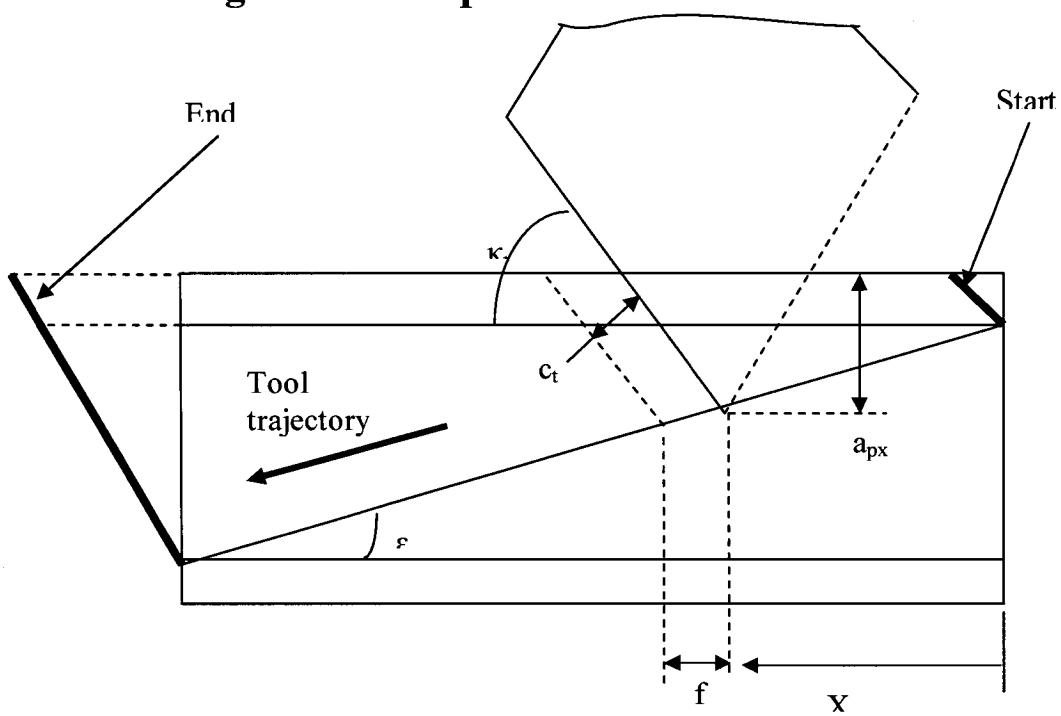

Figure 8.25. NR: The section removed when the ramp is negative, during the second pass.

$$Ct=f.\frac{\sin(\kappa r+\varepsilon)}{\cos(\varepsilon)} \qquad a_{px}=B+X.\tan(\varepsilon) \qquad Fx=Ks.ds \qquad Px=Fx.Vcx$$

$$X=[0;L] \qquad ds=C_t.\frac{a_{px}}{\sin(\kappa_r)}+\frac{f2}{2}\tan(\varepsilon)(1+\frac{\tan(\varepsilon)}{\tan(\kappa_r)}) \qquad Vcx=Dinit-2a_{px}$$

C_t: The chip thickness

ds: The cutting section

L: The cutting length

a_{px}: The depth of cut at the position X

ε: The slope

κ_r :The lead angle

F_x, P_x and V_{cx}, D_{init}; The cutting force, the cutting power, and the cutting speed at the position X, and the initial diameter.

II.6. NAD: The section removed at the beginning when the tool enter into the material when

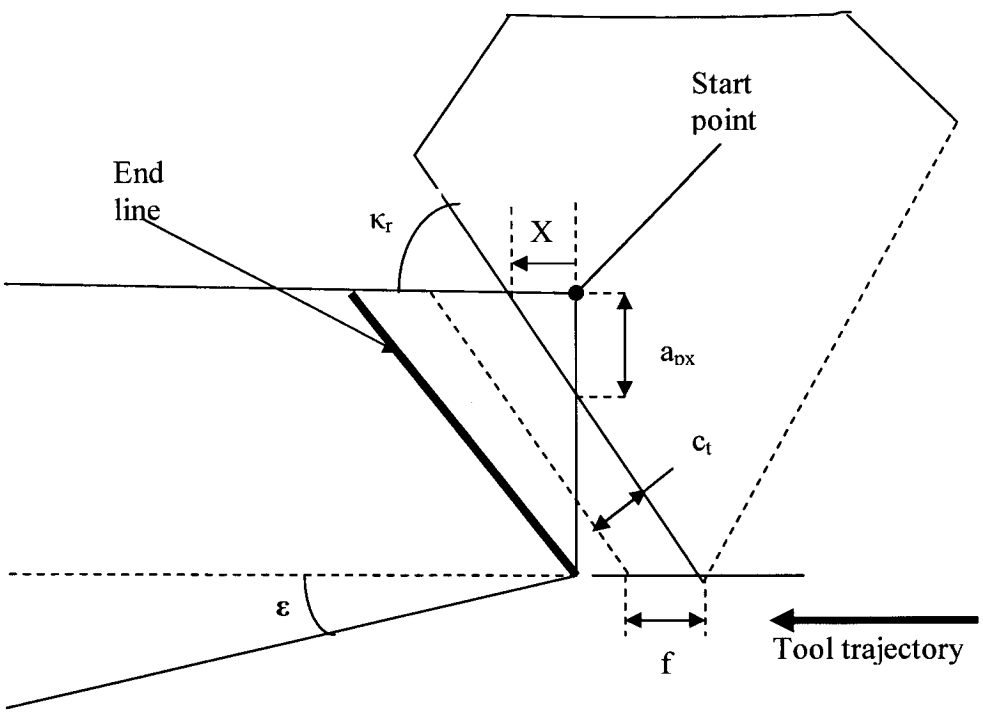

Figure 8.26. NAD: The section removed at the beginning when the tool enter into the material when

$Ct=f\sin(\kappa_r)$ $a_{px}=X.\tan(\kappa_r)$ $ds=\tan(\kappa_r)(f.X+\frac{f2}{2})$

$Fx=Ks.ds$ $X=[0;\frac{B}{\tan(\kappa_r)}]$ $Px=Fx.Vcx$ $Vcx=Dinit-2B$

C_t: The chip thickness

ds: The cutting section

L: The cutting length

a_{px}: The depth of cut at the position X

ε: The slope

κ_r :The lead angle

F_x, P_x and V_{cx}, D_{init}; The cutting force, the cutting power, and the cutting speed at the position X, and the initial diameter.

II.7. NRD: The section removed at the beginning when the tool enter into the material when the ramp is negative, during the second pass.

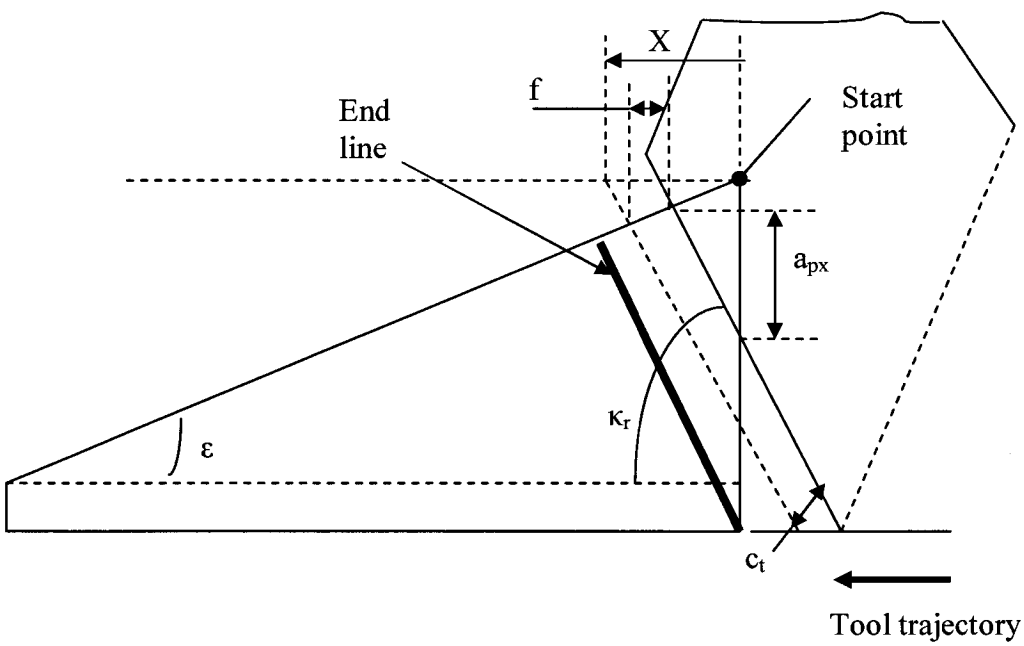

Figure 8.27. NRD: The section removed at the beginning when the tool enters into the material when the ramp is negative, during the second pass.

C_t: The chip thickness

$$a_{px}=X.\tan(\kappa_r) \qquad Vcx=Dinit-2(A+B) \qquad X=[0;\frac{A}{\tan(\kappa_r)+\tan(\varepsilon)}] \qquad Ct=f\sin(\kappa_r)$$

$$Fx=Ks.ds \qquad Px=Fx.Vcx$$

$$ds=\frac{f^2}{2}\tan(\kappa_r)+(X\tan(\kappa_r)-\frac{f}{2}\tan(\varepsilon)\frac{f.tan(\kappa_r)}{\tan(\kappa_r)+\tan(\varepsilon)}$$

ds: The cutting section

L: The cutting length

a_{px}: The depth of cut at the position X

ε: The slope

κ_r :The lead angle

F_x, P_x and V_{cx}, D_{init}; The cutting force, the cutting power, and the cutting speed at the position X, and the initial diameter.

II.8. NR: The section removed when the ramp is negative, during the second pass.

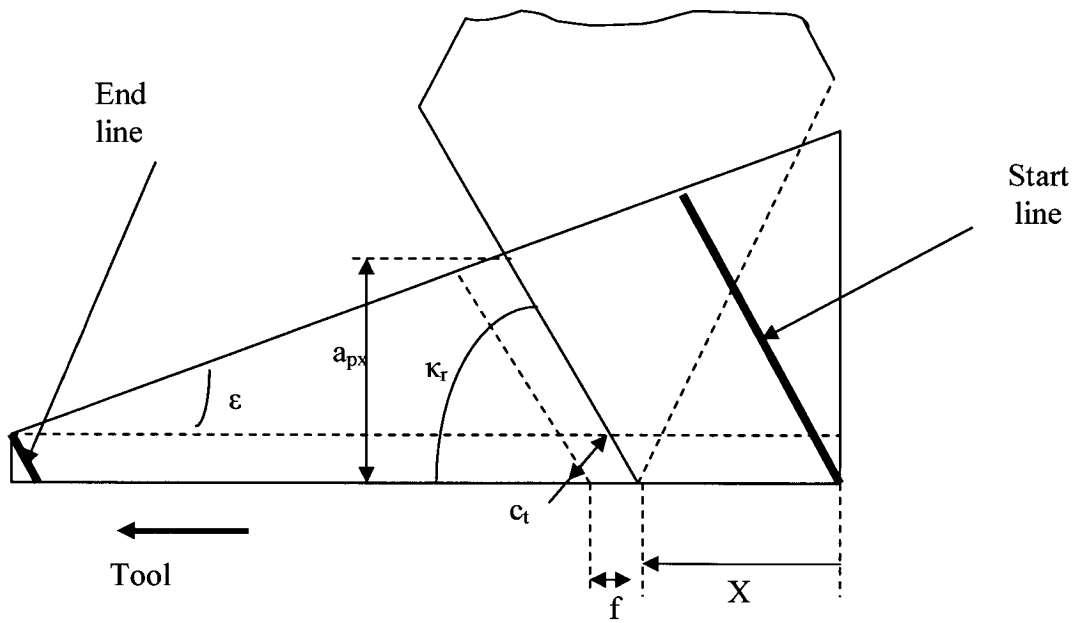

Figure 8.28. NR: The section removed when the ramp is negative, during the second pass.

$$Ct=f\sin(\kappa_r) \qquad a_{px}=\tan(\kappa_r)\frac{A-X.\tan(\varepsilon)}{\tan(\kappa_r)+\tan(\varepsilon)} \qquad X=[0;L-\frac{B}{\tan(\kappa_r)}]$$

$$ds=f.a_{px}-\frac{f2}{2}.\frac{\tan(\varepsilon)tan(\kappa_r)}{\tan(\kappa_r)+\tan(\varepsilon)}) \qquad Fx=Ks.ds \qquad Px=Fx.Vcx \qquad Vcx=Dinit-2(A+B)$$

C_t: The chip thickness

ds: The cutting section

L: The cutting length, a_{px}: The depth of cut at the position X

ε: The slope

κ_r: The lead angle

F_x, P_x and V_{cx}, D_{init}; The cutting force, the cutting power, and the cutting speed at the position X, and the initial diameter.

II.9. ITN and ITP: The remaining material when the ramp is negative or Positive during the second pass.

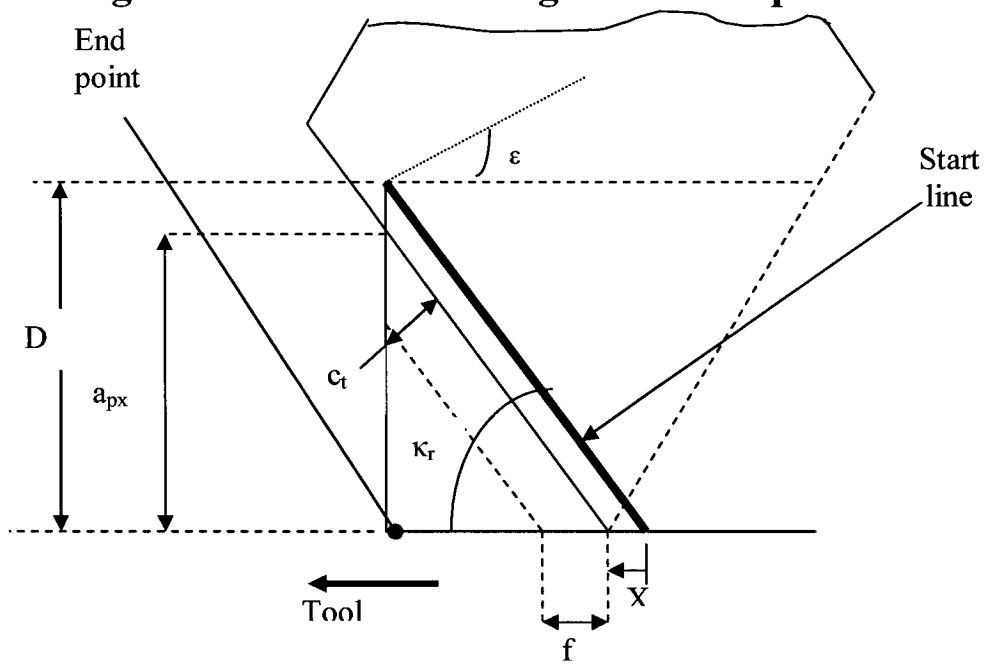

Figure 8.29. ITN and ITP: The remaining material when the ramp is negative or Positive during the second pass.

When the ramp is positive D=A and if the ramp is negative D=B.

$$ds = f.(D-(x+f).\tan(\kappa_r)) + \frac{f^2}{2}\tan(\kappa_r) \qquad Ct = f\sin(\kappa_r) \qquad Vcx = Dinit - 2(A+B)$$

$$a_{px} = D - X.\tan(\kappa_r) \qquad X = [0; \frac{D}{\tan(\kappa_r)}] \qquad Fx = Ks.ds \qquad Px = Fx.Vcx$$

C_t: The chip thickness

ds: The cutting section

L: The cutting length

a_{px}: The depth of cut at the position X

ε: The slope

κ_r: The lead angle

F_x, P_x and V_{cx}, D_{init}; The cutting force, the cutting power, and the cutting speed at the position X, and the initial diameter.

APPENDIX III. Cutting data

Test number	Insert Type	Observations	Insert	Rau	ap (in)	f (in/rev)	Vc (ft/min)	RPM
1	Ky1540	Constant depth of cut	Round	1	0,07	0,005	500	
	Ky1540	Constant depth of cut	Round	1	0,07	0,005	500	
	Ky1540	Constant depth of cut	Round	1	0,07	0,005	500	
2	KY1540	Constant depth of cut	Round	1	0,07	0,007	900	
	KY1540	Constant depth of cut	Round	1	0,07	0,007	900	
3	GA 5026	Constant depth of cut	80 degree	1	0,07	0,007	230	150
	GA 5026	Constant depth of cut	80 degree	1	0,07	0,007	230	
4	TiALN	Constant depth of cut	80 degree	1	0,07	0,007	230	150
		0		1	0,07	0,007	230	
5	TiALN	1 Ramp negative (first pass)	80 degree	0,1	0,14	0,007		150
6	TiAlN	1 Ramp positive (first pass)	80 degree	0,1	0,14	0,007		150
		1 Ramp positive (second pass)	80 degree	0,1	0,14	0,007		150
7	TiAlN	1 Ramp positive (first pass)	80 degree	0,3	0,14	0,007		150
		1 Ramp positive (second pass)	80 degree	0,3	0,14	0,007		150
8	TiAN	2 ramps (first pass)	80 degree	0,3	0,14	0,007		150
		2 ramps (second pass)	80 degree	0,3	0,14	0,007		150
9	TiAN	3 ramps (first pass)	80 degree	0,3	0,14	0,007		150
		3 ramps (second pass)	80 degree	0,3	0,14	0,007		150
const	WG300	First pass constant depth	45 degree	0,3	0,14	0,007	900	
		second pass constant depth	45 degree	0,3	0,14	0,007	900	0

Test number	Time (s)	DT (s)	Dap (in)	Dap/DT	VB (mm)	VBmax (mm)	Vn (mm)	VBc (mm)
1	1,20	0	0	0,00000	0,19	0,19	0,19	0,19
	4,21	0	0	0,00000	0,31	0,32	0,39	0,39
	7,22	0	0	0,00000	0,39	0,47	0,51	0,51
2	1,00	0	0	0,00000	0,31	0,35	0,49	0,48
	2,00	0	0	0,00000	0,67	0,67	0,67	1,01
3	2,60	0	0	0,00000	0,20	0,23	0,28	0,12
	5,08	0	0	0,00000	0,26	0,30	0,43	0,16
4	2,60	156	0	0,00000	0,17	0,17	0,22	0,17
	5,07	0	0	0,00000	0,23	0,00	0,00	0,00
5	2,60	156	0	0,00000	0,13	0,19	0,92	0,27
6	2,60	156	0,1145	0,00073	0,13	0,13	0,21	0,21
	5,20	156	0	0,00000	0,25	0,33	0,58	0,25
7	2,60	156	0,0754	0,00048	0,16	0,16	0,16	0,23
	5,20	156	0	0,00000	0,19	0,23	0,43	0,30
8	2,60	78	0,0754	0,00097	0,29	0,37	0,51	0,13
	5,20	78	0	0,00000	0,32	0,38	0,52	0,16
9	2,60	52	0,0754	0,00145	0,13	0,17	0,15	0,20
	5,20	52	0	0,00000	0,16	0,16	0,48	0,16
const	1,56	78	0	0,00000	0,12	0,12	0,46	0,12
	3,05	78	0	0,00000	0,16	0,16	0,59	0,15

Test number	Insert Type	Observations	Insert	Rau	ap (in)	f (in/rev)	Vc (ft/min)	RPM
3 ramps	WG300	3 ramps (first pass)	45 degree	0,3	0,14	0,007	900	
		3 ramps (second pass)	45 degree	0,3	0,14	0,007	900	
10	KC5010	finishing	VNGG	1	0,01	0,007	150	
				1	0,01	0,007	150	
				1	0,01	0,007	150	
11	KC5010	finishing	VNGG	1	0,01	0,005	210	
				1	0,01	0,005	210	
				1	0,01	0,005	210	
12	KC5010	finishing	VNGG	1	0,01	0,005	350	
				1	0,01	0,005	350	
				1	0,01	0,005	350	
13	WG 300		Square	1	0,07	0,007	900	
				1	0,07	0,007	900	
				1	0,07	0,007	900	
				1	0,07	0,007	900	
				1	0,07	0,007	900	
14	WG 300		Square	1	0,07	0,009	1000	
				1	0,07	0,009	1000	
				1	0,07	0,009	1000	
15	WG300		Round	1	0,07	0,007	900	
				1	0,07	0,007	900	
				1	0,07	0,007	900	
16	WG 300		Square	1	0,07	0,007	1000	
				1	0,07	0,007	1000	
				1	0,07	0,007	1000	
				1	0,07	0,007	1000	
				1	0,07	0,007	1000	

Test number	Time (s)	DT (s)	Dap (in)	Dap/DT	VB (mm)	VBmax (mm)	Vn (mm)	VBc (mm)
3 ramps	1,30	19,5	0	0,00000	0,08	0,08	0,08	0,12
	2,60	19,5	0	0,00000	0,13	0,13	0,09	0,13
10	12,97	0	0	0,00000	0,14	0,15	0,15	0,18
	19,43	0	0	0,00000	0,14	0,14	0,14	0,17
	25,88	0	0	0,00000	0,16	0,16	0,16	0,18
11	6,42	0	0	0,00000	0,17	0,17	0,17	0,17
	12,83	0	0	0,00000	0,11	0,11	0,17	0,17
	25,58	0	0	0,00000	0,14	0,14	0,18	0,18
12	3,81	0	0	0,00000	0,10	0,10	0,14	0,14
	7,61	0	0	0,00000	0,12	0,12	0,12	0,16
	15,17	0	0	0,00000	0,15	0,15	0,15	0,18
13	1,00	0	0	0,00000	0,09	0,09	0,09	0,09
	2,00	0	0	0,00000	0,14	0,14	0,37	0,14
	3,00	0	0	0,00000	0,15	0,16	0,38	0,15
	3,85	0	0	0,00000	0,19	0,19	0,47	0,23
	3,44	0	0	0,00000	0,00	0,00	0,00	0,00
14	1,00	0	0	0,00000	0,08	0,08	0,13	0,08
	1,96	0	0	0,00000	0,13	0,13	0,21	0,13
	3,86	0	0	0,00000	0,19	0,19	0,55	0,19
15	1,00	0	0	0,00000	0,13	0,13	0,13	0,15
	2,65	0	0	0,00000	0,20	0,20	0,20	0,20
	5,21	0	0	0,00000	0,31	0,33	0,43	0,33
16	1,00	0	0	0,00000	0,13	0,13	0,14	0,13
	2,00	0	0	0,00000	0,14	0,14	0,29	0,14
	2,58	0	0	0,00000	0,14	0,14	0,29	0,14
	3,54	0	0	0,00000	0,19	0,19	0,75	0,19
	4,47	0	0	0,00000	0,21	0,21	1,60	0,27

Table 27: Notch wear for different machining time in function of cutting speed

	3 min	5 min	7 min
400	0,16	0,19	0,25
800	0,19	0,23	0,28
900	0,2	0,26	0,57

Table 28: Tool life as a function of feed with a_p=0.07 in, Vc=900 ft/min

Vc (ft/min)	feed (in/rev)	a_p (in)	Tool life (min) for VB=0,3	Tool life (min) for VBc=0,3
900	0,007	0,07	7	7,6
900	0,009	0,07	6,7	6

Table 29: Tool life as a function of feed for Vc=800 ft/min, ap=0.0175 in

Vc	f (in/rev)	a_p (in)	TB (min)	TBc
800	0,005	0,0175	10,9295814	9,62360784
800	0,007	0,0175	11,2837748	8,63451082
800	0,009	0,0175	12,3868517	11,3646648

APPENDIX IV. Cutting forces

Table 30: Cutting forces data

	a_p (in)	Vc (in)	f (in)	Fr (N)	F_f (N)	F_t (N)
1	0,01	500	0,006	140,9581	33,8506	132,4285
2	0,01	500	0,007	197,0872	56,8691	160,221
3	0,01	500	0,008	169,5604	39,7762	165,9429
4	0,01	700	0,006	149,0876	51,9279	130,9522
5	0,01	700	0,007	211,6389	60,5484	161,278
6	0,01	700	0,008	206,3364	52,9373	172,4147
7	0,01	800	0,006	167,3881	44,4009	133,3393
8	0,01	800	0,007	218,656	63,2245	161,7173
9	0,01	800	0,008	186,8057	45,9685	166,1162
10	0,02	500	0,006	291,3891	125,447	261,7636
11	0,02	500	0,007	351,846	163,7934	314,8483
12	0,02	500	0,008	331,2867	128,3751	321,6765
13	0,02	700	0,006	323,2696	152,8809	271,9685
14	0,02	700	0,007	365,6288	170,9052	308,2436
15	0,02	700	0,008	351,8453	156,2072	330,3716
16	0,02	800	0,006	323,6825	137,0271	263,7624
17	0,02	800	0,007	383,5836	177,9305	308,7945
18	0,02	800	0,008	339,055	143,3647	321,4685
19	0,05	500	0,006	530,9236	305,2569	592,5725
20	0,05	500	0,007	332,6755	233,146	640,0034
21	0,05	500	0,008	590,8764	327,7443	732,5549
22	0,05	700	0,006	252,5875	172,2286	524,7883
23	0,05	700	0,007	366,0506	259,6875	638,5853
24	0,05	700	0,008	299,2658	197,1149	675,3941
25	0,05	800	0,006	604,6794	343,5371	589,7254
26	0,05	800	0,007	415,8871	297,711	650,3732
27	0,05	800	0,008	244,5644	149,0207	637,2559
28	0,02	700	0,007	382,09	181,27	313,16

Table 31: Cutting force data transformed into logarithm

$\ln(a_p)$	ln(Vc)	ln(f)	ln(Fr)	$\ln(F_f)$	$\ln(F_t)$
-4,605	6,215	-5,116	4,948	3,522	4,886
-4,605	6,215	-4,962	5,284	4,041	5,077
-4,605	6,215	-4,828	5,133	3,683	5,112
-4,605	6,551	-5,116	5,005	3,950	4,875
-4,605	6,551	-4,962	5,355	4,103	5,083
-4,605	6,551	-4,828	5,330	3,969	5,150
-4,605	6,685	-5,116	5,120	3,793	4,893
-4,605	6,685	-4,962	5,387	4,147	5,086
-4,605	6,685	-4,828	5,230	3,828	5,113
-3,912	6,215	-5,116	5,675	4,832	5,567
-3,912	6,215	-4,962	5,863	5,099	5,752
-3,912	6,215	-4,828	5,803	4,855	5,774
-3,912	6,551	-5,116	5,778	5,030	5,606
-3,912	6,551	-4,962	5,902	5,141	5,731
-3,912	6,551	-4,828	5,863	5,051	5,800
-3,912	6,685	-5,116	5,780	4,920	5,575
-3,912	6,685	-4,962	5,950	5,181	5,733
-3,912	6,685	-4,828	5,826	4,965	5,773
-2,996	6,215	-5,116	6,275	5,721	6,384
-2,996	6,215	-4,962	5,807	5,452	6,461
-2,996	6,215	-4,828	6,382	5,792	6,597
-2,996	6,551	-5,116	5,532	5,149	6,263
-2,996	6,551	-4,962	5,903	5,559	6,459
-2,996	6,551	-4,828	5,701	5,284	6,515
-2,996	6,685	-5,116	6,405	5,839	6,380
-2,996	6,685	-4,962	6,030	5,696	6,478
-2,996	6,685	-4,828	5,499	5,004	6,457
-3,912	6,551	-4,962	5,946	5,200	5,747

IV.1. Effect estimates for the feed component F_f of the cutting force

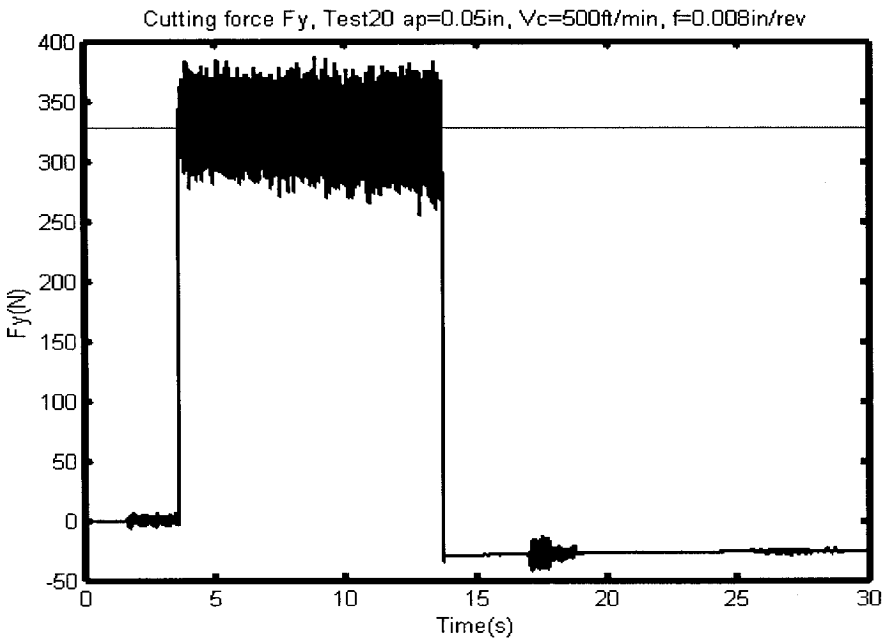

Figure 8.30. An example curve of the component $F_f = F_y$ of the cutting force

Table 32: Effect estimates for the feed component F_f of the cutting force (F_y=F_f)

	Effect	Std.Err.	t(21)	p	-95,% Cnf.Limt	+95,% Cnf.Limt	Coeff.	Std.Err. Coeff.
Mean/Interc.	4,85	0,06	78,40	0,00%	4,72	4,98	4,85	0,06
(1)Ln(a_p) (L)	1,60	0,15	10,43	0,00%	1,28	1,92	0,80	0,08
1L by 2L	-0,21	0,18	-1,18	25,04%	-0,58	0,16	-0,11	0,09
1L by 3L	-0,15	0,18	-0,81	42,80%	-0,53	0,23	-0,07	0,09
2L by 3L	-0,13	0,18	-0,75	46,15%	-0,51	0,24	-0,07	0,09
(2)LNVC (L)	0,05	0,15	0,33	74,74%	-0,26	0,35	0,02	0,07
(3)LNF (L)	-0,01	0,15	-0,07	94,15%	-0,33	0,31	-0,01	0,08

For a p of 5% the feed component of the cutting force depend only on the depth of cut.

Table 33: Regression coefficient of F_f when ignoring some effects

Regr. Coefficients; Var.:LnF_f; R-sqr=,81875; Adj:,81178 3 3-level factors, 1 Blocks, 28 Runs; MS Residual=,0942655 DV: LnF_f						
	Regressn Coeff.	Std.Err.	t(26)	p	-95,% Cnf.Limt	+95,% Cnf.Limt
Mean/Interc.	5,40	0,0794	68,004	0,00%	5,2394	5,566
(1)Ln(a_p) (L)	0,97	0,0896	10,837	0,00%	0,787	1,15548

The equation of feed component can be expressed by:

$\ln(F_f)=5.4+0.97\ln(a_p)$

$F_f=222a_p^{0.97}$ F_f expressed in (N) and a_p(mm)

IV.2. Effect estimates for the Z component (Fz=Ft)

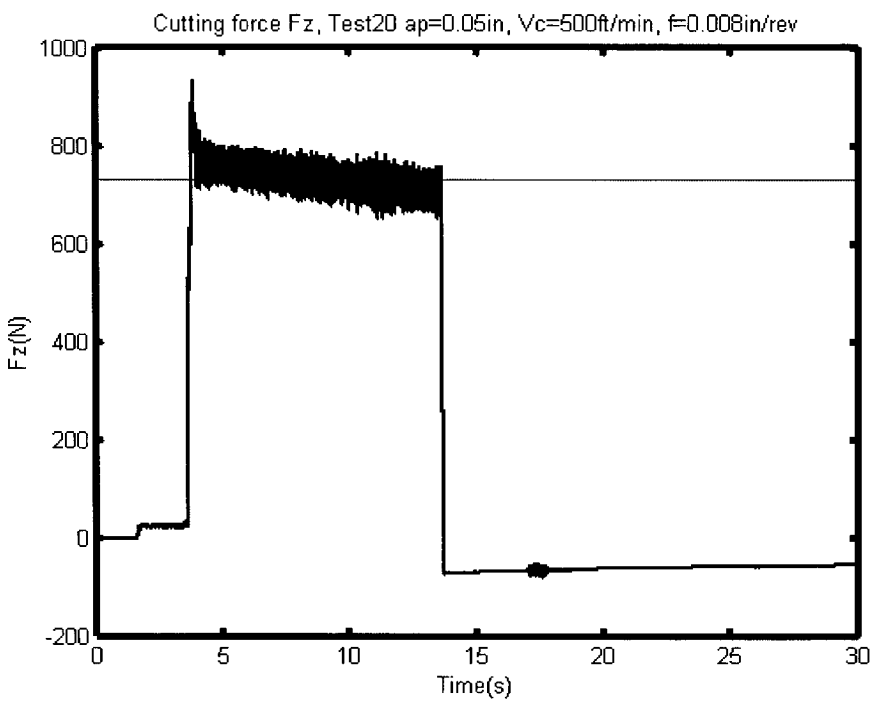

Figure 8.31. A sample curve of the component F_t of the cutting force

Table 34: Effect estimates for the tangential component F_t of the cutting force

	Effect	Std.Err.	t(21)	p	-95,% Cnf.Limt	+95,% Cnf.Limt	Coeff.	Std.Err. Coeff.
Mean/Interc.	5,76	0,01	547,01	0,00%	5,74	5,78	5,76	0,01
(1)Ln(a_p) (L)	1,41	0,03	54,20	0,00%	1,36	1,47	0,71	0,01
(3) Ln(f) (L)	0,21	0,03	8,04	0,00%	0,16	0,26	0,11	0,01
1L by 2L	-0,03	0,03	-1,03	31,36%	-0,09	0,03	-0,02	0,02
1L by 3L	-0,03	0,03	-0,96	34,86%	-0,10	0,04	-0,02	0,02
2L by 3L	-0,02	0,03	-0,51	61,31%	-0,08	0,05	-0,01	0,02
(2) Ln(V_C) (L)	-0,01	0,02	-0,54	59,31%	-0,07	0,04	-0,01	0,01

According to Table 34 Ln(F_t) depends mainly on ln(a_p) and ln(f). The other coefficients can be neglected since the value of p is higher than 5%.

Table 35: Regression coefficient of F_t when ignoring some effects

Regr. Coefficients; Var.:LnF_t; R-sqr=,9924; Adj:,9918 3 3-level factors, 1 Blocks, 28 Runs; MS Residual=,0028063 DV: LnF_t						
	Regressn Coeff.	Std.Err.	t(25)	p	-95,% Cnf.Limt	+95,% Cnf.Limt
Mean/Interc.	7,52	0,151	49,791	0,00%	7,2067	7,8286
(1) Ln(a_p) (L)	0,87	0,0155	56,532	0,00%	0,8423	0,90602
(3) Ln(f) (L)	0,73	0,0867	8,3959	0,00%	0,5495	0,90675

The tangential component of the cutting force can than be expressed:

$$\ln(F_t)=7.52+0.87\ln(a_p)+0.73\ln(f)$$

$F_t=1840a_p^{0.87} f^{0.73}$ (Ft is expressed in N, a_p in mm and f in mm/rev)

APPENDIX V. Force constant calculation

Determination of the constant K_c using the tangential cutting force equation.

In the range of a_p=[0.254;1.27 mm]=[a_{p1};a_{p2}] and f=[0.127;0.229 mm]=[f_1;f_2] which are the measurements ranges, the cutting force results gave:

$F_t=1840a_p^{0.87}\,f^{0.73}=C\,a_p^{\alpha}f^{\beta}$

Let's suppose that the average F_t : $\overline{F}_t=K_c\bar{a}_p\bar{f}$

This average must be equal to the average calculated with $F_t=C\,a_p^{\alpha}f^{\beta}$

So $$\overline{F}_t=\frac{C(a_{p2}^{\alpha+1}-a_{p1}^{\alpha+1})(f_2^{\beta+1}-f_1^{\beta+1})}{(\alpha+1)(\beta+1)(a_{p2}-a_{p1})(f_2-f_1)}=K_c\bar{a}_p\bar{f}$$

Then $$Kc.=\frac{C(a_{p2}^{\alpha+1}-a_{p1}^{\alpha+1})(f_2^{\beta+1}-f_1^{\beta+1})}{(\alpha+1)(\beta+1)(a_{p2}-a_{p1})(f_2-f_1)\bar{a}_p\bar{f}}$$

With the values C=1840, α = 0.87, β=0.73

K_c=3003 N/mm2

Than F_t=3003.ap.f, for a constant depth of cut machining.

Where a_p (mm) and f (mm)

APPENDIX VI. Ramping configurations

The rough estimation of the trajectory time to remove the material for the strategies (I), (II) and (III) is shown on Figure 8.27. This estimation is based on the trajectory of the tool in real machining. For the three cases the trajectory time is :

(I) Time= $4\Delta T+3T_h$

(II) Time= $4\Delta T+5T_h$

(II) Time= $4\Delta T+7T_h$

T_h: The time to traverse a height equal to the depth of cut.

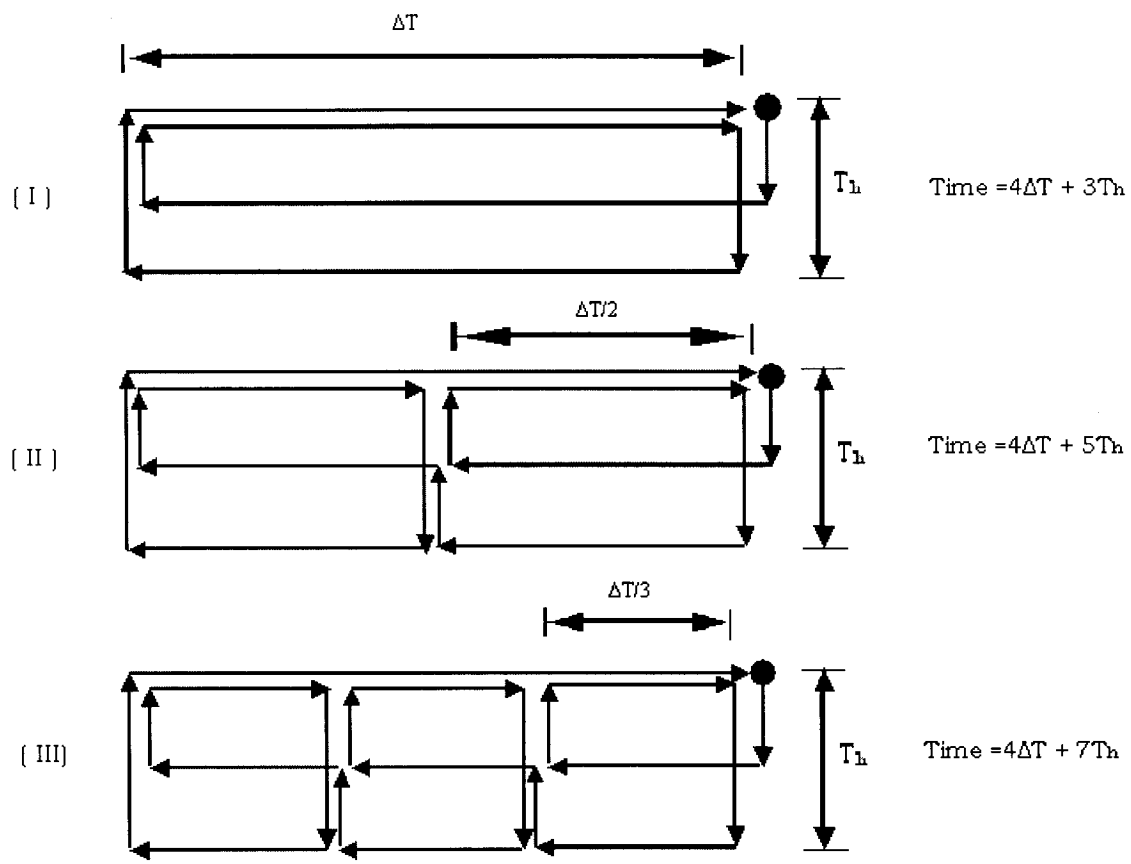

Figure 8.32. Trajectory times when making a multiple pass ramping

According to Figure 8.27 the trajectory time is higher when the length to machine is divided by 2 and 3.

Figure 8.28 shows a set of configurations with a positive slope A (higher depth of cut to smaller depth of cut) and a negative slope B (smaller depth of cut to higher depth of cut). The combinations which will give a minimum tool trajectory time are the combinations where there is a succession of A and B, (A, B, AB, BA, ABA, and BAB)

The tool trajectory times for these six configurations are equal to the time of configuration (A) Figure 4.8.

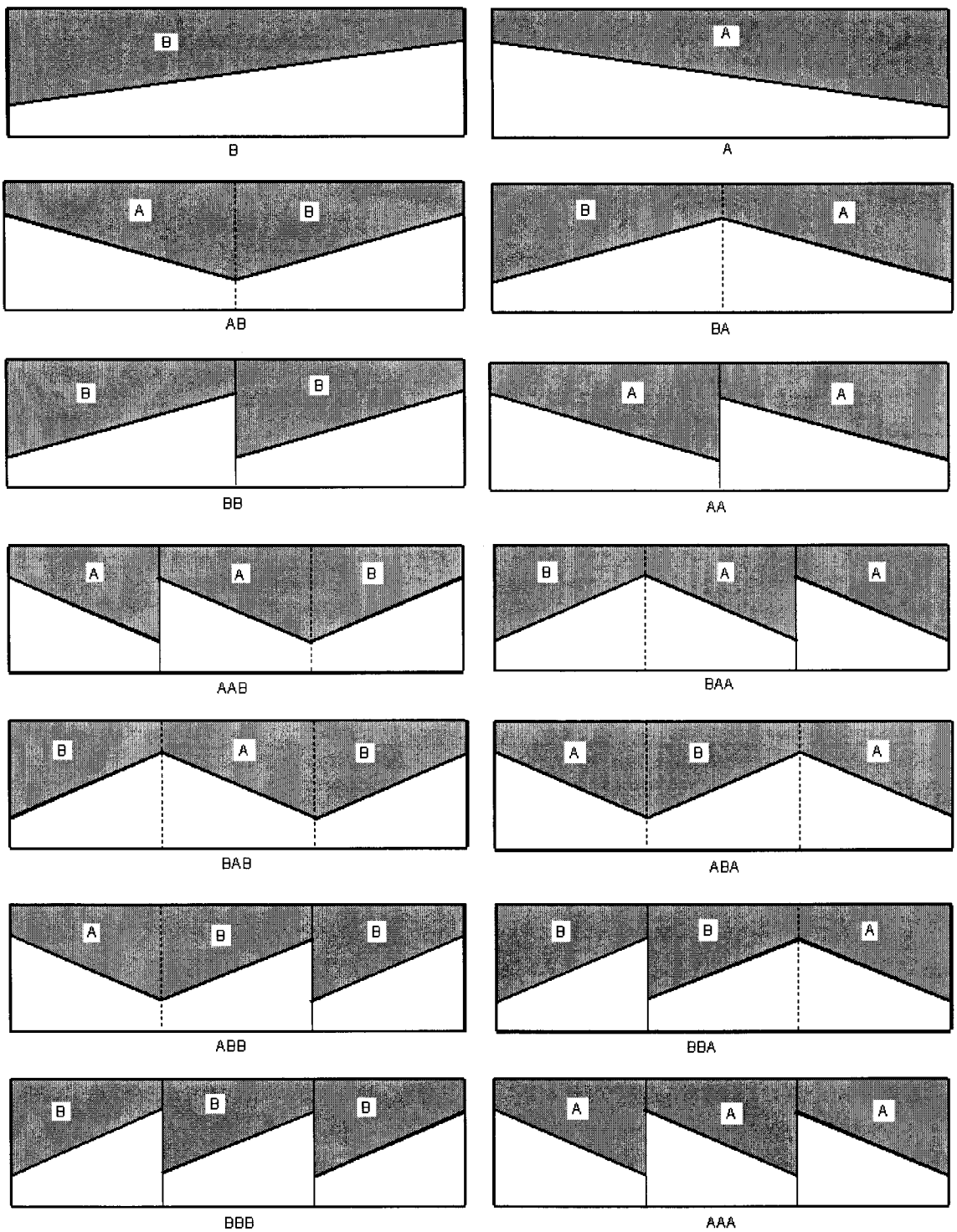

Figure 8.33. The full set of combination with positive slope configuration A and negative slope configuration B

The other combinations give higher tool trajectory times and those configurations give and idea of how the depth of cut variation can be built according to a mathematical function, for example a sinusoid or all kind of mathematical function, which will give a good depth of cut line variation to minimize the notch wear.

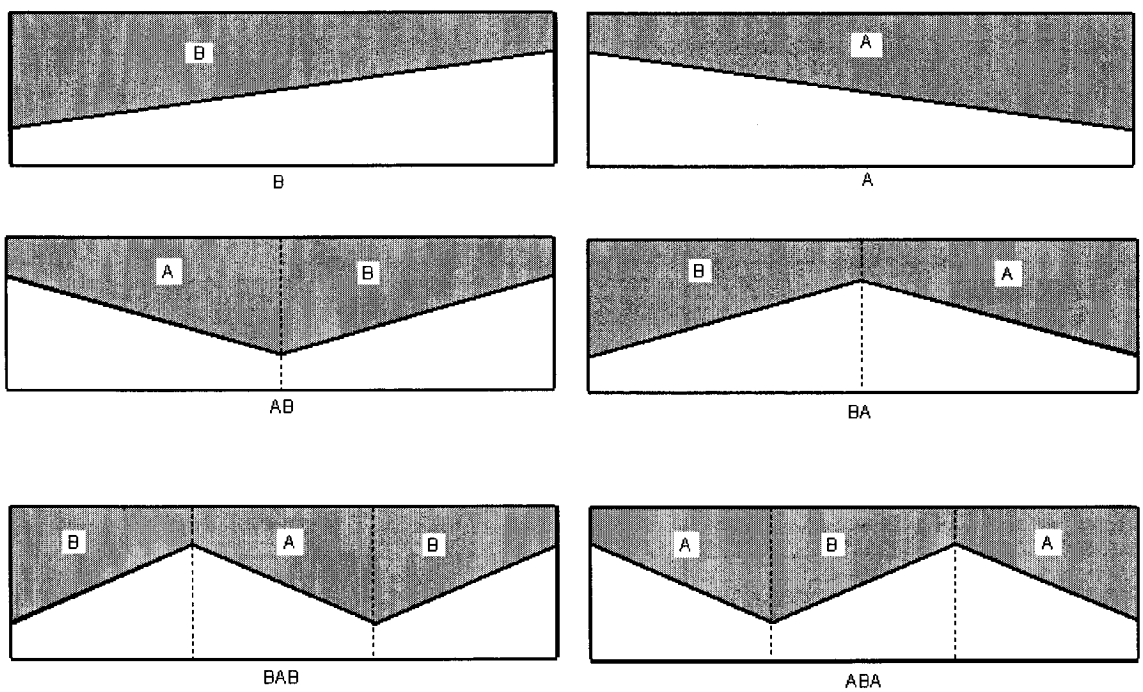

Figure 8.34. The six ramping configurations to test

APPENDIX VII. Machining overview

The PW307 machining in roughing and semi finishing requires many operations. The straight turning, facing, recessing, grooving and boring. The machining operations which do not require a big amount of material removal like grooving are annex operations. These operations are not studied in this document, but cutting tool suggestions are made.

Figure 8.35 shows the conditions where facing operations are performed.

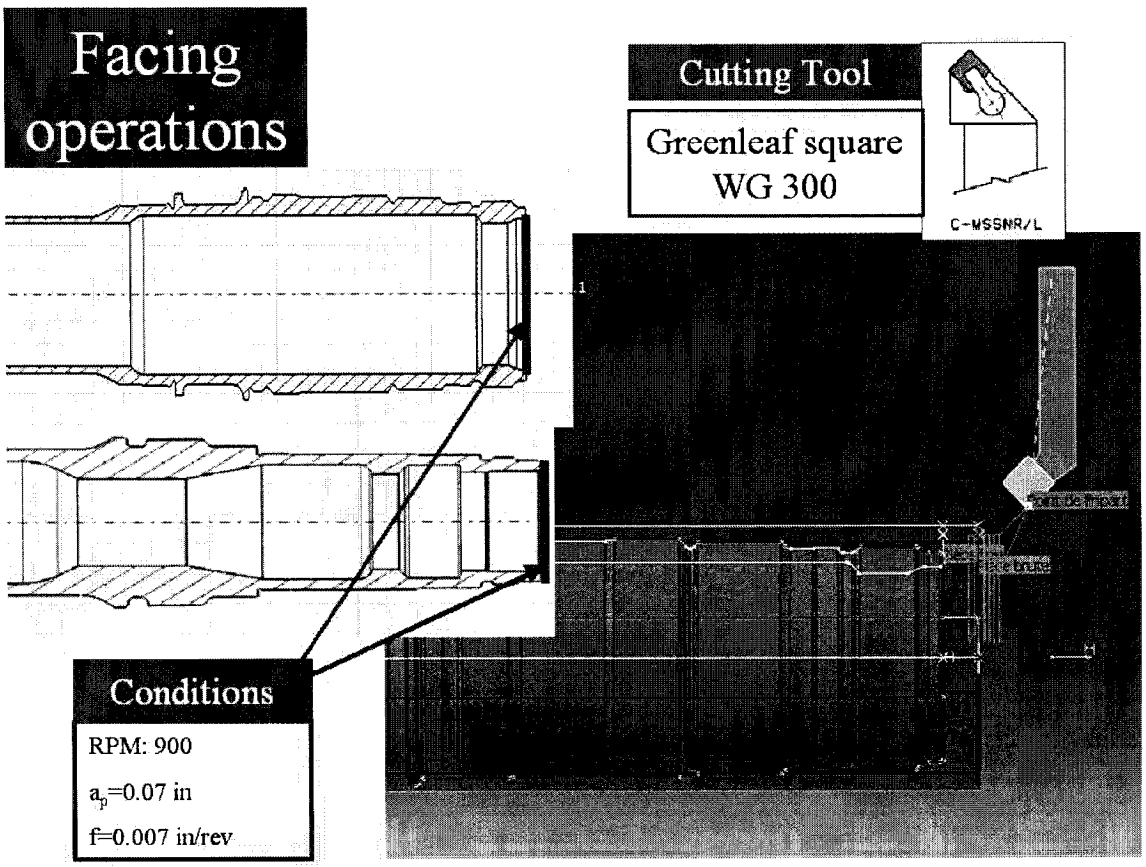

Figure 8.35. Facing operations

An important issue when machining the PW307 shaft is the steady-rest positioning. This positioning depends on the machine tool vibration conditions. The positioning steps is empiric, so let's take it first in the middle of the shaft. Figure 8.36 shows different machining zones depending on the steady rest position. The machining zone 1 is the roughing zone where the machining conditions are taken according to Table 19.

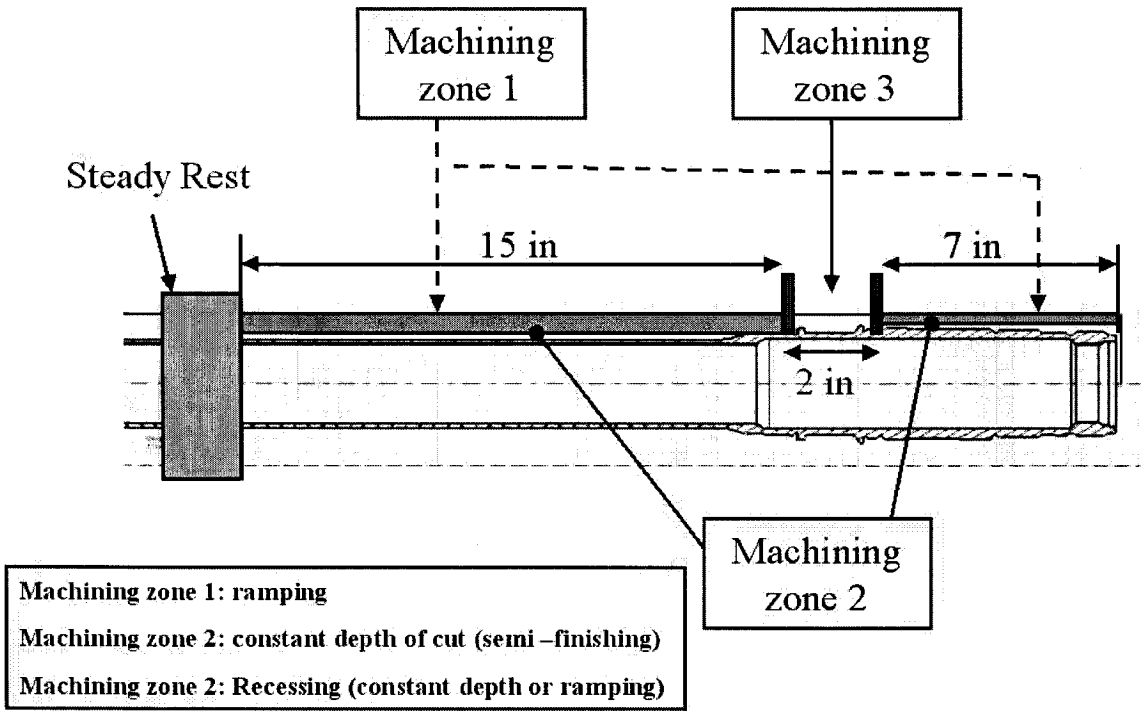

Figure 8.36. Machining zones.

The machining zone 2 is the semi finished zone where no ramping method is possible. The objective is to leave a width of material of a_p=0.01in around the shaft for the finishing operations. The machining zone 3 is a recessing zone for recessing operations.

VII.1. Ramping

The ramping operation conditions are given by Table 19 according to material hardness. Figure 8.37 shows that the ramping length is a parameter to calculate each time according to the feed, the RPM, and the time Δt. In Catia V5 the ramping process icon should not be used for this ramping strategy since some functionalities does not exist. The ramping strategy should therefore be carried out by the point to point method.

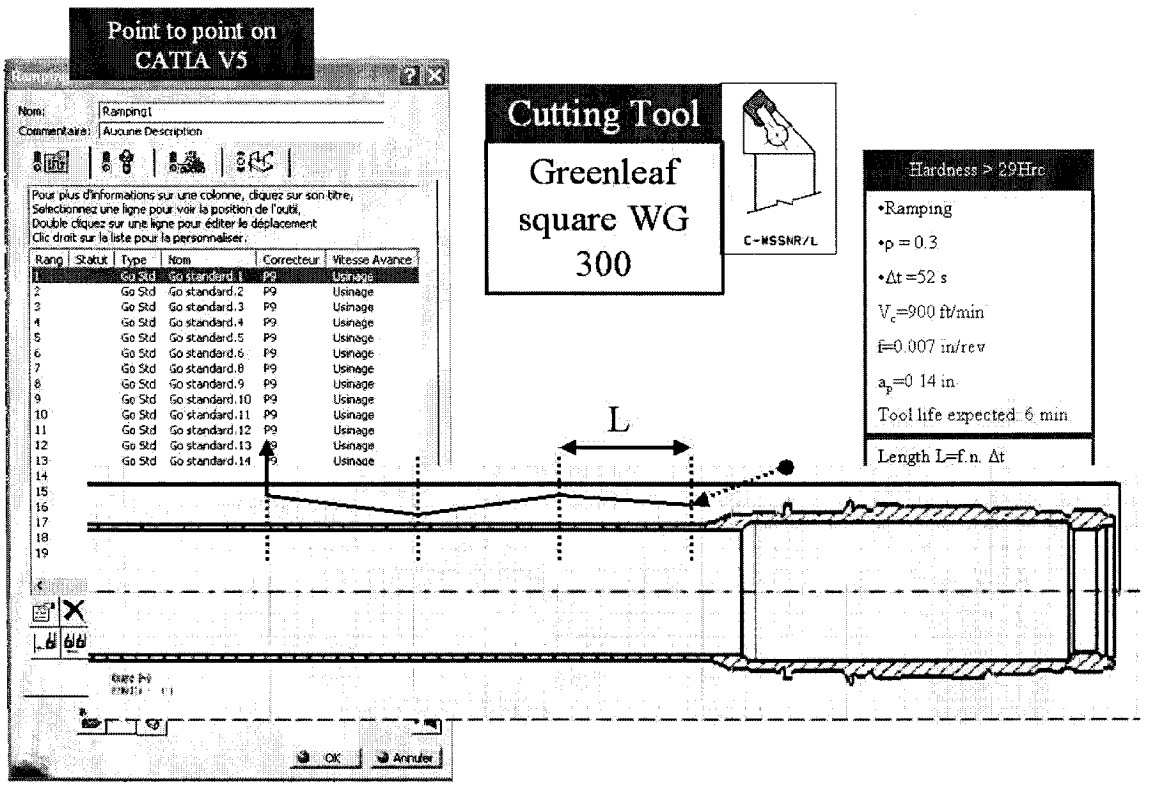

Figure 8.37. Ramping side 1

The point to point method requires the use of many point positioning in the NCGEO assembly (for Pratt & Whitney users). This operation is time consuming but mandatory

to succeed the ramping strategy. Like Figure 3.37, Figure 8.38 indicates that the ramping should be done on both side of the shaft.

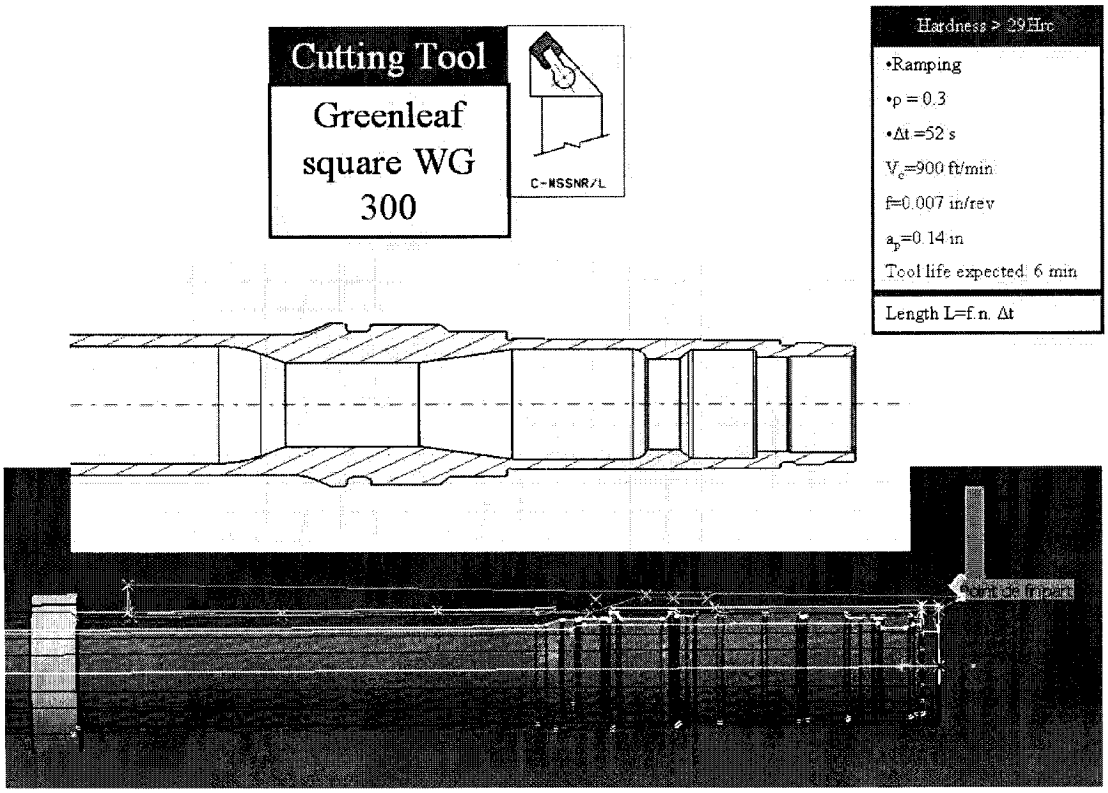

Figure 8.38. Ramping Side 2

Since it is not possible to machine the all shat by ramping, even if the material hardness recommend it, a constant depth of cut machining is required.

VII.2. Constant depth of cut.

As shown in Table 19, the constant depth of cut machining can be benefit when the Inconel 718 hardness is low. But, for semi finishing, the constant depth of cut machining is mandatory. Figure 3.39 shows that the semi finishing conditions is carried out on the whole length of the shaft.

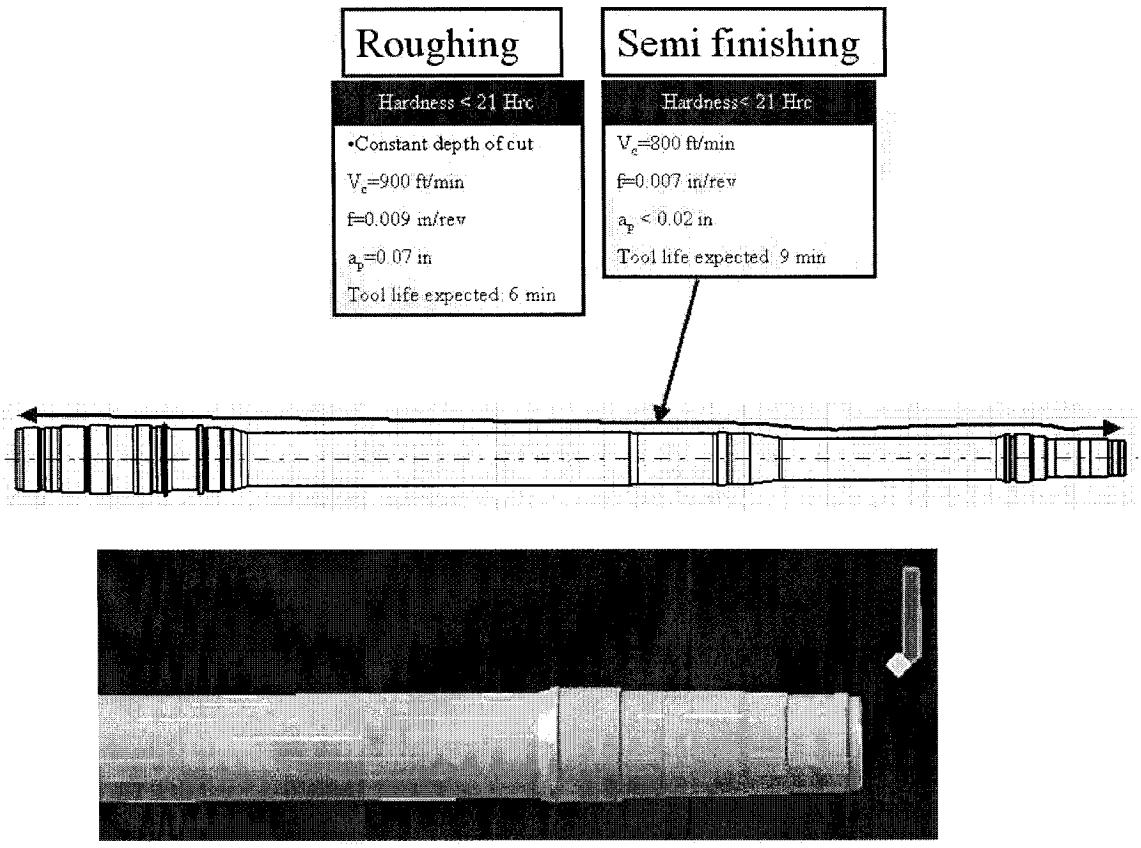

Figure 8.39. Semi finishing on the whole length of the shaft

VII.3. Recessing operations

Recessing operations are made by the same square WG 300 insert as for the straight turning and the facing. This operation is made according to the data Table 19. If the material hardness at this point requires the use of ramping, only one ramp will be made for this part, and the feed should be reduced to f_N (see Equation (33)), so that the cutting force is reduced when ramping. A smaller feed around f=0.005 in/rev could be used. Figure 8.40 show how this operation can be performed on Catia V5.

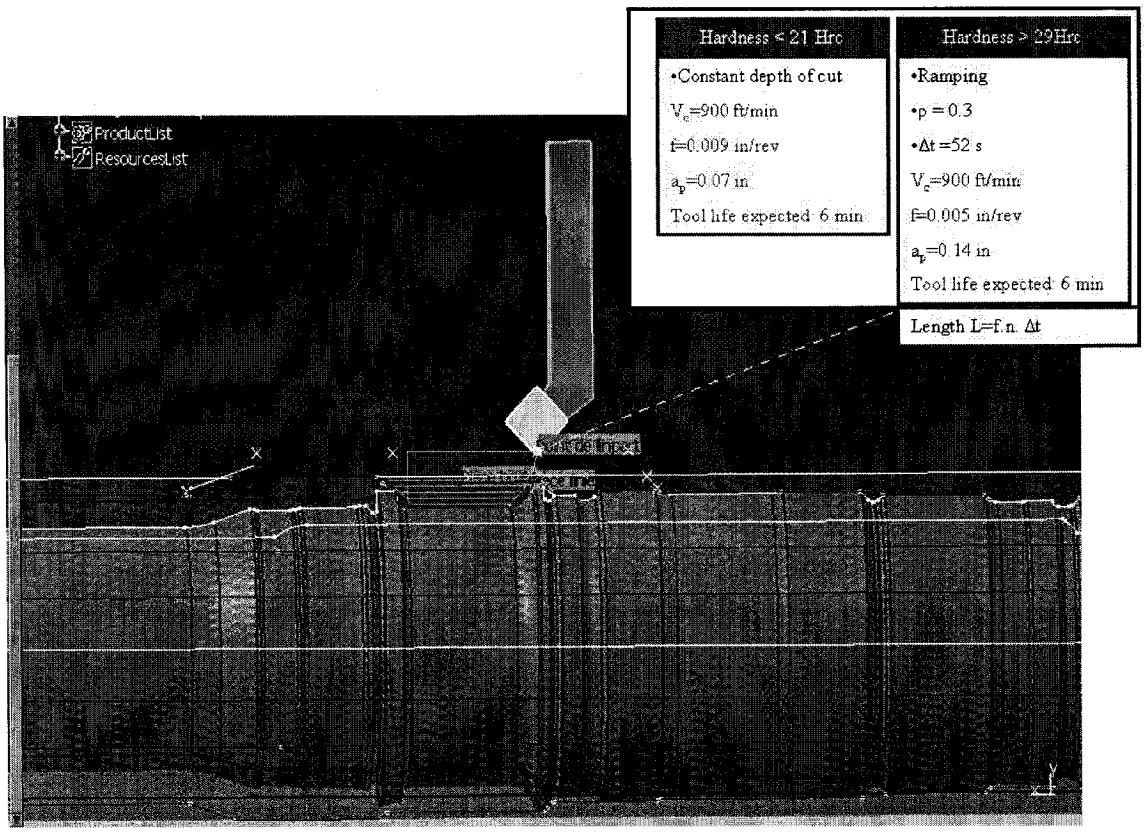

Figure 8.40. Recessing operation

VII.4. Boring operations

The boring operations are made in the same conditions as straight turning operations. The difference is that they are made in the Id. The square WG 300 insert of Greenleaf can be used for this operation, and the exact boring bar will depend on the lath to use. Figure 8.41 shows the inner diameter zone concerned by this operation.

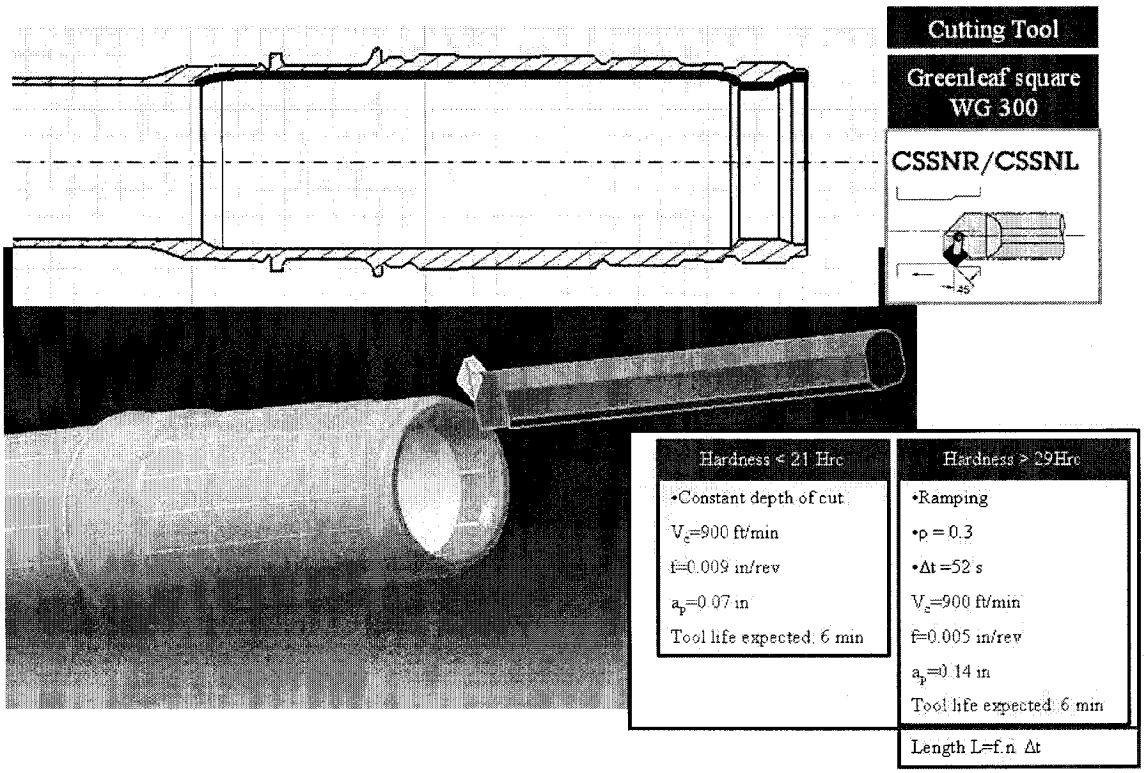

Figure 8.41. Boring operations

VII.5. Grooving operations

Grooving operation conditions are not particularly studied in this document. But these operation are necessary to machine the PW307 shaft. These operation are generally carried out in finishing. Figures 8.42 and 8.43 indicate the cutting tool suggestion for these operations and the shaft zone concerned for it. The top notch grooving insert KC5010 or KC1525 from Kennametal which is a TIALN coated insert may be a good suggestion.

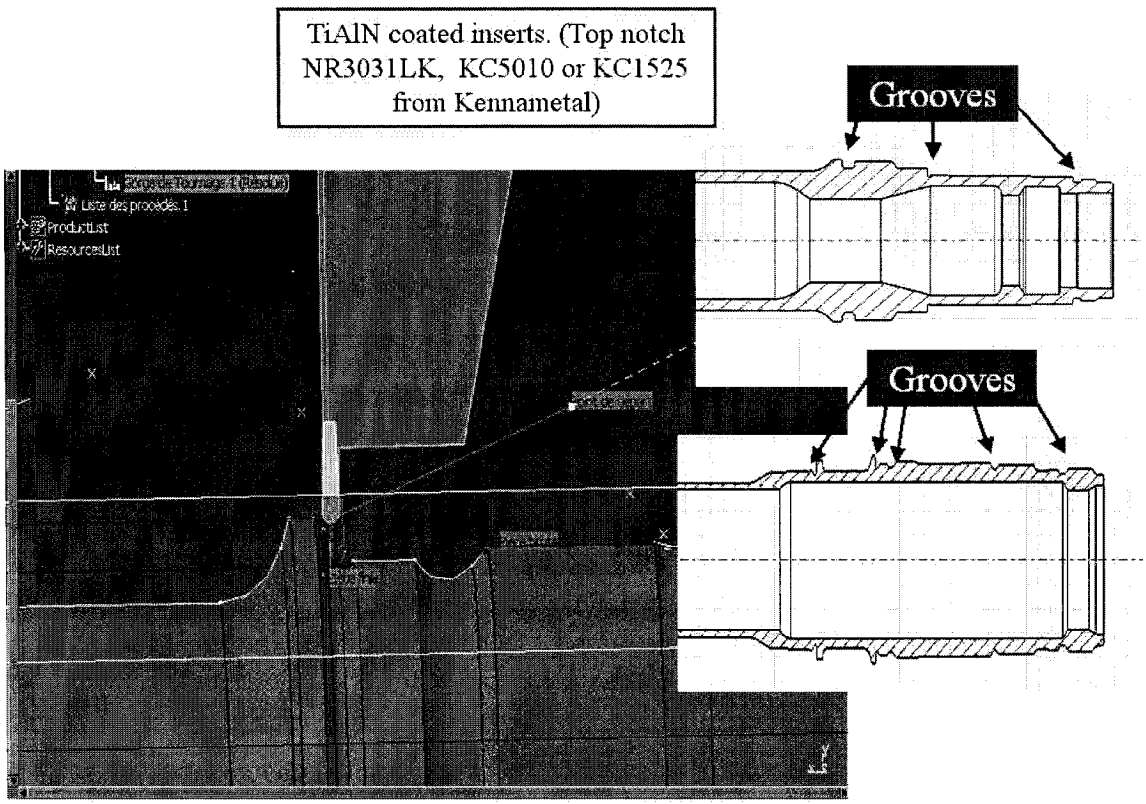

Figure 8.42. Top notch insert for Od grooving operations

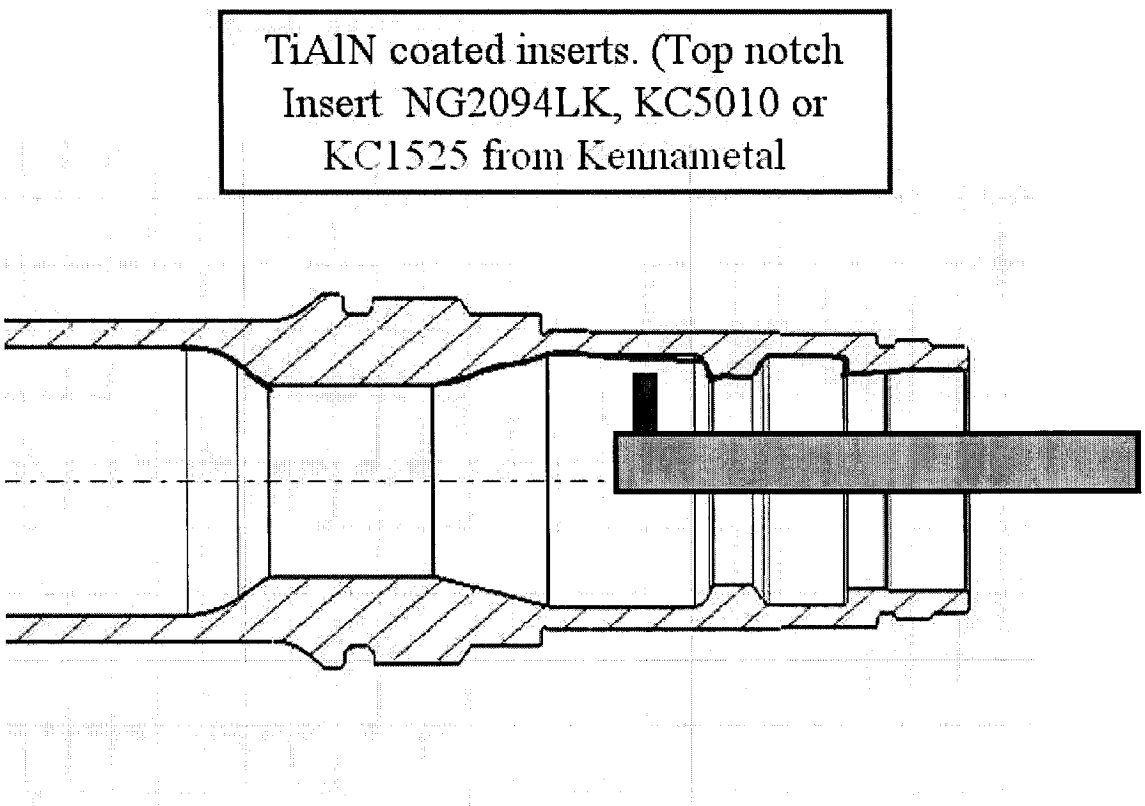

Figure 8.43. Top notch insert for Id grooving operations